ECF-300FF5-19-0089
Revision 0

GEOCHEMICAL EVALUATIONS AND REACTIVE TRANSPORT MODELING IN SUPPORT OF STAGE B ENHANCED ATTENUATION REMEDY AT 300-FF-5 OPERABLE UNIT

Prepared for the U.S. Department of Energy
Assistant Secretary for Environmental Management

Contractor for the U.S. Department of Energy
under Contract DE-AC06-08RL14788

CH2MHILL
Plateau Remediation Company

P.O. Box 1600
Richland, Washington 99352

Approved for Public Release;
Further Dissemination Unlimited

ECF-300FF5-19-0089
Revision 0

GEOCHEMICAL EVALUATIONS AND REACTIVE TRANSPORT MODELING IN SUPPORT OF STAGE B ENHANCED ATTENUATION REMEDY AT 300-FF-5 OPERABLE UNIT

Date Published
April 2020

Prepared for the U.S. Department of Energy
Assistant Secretary for Environmental Management

Contractor for the U.S. Department of Energy
under Contract DE-AC06-08RL14788

CH2MHILL
Plateau Remediation Company
P.O. Box 1600
Richland, Washington 99352

APPROVED
By Julia Raymer at 1:00 pm, Apr 27, 2020

Release Approval Date

Approved for Public Release;
Further Dissemination Unlimited

TRADEMARK DISCLAIMER

Reference herein to any specific commercial product, process, or service by tradename, trademark, manufacturer, or otherwise, does not necessarily constitute or imply its endorsement, recommendation, or favoring by the United States Government or any agency thereof or its contractors or subcontractors.

This report has been reproduced from the best available copy.

Printed in the United States of America

ENVIRONMENTAL CALCULATION COVER PAGE

SECTION 1 - Completed by the Responsible Manager

Project:
300-FF-5 Uranium Sequestration

Date: 04/06/2020

Calculation Title and Description:
Geochemical Evaluations and Reactive Transport Modeling in Support of Stage B Enhanced Attenuation Remedy at 300-FF-5-Operable Unit

RELEASE / ISSUE

DATE:
Apr 27, 2020
HANFORD RELEASE

Qualifications Summary

Preparer(s):

Name: Ryan Nell

Degree, Major, Institution, Year: PhD, Environmental Chemistry, University of Notre Dame, 2016
BA, Geology, University of Colorado, 2010

Professional Licenses:

Brief Narrative of Experience: Ryan Nell brings applied and theoretical laboratory experience in geochemistry and environmental science, and research expertise in designing and executing experiments pertaining to heavy metal remediation using biotic systems. His experience includes collecting and analyzing data to evaluate metal fate and transformation in microbial ecosystems, developing standard operating procedures for fluorescent microscopy imaging of manganese oxidizing fungi, and preparing biological samples for x-ray adsorption spectroscopy analysis. He also led field data collection and analysis of dioritic rock samples for U-Th/He analysis. Ryan has presented the results of his work at conferences and authored several publications in peer-reviewed journals, including Geochimica et Cosmochimica Acta and Chemical Geology.

ENVIRONMENTAL CALCULATION COVER PAGE (Continued)

Checker(s):

Name: Randy Arthur

Degree, Major, Institution, Year: PhD, Geochemistry and Mineralogy, The Pennsylvania State University, 1983
BS, Geology, San Diego State University, 1975

Professional Licenses:

Brief Narrative of Experience: Randolph "Randy" Arthur's experience encompasses field, laboratory, and geochemical modeling gained from projects ranging from the commercial development of mineral and water resources to the final disposal of radioactive materials in geologic repositories. His primary area of expertise is focused on the use of geochemical thermodynamics to develop conceptual and numerical models of fluid-rock interactions. He has applied this expertise to various mining related projects, including the planning and execution of exploration campaigns for uranium and gold deposits, experimental investigations of the recovery of base and precious metals from geothermal brines, due diligence assessments of proposed potash mining operations, and evaluations of engineered systems for the mitigation of contaminant transport from mill tailings and waste rock. Randy also has experience in the characterization of groundwater resources based on critical evaluations of the analytical quality and representativeness of hydrochemical and isotopic data collected in borehole investigations, and the application of empirical, geostatistical, and geochemical modeling tools to identify equilibrium and kinetic constraints on water chemistry. Technical investigations supporting these projects have included the construction of internally consistent thermodynamic databases for geochemical and geo-engineered (e.g., clay-based and cementitious) systems, and the development of reactive-transport models of waste form dissolution. He has authored or co-authored more than 60 peer-reviewed journal articles, book chapters, and technical reports.

ENVIRONMENTAL CALCULATION COVER PAGE (Continued)

Senior Reviewer(s):

Name: Sunil Mehta

Degree, Major, Institution, Year: PhD, Geology (Hydrogeology Emphasis), University of Kentucky, 2000
MS, Geology, University of Louisiana, 1996
MS, Geology, University of Poona, India, 1990
BS, Chemistry, Zoology, and Geology, University of Jodhpur, India, 1988

Professional Licenses:

Brief Narrative of Experience: Sunil Mehta's professional experience as a hydrogeologist has been focused on flow and transport modeling under variably saturated conditions, reactive transport modeling, performance assessment, and uncertainty analysis. He has gained this experience on projects involving deep geologic isolation of high-level radioactive wastes, shallow disposal of low-level radioactive waste, and environmental restoration activities in accordance with local and federal regulations. Sunil's experience includes designing, developing, and applying numerical models to evaluate the performance of radioactive waste storage and disposal facilities. His work has encompassed developing flow and reactive transport models for transuranics, conducting process and component modeling (e.g., unsaturated and saturated zone flow, colloid facilitated transport, waste form degradation) and combining these models into a comprehensive probabilistic assessment tool used to forecast post-closure performance of a storage facility. In the area of environmental restoration, he has performed hydrogeological studies and groundwater flow and contaminant transport modeling to support the design of remedial systems to sequester and capture contaminants such as uranium and hexavalent chromium in periodically rewetted zones influenced by aquifer-river interactions. In addition, Sunil's water resources experience includes evaluating aquifer resource potential for agricultural needs through the interpretation of geophysical logs and analysis of pumping test data, and using remote sensing techniques to support groundwater exploration.

SECTION 2 - Completed by Preparer

Calculation Number: ECF-300FF5-19-0089 | Revision Number: 0

Revision History

Revision No.	Description	Date	Affected Pages
0	Initial issue		All

SECTION 3 - Completed by the Responsible Manager

Document Control:

Is the document intended to be controlled within the Document Management Control System (DMCS)? ◉ Yes ○ No

Does document contain scientific and technical information intended for public use? ◉ Yes ○ No

Does document contain controlled-use information? ○ Yes ◉ No

ENVIRONMENTAL CALCULATION COVER PAGE (Continued)

SECTION 4 - Document Review and Approval

Preparer(s):

Print First and Last Name	Position	Signature	Date
Ryan Nell	Hydrogeologist	Approved Via Attached	06/17/2020

Checker(s):

Print First and Last Name	Position	Signature	Date
Randy Arthur	Pr. Geochemist	Approved Via Attached	06/17/2020

Senior Reviewer(s):

Print First and Last Name	Position	Signature	Date
Sunil Mehta	Pr. Hydrogeologist	Approved Via Attached	06/17/2020

Responsible Manager(s):

Print First and Last Name	Position	Signature	Date
Alaa Aly	Risk & Model Integr Mgr	Approved Via Attached	06/17/2020

SECTION 5 - Applicable if Calculation is a Risk Assessment or Uses an Environmental Model

Prior to Initiating Modeling:

Required training for modelers completed:
Integration Lead:

Print First and Last Name	Signature	Date
William Nichols	Approved Via Attached 06/17/2020	07/11/2019

Safety Software Approved:
Integration Lead:

Print First and Last Name	Signature	Date
William Nichols	Approved Via Attached 06/17/2020	07/11/2019

Calculation Approved:
Risk/Modeling Integration Manager:

Print First and Last Name	Signature	Date
Alaa Aly	Approved Via Attached	06/17/2020

From: PRC SharePoint
To: Dodge, Bonnie J
Cc: Dodge, Bonnie J
Subject: Electronic Approval has completed for document: ECF-300FF5-19-0089-00.
Date: Wednesday, June 17, 2020 9:43:07 AM

Electronic Approval has completed for document: ECF-300FF5-19-0089-00.

Please include this email as the Electronic Approval page.

Electronic Approval for document: ECF-300FF5-19-0089-00 has successfully COMPLETED.

Electronic Approval started by Dodge, Bonnie J on 6/17/2020 5:50 AM
Comment: CHPRC does not recognize digital signatures, please reapprove. Thank you.

Approved by Nichols, William E on 6/17/2020 6:38 AM
Comment:

Approved by Nell, Ryan M on 6/17/2020 8:48 AM
Comment:

Approved by Mehta, Sunil on 6/17/2020 9:19 AM
Comment:

Approved by Aly, Alaa H on 6/17/2020 9:42 AM
Comment:

From: Randy Arthur
To: Dodge, Bonnie J
Cc: Ryan Nell
Subject: RE: Approval: ECF-300FF5-19-0089_R0
Date: Wednesday, June 17, 2020 11:46:59 AM
Attachments: image001.png

No, I don't see them, but approved.

Thanks.

From: Dodge, Bonnie J <bonnie_j_dodge@rl.gov>
Sent: Wednesday, June 17, 2020 12:39 PM
To: Randy Arthur <rarthur@intera.com>
Subject: RE: Approval: ECF-300FF5-19-0089_R0

Upper left corner. If you don't see them, you can reply approved.

Thank you.

Bonnie Dodge
Remedy Selection and Implementation
Records Specialist
Document Processing
Operating Record
Administrative Record

D 509-373-4284/M 509-713-0053 bonnie_j_dodge@rl.gov

The contents of this message may be personal and do not reflect the views or position of the U.S. Department of Energy or the Federal Government.

From: Randy Arthur <rarthur@intera.com>
Sent: Wednesday, June 17, 2020 11:09 AM
To: Dodge, Bonnie J <bonnie_j_dodge@rl.gov>
Subject: RE: Approval: ECF-300FF5-19-0089_R0

Sorry Bonnie…where are the "voting buttons"?

From: Dodge, Bonnie J <bonnie_j_dodge@rl.gov>

Sent: Wednesday, June 17, 2020 11:55 AM
To: Randy Arthur <rarthur@intera.com>
Cc: Nell, Ryan M <ryan_m_nell@rl.gov>
Subject: Approval: ECF-300FF5-19-0089_R0

Randy,

CHPRC does not recognize digital signatures, please use the voting buttons in the upper left corner to approve and I will finalize the document. I have received all other approvals.

Thank you.

Bonnie Dodge
Remedy Selection and Implementation
Records Specialist
Document Processing
Operating Record
Administrative Record

D 509-373-4284/M 509-713-0053 bonnie_j_dodge@rl.gov

The contents of this message may be personal and do not reflect the views or position of the U.S. Department of Energy or the Federal Government.

Contents

1 Purpose 1-1

2 Background 2-1

3 Methodology 3-1

4 Assumptions 4-1

4.1 Observations and Conceptual Model Development 4-1

4.1.1 300 Area Geologic Framework 4-1

4.1.2 300 Area Groundwater Flow System 4-1

4.1.3 Stage B EAA Polyphospate Injection 4-3

4.1.4 Electrical Resistivity Tomography 4-5

4.1.5 Comparison of Pre- and Post-Treatment Samples 4-26

4.2 Three-Dimensional Reactive Transport Modeling 4-38

4.2.1 Bulk Uranium Kinetic Rate Model Description 4-40

5 Software Applications 5-1

5.1 Approved Software 5-2

5.1.1 Description 5-2

5.1.2 Software Installation and Checkout 5-2

5.1.3 Statement of Valid Software Application 5-2

6 Calculation 6-1

6.1 One-Dimensional Column Leaching Simulations 6-1

6.2 Three-Dimensional Remedy Injection Modeling 6-5

6.2.1 Model Domain 6-5

6.2.2 Fate and Transport Parameters 6-6

6.2.3 Boundary Conditions 6-8

6.2.4 Development of PHREEQC Reactive Transport Parameters 6-11

6.2.5 Chemistry Domain Assignment 6-18

6.2.6 Sensitivity Analysis 6-20

6.3 Supplemental Thermodynamic Geochemical Assessment 6-25

7 Results 7-1

7.1 One-Dimensional Column Leaching Simulation Results 7-1

7.2 Three-Dimensional Remedy Injection Model Results 7-5

7.2.1 Remedy Injection Flow Field 7-5

7.2.2 Geochemical Evolution 7-7

7.2.3 Sensitivity Analysis 7-24

8 Conclusions 8-1

9 References 9-1

Appendices

A. Monitoring Data for Stage B EAA Extended Well Network ..... A-i
B. Additional Evaluations ..... B-i
C. One-Dimensional Column Leaching Simulation PHREEQC Input Files ..... C-i
D. Remedy Injection Modeling PHREEQC Input File ..... D-i
E. Software Installation and Checkout Forms E-1

Figures

Figure 1-1. 300 Area Industrial Complex and the Stage A and Stage B Enhanced Attenuation Areas 1-3
Figure 4-1. View of the 300 Area Geoframework Model 4-1
Figure 4-2. 300 Area Process Trenches Water Table, February 2018 4-2
Figure 4-3. Injection Well Locations for Stage B EAA 4-4
Figure 4-4. Average Daily Measured pH of the Injection Solution for a) Skid 1, and b) Skid 2 4-5
Figure 4-5. ERT Cluster Locations in Stage B EA Area 4-6
Figure 4-6. Distances between ERT Instruments and Nodes from PNNL-28619 4-7
Figure 4-7. Pre-treatment Baseline ERT Images in the A-A' Plane for Each Cluster (Top) and the Corresponding Geologic Structure Interpretations (Bottom) 4-8
Figure 4-8. Maximum Change in Bulk Conductivity during Remedy Injections for Each ERT Cluster Monitoring Results for Stage B EAA Treatment 4-9
Figure 4-9. Comparison of Uranium to Phosphate for Wells 399-1-72 and 399-1-73 4-11
Figure 4-10. Comparison of Uranium to Phosphate for Wells 399-1-159 and 399-1-152 4-12
Figure 4-11. Comparison of Uranium to Phosphate for Wells 399-1-17A and 399-1-164 4-13
Figure 4-12. Comparison of Phosphate to Bicarbonate Ratio to pH for Wells 399-1-72 and 399-1-73 4-14
Figure 4-13. Comparison of Phosphate to Bicarbonate Ratio to pH for Wells 399-1-159 and 399-1-152 4-15
Figure 4-14. Comparison of Phosphate to Bicarbonate Ratio to pH for Wells 399-1-17A and 399-1-164 4-16
Figure 4-15. Comparison of Uranium to Calcium for Wells 399-1-72 and 399-1-73 4-17
Figure 4-16. Comparison of Uranium to Calcium for Wells 399-1-159 and 399-1-152 4-18
Figure 4-17. Comparison of Uranium to Calcium for Wells 399-1-17A and 399-1-164 4-19
Figure 4-18. Comparison of Phosphate to Calcium for Wells 399-1-72 and 399-1-73 4-20
Figure 4-19. Comparison of Phosphate to Calcium for Wells 399-1-159 and 399-1-152 4-21

Figure 4-20. Comparison of Phosphate to Calcium for Wells 399-1-17A and 399-1-164 4-22
Figure 4-21. Comparison of Calcium to Sodium Ratio to pH for Wells 399-1-72 and 399-1-73 4-23
Figure 4-22. Comparison of Calcium to Sodium Ratio to pH for Wells 399-1-159 and 399-1-152 4-24
Figure 4-23. Comparison of Calcium to Sodium Ratio to pH for Wells 399-1-17A and 399-1-164 4-25
Figure 4-24. Stage B EAA Post-Injection Borehole Location Map 4-26
Figure 4-25. Uranium and Phosphorus Soil Concentration with Depth for C9646/C9731, C9647/C9733, and C9667/C9729 Borehole Pairs 4-28
Figure 4-26. Uranium and Phosphorus Soil Concentration with Depth for C9673/C9728, C9677/C9730, and C9683/C9732 Borehole Pairs 4-29
Figure 4-27. Uranium and Phosphorus Soil Concentration with Depth for C9734, C9735, and C9736 Post-Treatment Boreholes 4-30
Figure 4-28. Average Change of the Uranium Fraction in 19 Pre- and Post-Treatment Pairs Based on Sequential Extractions 4-32
Figure 4-29. Change in Uranium Sequential Extractions among 19 Pairs of Sediment Samples, in terms of a) Uranium Concentration (μg/g), and (b) Fraction of Total Uranium 4-33
Figure 4-30. a) Iron Concentration, and b) Calcium Concentration in Pre-treatment Sample Sequential Extraction Results 4-33
Figure 4-31. Effluent Uranium Concentration and Cumulative Fraction Uranium Removed Column Leaching Experiment Results for a) C9683/C9732 22.5-25 ft Interval, b) C9673/C9728 27.5-30 ft Interval, and c) C9673/C9728 30-32.5 ft Interval Sample Pairs 4-35
Figure 4-32. Change in Uranium Mass Leaching among Pre- and Post-Treatment Sample in 1-D Column Experiments: (a) Linear Scale, and (b) Log Scale 4-36
Figure 4-33. Effluent pH as a Function of Pore Volumes for Select Pre-treatment and Post-Treatment 1-D Column Leaching Experiments 4-36
Figure 4-34. Change in Uranium Mobility as Shown in 1000-hr Carbonate Extractions on 10 Pre- and Post-Treatment Pairs of Sediments 4-37
Figure 4-35. Uranium Sequestration Mechanisms via Phosphate Addition as an In-Situ Remediation Approach 4-38
Figure 4-36. Uranium Conceptual Model Implementation 4-40
Figure 4-37. Numerical Modeling Results For 1-D Column Leaching Kinetic Rate Parameter Estimation for a) Forward and Reverse Rate Constants, and b) Kd Estimates 4-42
Figure 6-1. The One-Dimensional Column Leaching Simulation Domain 6-2
Figure 6-2. The VS2DRTI Remedy Injection Model Domain 6-6
Figure 6-3. Distribution of Hydrogeologic Units 6-7
Figure 6-4. Boundary Conditions for a) Initial Conditions and Non-Injection, b) PRZ Injection, and c) LVZ Injection Periods 6-10
Figure 6-5. Initial Pressure Head STOMP Abstraction 6-11
Figure 6-6. Schoeller Diagram of Injected Remedy and Porewater Solutions 6-16
Figure 6-7. Distribution of Chemistry Classes 6-19
Figure 6-8. Two-Dimensional Remedy Injection Groundwater Model Domain 6-22
Figure 6-9. Distribution of Hydrogeologic Units in the 3-D Heterogeneous Remedy Injection Model 6-24

Figure 7-1. Bromide Result History Comparison for a) Pretreatment Sample G21, and b) Post-Treatment Sample G113 7-2

Figure 7-2. Uranium Result History Comparison for a) Pretreatment Sample G21, and b) Post-Treatment Sample G113 7-3

Figure 7-3. Uranium Kinetic Release Parameter Comparison between a) Pretreatment, and b) Post-Treatment Simulations 7-4

Figure 7-4. 3-D Remedy Injection Model Aqueous Saturation Profiles a) Before Injections, b) After the First PRZ, c) Second PRZ, d) First LVZ, and e) Second LVZ Injection Periods 7-6

Figure 7-5. Observation Node Locations Used for Timeseries Plots 7-7

Figure 7-6. 3-D Remedy Injection Model Geochemical Evolution Timeseries Plots for a) 0.5 m Distance from LVZ Injection Screen, and b) 0.5 m Distance from PRZ Injection Screen with Injection Periods Indicated by Black Bars 7-9

Figure 7-7. 3-D Remedy Injection Model Geochemical Evolution Timeseries Plots for Phosphorus Species 0.5 m Distance from PRZ Injection Screen with Injection Periods Indicated by Black Bars 7-10

Figure 7-8. 3-D Remedy Injection Model Cation Exchange Site Timeseries Plots for a) 0.5 m Distance from LVZ Injection Screen, and b) 0.5 m Distance from PRZ Injection Screen with Injection Periods Indicated by Black Bars 7-11

Figure 7-9. 3-D Remedy Injection Model Mineral Timeseries Plots for a) 0.5 m Distance from LVZ Injection Screen, and b) 0.5 m Distance from PRZ Injection Screen with Injection Periods Indicated by Black Bars 7-12

Figure 7-10. 3-D Remedy Injection Model log Molar Ratio HPO4/HCO3 and pH Timeseries Plots (Left) for 0.5 m Distance from a) LVZ Injection Screen, and c) PRZ Injection Screen with Injection Periods Indicated by Black Bars and Phase Diagrams (Right) b) with Uranium, and d) without Uranium 7-14

Figure 7-11. Comparison of Remaining Amount of Generic Uranium-Bearing Solid per kg Water between Simulated 3-D Remedy Injection Model and No Action Case (NAC) 7-15

Figure 7-12. 3-D Remedy Injection Model HPO_4^{2-} Profile a) Before Injections, b) After the First PRZ, c) Second PRZ, d) First LVZ, and e) Second LVZ Injection Periods 7-17

Figure 7-13. 3-D Remedy Injection Model Generalized Uranium-Bearing Solid Profile a) Before Injections, b) After the First PRZ, c) Second PRZ, d) First LVZ, and e) Second LVZ Injection Periods 7-18

Figure 7-14. 3-D Remedy Injection Model Total Aqueous Uranium Profile a) Before Injections, b) After the First PRZ, c) Second PRZ, d) First LVZ, and e) Second LVZ Injection Periods 7-19

Figure 7-15. 3-D Remedy Injection Model Calcite Profile a) Before Injections, b) After the First PRZ, c) Second PRZ, d) First LVZ, and e) Second LVZ Injection Periods 7-20

Figure 7-16. 3-D Remedy Injection Model pH Profile a) Before Injections, b) After the First PRZ, c) Second PRZ, d) First LVZ, and e) Second LVZ Injection Periods 7-21

Figure 7-17. 3-D Remedy Injection Model Hydroxylapatite Profile a) Before Injections, b) After the First PRZ, c) Second PRZ, d) First LVZ, and e) Second LVZ Injection Periods 7-22

Figure 7-18. 3-D Remedy Injection Model Andersonite Profile a) Before Injections, b) After the First PRZ, c) Second PRZ, d) First LVZ, and e) Second LVZ Injection Periods 7-23

Figure 7-19. Model Component Sensitivity Case Geochemical Timeseries Plots for a) Case 1, b) Case 2, and c) Case 3 from PRZ Injection Screen with Injection Periods Indicated by Black Bars 7-25
Figure 7-20. Model Component Sensitivity Case Saturation Index Timeseries Plots for a) Case 1, b) Case 2, and c) Case 3 from PRZ Injection Screen with Injection Periods Indicated by Black Bars 7-26
Figure 7-21. Horizontal Groundwater Velocity in 2-D Remedy Injection Groundwater Model 7-27
Figure 7-22. 2-D Remedy Injection Groundwater Flow Model Geochemical Evolution Timeseries Plots for 10 m Distance Downgradient from PRZ Injection Screen with Injection Periods Indicated by Black Bars 7-28
Figure 7-23. 2-D Remedy Injection Groundwater Flow Model Phosphate to Bicarbonate Indicator Timeseries Plots for 10 m Distance Downgradient from PRZ Injection Screen with Injection Periods Indicated by Black Bars 7-29
Figure 7-24. 2-D Remedy Injection Groundwater Flow Model Calcium to Sodium Ratio Indicator Timeseries Plots for 10 m Distance Downgradient from PRZ Injection Screen with Injection Periods Indicated by Black Bars 7-30
Figure 7-25. 2-D Groundwater Model Uranium Profile a) Before Injections, b) After the First PRZ Injection, c) After the Second PRZ Injection, d) 4 Days, and e) 10 Days 7-31
Figure 7-26. 3-D Heterogeneous Remedy Injection Model Aqueous Saturation Profiles a) Before Injections, b) After the First PRZ, c) Second PRZ, d) First LVZ, and e) Second LVZ Injection Periods 7-33
Figure 7-27. Maximum Change in Bulk Electrical Conductivity (Left) and Change in Aqueous Saturation between Days 0 and 4 for the 3-D Heterogeneous Remedy Injection Model (Right) 7-34
Figure 7-28. Comparison of Geochemical Evolution Timeseries Plots for Base Case 3-D Remedy Injection Model (Left) and 3-D Heterogeneous Remedy Injection Model (Right) with Injection Periods Indicated by Black Bars 7-35
Figure 7-29. Comparison of Mineral Timeseries Plots for Base Case 3-D Remedy Injection Model (Left) and 3-D Heterogeneous Remedy Injection Model (Right) with Injection Periods Indicated by Black Bars 7-36
Figure 7-30. 3-D Heterogeneous Remedy Injection Model Hydroxylapatite Profiles a) Before Injections, b) After the First PRZ, c) Second PRZ, d) First LVZ, and e) Second LVZ Injection Periods 7-37
Figure 7-31. 3-D Heterogeneous Remedy Injection Model Andersonite Profiles a) Before Injections, b) After the First PRZ, c) Second PRZ, d) First LVZ, and e) Second LVZ Injection Periods 7-38

Tables

Table 6-1. One-Dimensional Column Leaching Simulation Solver Options 6-1
Table 6-2. One-Dimensional Column Leaching Simulation Chemistry Class Assignment [a] 6-2
Table 6-3. One-Dimensional Column Leaching Simulation Recharge Periods 6-3
Table 6-4. 1-D Column Leaching Flow Parameters 6-3
Table 6-5. Kinetic Desorption Rate Parameters 6-4
Table 6-6. Kinetic Desorption Rate Parameter Comparison 6-5

Table 6-7. Three-Dimensional Remedy Injection Model Solver Options 6-5
Table 6-8. 3-D Remedy Injection Model Textural Class Hydraulic Properties 6-7
Table 6-9. 3-D Remedy Injection Model Textural Class Solute Transport Properties 6-7
Table 6-10. Three-Dimensional Remedy Injection Model Recharge Periods 6-8
Table 6-11. Aqueous Uranium and Phosphate Species.....6-12
Table 6-12. Uranium Mineral Phases.....6-13
Table 6-13. Surface Complexation Site Reactions.....6-14
Table 6-14. Solution Card Chemistries 6-15
Table 6-15. Mineral Kinetic Parameters 6-18
Table 6-16. Three-Dimensional Remedy Injection Base Case Model Chemistry Classes [a] 6-19
Table 6-17. PHREEQC Input File Modifications 6-20
Table 6-18. Sensitivity Cases 1 and 2 Chemistry Classes [a] 6-21
Table 6-19. Two-Dimensional Groundwater Model Solver Options.....6-21
Table 6-20. Two-Dimensional Remedy Injection Groundwater Model Recharge Periods 6-23
Table 6-21. 3-D Heterogeneous Remedy Injection Model Textural Class Flow Properties.....6-24
Table 6-22. 3-D Heterogeneous Remedy Injection Model Textural Class Solute Properties.....6-25
Table 6-23. Act2 Inputs.....6-25

Terms

1-D	one-dimensional
2-D	two-dimensional
3-D	three-dimensional
µ-EXAFS	micro extended X-ray absorption fine structure
µ-XANES	micro X-ray absorption near-edge spectroscopy
µ-XRF	micro X-ray fluorescence
ANOVA	analysis of variance
APS	Advanced Photon Source
CHPRC	CH2M HILL Plateau Remediation Company
COC	contaminant of concern
DOE	Department of Energy
EA	Enhanced Attenuation
EAA	enhanced attenuation area
ECF	environmental calculation file
EHM	equivalent homogenous medium
EPA	Environmental Protection Agency
ERT	Electrical Resistivity Tomography
gpm	gallons per minute
GWB	Geochemist's Workbench
Hf	Hanford formation
HSU	hydrostratigraphic unit
LVZ	lower vadose zone
OU	Operable Unit
NAC	no action case
NPP	North Process Pond
PNNL	Pacific Northwest National Lab
PRZ	periodically rewetted zone
Rlm	Ringold Formation member of Wooded Island lower mud unit

ROD	record of decision
Rwie	Ringold Formation member of the Wooded Island unit E
SAP	sampling analysis plan
SEM	Scanning electron microscopy
STOMP	Subsurface Transport Over Multiple Phases
USGS	United States Geological Survey

1 Purpose

Completion of the 300 Area cleanup on the Hanford Site will be accomplished under the 2013 U.S. Environmental Protection Agency (EPA) and U.S. Department of Energy (DOE) record of decision (ROD) and amendment (EPA and DOE, 2013, *Hanford Site 300 Area Record of Decision for 300-FF-2 and 300-FF-5, and Record of Decision Amendment for 300-FF-1* [hereinafter referred to as the 300 Area ROD/ROD Amendment]), which identifies uranium as a contaminant of concern (COC) in both soil and groundwater. Enhanced attenuation (EA) was chosen as part of the remedy for uranium contamination in the periodically rewetted zone (PRZ) and top of aquifer over a 12,140 m^2 (3 ac) area using polyphosphate solutions. The intent of the remedy is to deliver high concentration polyphosphate solution to the vadose zone and top of the aquifer where uranium is present and bind, or sequester, labile uranium via multiple mechanisms including: sorption of aqueous uranium to calcium phosphate solids (e.g., hydroxylapatite), formation of uranium bearing minerals, formation of secondary mineral coatings reducing uranium mobility, and uranium incorporation (by either co-precipitation or structural substitution of uranium for calcium) in calcium phosphate solids (Mehta et al., 2016, "Effect of reaction pathway on the extent and mechanism of uranium(VI) immobilization with calcium and phosphate").

The EA remedy was implemented in two sequential stages (Stage A and Stage B shown in Figure 1-1) covering 3,035 m^2 (0.75 ac) and 9,105 m^2 (2.25 ac), respectively. Stage A was implemented during November 2015 by injecting polyphosphate solution in the deeper portion of the vadose zone and at the top of the aquifer along with near-surface infiltration (SGW-59455, *300-FF-5 Operable Unit Stage A Uranium Sequestration System Installation Report)*. Review of the Stage A remedy resulted in operational refinements, and in September 2018 (from September 4 to 20) Stage B was conducted by injecting polyphosphate solutions into the vadose zone at two target depths—the deeper portion that gets periodically rewetted from seasonal water table fluctuations and the lower vadose zone (LVZ), the portion that is just above the PRZ (SGW-60778, *300-FF-5 Operable Unit Stage B Uranium Sequestration System Installation Report*).

This report uses a geochemical modeling approach to evaluate the fate of uranium in the vadose zone and aquifer in the vicinity of the Stage B EA area during and after remedy implementation. Data collected during geochemical evaluations of pre-treatment and post-treatment soil samples, sequential extraction tests, batch desorption and flow-through column tests, mineral phase analysis, and observations made in groundwater uranium and phosphate concentrations are all used to develop parameters and conceptual models for the reactive transport modeling.

The purpose of this environmental calculation file (ECF) is to:

1. Synthesize relevant information for conducting reactive transport modeling. This involves evaluating groundwater sampling data, results of electrical resistivity tomography (ERT), and soil characterization data prior to and following polyphosphate injection.

2. Develop conceptual models of potential geochemical processes occurring during and following injection.

3. Develop parameter estimates for conducting reactive transport modeling. Parameter estimates are based on evaluation of sequential extraction tests, batch desorption and flow-through column tests, mineral phase analysis, and observations made in the aquifer. Bulk kinetic sorption-desorption parameters are estimated from the flow-through column tests and their adequacy in implementation is judged by comparing the simulated one-dimensional (1-D) model results to the flow-through column experimental data.

4. Conduct detailed reactive transport modeling to evaluate the geochemical changes from injecting concentrated polyphosphate solutions in the subsurface on uranium sequestration. Fate and transport modeling was performed by using VS2DRTI software (Healy et al., 2018, "VS2DRTI: Simulating Heat and Reactive Solute Transport in Variably Saturated Porous Media") to simulate injection at one representative well location under variably saturated conditions. The flow and transport model was coupled with the geochemical model for performing reactive transport in a three-dimensional (3-D) radial coordinate system at each time step within the model domain. The model incorporates the entire thickness of the vadose zone and a significant portion of the saturated zone.

5. Perform sensitivity cases in order to evaluate: 1) model components (e.g., kinetic release, precipitation of calcium-phosphate minerals, and surface complexation) effectiveness on representing monitoring data observations; 2) the fate of uranium and its transport within the highly conductive saturated zone by developing a two-dimensional (2-D) cross-section model in cartesian coordinates; and 3) the effect of lithologic heterogeneity on uranium transport within the vadose zone, a 3-D vadose zone heterogeneous model is developed in radial coordinates based on ERT time-lapse imaging.

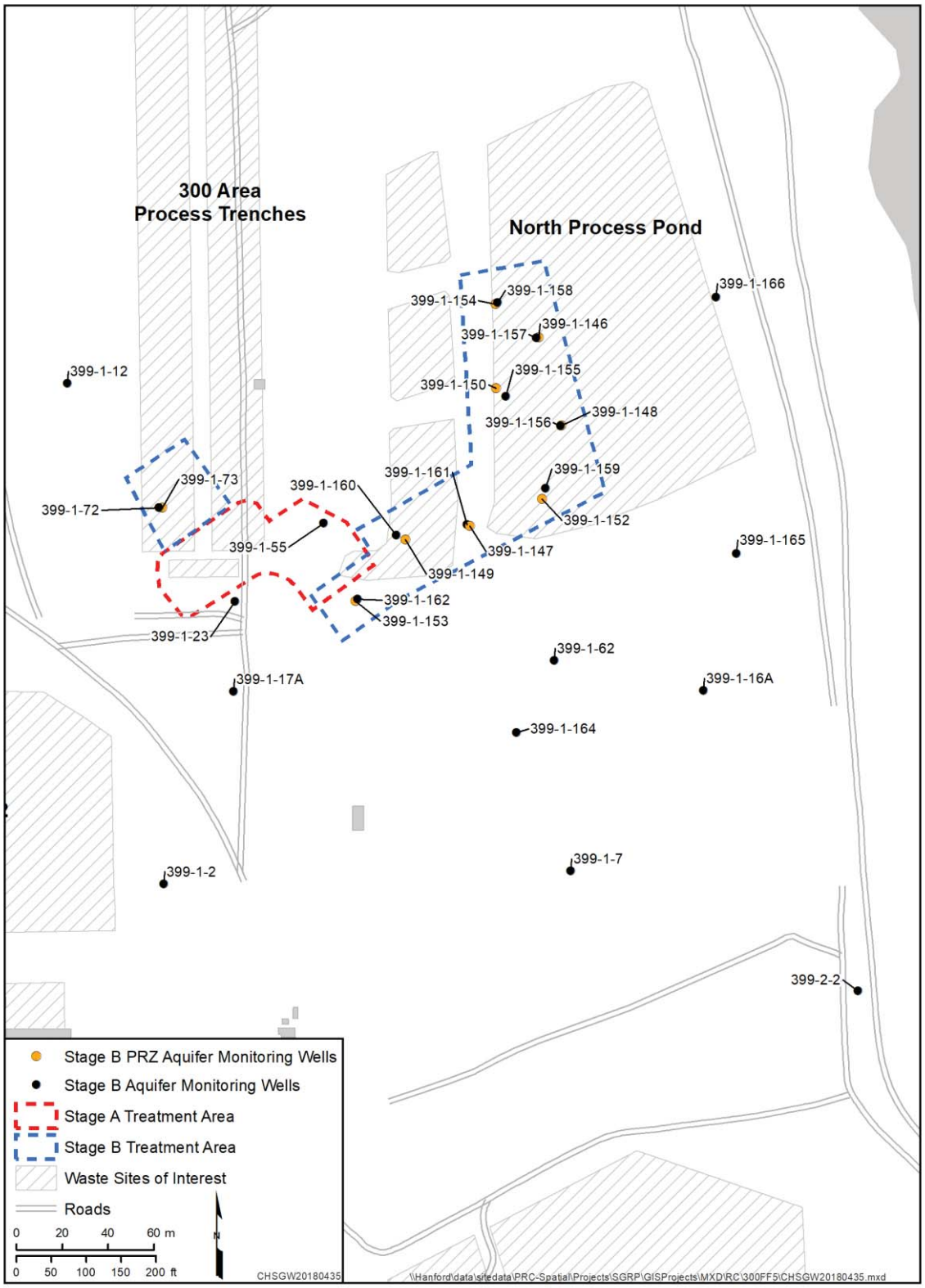

Figure 1-1. 300 Area Industrial Complex and the Stage A and Stage B Enhanced Attenuation Areas

This page intentionally left blank.

2 Background

The 300 Area encompasses approximately 105 km^2 (40 mi^2) in the southeastern portion of Hanford Site adjacent to the Columbia River. Within the 300 Area, the smaller 300 Area Industrial Complex was home to uranium fuel production as well as experimental and laboratory facilities which generated solid waste that was placed in burial grounds and shallow landfills and liquid waste discharged to ponds and trenches designed for infiltration into the vadose zone. An outcome of these activities was soil and groundwater uranium contamination. Though most of the 300 Area Industrial Complex waste sites have been remediated, persistent uranium groundwater plumes exist.

The sampling and analysis plan (SAP) (DOE/RL-2014-42, *300-FF-5 Operable Unit Remedy Implementation Sampling and Analysis Plan*) presents plans for the 300-FF-5 Groundwater Operable Unit (OU) remedy implementations, performance monitoring, and groundwater monitoring. The uranium sequestration remedy was planned as two stages (Stage A and Stage B) per DOE/RL-2014-13-ADD2, *Remedial Design Report/Remedial Action Work Plan Addendum for the 300 Area Groundwater*. Stage A consisted of polyphosphate injection into the vadose zone and surface infiltration and completed in November of 2015 with flow and transport modeling documented in ECF-300FF5-16-0091, *Uranium Transport Modeling in Support of the Stage A Enhanced Attenuation Remedy at 300-FF-5 Operable Unit*. Stage B was implemented as polyphosphate injections into the LVZ and PRZ near the top of aquifer from September 4 through 20, 2018, with an extended monitoring network sampled for 6 to 12 months after injections (Figure 1-1). Treatment effectiveness will also be evaluated based on Stage B implementation, such as phosphate distribution efficiency, the degree of uranium mobilization to groundwater, and changes to hydraulic conductivity of the aquifer due to precipitation of phosphate minerals.

The report is structured in the following manner:

- Section 3 discusses the method used for evaluating geochemical data to develop parameters for the reactive transport model
- Section 4 provides a discussion of key observations from monitoring and subsequent conceptual model development
- Section 5 describes the software used
- Section 6 summarizes the modeling approach calculation
- Section 7 discusses the results of the various model simulations
- Section 8 summarizes the conclusions
- Appendix A provides supplemental extended monitoring network groundwater geochemical indicator data
- Appendix B discusses additional statistical and geochemical data evaluations
- Appendix C includes the PHREEQC inputs for one-dimensional leaching simulations
- Appendix D includes the PHREEQC input for remedy injection modeling
- Appendix E provides software installation and checkout forms

This page intentionally left blank.

3 Methodology

The following steps were used to simulate post-treatment geochemical evolution near the injection zone:

1. Obtain detailed information on the operational parameters and outcomes of the injections conducted in the Stage B enhanced attenuation area (EAA).
    a. Evaluate chemical composition of the injection solution.
    b. Evaluate injection rates and durations during operations.
2. Evaluate data from 21 groundwater monitoring wells used in Stage B EAA.
    a. Evaluate uranium and phosphate concentrations before, during, and after treatment in the groundwater monitoring network surrounding the Stage B EAA.
    b. Evaluate geochemical indicators before, during, and after treatment in the groundwater monitoring wells.
3. Assess data from six pretreatment and nine post-treatment soil characterization boreholes.
    a. Compare depth discrete uranium and phosphate sediment concentrations.
    b. Compare sequential extraction data between pre-treatment and post-treatment samples.
    c. Compare leaching behavior of contaminants from sediments before and after treatment.
    d. Review batch leach tests and mineral phase analyses.
4. Develop a conceptual model of possible geochemical reactions that occurred within the host rock as a result of treatment that led to sequestration of uranium. Build detailed reactive transport input files.
5. Simulate reactive transport model in the vadose zone and unconfined groundwater aquifer to evaluate the geochemical evolution of near field reactions present at the Stage B EAA injection zones. Longer term performance evaluation is conducted using Subsurface Transport Over Multiple Phases (STOMP; ECF-300FF5-19-0086, *STOMP Modeling in Support of Stage B Sequestration of Uranium at 300-FF-5 Operable Unit*)
6. Conduct conceptual model sensitivity by evaluation of model components, uranium transport via 2-D groundwater flow, and 3-D heterogeneity in the unsaturated zone.

This page intentionally left blank.

4 Assumptions

Details on conceptual model assumptions related to reactive transport modeling are discussed in this section. Conceptual model development is discussed in Section 4.1, while 3-D reactive transport modeling is described in Section 4.2.

4.1 Observations and Conceptual Model Development

4.1.1 300 Area Geologic Framework

Leapfrog® Geo (version 3.0.0) was used to develop a 3-D solid geologic framework model within the 300 Area (Figure 4-1) (ECF-300FF5-16-0087, *Determination of Vadose Zone Uranium Concentration Distribution Extents and Development of a Three-Dimensional Geologic Framework Model for the 300-FF-5 Operable Unit, Hanford, Washington*). Beneath the 300 Area, the Hanford formation (Hf) is comprised of unconsolidated sandy gravels containing variable amounts of silts and clays. Hf sediments are underlain by more consolidated materials of the Ringold Formation member of the Wooded Island unit E (Rwie) (WHC-EP-0500, *Geology and Hydrology of the 300 Area and Vicinity, Hanford Site, South-Central Washington*). Underlying Rwie is the Ringold Formation member of Wooded Island lower mud unit (Rlm), consisting of predominantly silts and clays, and the top of the Columbia River Basalt Group is the bedrock defining the base of the model.

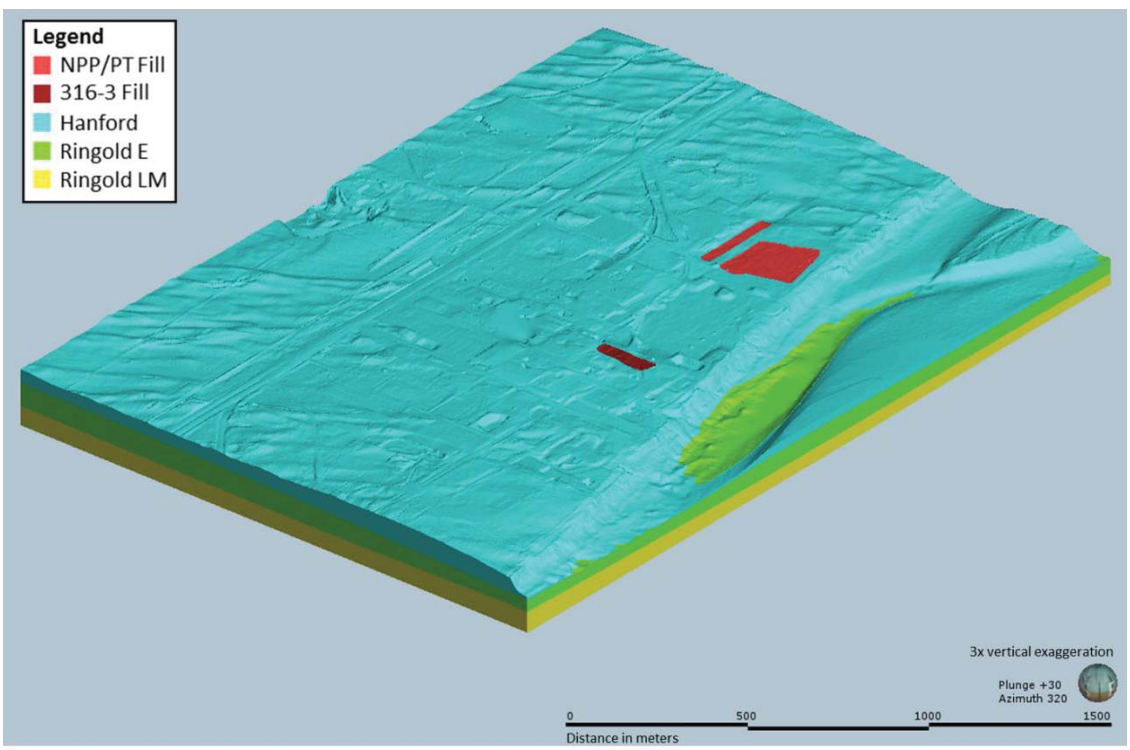

Figure 4-1. View of the 300 Area Geoframework Model

4.1.2 300 Area Groundwater Flow System

Regionally, groundwater in the unconfined aquifer beneath the 300 Area Stage B footprint generally flows southeast toward the Columbia River (Figure 4-2). This is due to a confluence of regional flow directions from the northwest, west, and southwest. A strong influence from the river-stage fluctuations

® Leapfrog is a registered trademark of ARANZ Geo Limited, Christchurch, New Zealand.

manifests in seasonally changing groundwater flow direction. These groundwater elevation fluctuations are an important factor in uranium contaminant leaching from the PRZ, with subsequent changes in uranium concentrations in the aquifer. Furthermore, groundwater flow impacts contaminant dilution when moving from the vadose zone porewaters to the saturated aquifer conditions. DOE/RL-2018-66, *Hanford Site Groundwater Monitoring Report for 2018*, determined a groundwater gradient of 3.4e-4 m/m by trend surface analysis using late February 2018 data.

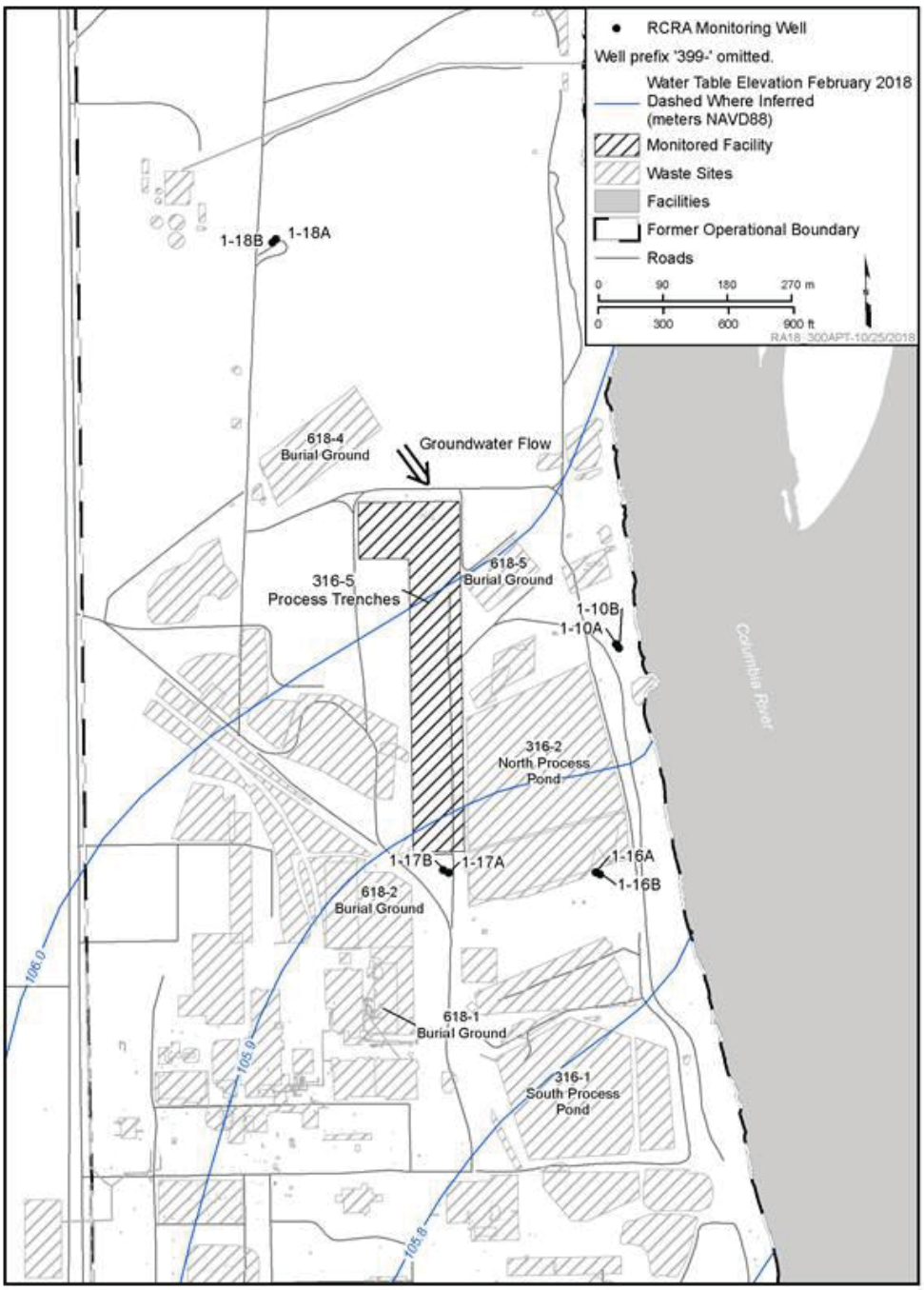

References: DOE/RL-2018-66, *Hanford Site Groundwater Monitoring Report for 2018*; NAVD88, *North American Vertical Datum of 1988*.

Figure 4-2. 300 Area Process Trenches Water Table, February 2018

4.1.3 Stage B EAA Polyphospate Injection

Stage B EAA remediation injections were performed from 9/4/2018 through 9/20/2018. Two mixing skids were used to deliver a blend of filtered river water and concentrated polyphosphate solution to injection wells in the Stage B EA area to achieve a target phosphorus concentration of approximately 2,700 mg/L (roughly 8,300 mg/L as total phosphate) (DOE/RL-2014-42-ADD1, *300-FF-5 Operable Unit Remedy Implementation Sampling and Analysis Plan Addendum for Stage B Uranium Sequestration*). An equivalent of roughly three pore volumes, or 51,000 gallons of solution per PRZ screen and 38,400 gallons per LVZ screen, was the target amount of solution to be delivered (DOE/RL-2014-42-ADD1). Each skid was capable of injecting 6 wells at a time for a total of 12 wells simultaneously. A total of 48 injection wells were used (Figure 4-3) in a series of four injection zones (phases) which used 12 wells at a time. Injection solution volumes and flow rates were monitored daily, with data compiled in ECF-300FF5-19-0005, *Injection Volumes for 300-FF-5 Stage B Injections and Sampling*. Injection rates ranged from 43 to 68 gallons per minute (gpm) with an average rate of 48 gpm between the two skids. Injections durations typically lasted between 6 to 9 hours from 9/4/2018 to 9/19/2018 with an average of 7.75 hours. The last day of injections (9/20/2018) lasted 4 hours. Injection volumes ranged from 39,623 to 64,101 gallons delivered to the PRZ with an average of 49,954 gallons (189,096 L) which is within 5% of the target volume. Similarly, a range of injection volumes from 26,376 to 45,624 gallons were delivered to the LVZ with an average of 38,997 gallons (147,619 L), also within 5% of the target delivery volume.

Injection solution composition was sampled twice daily, while solution pH was measured three times daily with results reported in the Hanford Environmental Information System (HEIS). Solution pH was maintained at an average value of 7.55 and 7.60 for Skid 1 and Skid 2, respectively (Figure 4-4). Anomalously low pH readings of 7.0 and 7.2 were measured, though additional measurement readings of 7.5 and 7.45 were reported those days (9/4/2018 and 9/18/2018, respectively). Similarly, anomalously high pH measurements of 9.9 occurred on 9/6/2018 for both skids, though the other measurements for the day were at a pH of 7.6. An average measured phosphorus concentration of 2,769 mg/L (approximately equivalent to 8,490 mg/L phosphate) was maintained in the injected solution during remedy implementation. On average, 1,605 kg of phosphate was delivered per PRZ well screen while 1,253 kg was delivered per LVZ well screen.

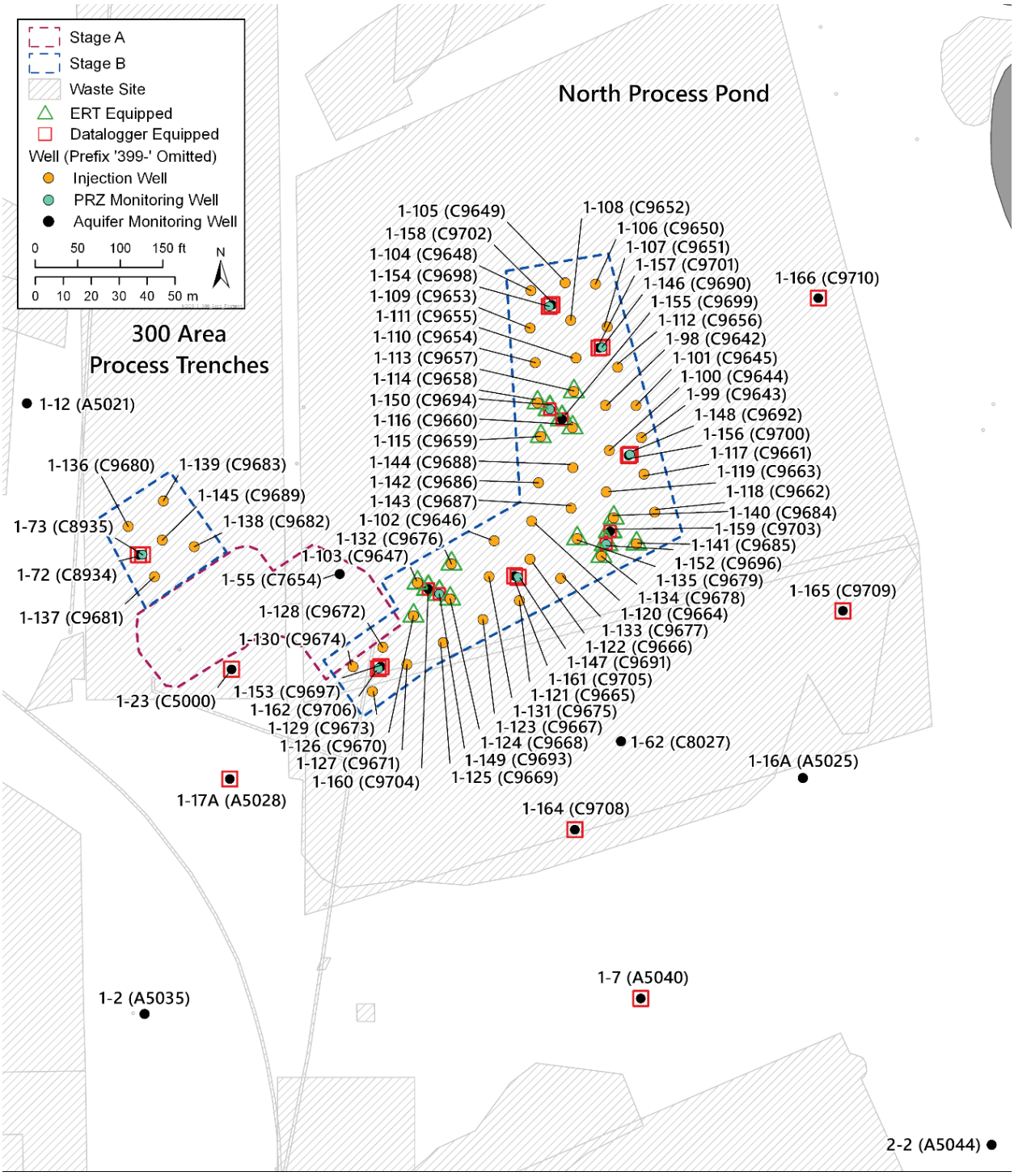

Figure 4-3. Injection Well Locations for Stage B EAA

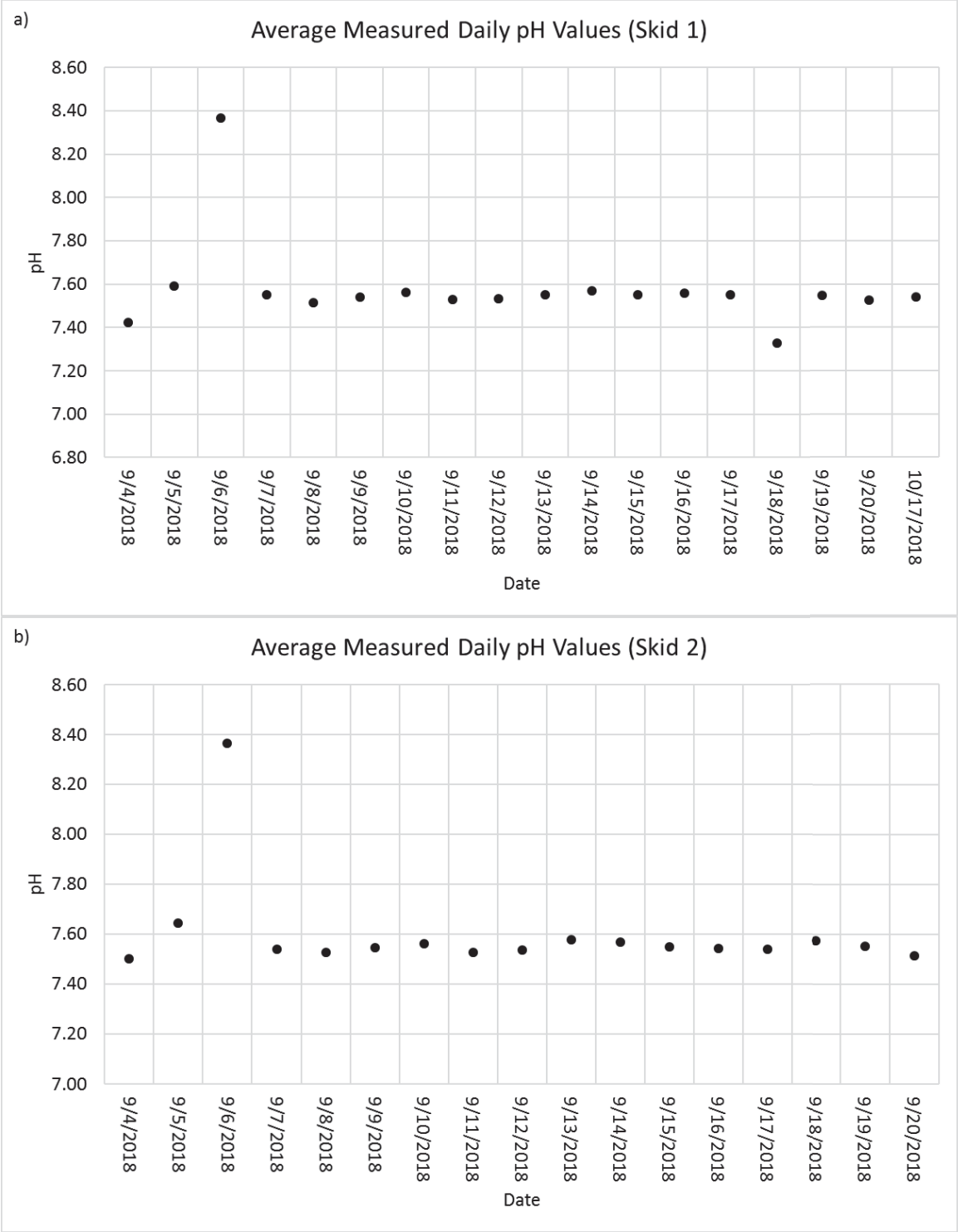

Figure 4-4. Average Daily Measured pH of the Injection Solution for a) Skid 1, and b) Skid 2

4.1.4 Electrical Resistivity Tomography

Real-time cross-borehole ERT was used to evaluate remedy solution delivery by imaging the spatial and temporal distribution of the change in subsurface electrical conductivity caused by polyphosphate solution migration (PNNL-28619, *Stage B Uranium Sequestration Amendment Delivery Monitoring Using Time-*

Lapse Electrical Resistivity Tomography). ERT imaging surveys were conducted continuously using wellbore annulus electrodes installed in three clusters of injection and monitoring boreholes (Figure 4-5). On each cluster, surveys were conducted every 52 minutes over the duration of the remedy injection period.

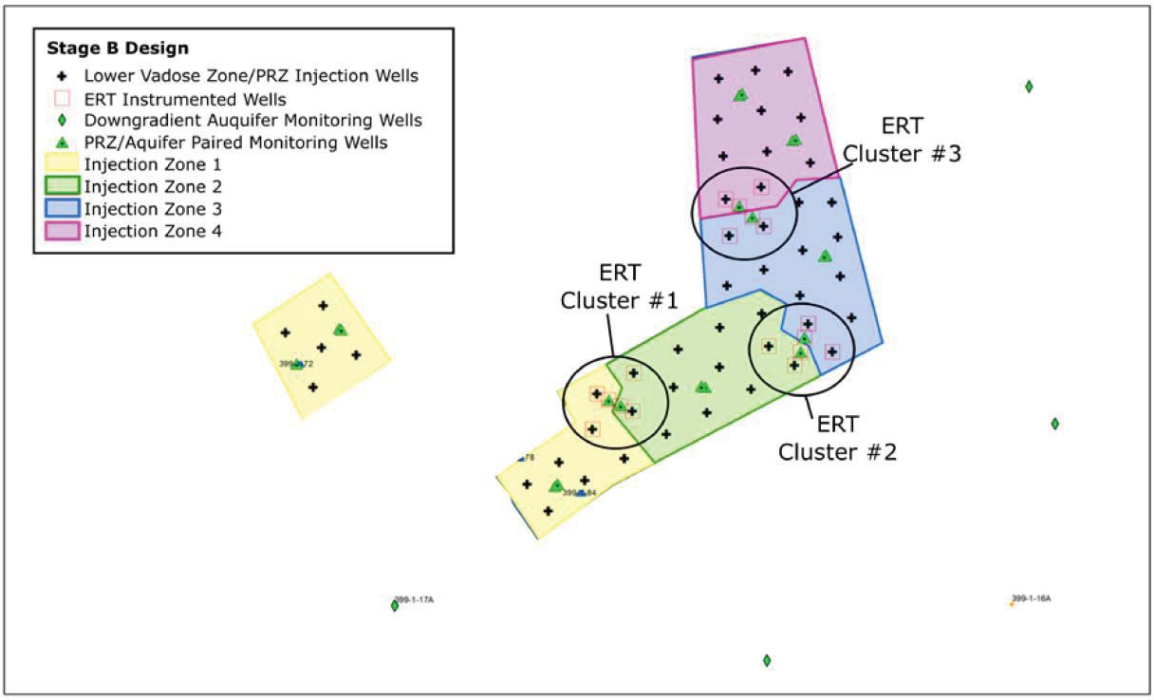

Figure 4-5. ERT Cluster Locations in Stage B EA Area

Plan view distances between each ERT instrumentation for each monitoring cluster and diagrams of down borehole electrode distributions are shown in Source: PNNL-28619, *Stage B Uranium Sequestration Amendment Delivery Monitoring Using Time-Lapse Electrical Resistivity Tomography*.

Figure 4-6. Total distance across A-A' transects for cluster 1, 2, and 3 were 13.2 ft (4.02 m), 14.5 ft (4.42 m), and 15.3 ft (4.66 m), respectively, with depths reaching below the water table.

Baseline ERT readings were conducted on September 4, 2018, to determine the background bulk conductivity prior to remedy injections (Figure 4-7). Regions of elevated baseline electrical conductivity are generally interpreted as representing finer grained sediment regions with lower permeability and elevated saturation and possibly elevated pore fluid conductivity resulting from past waste-discharge operations (PNNL-28619). Interpretations of zones with similar geologic structure are shown via solid black lines in Figure 4-7.

All new readings captured through the remedy period were then subtracted from the baseline measurements. Changes in bulk electrical conductivity during this time are due to increases in saturation and remedy solution composition conductivity. Maximum changes in bulk electrical conductivity are shown for each cluster as solid white lines in Figure 4-8 representing the maximum extents of remedy injection. Alternative interpretations of amendment distribution are shown in dashed white lines.

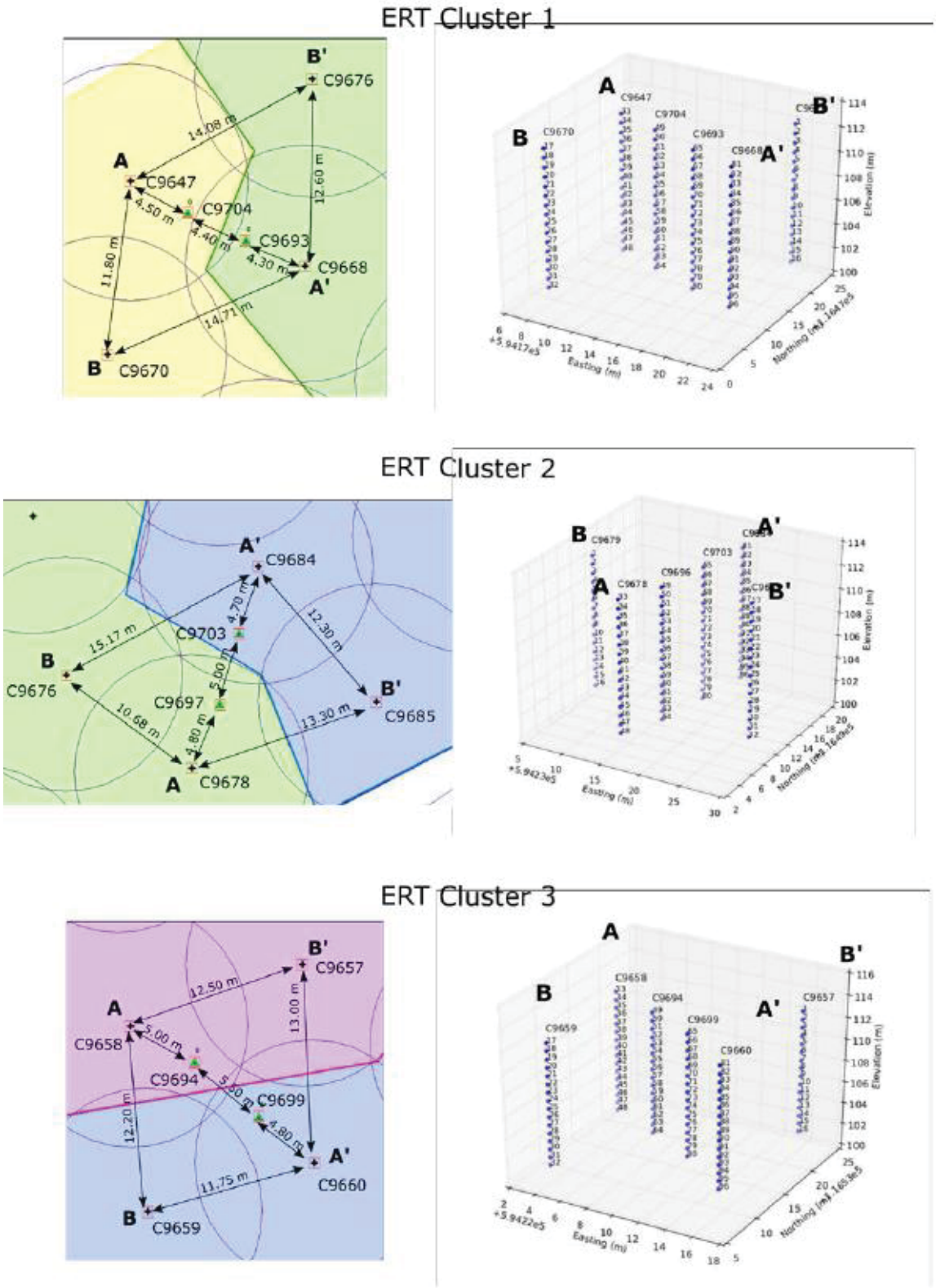

Source: PNNL-28619, *Stage B Uranium Sequestration Amendment Delivery Monitoring Using Time-Lapse Electrical Resistivity Tomography*.

Figure 4-6. Distances between ERT Instruments and Nodes from PNNL-28619

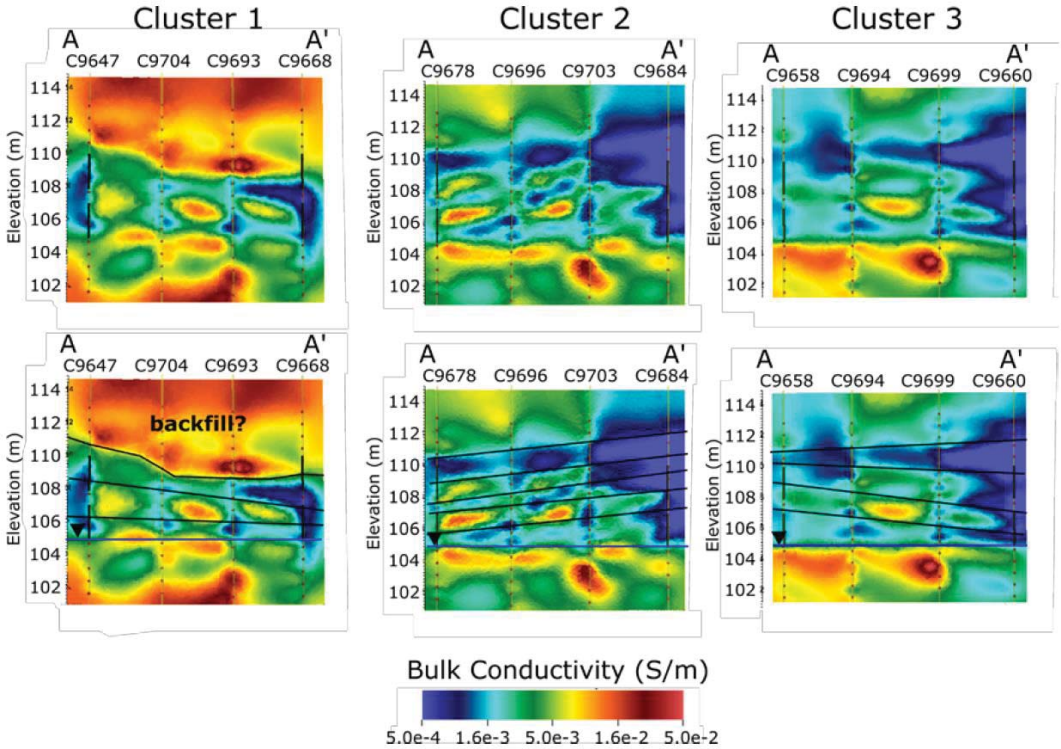

Source: Figure 15, PNNL-28619, *Stage B Uranium Sequestration Amendment Delivery Monitoring Using Time-Lapse Electrical Resistivity Tomography*

Figure 4-7. Pre-treatment Baseline ERT Images in the A-A' Plane for Each Cluster (Top) and the Corresponding Geologic Structure Interpretations (Bottom)

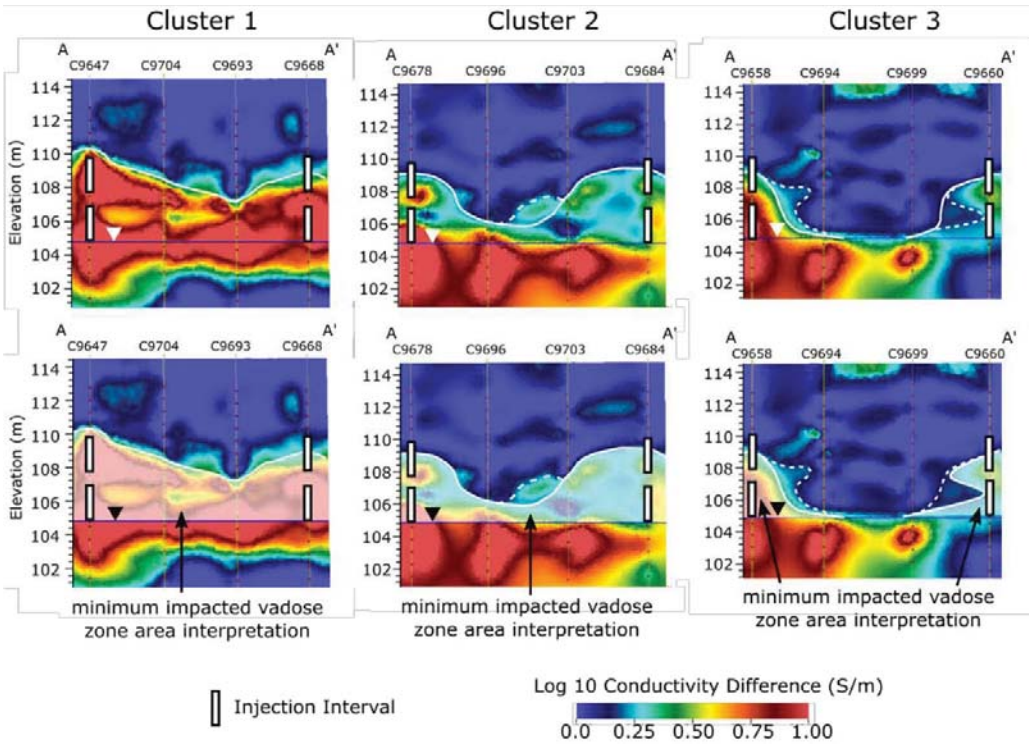

Source: Figure S.1, PNNL-28619, *Stage B Uranium Sequestration Amendment Delivery Monitoring Using Time-Lapse Electrical Resistivity Tomography*

Figure 4-8. Maximum Change in Bulk Conductivity during Remedy Injections for Each ERT Cluster Monitoring Results for Stage B EAA Treatment

A network of 15 groundwater monitoring wells and 9 PRZ wells was sampled daily from 9/4/18 through 9/27/18, with weekly sampling through October 2018. Subsequent monthly groundwater sampling was conducted using an expanded network of groundwater monitoring wells (Figure 1-1). Several geochemical indicators were examined to provide information on how dissolved uranium concentrations were impacted by the Stage B EAA remedy. Select well pairs are presented in this section for the following parameters:

- Phosphate to bicarbonate molar ratio compared to pH
- Concentration of dissolved uranium compared to aqueous calcium concentration
- Concentration of dissolved uranium compared to aqueous phosphate concentration
- Concentration of calcium compared to aqueous phosphate concentration
- Calcium/sodium ratio in milliequivalents per liter compared to pH

Two well pairs are presented (399-1-72/399-1-73 and 399-1-159/399-1-152), comprised of one groundwater monitoring well and one well screened in the PRZ, respectively, within the Stage B EAA. Two additional groundwater monitoring wells located outside the injection area are included (399-1-17A and 399-1-164) to assess the impact on the aquifer outside the Stage B EAA remedy footprint. Additional indicator data are presented in Appendix A for the remaining monitoring network. All data shown represent unfiltered maximum values for a given sampling period.

4.1.4.1 Uranium Concentration Compared to Phosphate Concentration

Figures 4-9 through 4-11 show the concentrations of uranium and phosphate for selected wells during remedy injections and up to one year prior. Uranium concentrations show a steep decline as phosphate breakthrough occurs and concentrations increase resulting from injections. A slight delay in phosphate breakthrough is observed for wells outside the remedy boundary. Most aquifer wells show an increase in uranium concentration as phosphate concentrations decline, though remaining at lower concentrations than during remedy injections months after remedy delivery.

Phosphate concentrations exhibit a sharp increase in concentration during injections within the Stage B EAA with delayed peaks observed with distance. Residual aqueous phosphate concentrations vary from a steep decline observed at wells 399-1-72 and 399-1-73 (Figure 4-9) to a much more gradual reduction in concentration over the course of months (e.g., well 399-1-164, Figure 4-11) reflecting the east-southeast flow direction.

4.1.4.2 Phosphate to Bicarbonate Ratio Compared to pH

Figures 4-12 through 4-14 compare the phosphate to bicarbonate molar ratio to pH for select wells. More phosphate is available relative to bicarbonate at higher molar ratios, providing more favorable conditions for uranium to react with phosphate. The phosphate to bicarbonate ratio sharply increases during the period of injections for all wells within the Stage B EAA boundary. Changes in pH occur briefly during remedy injections in all groundwater monitoring wells including well 399-1-73 with a lower elevation screen interval, dropping to values ~7.1, then quickly rebounding to ~7.5. This is not observed in PRZ well 399-1-152, though sampling was less frequent and could have been missed.

4.1.4.3 Uranium Concentration Compared to Calcium Concentration

Comparisons between uranium and calcium concentrations for select wells are provided in Figures 4-15 through 4-17. All groundwater wells (including 399-1-73) within the Stage B EAA show a sharp increase in calcium during remedy injections followed by a sharp decline directly as it is consumed in the reactions. PRZ well 399-1-152 does not show this as samples were not collected during injections. The peak is less dramatic with distance as shown in Figure 4-17 by little to no noticeable peak observed at well 399-1-164 compared to 399-1-17A indicating complex flow pathways in the aquifer. Wells 399-1-72 and 399-1-73 both exhibit slow rebounding over the course of the subsequent monthly sampling period to approximately the same calcium concentrations as during injections.

4.1.4.4 Calcium Concentration Compared to Phosphate Concentration

Observed phosphate and calcium concentrations for select wells are shown in Figures 4-18 through 4-20. One objective of the Stage B EA remedy is to form calcium-phosphate-uranium complexes and precipitates. As shown in Figure 4-18 through Figure 4-20, in situ calcium is available during remedy injections allowing for favored complexation/precipitation conditions.

4.1.4.5 Calcium to Sodium Ratio Compared to pH

Figures 4-21 through 4-23 show the ratio of calcium to sodium (in milliequivalents per liter) along with pH. A decrease in the Ca:Na ratio indicates an increase in the amount of sodium in the system due to the sodium-rich remedy injection solution. Because of concurrent geochemical reactions, pH declines during injections (also shown by decreasing Ca:Na ratio) with rapid rebounding.

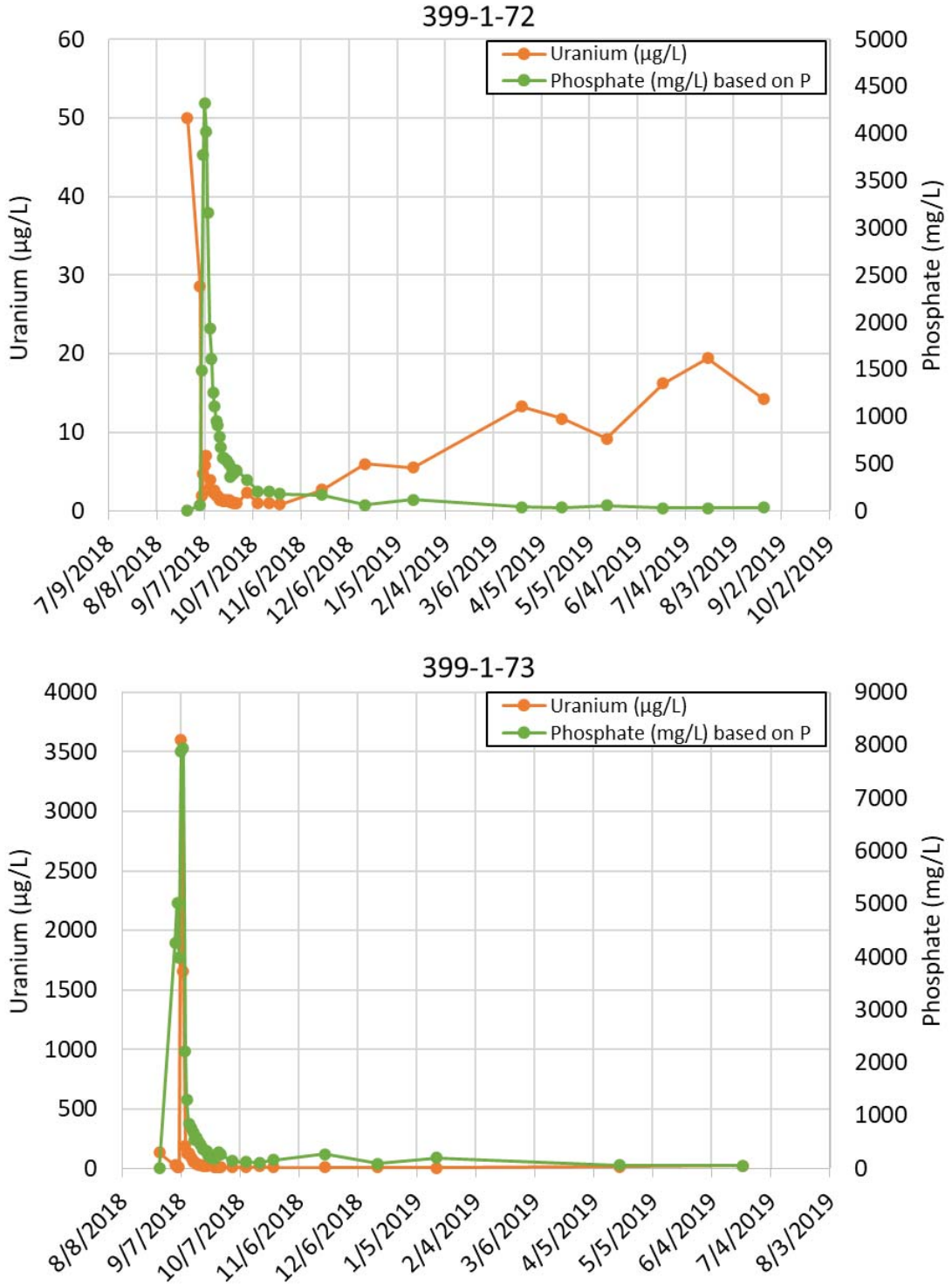

Figure 4-9. Comparison of Uranium to Phosphate for Wells 399-1-72 and 399-1-73

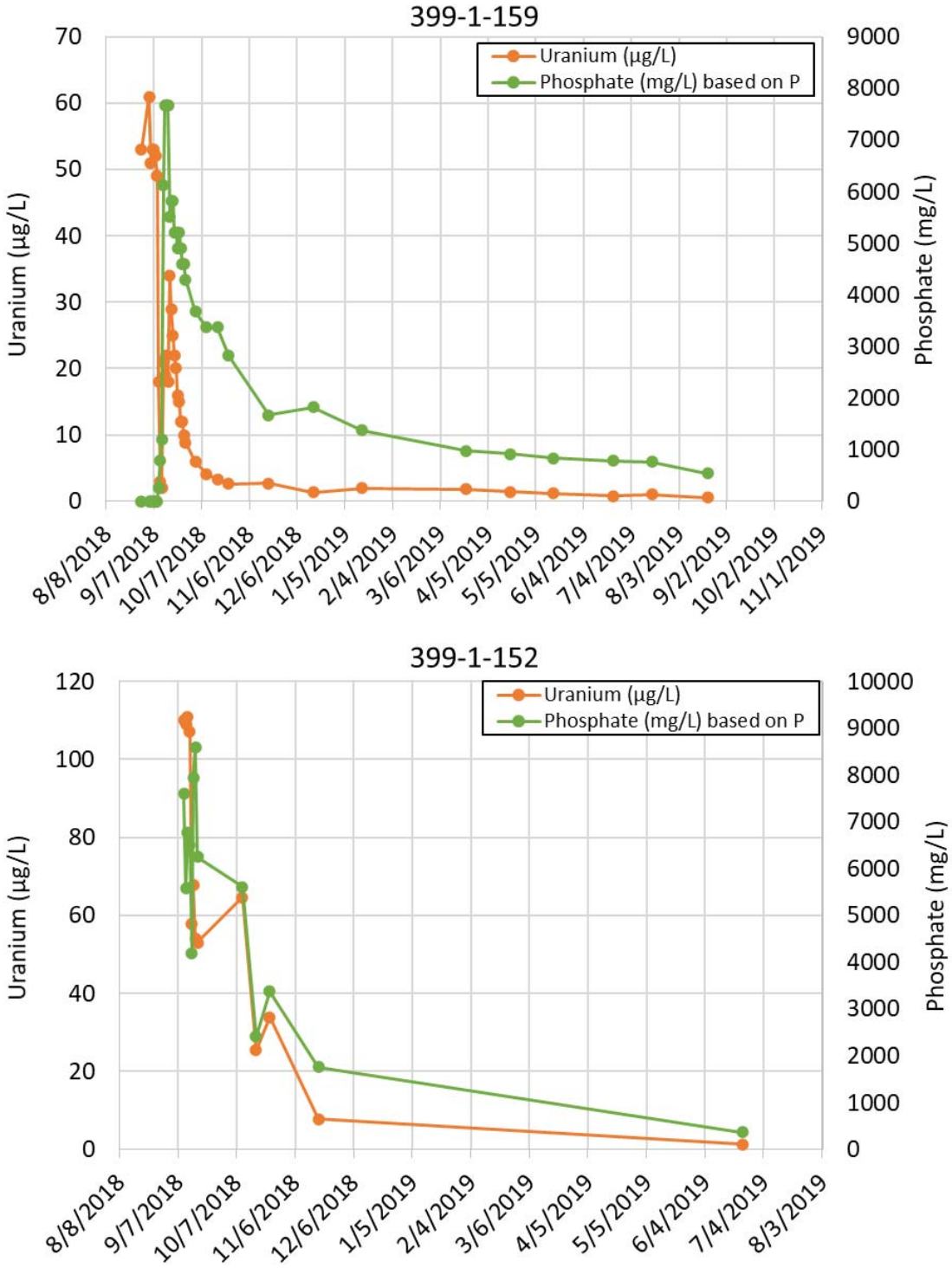

Figure 4-10. Comparison of Uranium to Phosphate for Wells 399-1-159 and 399-1-152

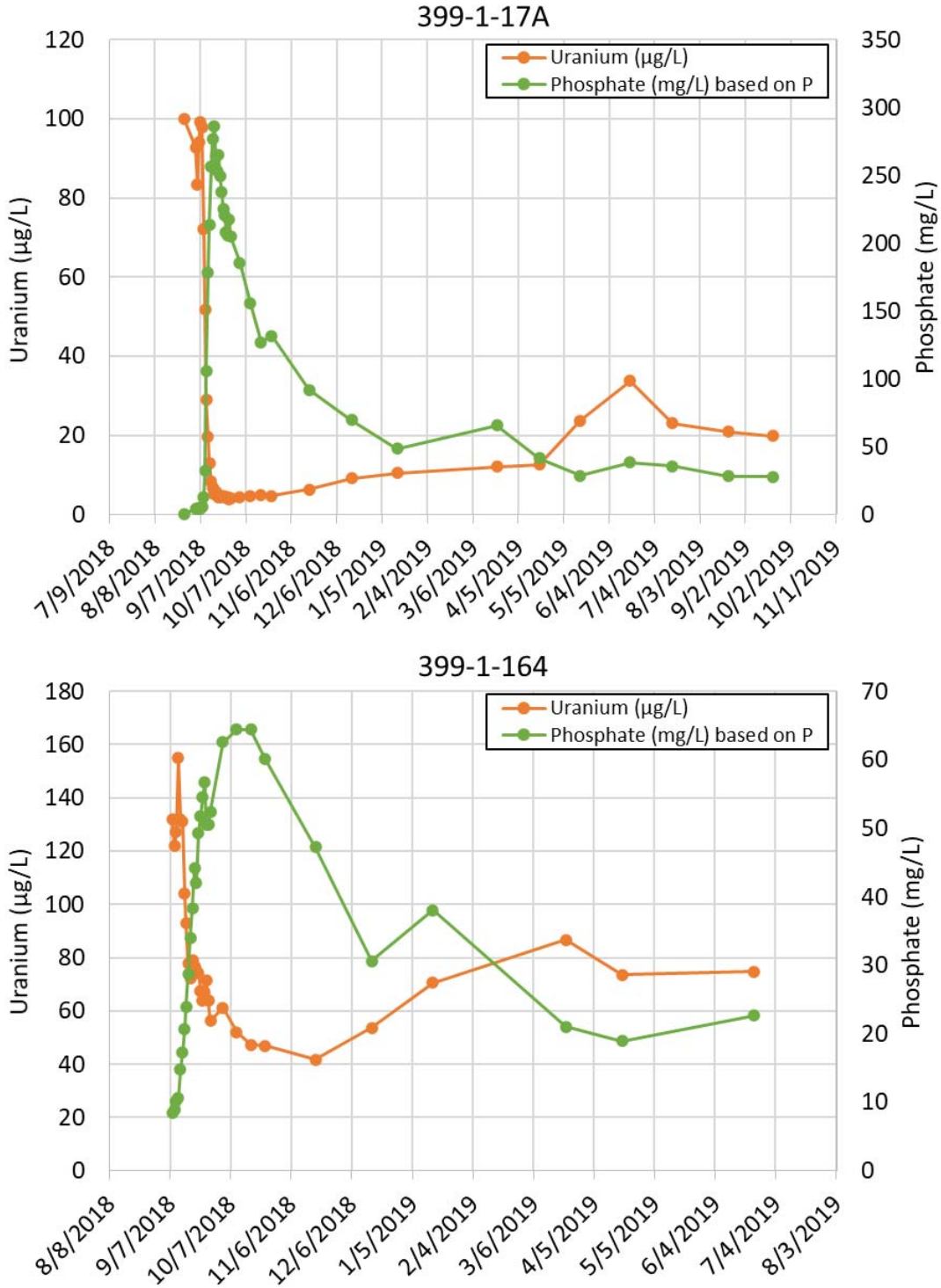

Figure 4-11. Comparison of Uranium to Phosphate for Wells 399-1-17A and 399-1-164

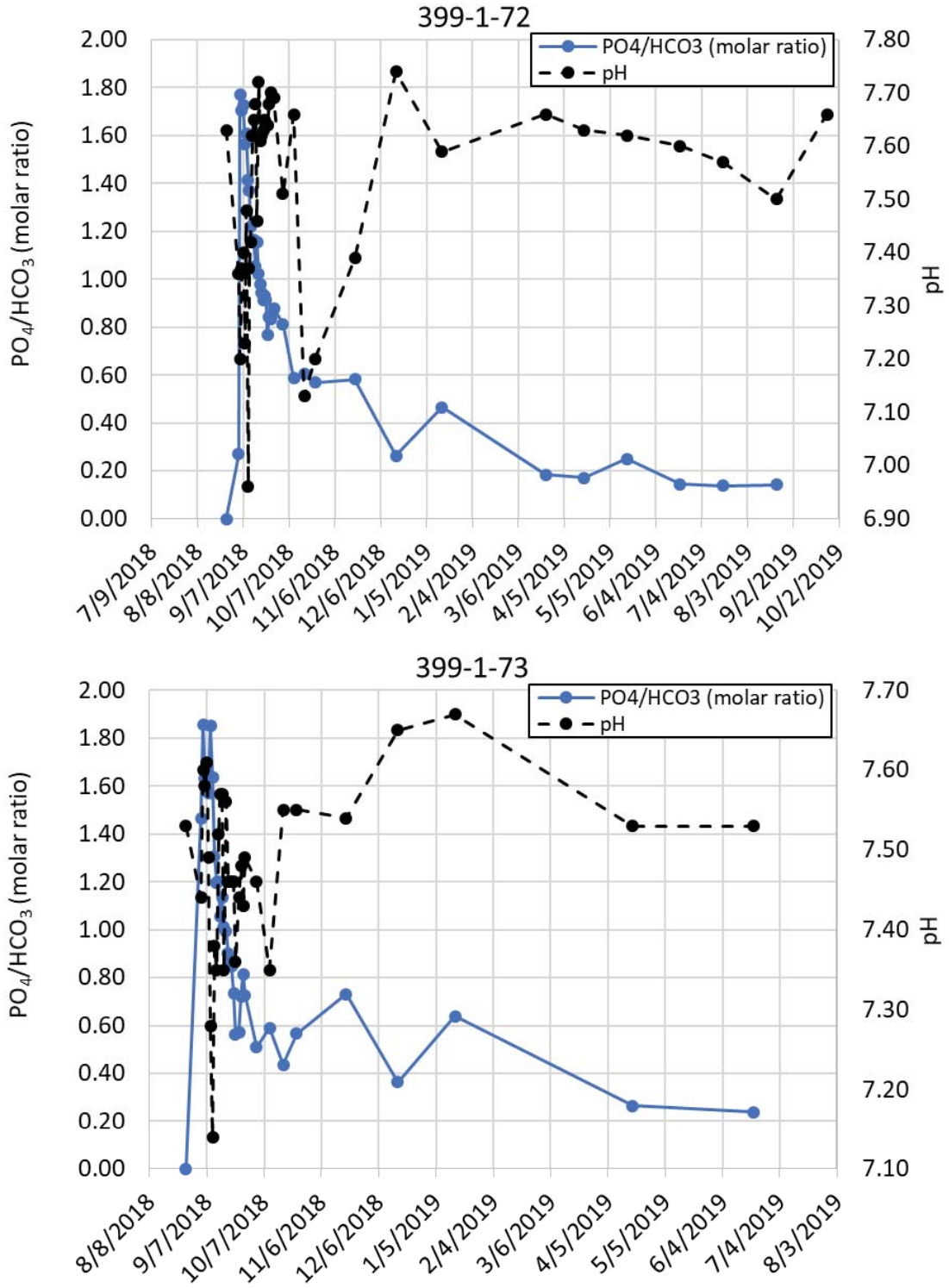

Figure 4-12. Comparison of Phosphate to Bicarbonate Ratio to pH for Wells 399-1-72 and 399-1-73

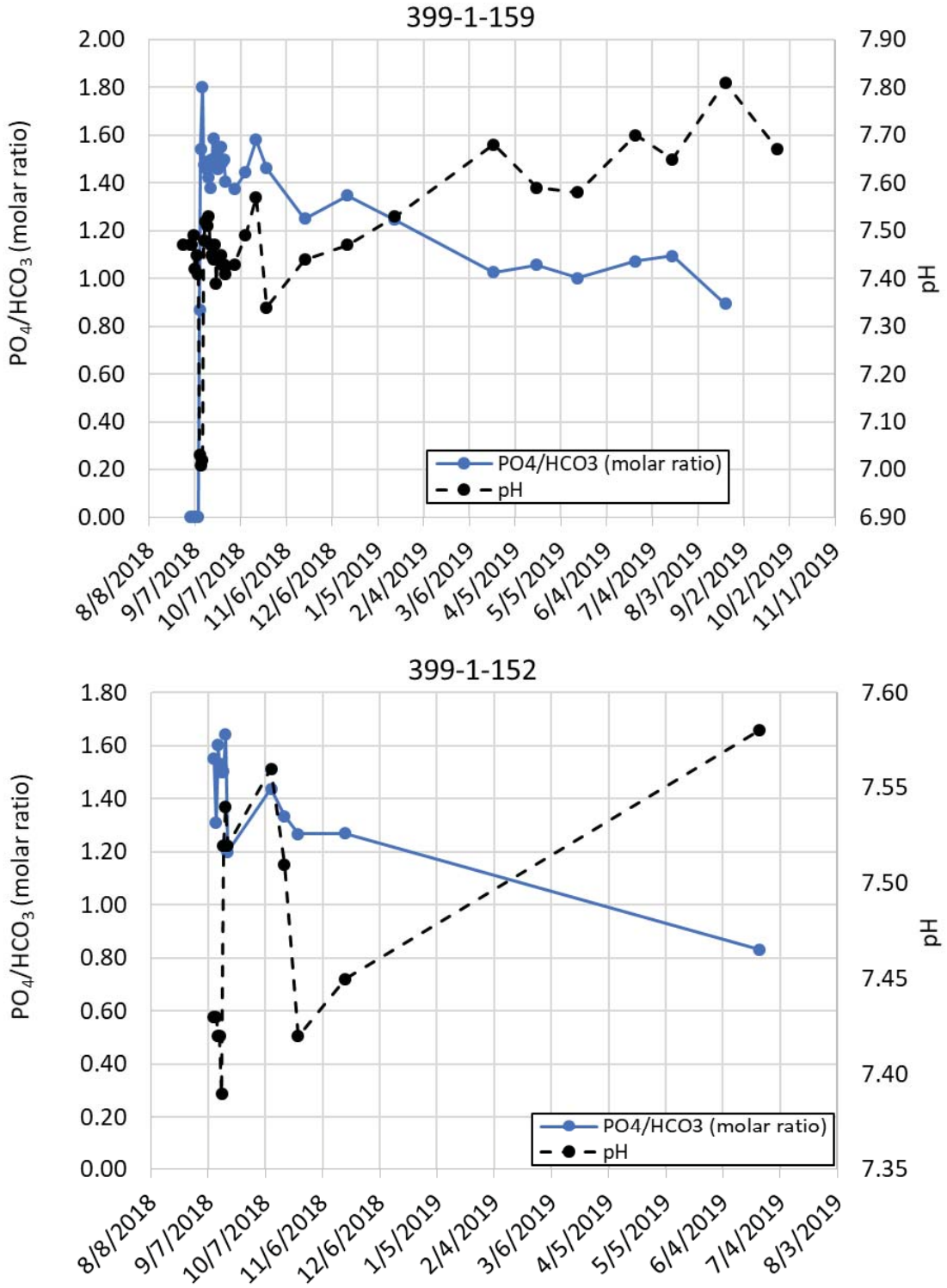

Figure 4-13. Comparison of Phosphate to Bicarbonate Ratio to pH for Wells 399-1-159 and 399-1-152

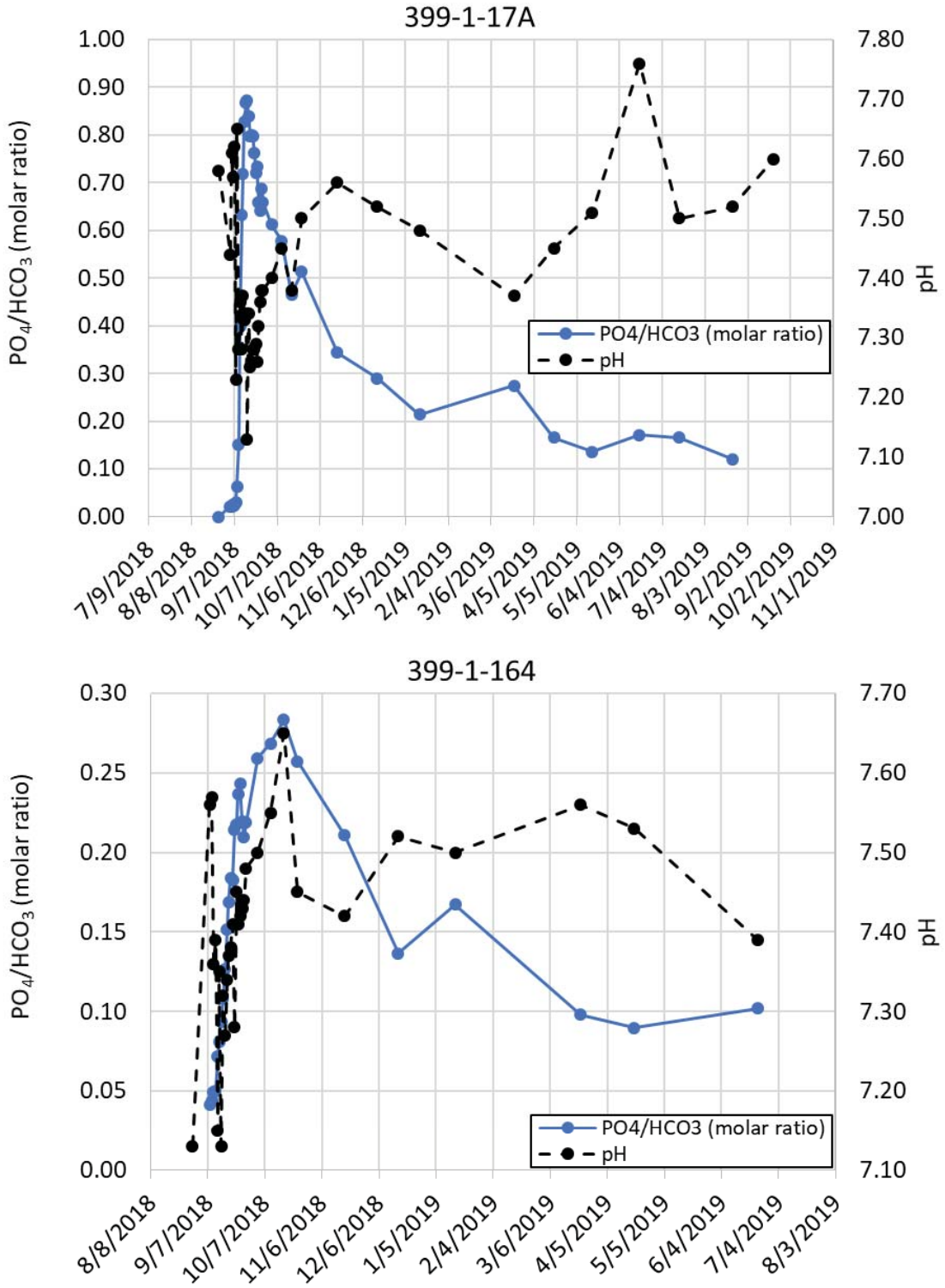

Figure 4-14. Comparison of Phosphate to Bicarbonate Ratio to pH for Wells 399-1-17A and 399-1-164

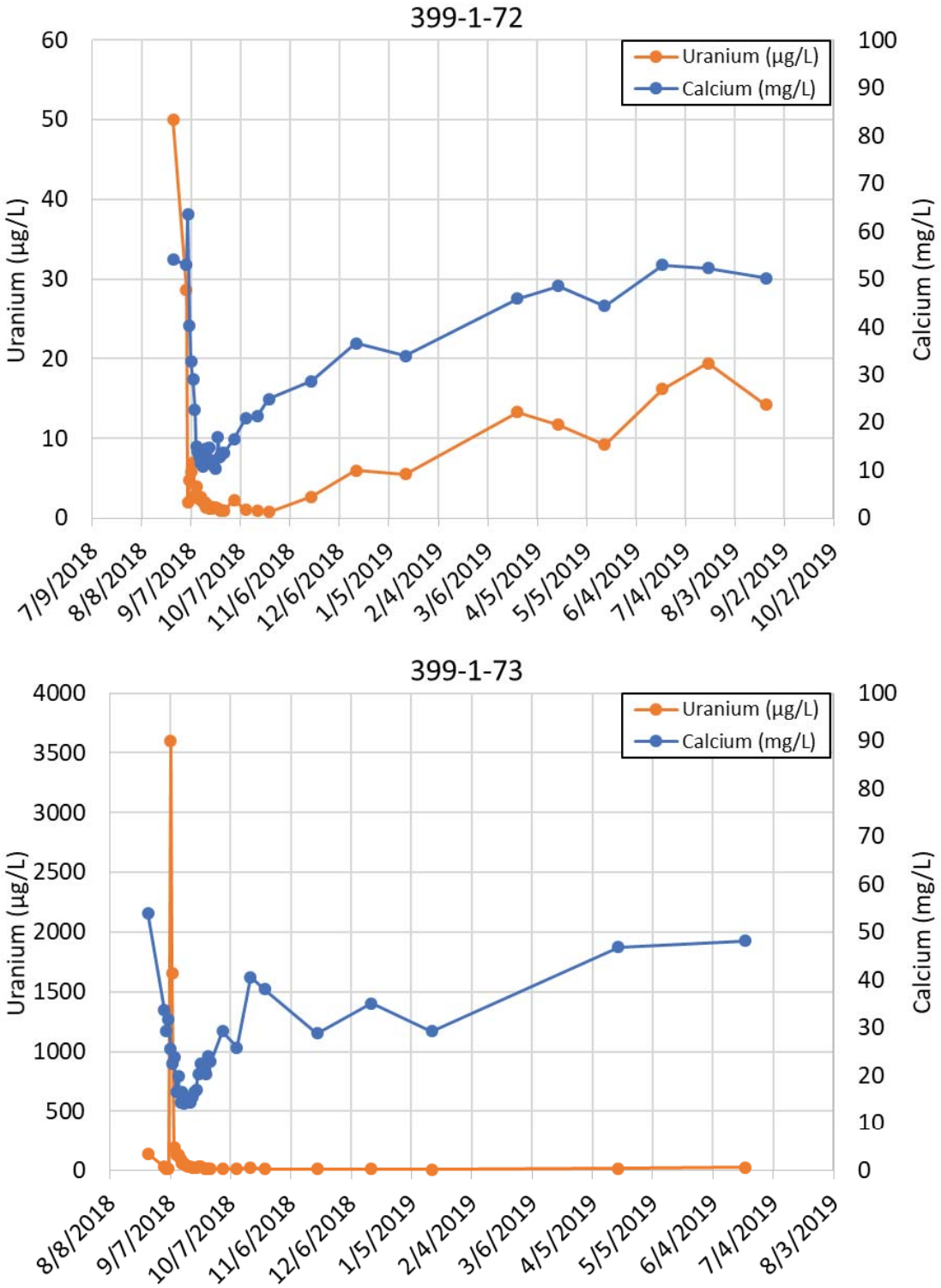

Figure 4-15. Comparison of Uranium to Calcium for Wells 399-1-72 and 399-1-73

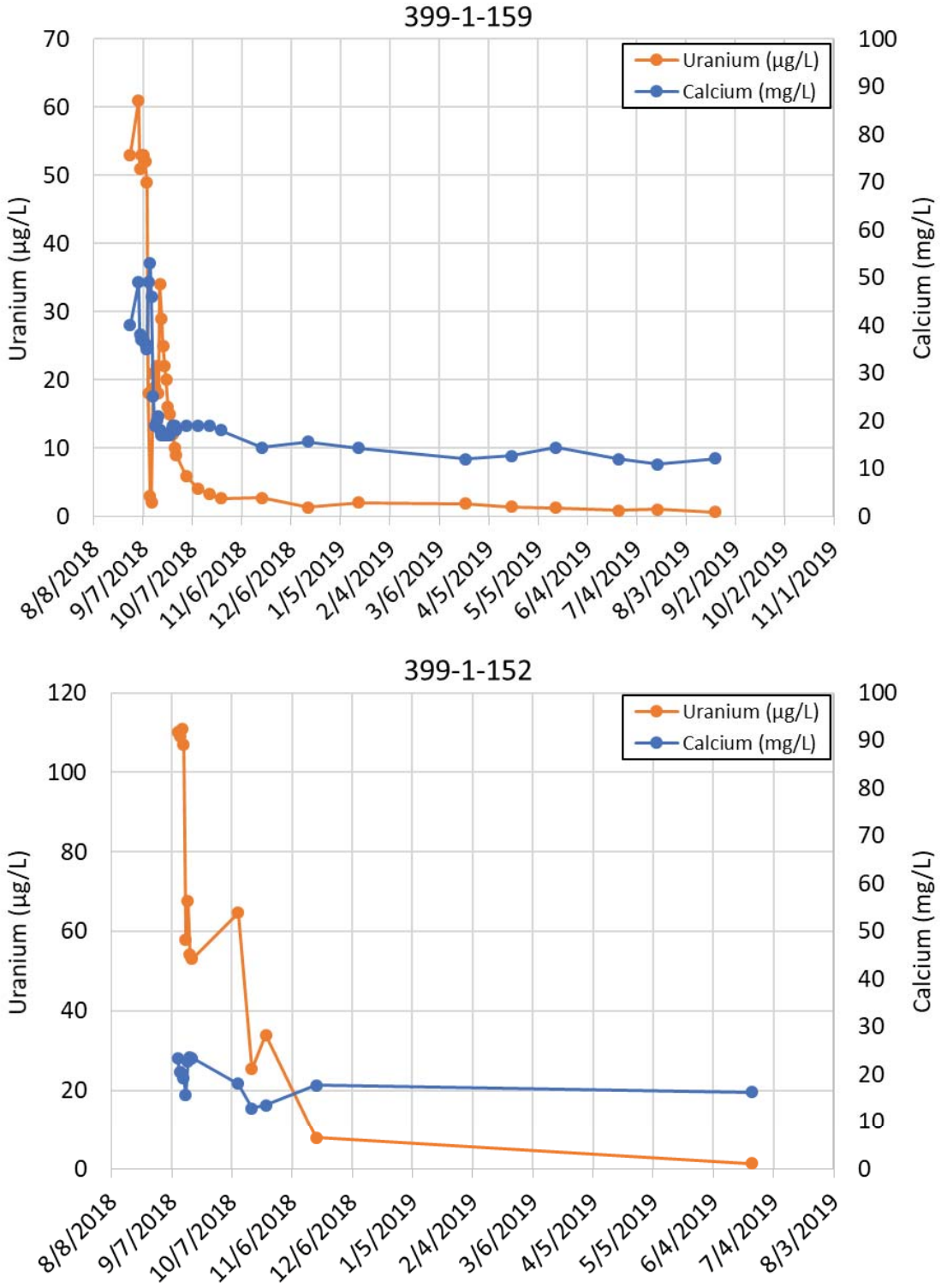

Figure 4-16. Comparison of Uranium to Calcium for Wells 399-1-159 and 399-1-152

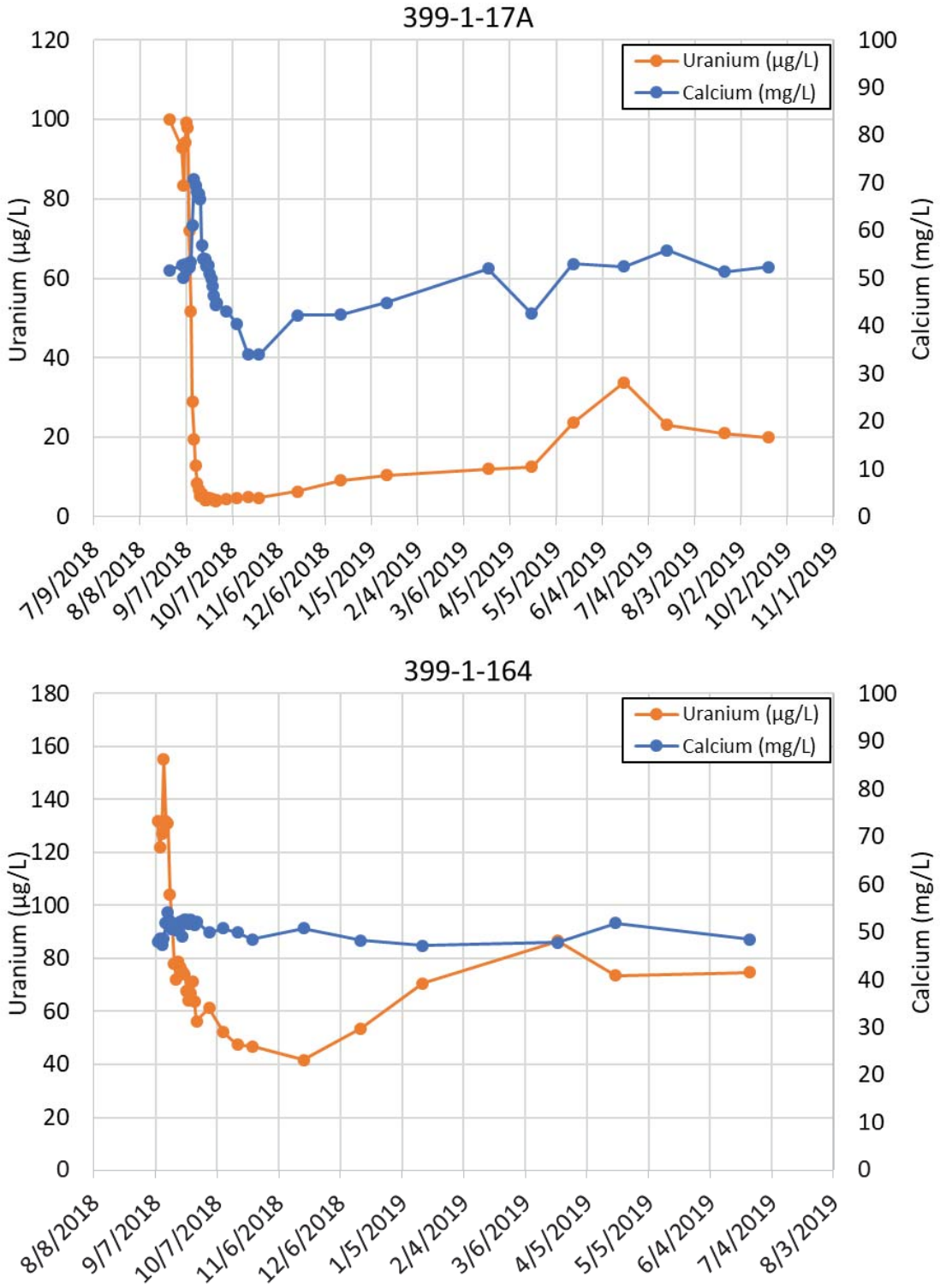

Figure 4-17. Comparison of Uranium to Calcium for Wells 399-1-17A and 399-1-164

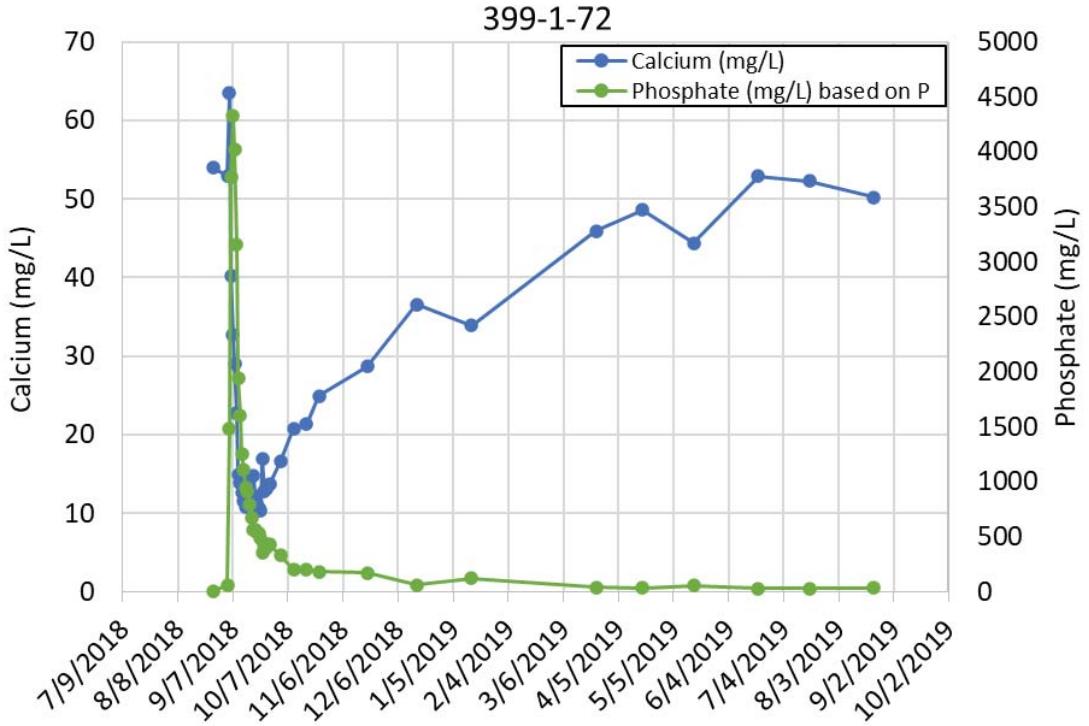

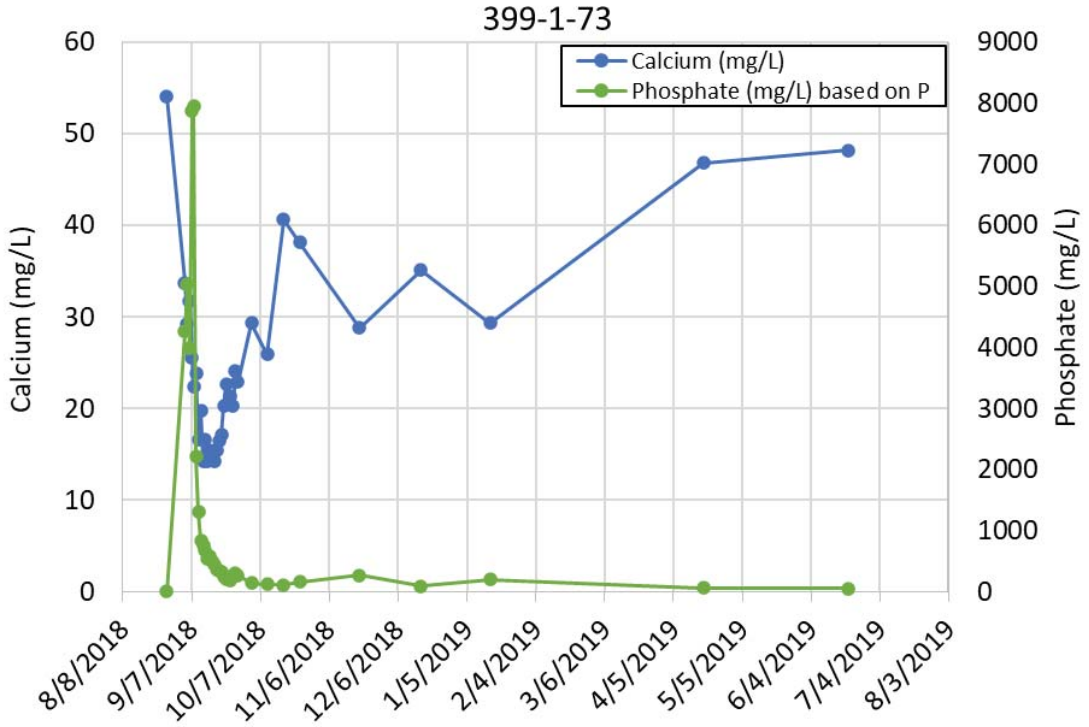

Figure 4-18. Comparison of Phosphate to Calcium for Wells 399-1-72 and 399-1-73

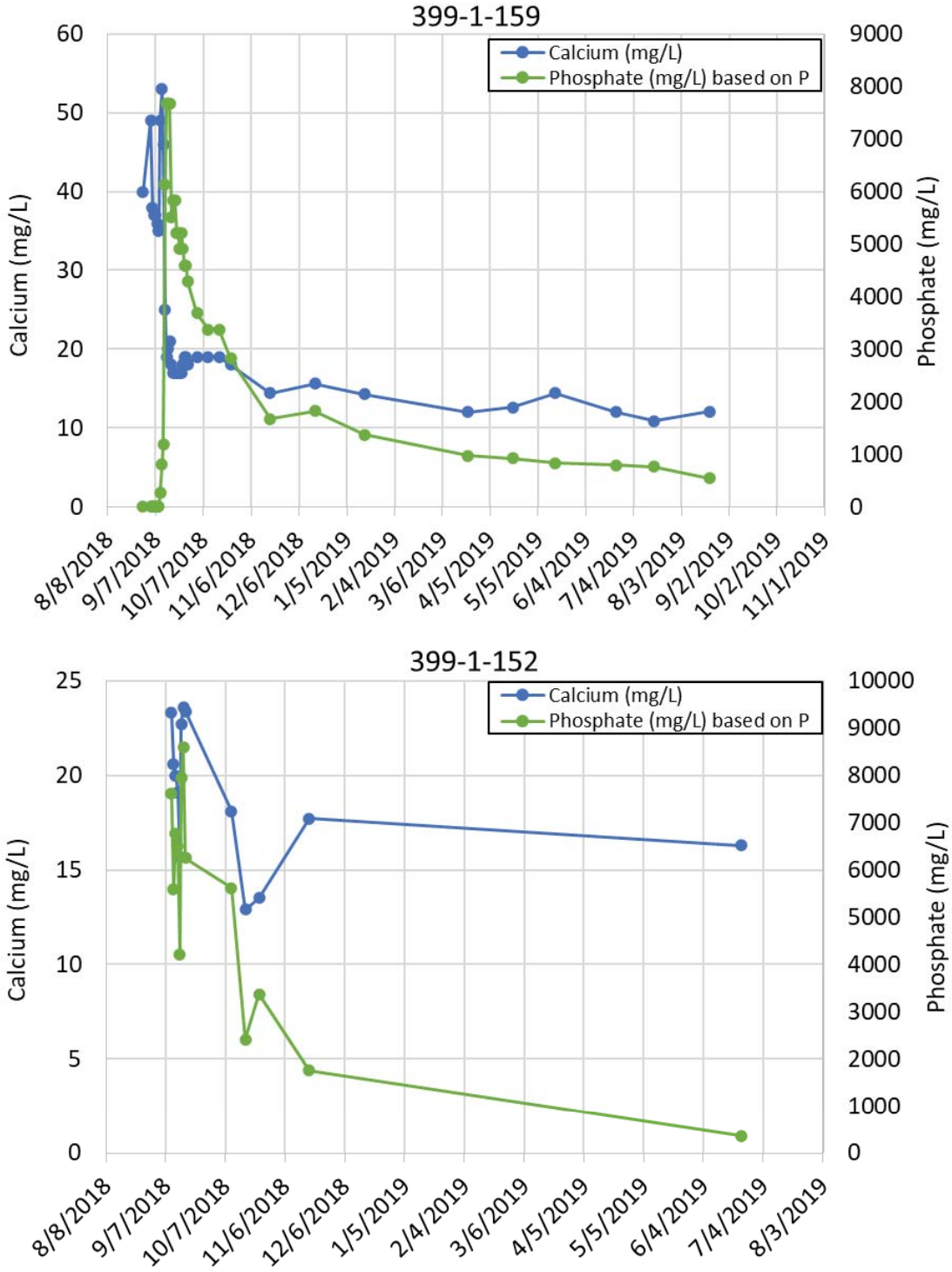

Figure 4-19. Comparison of Phosphate to Calcium for Wells 399-1-159 and 399-1-152

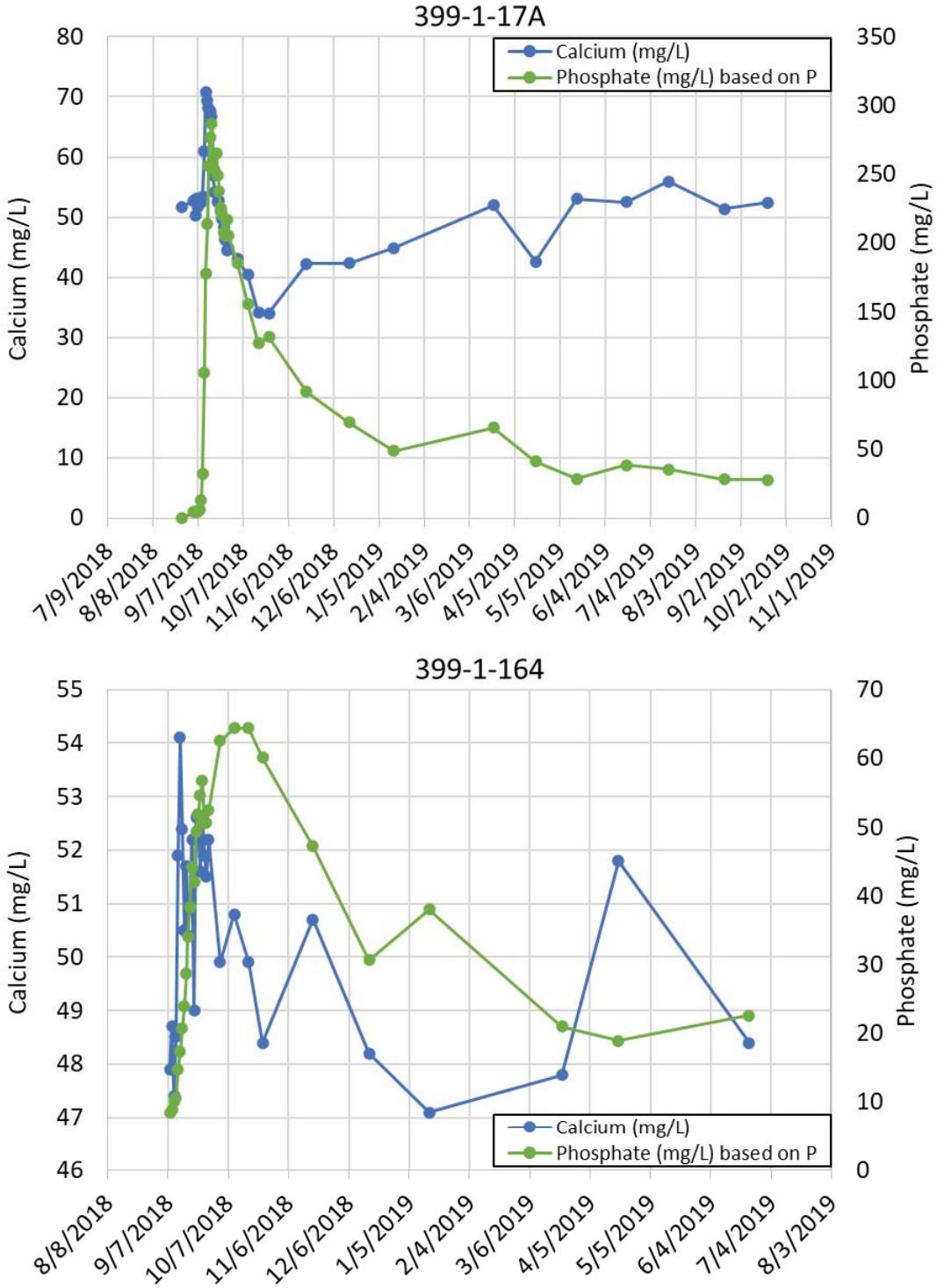

Figure 4-20. Comparison of Phosphate to Calcium for Wells 399-1-17A and 399-1-164

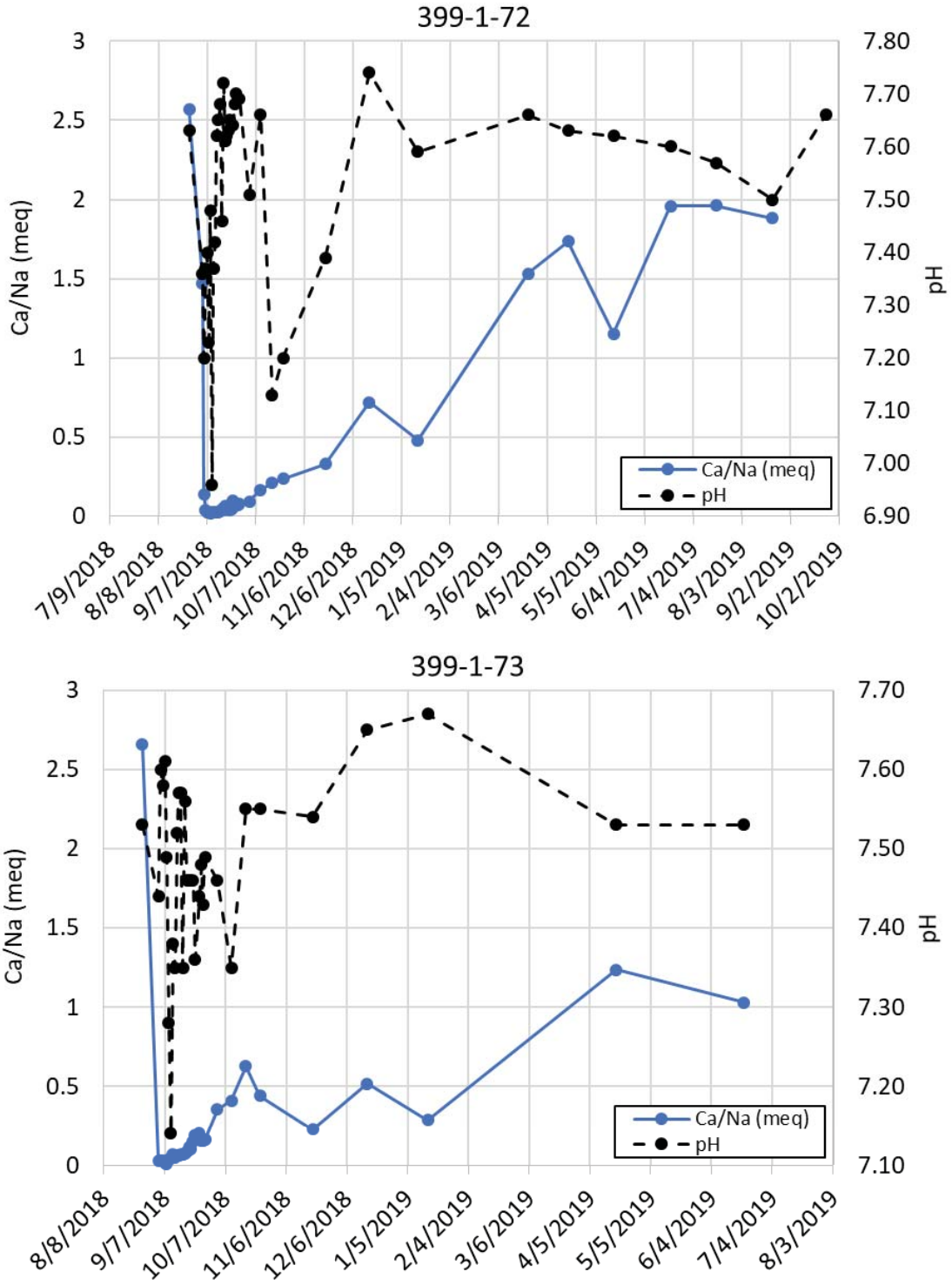

Figure 4-21. Comparison of Calcium to Sodium Ratio to pH for Wells 399-1-72 and 399-1-73

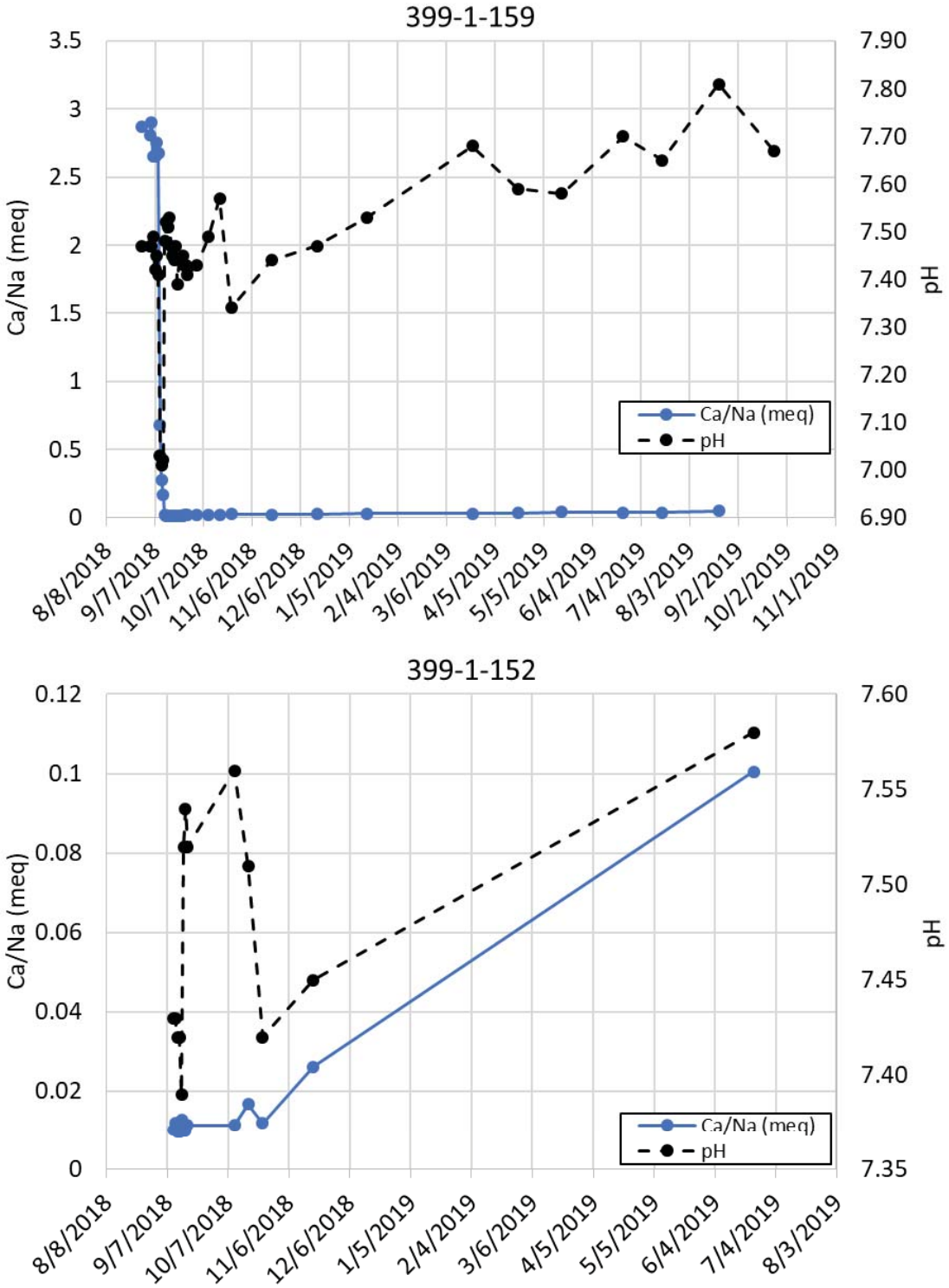

Figure 4-22. Comparison of Calcium to Sodium Ratio to pH for Wells 399-1-159 and 399-1-152

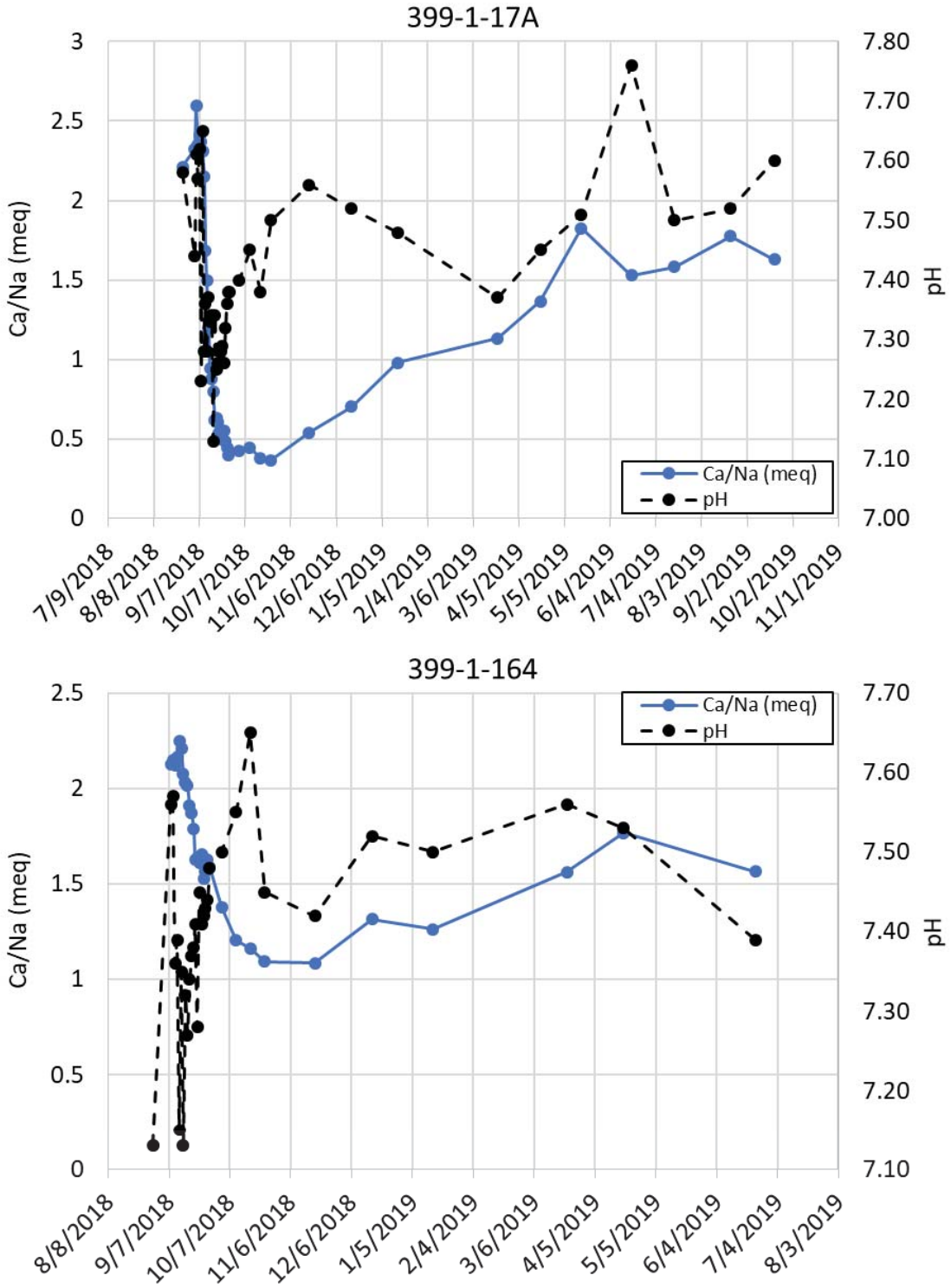

Figure 4-23. Comparison of Calcium to Sodium Ratio to pH for Wells 399-1-17A and 399-1-164

4.1.5 Comparison of Pre- and Post-Treatment Samples

Evaluation of uranium mobility changes due to treatment impacts was conducted by comparing samples from nine post-treatment borehole locations against six pre-treatment locations (Figure 4-24). Six pre-/post-injections borehole pairs were within 3.61 ft (1.1 m) of each other: C9646/C9731, C9647/C9733, C9667/C9729, C9673/C9728, C9677/C9730, and C9683/C9732. Three additional boreholes (C9734, C9735, and C9736) were used to evaluate spatial variability with greater distances from injection wells in addition to variations present within the Stage B EAA footprint. Select samples from these 15 boreholes were selected for sequential extraction, one-dimensional flow through column leaching experiments, labile uranium extractions, and mineral phase identification.

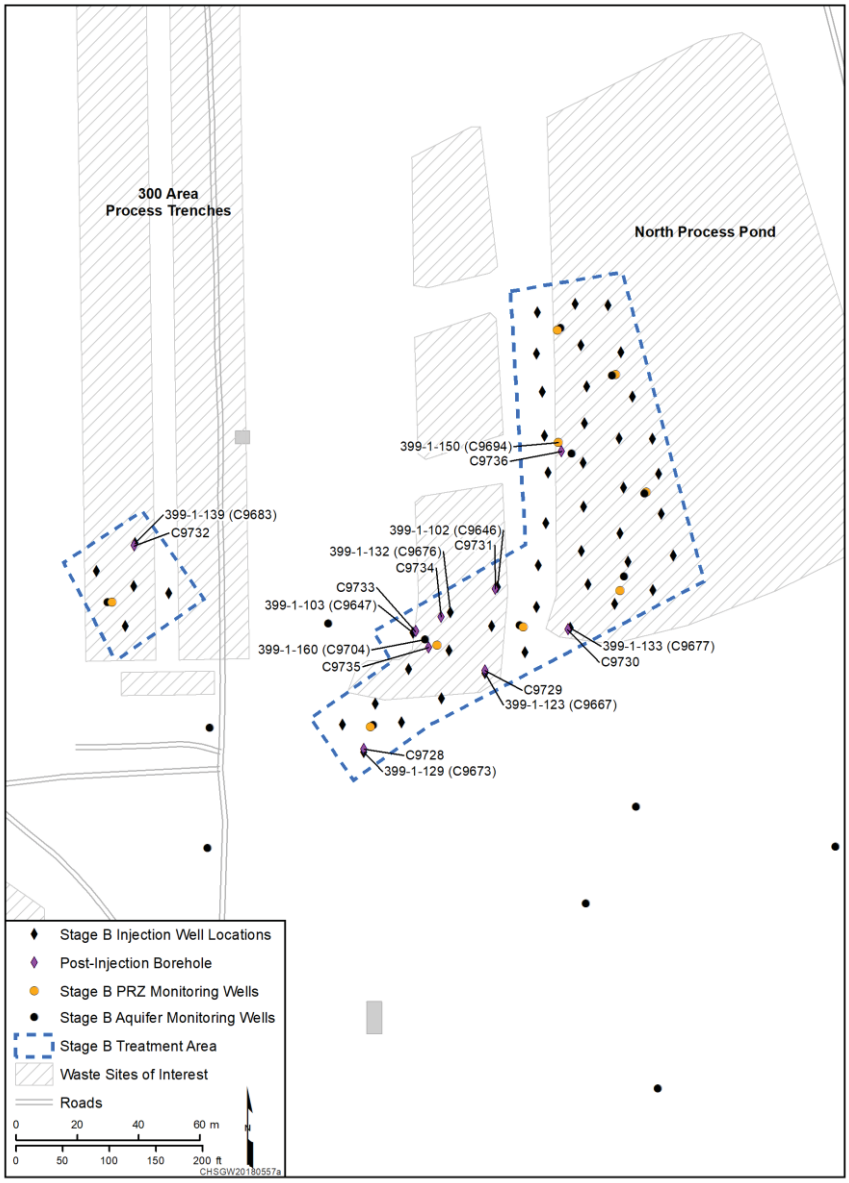

Figure 4-24. Stage B EAA Post-Injection Borehole Location Map

4.1.5.1 Depth Discrete Uranium and Phosphate Sampling

Figures 4-25 and 4-26 compare total uranium and phosphorus soil concentrations with depth between pre-/post-injection well pairs. Total uranium and phosphorus soil concentrations were conducted by outside laboratories separate from analyses performed by Pacific Northwest National Laboratory (PNNL). Three non-paired post-treatment borehole uranium and phosphate soil concentrations are included in Figure 4-27. Uranium soil concentrations vary widely with depth and between pre- and post-injection pairs where available with no discernable trends. A mean pretreatment soil concentration of 21.9 ± 23.0 mg/kg is very similar to post-treatment sample mean of 23.4 ± 25.1 mg/kg. A single-factor analysis of variance (ANOVA) analysis was conducted to compare the effect of remedy injections on uranium soil concentration (as log-normalized uranium soil concentrations) in pre-/post-injection populations (see Appendix B for additional details). Results indicate a failure to reject the null hypothesis due to no statistically significant difference between pre- and post-injection uranium soil samples [$F(1,101)=0.901$, $p=0.345$]. Because no significant difference is observed, no changes in the total uranium concentration in soil samples is observed as a result of remedy injections.

Similarly, phosphorus soil concentrations show no discernable trend as a function of depth. Mean phosphorus soil concentrations for pre- and post-injection samples are 1180.84 ± 341.78 mg/kg and 1685.19 ± 431.89 mg/kg, respectively. A single-factor ANOVA analysis was conducted to compare the effect of remedy injections on phosphorus soil concentration in pre-/post-injection populations (see Appendix B for additional details). Unlike uranium soil concentrations, phosphorus soil concentrations reject the null hypothesis, showing statistically significant difference between pre- and post-injection samples [$F(1,99)=42.02$, $p=3.56E-9$]. Implications indicate residual phosphorus roughly 6 months after treatment implementation remain greater than pre-injection background soil concentrations as a result of remedy injections.

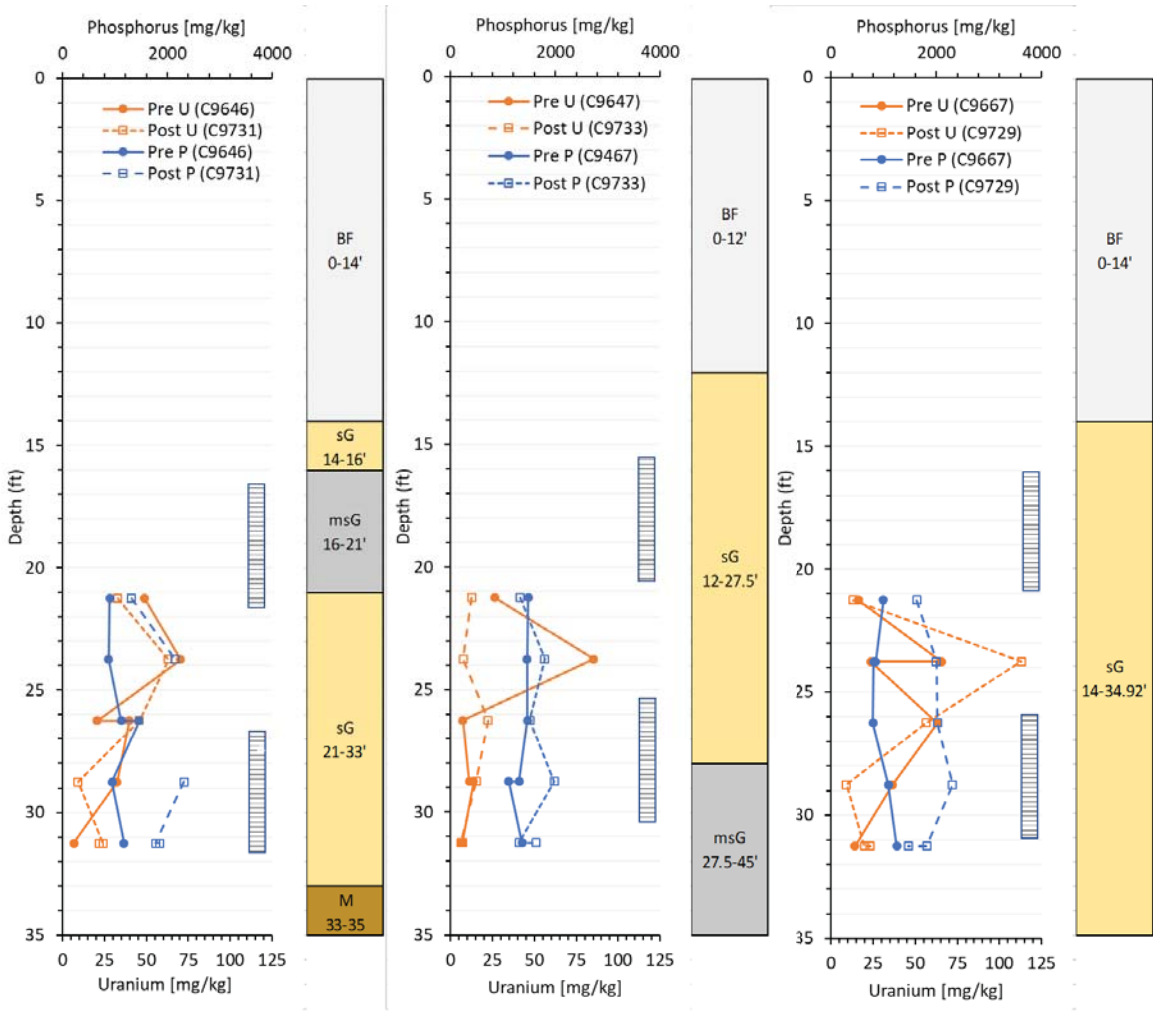

Note: Approximate depths for LVZ and PRZ well screens shown. Borehole logs presented for pretreatment boreholes. BF, msG, sG, G, and M refer to backfill, silty sandy gravel, sandy gravel, gravel, and silt sediment textures, respectively.

Figure 4-25. Uranium and Phosphorus Soil Concentration with Depth for C9646/C9731, C9647/C9733, and C9667/C9729 Borehole Pairs

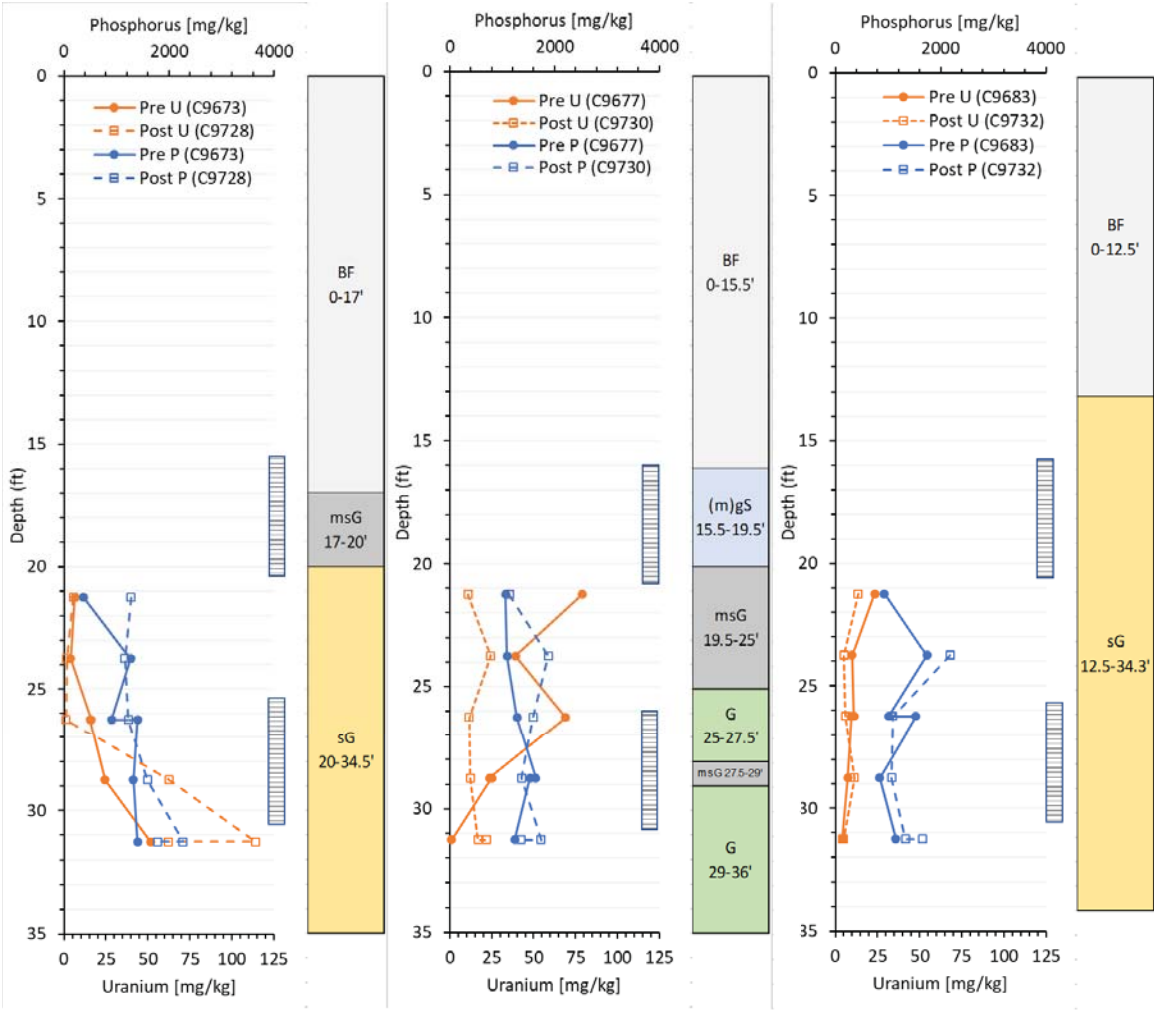

Note: Approximate depths for LVZ and PRZ well screens shown. BF, msG, sG, G, and (m)gS refer to backfill, silty sandy gravel, sandy gravel, gravel, and silty gravely sand sediment textures, respectively.

Figure 4-26. Uranium and Phosphorus Soil Concentration with Depth for C9673/C9728, C9677/C9730, and C9683/C9732 Borehole Pairs

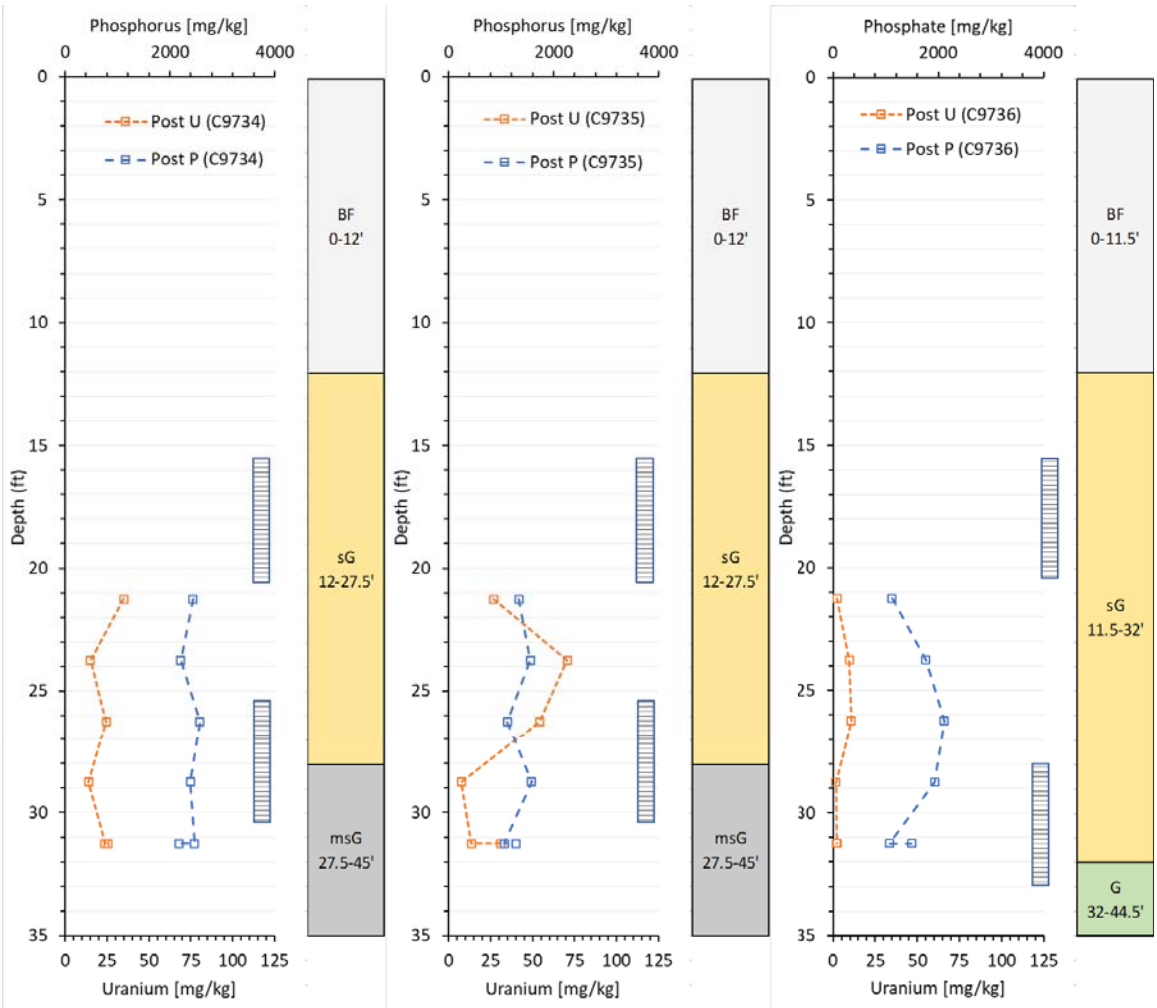

Note: Approximate depths for LVZ and PRZ well screens shown. BF, msG, sG, and G refer to backfill, silty sandy gravel, sandy gravel, and gravel sediment textures, respectively.

Figure 4-27. Uranium and Phosphorus Soil Concentration with Depth for C9734, C9735, and C9736 Post-Treatment Boreholes

4.1.5.2 Sequential Extraction

Sequential extractions were conducted on selected samples to assess how uranium is present in sediments (PNNL-29650, *Evaluation of the Change in Uranium Mobility in Sediments from Hanford 300-FF-5 Stage B Polyphosphate Field Injection*). Determination of the labile uranium fraction (weakly bound aqueous and adsorbed phases), readily extractable fraction, and strongly bound uranium fraction was accomplished by a succession of six sequential extraction solutions targeted to dissolve targeted phases with each step (PNNL-29650):

Extraction 1 targets the aqueous contaminant fraction, extraction 2 focuses on the adsorbed contaminant fraction, and the remaining extractions, 3 through 6, are operationally defined and designed to remove metals from different assemblages of precipitates. Extraction 3 was a weak acid (pH 5 acetate reacted for 1 hour) extraction that dissolves some carbonates and iron oxides; extraction 4 was based on stronger acetic acid and longer reaction time (pH 2.3 for 5 days) designed to dissolve carbonates (if present) and other phases; extraction 5 was an ammonium oxalate extraction designed to dissolve iron oxides (reaction time is 1 hr); and extraction 6 was an 8 M HNO_3 at 95°C (reacted for 2 hr) designed to dissolve the

remaining portion of sediment minerals. The 8 M HNO_3 extraction is a strong but incomplete digestion that is expected to dissolve elements that are potentially environmentally available. Sequential extractions 1 through 5 were conducted at a 1:2 sediment mass:liquid volume ratio at room temperature (20°C to 25°C).

Experiments were conducted on 19 pre- and post-injection sample pairs (from collocated six pre- and post-treatment boreholes) along with 6 additional post-injection samples collected from three non-paired post-injection boreholes. Results of sequential uranium extractions conducted on the 19 paired samples are summarized in Figure 4-28 as the fraction of total uranium extracted. Figure 4-29 presents the information in terms of relative change in uranium concentration for each extraction (relative to pre-treatment concentration). A comparison of changes in uranium sequential extractions shows that there is a loss in extraction 1 and 2 (the aqueous and adsorbed uranium) and in extraction 4 for nearly all sediment pairs, both in terms of uranium concentration (Figure 4-29a) and in fraction of total uranium (Figure 4-29b). There is a corresponding increase in extraction 6 for most sediments. Decreases in aqueous and adsorbed uranium are likely due to transient increase in flow during injection in addition to formation of calcium-phosphate minerals when in contact with the polyphosphate solution (Mehta et al., 2016; PNNL-21733, *Use of Polyphosphate to Decrease Uranium Leaching in Hanford 300 Area Smear Zone Sediment*). Supplemental solubility experiments were conducted to evaluate the effects of polyphosphate solutions on uranium leaching. Minerals typically associated with extractions 3 and 4 (e.g., moderate-solubility hydrous uranium silicates, such as uranophane and Na-boltwoodite, and uranium substituted in calcite) were found to be somewhat soluble is in these solutions. These findings suggest the decrease in extraction 4 and coincident increase in extraction 6 is an indication of dissolution of relatively soluble uranium bearing minerals present in the contaminated sediments and reprecipitation/co-precipitation of uranium with more stable calcium-phosphate and calcium-carbonate-phosphate solid phases (Mehta, 2017, "Geochemical evaluation of uranium sequestration from field-scale infiltration and injection of polyphosphate solutions in contaminated Hanford sediments"). Extraction experiments indicate various mechanisms binding uranium in sediments with a range of uncertainty concerning any one mechanism's (e.g., specific mineral phase present in what abundance, etc.).

Extractions 3 through 5 are most generally associated with mineral phases in sediments. Iron and calcium were among the many metals measured during sequential extraction experiments, used as proxy for quantifying iron-bearing reactive mineral phases and calcite, respectively. Figure 4-30a shows results for extractions 3, 4, and 5 for iron while Figure 4-30b provides results for extractions 3 and 5 for calcium in pre-treatment sediment samples. Extraction 4 is excluded from calcium analysis as the solution is primarily composed of $Ca(NO_3)_2 \bullet 4H_2O$. The majority of iron in sediments is from extraction 5, with decreasing amounts in extractions 4 and 3, having an average total combined iron content of approximately 500 μg/g. For calcium, extraction 3 holds the highest concentration followed by extraction 5. An average total calcium concentration of approximately 400 μg/g was found for pre-treatment samples, though the total is likely greater assuming equivalent concentrations would occur in extractions 3 and 4.

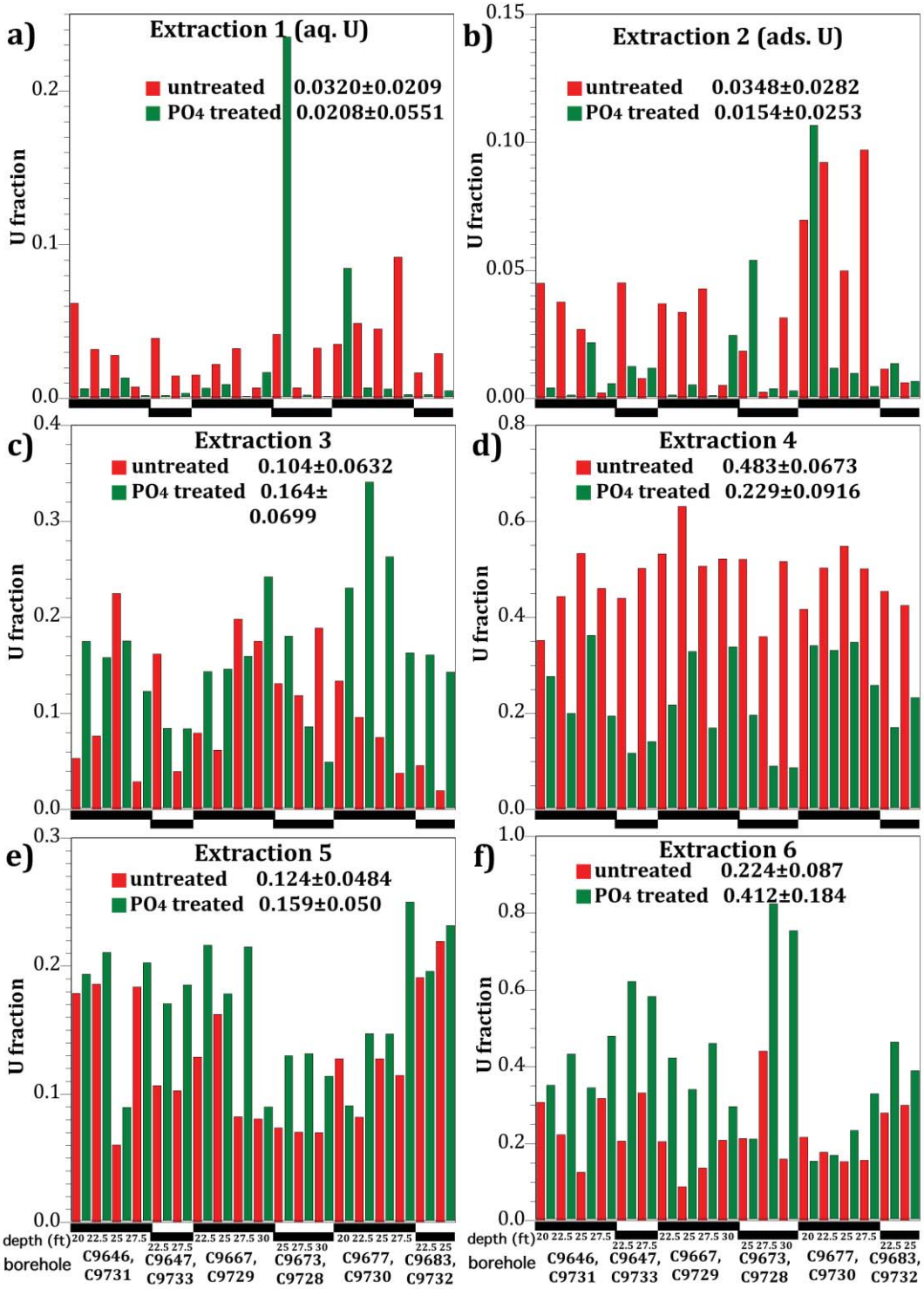

Source: Figure 4.17, PNNL-29650, *Evaluation of the Change in Uranium Mobility in Sediments from Hanford 300-FF-5 Stage B Polyphosphate Field Injection*.

Note: Pre-treatment samples are indicated as "untreated" while post-treatment samples are indicated as "PO4 Treated."

Figure 4-28. Average Change of the Uranium Fraction in 19 Pre- and Post-Treatment Pairs Based on Sequential Extractions

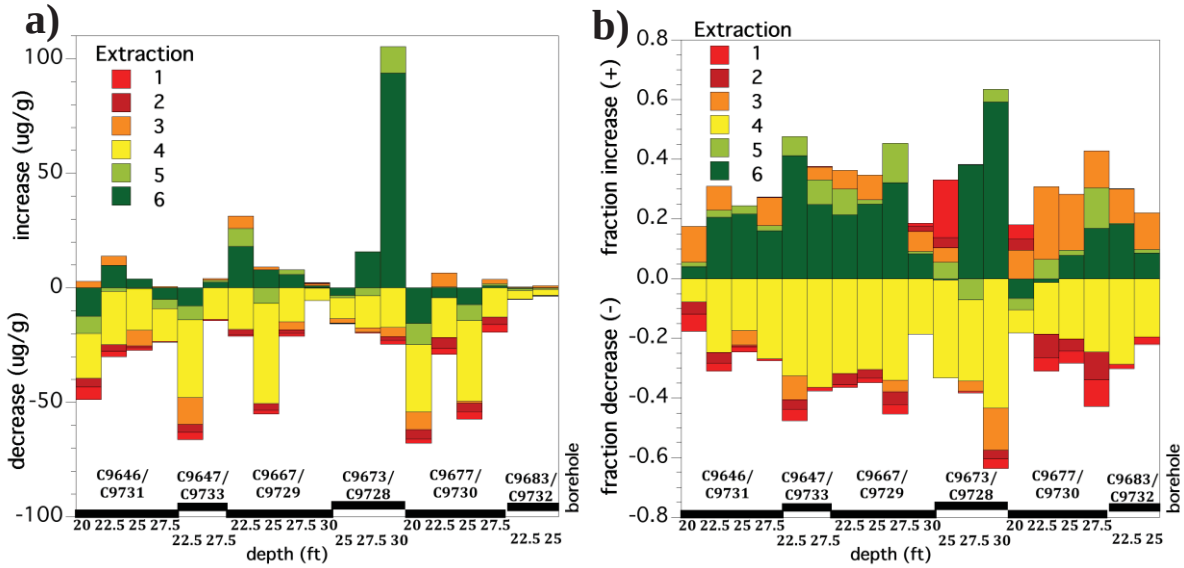

Source: Figure 5.4, PNNL-29650, *Evaluation of the Change in Uranium Mobility in Sediments from Hanford 300-FF-5 Stage B Polyphosphate Field Injection*.

Note: Results presented relative to the pre-treatment sample values.

Figure 4-29. Change in Uranium Sequential Extractions among 19 Pairs of Sediment Samples, in terms of a) Uranium Concentration (µg/g), and (b) Fraction of Total Uranium

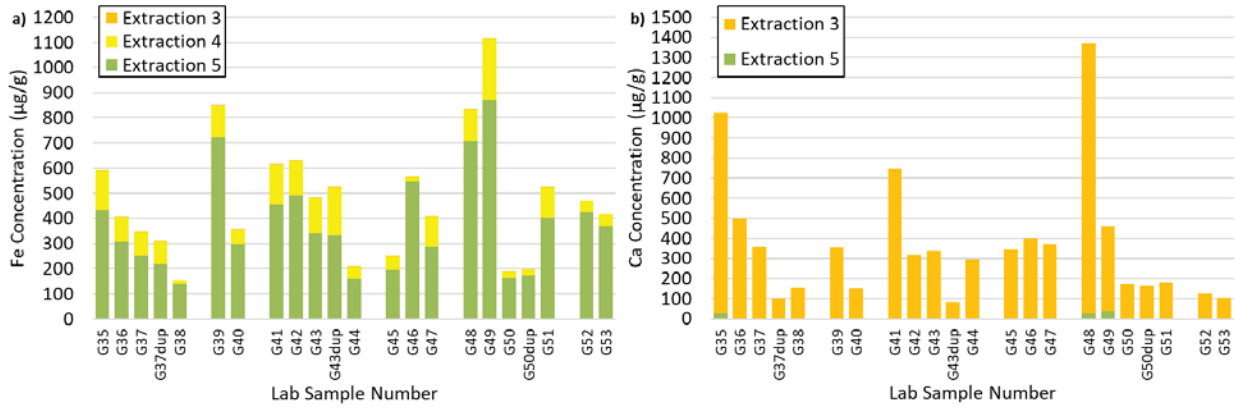

Figure 4-30. a) Iron Concentration, and b) Calcium Concentration in Pre-treatment Sample Sequential Extraction Results

4.1.5.3 Select Flow-Through Column Leaching Tests

1-D column leaching experiments were conducted with pre- and post-treatment sediments to measure the change in uranium mobility (i.e., uranium mass and concentration released) as a result of the field-injected phosphate treatment, and to measure the rate of uranium release from the sediment (PNNL-29650). These 1-D column leach tests were conducted on 10 pairs of pre- and post-treatment sediments along with four additional post-treatment sediments. In these experiments, approximately 100 pore volumes of artificial groundwater were injected into the sediments and effluent samples were collected and analyzed for uranium concentration. A bromide tracer was added to the artificial groundwater in order to track breakthrough of the injected groundwater.

Select column leaching pre-/post-treatment sample pair results from C9683/C9732 (22.5-25 ft depth interval) and C9673/C9728 (27.5-30 ft and 30-32.5 ft depth intervals) are shown in Figure 4-31. For all sample pairs, initial effluent uranium concentrations decrease rapidly within the first 10 pore volumes and remain steady for the remainder of the experiment except for the sample from C9728 30-32.5 ft interval which continues to decrease slowly. For both the C9683/C9732 sample pair and C9673/C9728 30-32.5 ft interval sample pair, the post-treatment sample shows a significantly lower initial concentration by approximately two orders of magnitude with respect to the pre-treatment sample. In the case of the C9673/C9728 27.5-30 ft interval sample pair, the post-treatment initial uranium concentration is lower than the pre-treatment sample, though only by approximately one order of magnitude.

For all three sample pairs, cumulative fraction of uranium removed during column leaching experiments was greater in pre-treatment samples than post-treatment samples. With total whole sediment uranium soil concentrations of 3.19 and 0.383 µg/g for samples from C9683 and C9732, respectively, cumulative fraction of uranium removed from the system shows pre-treatment sample removes roughly 21% of the uranium while post-treatment sample removes ~6% (Figure 4-31a). C9673/C9728 27.5-30 ft interval sample pair have total whole sediment uranium soil concentrations of 18.04 and 12.05 µg/g, respectively, and roughly 6% of the uranium removed in pre-treatment sample while post-treatment sample removes ~1% (Figure 4-31b). Finally, the cumulative fraction of uranium removed for the C9673/C9728 30-32 ft interval sample pair (whole sediment uranium soil concentrations of 18.40 and 29.13 µg/g, respectively) was ~72% in the pre-treatment sample and ~1% in the post-treatment sample (Figure 4-31c).

Comparing all pre- to post-injection leach experiments, there was a 59.9 ± 53.8% decrease in uranium leaching, as defined from the fraction leached to total uranium for each leach experiment (PNNL-29650). Of the 10 pre-/post-injection pairs, 9 pairs showed a decrease in uranium leaching for the post-injection experiment, and 1 pair showed an increase (Figure 4-32). The change in uranium leaching was dependent on the amount of phosphate (if any) delivered to that location, defined by aqueous phosphate in the first few effluent samples of each leach experiment. Of 13 post-injection sediments, 10 received high phosphate and, as a result, had a large decrease in uranium leaching compared to pre-injection sediments. In contrast, three post-injection sediments show that (after 6 months) low phosphate or no detectable aqueous phosphate was present. These locations showed little decrease in uranium leaching (i.e., the fraction uranium leached was similar to untreated sediments), which implied that little phosphate precipitated at these locations.

Effluent pH was also monitored during column leaching experiments. A comparison of selected pre- and post-injection pairs are provided in Figure 4-33 for the first couple of pore volumes. In general, post-treatment effluent samples were higher in pH than their corresponding pre-treatment pair, ranging from approximately 8 to 9.4. Changes in pH suggest geochemical reactions occurring in sediments as a result of remedy solution injections as both ambient sediment porewater pH (varies from 7.5 to 8.5) and remedy solution pH (varies from 7.4 to 7.6) are appreciably lower.

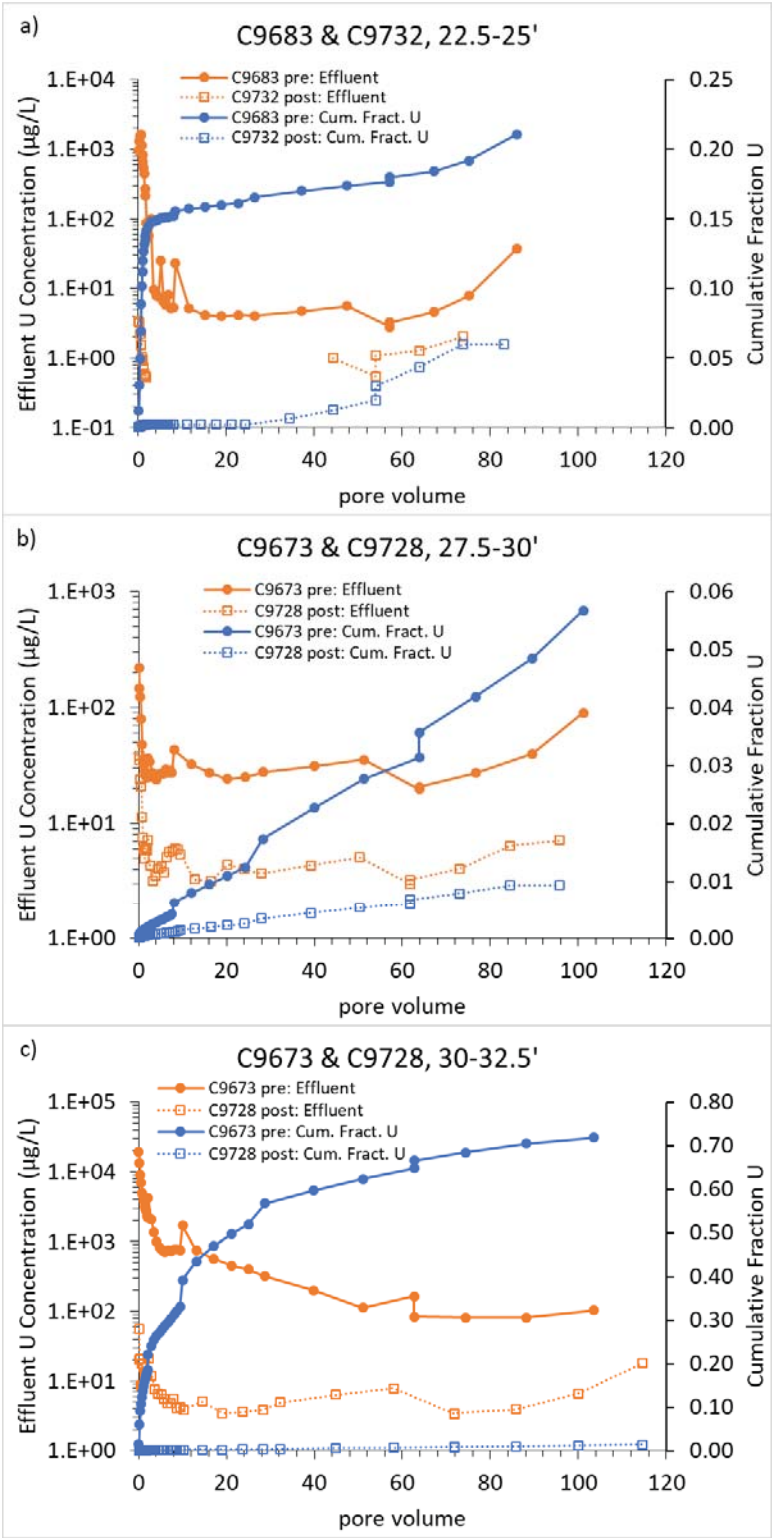

Figure 4-31. Effluent Uranium Concentration and Cumulative Fraction Uranium Removed Column Leaching Experiment Results for a) C9683/C9732 22.5-25 ft Interval, b) C9673/C9728 27.5-30 ft Interval, and c) C9673/C9728 30-32.5 ft Interval Sample Pairs

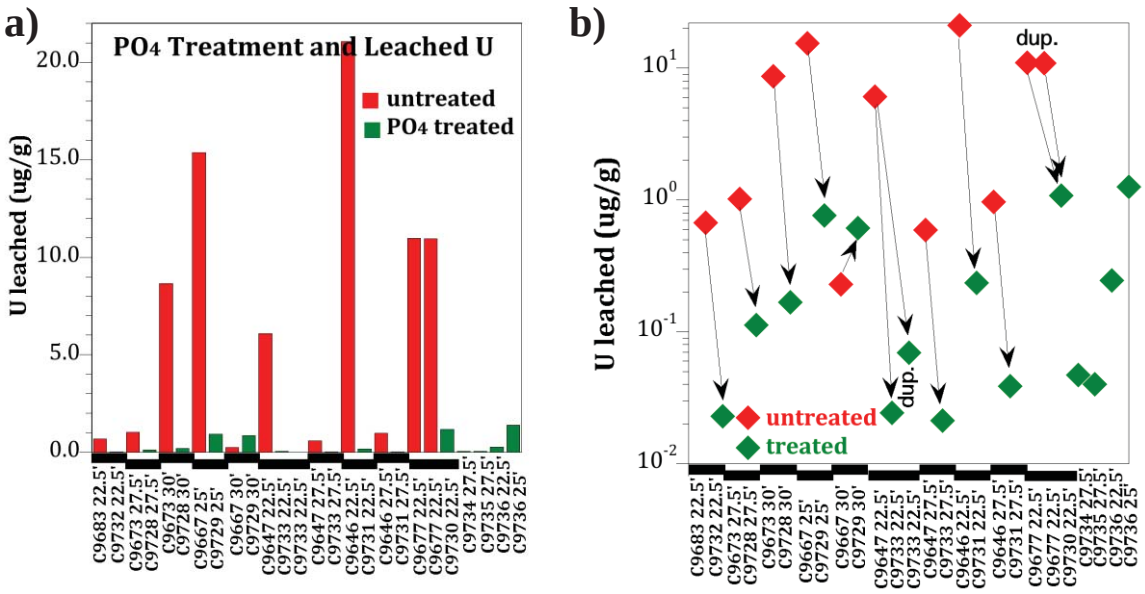

Reference: PNNL-29650, *Evaluation of the Change in Uranium Mobility in Sediments from Hanford 300-FF-5 Stage B Polyphosphate Field Injection*.

Figure 4-32. Change in Uranium Mass Leaching among Pre- and Post-Treatment Sample in 1-D Column Experiments: (a) Linear Scale, and (b) Log Scale

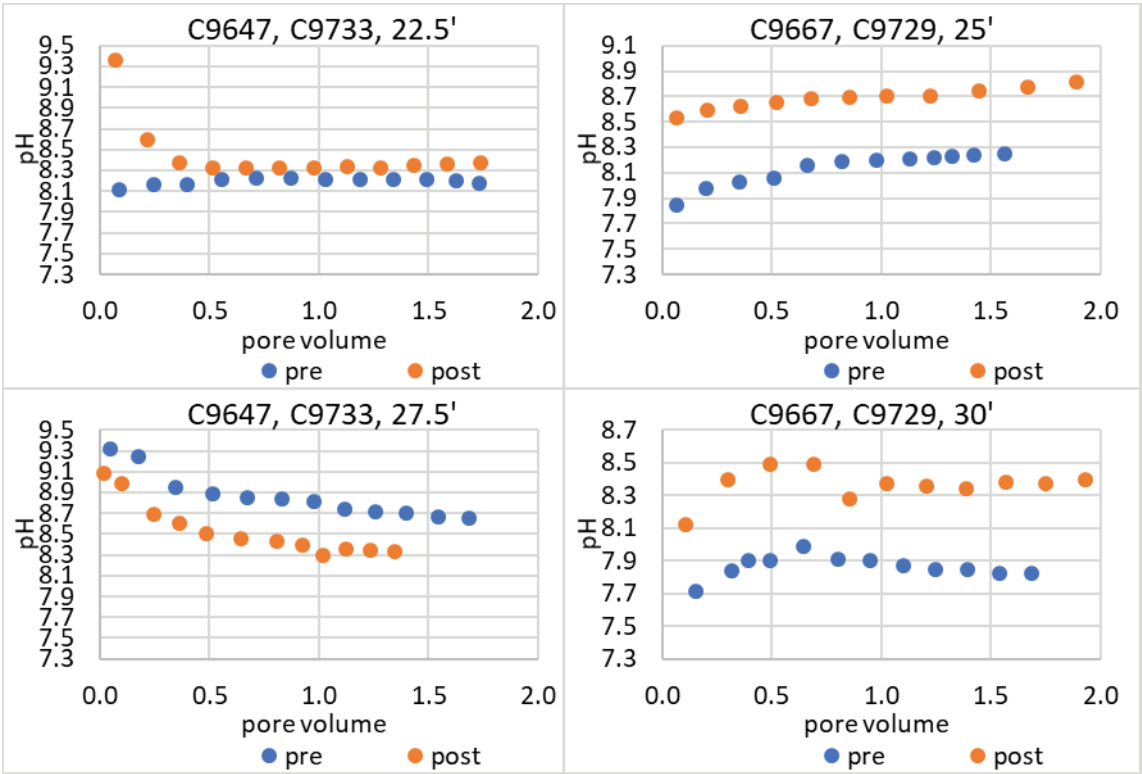

Figure 4-33. Effluent pH as a Function of Pore Volumes for Select Pre-treatment and Post-Treatment 1-D Column Leaching Experiments

4.1.5.4 Labile Uranium Batch Test

A total of 42 sediment 1000-hour batch carbonate extractions were conducted by PNNL to evaluate the leachable uranium mass from 10 pre-/post-treatment sample pairs and three un-paired post-treatment samples (PNNL-29650). Figure 4-34 shows the fraction of uranium mobility change from pre-treatment to post-treatment sample analysis due to polyphosphate injections. The mobile fraction uranium for pre-injection (i.e., untreated) sediments was 0.425 ± 0.096, and for post-injection samples is 0.156 ± 0.143, or an average of 63% less mobile uranium as a result of the polyphosphate treatment.

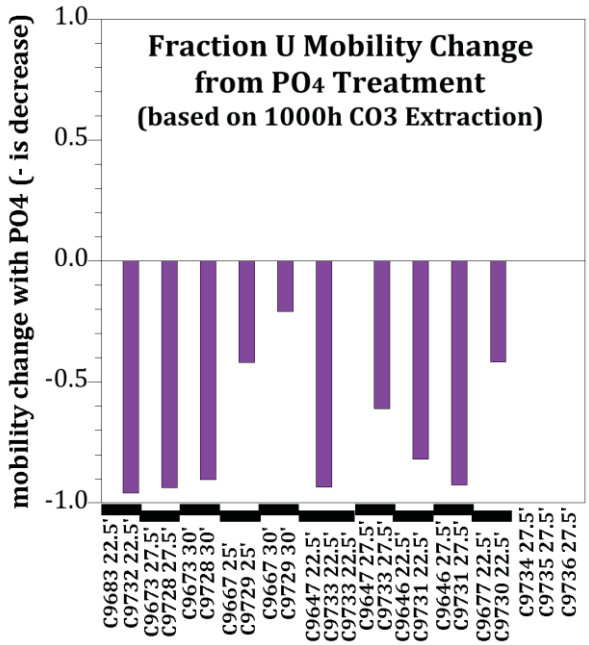

Source: PNNL-29650, *Evaluation of the Change in Uranium Mobility in Sediments from Hanford 300-FF-5 Stage B Polyphosphate Field Injection*.

Figure 4-34. Change in Uranium Mobility as Shown in 1000-hr Carbonate Extractions on 10 Pre- and Post-Treatment Pairs of Sediments

4.1.5.5 Identification of Mineral Phases Using Surface Analysis

A suite of low detection solid phase characterization techniques was conducted by PNNL on pre- and post-treatment sediment samples as uranium soil concentrations ranged from 0.3 to 140 µg/g (Section 4.1.5.1). Measurements were conducted at the Advanced Photon Source (APS) at Argonne National Laboratory using micro X-ray fluorescence (µ-XRF), micro extended X-ray absorption fine structure (µ-EXAFS), and micro X-ray absorption near-edge spectroscopy (µ-XANES; for uranium valence state). Additional elements were identified using a scanning electron microscope (SEM) to better identify potential uranium minerals.

2-D elemental mapping using XRF, XANES, and EXAFS indicate uranium coincident with copper consistent with previous studies identifying metatorbernite ($Cu(UO_2)_2(PO_4)_2 \cdot 8H_2O$) in the 300 Area (Arai et al., 2007, "Spectroscopic Evidence for Uranium Bearing Precipitates in Vadose Zone Sediments at the Hanford 300-Area Site"). Uranium was also shown to be associated to a lesser extent with iron and calcium (PNNL-29650). Calcium was identified surrounding uranium minerals and is assumed to be associated with apatite group coatings on particles. SEM measurements showed colocation of calcium and phosphorus in both pre- and post-treatment samples, with copper and phosphorus colocation identified only in post-treatment samples. Similarities in µ-EXAFS autunite and torbernite spectra did not allow for

specific identification of either mineral in sediment samples, though spectra fits to reference samples qualitatively associate uranium-phosphate minerals present in both pre- and post-treatment samples.

4.2 Three-Dimensional Reactive Transport Modeling

The purpose of this section is to describe the assumptions made for simulating the reactive fate and transport of uranium in the vadose zone and unconfined aquifer near the injection wells of the Stage B EAA. The modeling results are used to assess geochemical processes impacting uranium mobility and support larger scale fate and transport modeling. Previous work conducted by Mehta et al., 2016, present multiple mechanisms for uranium sequestration via phosphate addition for in situ remediation including: sorption of aqueous uranium to calcium phosphate solids (e.g., hydroxylapatite); formation of uranium bearing minerals including autunite; and uranium incorporation in calcium phosphate solids (Figure 4-35).

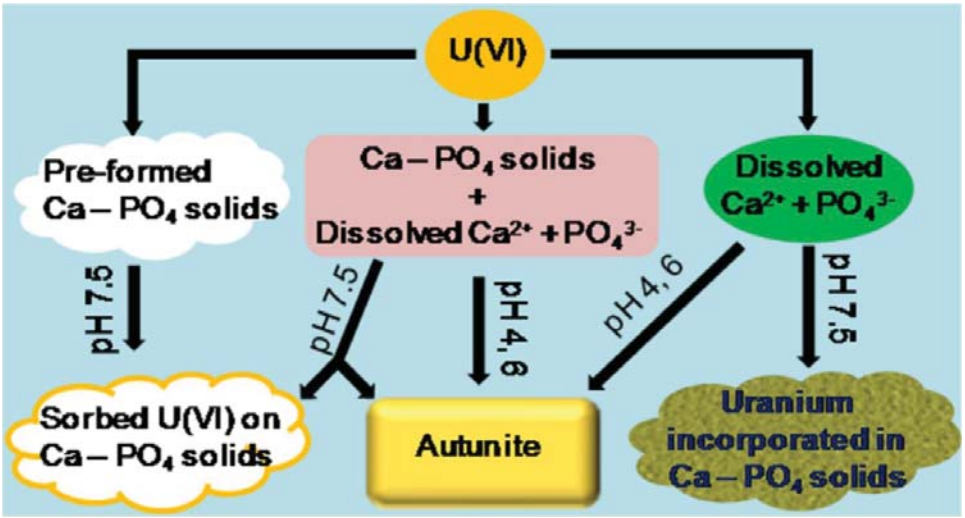

Figure 4-35. Uranium Sequestration Mechanisms via Phosphate Addition as an In-Situ Remediation Approach

A conceptual model of the 300-FF-5 OU is first developed, similar to the one developed during Stage A remedy evaluation (Mehta, 2017), by incorporating features, events, and processes that control uranium transport through the subsurface:

- Variably saturated flow conditions will exist during and following the injection of polyphosphate solutions in the vadose zone and need to be modeled appropriately given the non-linear change in unsaturated hydraulic conductivity as a function of saturation.
- Spatially and temporally varying concentrations of polyphosphate will exist in the vadose zone as the radius of injection expands leading to concentration gradients.
- The impact of injection on flow in the vadose zone and saturated zone needs to be considered in three dimensions.
- Ion-exchange reactions will occur as the available in-situ calcium exchanges with injected sodium and potassium rich solutions. Exchange sites on clay minerals have to be accounted.
- Surface complexation of uranium with iron (and manganese) mineral reactive surfaces present in the subsurface need to be considered.

- Impact of formation of calcium-phosphate solid precipitates and their effect on uranium leaching rates needs to be considered given that the past studies have shown uranium release to be kinetically controlled.
- Variability in geochemical evolution due to subsurface heterogeneity (as evidenced by ERT) needs to be considered when upscaling the parameters.

Though each mechanism is identified in uranium sequestration via phosphate injection (Mehta et al., 2016), little is understood on the individual component kinetic rates in a complex system. The approach taken in this ECF is to model the bulk uranium release behavior as determined by 1-D column leaching experiments described in Section 4.1.5.3. The bulk kinetic release behavior describes the rate of loss as a combination of all mechanisms relevant to uranium release including desorption and mineral dissolution. Two bulk kinetic release behaviors are defined as shown in Figure 4-36: Pre-remedy solid phase uranium representing bulk leaching behavior prior to injections and uranium incorporated and sorbed to calcium phosphate solids representing post-injection bulk leach behavior for regions impacted by polyphosphate treatment. Prior to injections (Initial Conditions, Figure 4-36), uranium is transformed from the pre-remedy solid phase to dissolved uranium at a rate defined by pre-injection 1-D column leaching experiments. The dissolved uranium can then interact with iron oxide reactive surface sites via surface complexation. The surface complexation reaction is assumed to be a rapid exchange when thermodynamically favorable and implemented as an equilibrium model.

As no bulk kinetic dissolution rates were explicitly measured during the time of injections, the rates measured using post-injection samples was applied. The post-injection bulk kinetic release rate of uranium occurs due to calcium phosphate precipitation reactions that either incorporate uranium as impurities or acts as a coating with phases (e.g., hydroxylapatite) that reduce uranium leachability. Similar to the initial conditions, uranium is transformed from the solid phase to dissolved uranium at a rate defined by post-injection sample 1-D column leaching experiments. A generalized assumption is made that only one uranium bulk kinetic release rate can occur at a single point in space and time: either by pre-injection bulk kinetic release rate or by post-injection bulk kinetic release rate for locations without or with polyphosphate solution present, respectively. Furthermore, any available dissolved uranium species could bind with phosphate instantaneously and form microcrystalline uranium bearing mineral phases under thermodynamically favorable conditions. Rates associated with the uranium mineral precipitation are undefined at this time. Instead, precipitation reactions are assumed to occur instantaneously as defined by an equilibrium model. Experimental analyses of uranium mineral phase identification were inconclusive (Section 4.1.5.5). Moreover, what uranium mineral phases did precipitate proved to be incredibly small (microns in size) and likely not the dominant driver in uranium kinetic release post remedy injection.

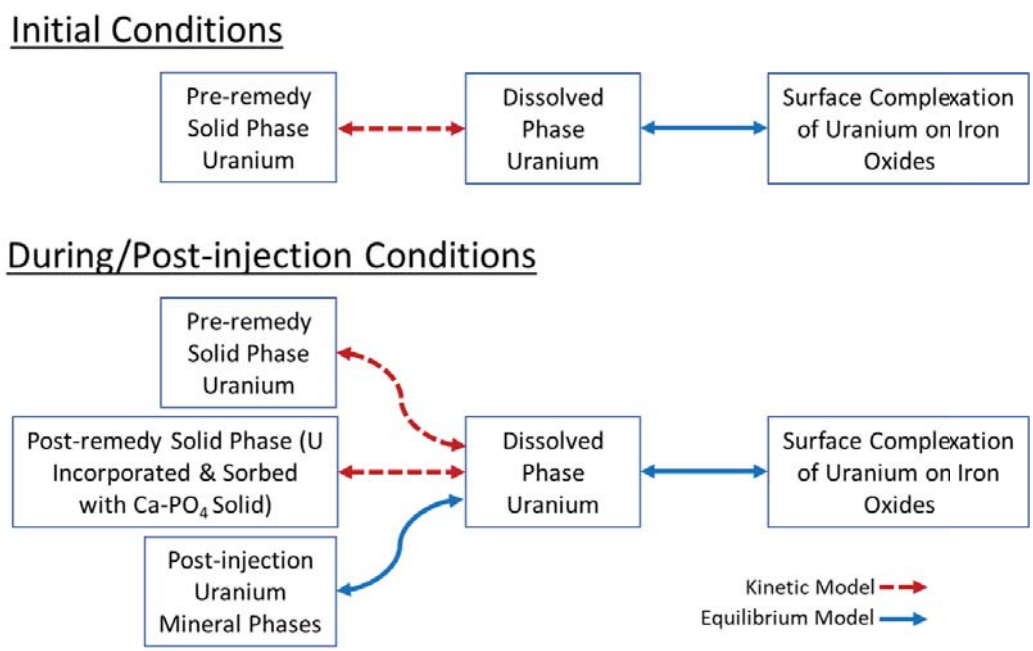

Figure 4-36. Uranium Conceptual Model Implementation

The 3-D simulation of a single generalized injection well is undertaken to evaluate the geochemical impacts during and directly after polyphosphate injections into the PRZ and LVZ on uranium mobility in the vadose zone and unconfined aquifer. The results can be considered representative of conditions that would exist within the Stage B injection area. Because the 3-D axisymmetric model is constructed using radial coordinates to simulate the injection well (at the axis of model) a radial symmetry is assumed. In order to evaluate the effect of injection in aquifer under natural gradient conditions, a supplemental 2-D simulation in cartesian coordinates was developed, which provides insight on groundwater flow impacts on uranium mobility in the unconfined aquifer. An additional 3-D simulation was conducted to evaluate the impact of a generalized heterogeneous unsaturated zone on geochemical evolution during remedy injections.

4.2.1 Bulk Uranium Kinetic Rate Model Description

The flow-through column leach experiments described in Section 4.1.5.3 provide useful information for quantifying bulk desorption/dissolution rates of uranium from site specific samples. Three stop flow events were included in the experiment to evaluate release rates under stagnant conditions. While these rates are determined under fully saturated conditions they are being applied to unsaturated conditions without any further adjustments. Numerical modeling was conducted to estimate the bulk kinetic rates for 26 samples as described in ECF-300FF5-19-0086. A one-dimensional flow through model simulating infiltrating artificial groundwater spiked with bromide was designed to evaluate the estimated bulk kinetic rate parameters implementation in VS2DRTI.

The bulk kinetic sorption parameter estimation is modeled by forward and reverse reaction rates (ECF-300FF5-19-0086). The forward reaction rate (α_f) is defined as the mass transfer from the liquid phase to the solid phase while the reverse reaction (α_r) is the mass transfer from the solid to liquid phase.

The forward/reverse reaction rate constants are related by the following equation:

$$\alpha_r = \frac{\alpha_f}{K_d}\left(\frac{\theta}{\rho_b}\right) \quad \textbf{(Eq. 4-1)}$$

where:

α_r: reverse reaction rate constant (desorption) $[hr^{-1}]$

α_f: forward reaction rate constant (sorption) $[hr^{-1}]$

ρ_b: bulk density, matrix mass/bulk volume g/cm^3

θ: volumetric moisture content, water volume/bulk volume [dimensionless]

K_d: distribution coefficient, volume water/matrix mass $[mL/g]$.

The dissolved phase concentration based on sorption-desorption reaction rate constants can be defined as:

$$\frac{\partial C}{\partial t} = -(\alpha_f C - \alpha_r M) \quad \textbf{(Eq. 4-2)}$$

where:

C: dissolved mass of uranium per unit water volume $[\mu g_{U_diss}/mL_{water}]$

M: Uranium mass on Solid per unit water volume, $[\mu g_{U_solid}/mL_{water}]$.

The above equation can be rewritten as follows by combining Eq. 4-1 and 4-2:

$$\frac{\partial C}{\partial t} = -[\alpha_f C - \frac{\alpha_f}{K_d}\left(\frac{\theta}{\rho_b}\right) M] = -\alpha_f[C - \frac{M}{K_d}\left(\frac{\theta}{\rho_b}\right)] \quad \textbf{(Eq. 4-3)}$$

Metatorbernite [$Cu(UO_2)_2(PO_4)_2 \cdot 8H_2O$], uranophane [$Ca(UO_2)_2(HSiO_4)_2 \cdot 5H_2O$], disordered uranyl carbonate, and uranium adsorbed to muscovite (Arai et al., 2007; McKinley et al., 2007, "Geochemical controls on contaminant uranium in vadose Hanford formation sediments at the 200 area and 300 area, Hanford site Washington") following disposal of approximately 50 tons of copper and 30 tons of uranium to the North Process Pond (NPP) (WHC-MR-0440, *Multiple Missions: The 300 Area in Hanford Site History*) are well-documented mineral phases identified in sediments under the NPP (Wang et al., 2005, "Cryogenic laser induced U(VI) fluorescence studies of a U(VI) substituted natural calcite: Implications to U(VI) speciation in contaminated Hanford sediments"; PNNL-17031, *A Site-Wide Perspective on Uranium Geochemistry at the Hanford Site*). For the purpose of this model, all available uranium in the solid phase is assumed to be present as either generalized uranium solid or uranium incorporated and sorbed to calcium phosphate solids representing pre-treatment or post-treatment uranium solid phase assemblage, respectively (Figure 4-37). In doing so, the effective uranium release rate (R_U), in units of moles/Liter/second, is defined in terms of dissolved concentration and available solid phase uranium mass per unit water volume M_{U_solid} $[mol/L]$ assuming fully saturated conditions:

$$R_U = -\alpha_f * [C - \frac{M_{U_{solid}}}{K_d}\left(\frac{\theta}{\rho_b}\right)] \quad \textbf{(Eq. 4-4)}$$

As a result, when R_U is positive, uranium is released to solution.

Numerical modeling results for bulk kinetic rate parameter estimation are provided in Figure 4-37 (ECF-300FF5-19-0086). When comparing pre-treatment and post-treatment sample results, forward reaction rates showed little change between samples while reverse rates generally decreased from pre-

treatment to post-treatment samples (Figure 4-37a). As a result, an average ten-fold increase is observed between pre-treatment and post-treatment distribution coefficient (K_d) values (Figure 4-37b).

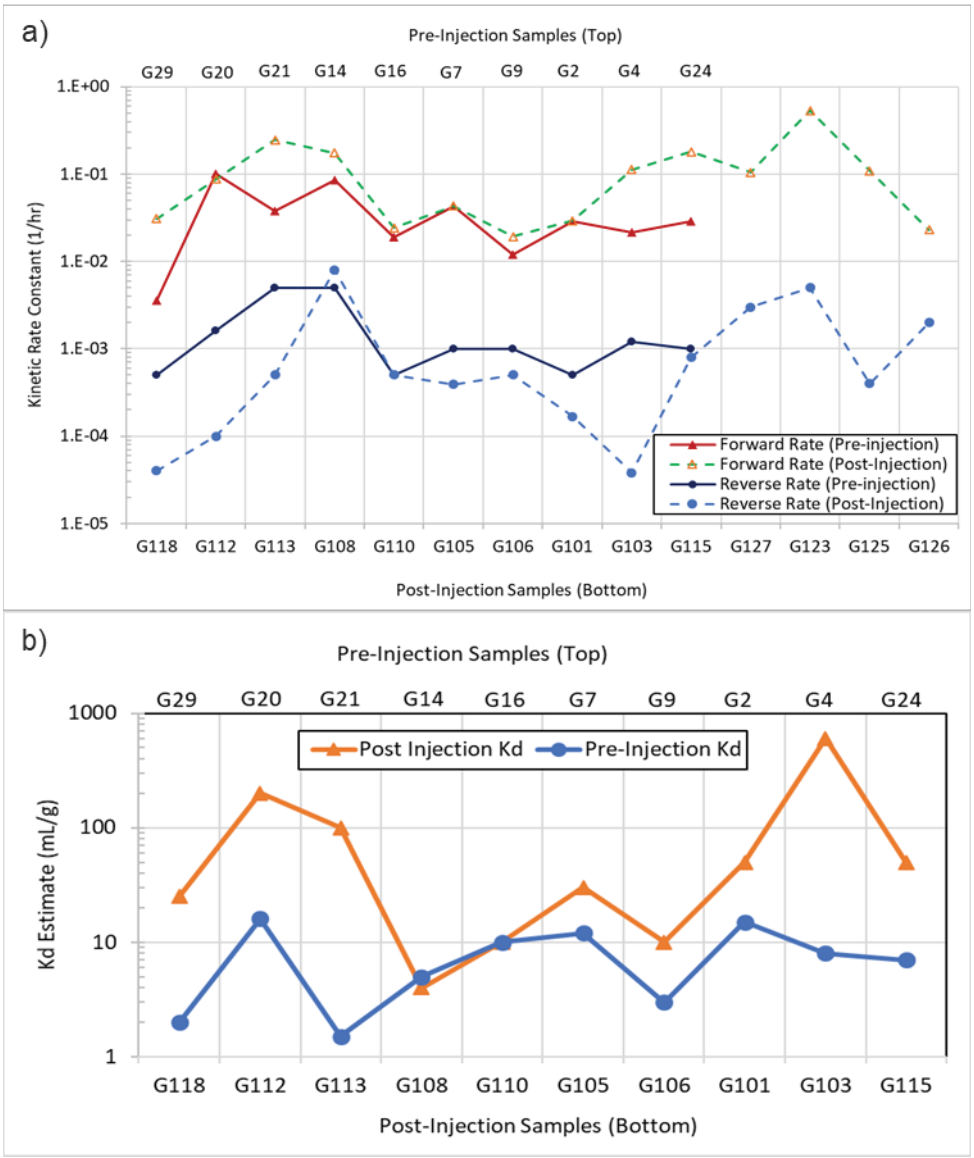

Note: Refer to Table 3.1 of PNNL-29650, *Evaluation of the Change in Uranium Mobility in Sediments from Hanford 300-FF-5 Stage B Polyphosphate Field Injection*, for sample IDs.

Figure 4-37. Numerical Modeling Results For 1-D Column Leaching Kinetic Rate Parameter Estimation for a) Forward and Reverse Rate Constants, and b) Kd Estimates

5 Software Applications

The primary software selected for geochemical evaluation during Stage B EAA remedy injections is VS2DRTI (developed by United States Geological Survey [USGS]: Healy et al., 2018). This is a CH2M HILL Plateau Remediation Company (CHPRC) approved software, managed and used in compliance with the requirements of PRC-PRO-IRM-309, *Controlled Software Management*. This selection was based on the following considerations:

1. VS2DRTI software is actively managed by CHPRC and approved for use at the Hanford Site as Level D software under a procedure that implements the requirements of DOE O 414.1D, *Quality Assurance*.

2. VS2DRTI software includes the tools a user needs to create, run, and view results for a simulation of flow and heat and reactive solute transport through variably saturated porous media.

VS2DRTI use in the development and application of the model described in this ECF is managed under the requirements of CHPRC-04166, *VS2DRTI Software Management Plan*.

Version 1.4 of the VS2DRTI software was used in the implementation of the models described in this ECF. This version was approved for use at the Hanford Site based on the status of requirements for this software and acceptance testing results reported in CHPRC-04168, *VS2DRTI Acceptance Test Report and Requirements Traceability Matrix*. All acceptance testing was performed to the requirements of CHPRC-04167, *VS2DRTI Software Test Plan*. Installation testing is also required for any computer system on which VS2DRTI (and hence, this calculation) is run. The installation test is specified in CHPRC-04167.

VS2DRTI is a graphical software package which utilizes VS2DRT (Haile, 2013, "VS2DRT: Variable saturated two dimensional reactive transport modeling in the vadose zone") as its underlying numerical model. VS2DRT links the VS2DT model for simulating solute transport (Healy, 1990, "Simulation of solute transport in variably saturated porous media with supplemental information on modifications to the U.S. Geological Survey's computer program VS2D"), VS2DH model for simulating heat transport (Healy and Ronan, 1996, "Documentation of computer program VS2DH for simulation of energy transport in variably saturated porous media: Modification of the U.S. Geological Survey's computer program VS2DT") and PhreeqcRM modules for simulating chemical equilibrium and kinetic reactions (Parkhurst and Wissmeier, 2015, "PhreeqcRM: A reaction module for transport simulators based on the geochemical model PHREEQC"). PhreeqcRM performs equilibrium and kinetic reaction calculations in conjunction with multicomponent solute-transport simulators with all the capabilities of the general-purpose geochemical reaction model PHREEQC (Parkhurst and Wissmeier, 2015). VS2DT calculates flow and transport equations independently from geochemical reactions using an operator-splitting approach. The flow, heat and solute transport equations are solved at each time step allowing simulated concentrations to be transported by advection and dispersion (Healy et al., 2018). Chemical concentrations for each model cell are then passed to PhreeqcRM to calculate geochemical reactions and returned to each model cell.

The Geochemist's Workbench (GWB) software was also used as a qualitative comparison tool to compare against VS2DRTI results. This is a CHPRC approved software, managed and used in compliance with the requirements of PRC-PRO-IRM-309. This selection was based on the following considerations:

1. GWB software is actively managed by CHPRC and approved for use at the Hanford Site as Level C software under a procedure that implements the requirements of DOE O 414.1D.

2. GWB software all the tools a user needs to create, run, and view results for mineral phase diagrams.

GWB use in the development and application of the model described in this ECF is managed under the requirements of CHPRC-01874, *The Geochemist's Workbench Integrated Software Management Plan: Version 12.0.4*.

Version 12 of the GWB software was used in select figure generation of this ECF. This version was approved for use at the Hanford Site based on the status of requirements for this software and acceptance testing results reported in CHPRC-01874 Section 15. All acceptance testing was performed to the requirements of CHPRC-01874 Section 14. Installation testing is also required for any computer system on which GWB (and hence, this calculation) is run. The installation test is specified in CHPRC-01874 Section 18.

5.1 Approved Software

For approved software used in this calculation, the required descriptions are provided in the following subsections.

5.1.1 Description

The following information has been identified for the VS2DRTI software package used in the calculation:

- Software Title: VS2DRTI
- Software Version: 1.4
- HISI Identification Number: 4582 (Level D)
- Workstation type and property number: Thinkpad Laptop INTERA-00873

The following information has been identified for the GWB software package used in the calculation:

- Software Title: Geochemist's Workbench
- Software Version: 12.0.4.0
- HISI Identification Number: 3845 (Level C)
- Workstation type and property number: INTERA-Blue

5.1.2 Software Installation and Checkout

A copy of the Software Installation and Checkout Form for the authorized user and workstation for the software used (VS2DRTI and GWB) that requires this documentation are provided in Appendix E to this ECF.

5.1.3 Statement of Valid Software Application

The preparers of this calculation attest that the software identified and used for this calculation is appropriate for the application and has been within the range of intended uses for which it was tested and accepted by CHPRC.

6 Calculation

This section discusses observations made during and following Stage B treatment operations relevant to reactive transport modeling. A conceptual model is first developed using field-scale and lab-scale data. 3-D reactive transport modeling is implemented based on the conceptual model. Uncertainty analysis of the unsaturated zone is evaluated by use of a 3-D heterogeneity model in the unsaturated zone.

6.1 One-Dimensional Column Leaching Simulations

This section provides model settings for the one-dimensional column leaching simulations. The purpose of these simulations was to evaluate the implementation of the kinetic sorption parameter estimation results using VS2DRTI by way of the Kinetics and Rates cards in PHREEQC. Sample pair G21 from borehole C9673 and G113 from borehole C9728 was selected as representative column leaching pre-treatment and post-treatment pair, respectively. The basic model setup includes assigning all units in terms of meters, hours, grams, and Joules with respect to length, time, mass, and energy. Simulating solute transport is selected to allow for reactive transport modeling. Flow options are comprised of pressure head contour assignment to specify the initial hydraulic conditions, arithmetic mean for computing relative intercell hydraulic conductivity, and tabular data for calculating hydraulic flow. Transport calculations are based on the finite differencing scheme centered in space and backward in time. Table 6-1 outlines the model solver options and corresponding values.

Table 6-1. One-Dimensional Column Leaching Simulation Solver Options

Parameter	Value
Relaxation Parameter	0.7
Minimum iterations per time step	2
Maximum iterations per time step	100
Maximum number of time steps	100,000
Closure criteria for head	1e-4
Closure criterion for concentration	1e-4

A one-dimensional model domain was designed such that the diameter and length of the column match the experimental setup of approximately 2.0 cm and 31 cm, respectively. A grid spacing with a width of 2 cm and length of 1 cm was used with a total of 30 nodes (Figure 6-1).

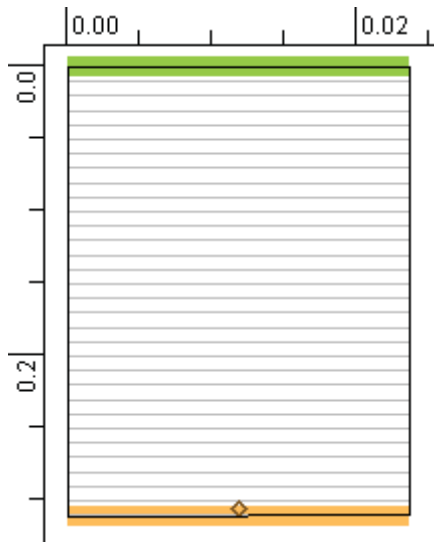

Note: Units in meters

Figure 6-1. The One-Dimensional Column Leaching Simulation Domain

Chemistry domains can be assigned for specific solution chemistries, equilibrium phases, exchange phases, surface phases, gas phases, solid solutions, and kinetic releases defined in the corresponding PHREEQC input file. A given Solution, Equilibrium Phase, Exchange, Surface, Gas, Solid Solution, and Kinetics PHREEQC card is assigned a number which can be read by VS2DRTI. A single chemistry class is defined for these one-dimensional column leaching simulations are shown in Table 6-2. Three solutions are defined in the simulation representing the initial column porewater, artificial groundwater injection solution spiked with bromide, and artificial groundwater solution without bromide compositions for Solutions 1, 2, and 3, respectively. Corresponding PHREEQC input cards are provided in Appendix C of this document.

Table 6-2. One-Dimensional Column Leaching Simulation Chemistry Class Assignment [a]

Name	Solution	Equilibrium Phases	Exchange	Surface	Gas Phase	Solid Solution	Kinetics
Inactive [b]	-1	-1	-1	-1	-1	-1	-1
Initial Concentration	1	-1	-1	-1	-1	-1	1
Artificial Groundwater w/ Br	2	-1	-1	-1	-1	-1	1
Artificial Groundwater w/out Br	3	-1	-1	-1	-1	-1	1

a. A value of -1 is assigned to deselect a card from the chemistry class.

b. Inactive class is used to define the domain extents.

Recharge periods are used to define changes in boundary conditions (e.g., periods of artificial groundwater flow and stop flow events) over specified lengths of time. This model follows the 1-D column leaching experimental setup such that three flow events and two stop flow events take place. The complete set of five recharge periods and corresponding criteria are outlined in Table 6-3.

Table 6-3. One-Dimensional Column Leaching Simulation Recharge Periods

Number	Period Length	Initial TS	TS Multiplier	Max. TS	Min. TS	TS Red. Factor	Max Head Change	SS Head Criterion	Max Ponding Height
1	3.8	0.01	1.2	0.5	0.5	0	100	0	0
2	50.8	0.01	1.2	0.5	0.5	0	100	0	0
3	14.7	0.1	1.2	0.5	0.5	0	100	0	0
4	79.6	0.1	1.2	0.5	0.5	0	100	0	0
5	104	0.1	1.2	0.5	0.5	0	100	0	0

SS = steady-state
TS = time step

Artificial groundwater injection fluid flux (Q, *mL/hr*) and stop flow times were recorded for each 1-D column leach experiment (PNNL-29650). An average vertical Darcy velocity (q, *m/hr*) was applied at the top of the model boundary by the following equation:

$$q = \frac{Q}{\pi(\frac{d}{2})^2} \qquad \textbf{(Eq. 6-1)}$$

where *d* is the measured diameter of the flow through column (Table 6-4). Small vertical Darcy velocities of <1e-7 m/hour were applied during stop flow events to allow the model to run. A seep face was applied to the outflow boundary for all time periods. Table 6-4 defines the corresponding inflow boundary condition as specified flux into the domain assigned by each recharge period (Table 6-3, periods 1 through 5) for pre- and post-treatment simulations. Although the experimental setup was such that flow migrated from bottom to top and the simulation runs top to bottom, the column remains saturated through the simulation and is assumed equivalent.

Table 6-4. 1-D Column Leaching Flow Parameters

Boundary Period	Length (hr)	Average Pretreatment Measured Q (mL/hr)	Pretreatment Sample Injection Darcy Velocity (m/hr) [a]	Average Post-Treatment Measured Q (mL/hr)	Post-Treatment Sample Injection Darcy Velocity (m/hr) [a]
1	3.8	25.884 [b]	0.059	20.475	0.047
2	50.8	stop flow	1.0e-9	stop flow	1.0e-7
3	14.7	23.148	0.053	24.364	0.057
4	79.6	stop flow	1.0e-9	stop flow	1.0e-9
5	104	23.423 [c]	0.052	26.322[c]	0.06

Table 6-4. 1-D Column Leaching Flow Parameters

Boundary Period	Length (hr)	Average Pretreatment Measured Q (mL/hr)	Pretreatment Sample Injection Darcy Velocity (m/hr) [a]	Average Post-Treatment Measured Q (mL/hr)	Post-Treatment Sample Injection Darcy Velocity (m/hr) [a]

a. Average measured flux divided by the column area, $\pi(2.36/2)^2$, for a given boundary period

b. The first recorded flux was not included in the average velocity calculation due to poor bromide (Br) curve fitting.

c. The last recorded flux was ignored due to high flow.

Flow properties are assigned by defining a textural class within the model domain. A single textural class is assigned within the entire column domain with a saturated conductivity of 1 m/hour to ensure flow within the column be defined by the inlet velocity. Zero solute dispersion is assigned in addition to very low specific storage (1e-4 m^{-1}). Experimentally derived porosity values of 0.3513 and 0.3509 are used for pre- and post-injection samples, respectively (PNNL-29650). Two tabular data entries are included such that the relative saturated conductivity and moisture content (equivalent to porosity under saturated conditions) remains the same at pressure head values of 0 and -1. A minimum of two entries are necessary for the model to run. Sample specific hydrologic and physical characterization data are included in VS2DRTI model design. Table 6-5 outlines parameters used in textural properties defined in VS2DRTI. Sample specific kinetic sorption parameter estimation results (ECF-300FF5-19-0086) are implemented via PhreeqcRM input file. Forward rates and distribution coefficients for pre-treatment and post-treatment samples are included in Table 6-5.

Table 6-5. Kinetic Desorption Rate Parameters

PNNL Sample #	Pre- or Post-Injection Sample	Borehole [a]	Dry Bulk Density (g/cm^3)	Porosity (cm^3/cm^3)	α_f (1/hr) [b]	K_d (mL/g)[b]	Initial Aq. Uranium Concentration (µg/L) [c]	Initial Total Uranium Bulk Sediment Concentration (µg/g) [d]
G21	Pre	C9673	1.765	0.3513	3.77e-2	1.5	19,000	10.0938
G113	Post	C9728	1.731	0.3509	2.47e-1	100	55.5	1.5521

a. Sample interval depth of 30-32.5 ft

b. ECF-300FF5-19-0086, *STOMP Modeling in Support of Stage B Sequestration of Uranium at 300-FF-5 Operable Unit*.

c. First effluent measurement recorded during the one-dimensional column leach experiment

d. Uranium bulk sediment concentrations based on 1000 hr carbonate leachable experimental data

PNNL = Pacific Northwest National Laboratory

Previously derived kinetic rate parameters used for supporting the uranium transport modeling for ECF-300FF5-11-0151, *Groundwater Flow and Uranium Transport Modeling in Support of the 300 Area FF-5 RI/FS*, are compared against parameters derived for Stage B evaluation. One-dimensional simulations representing pre-treatment and post-treatment scenarios were used to compare previously defined forward rate (α_f) and partition coefficient (K_d) parameters (ECF-300FF5-11-0151) with values implemented in this ECF (Table 6-15, Section 6.2.4.4). Dry bulk density, porosity, and initial aqueous and bulk sediment uranium concentrations were retained from pre-treatment and post-treatment samples

G21 and G113, respectively, for simulating pre-treatment and post-treatment simulations. A ratio of 10 is used between simulations for K_d values assigned to the models. Simulation parameters used for the comparison are compiled in Table 6-6.

Table 6-6. Kinetic Desorption Rate Parameter Comparison

Simulation	Dry Bulk Density (g/cm^3) [a]	Porosity (cm^3/cm^3) [a]	αf (1/hr) [b]	α_f (1/hr) [c]	Kd (mL/g) [b]	Kd (mL/g) [c]	Initial Aq. Uranium Concentration (µg/L) [a]	Initial Total Uranium Bulk Sediment Concentration (µg/g) [a]
Pretreatment	1.765	0.3513	9.31-3	3.87e-2	3.17	7.41	19,000	10.0938
Post-treatment	1.731	0.3509	9.31-3	3.87e-2	31.7	74.1	55.5	1.5521

a. Table 6-5 of this document

b. ECF-300FF5-11-0151, *Groundwater Flow and Uranium Transport Modeling in Support of 300 Area FF-5 RI/FS.*

c. Table 6-15 of this document

6.2 Three-Dimensional Remedy Injection Modeling

This section provides base case model settings for the 3-D remedy injection simulation. The basic model setup includes assigning all units in terms of meters, days, grams, and Joules with respect to length time, mass, and energy. Radial coordinates and simulating solute transport are selected to allow for 3-D injection modeling with reactive transport. Flow options are comprised of pressure head contour assignment to specify the initial hydraulic conditions, upstream weighting for computing relative intercell hydraulic conductivity, and van Genuchten functions for hydraulic flow. Transport calculations are based on the finite differencing scheme centered in both space and time. Table 6-7 outlines the model solver options and corresponding values.

Table 6-7. Three-Dimensional Remedy Injection Model Solver Options

Parameter	Value
Relaxation Parameter	0.1
Minimum iterations per time step	2
Maximum iterations per time step	1000
Maximum number of time steps	500,000,000
Closure criteria for head	0.1
Closure criterion for concentration	0.001

6.2.1 Model Domain

The 3-D VS2DRTI model domain has been selected in such a way that there is adequate coverage of a single generalized injection well both horizontally to capture the maximum horizontal saturation and vertically to incorporate both Hf and Rwie relevant saturated units.

The total domain dimensions of 16 m (52.5 ft) horizontally (radius length) and 20 m (65.6 ft) vertically were found sufficient to capture horizontal contaminant mobility in the vadose zone (Figure 6-2). The domain is generated in radial coordinates with the leftmost side representing the centerline of a 3-D cylinder and the rightmost side representing the outermost edge. A height of 0.25 m (0.82 ft) was used for the vertical cell discretization. Horizontal discretization was defined by successive cell widths increasing by a factor of 1.2 such that a minimum cell width of 0.01 m (0.033 ft) was located near the injection well (leftmost domain edge) and 2.68 m (8.53 ft) furthest from the well (rightmost domain edge). A total of 2,400 nodes, a single node centered in each grid cell, are used in calculations for the simulation.

Note: Units in meters

Figure 6-2. The VS2DRTI Remedy Injection Model Domain

6.2.2 Fate and Transport Parameters

VS2DRTI allows for each soil textural category defined in the model to have specific flow and solute transport properties assigned. An equivalent homogenous medium (EHM) approach is taken for each geologic unit defined such that the flow properties are equivalent throughout the defined domain for a given unit. Figure 6-3 shows the distribution of hydrogeologic units within the model domain consisting of unsaturated (or variably saturated) Hf, saturated Hf, and saturated Rwie. Average hydrostratigraphic unit (HSU) thicknesses were used based on a surface elevation of ~115 m (377 ft) and average water table elevation of 105 m (344.5 ft) such that Hf unsaturated zone is 10 m, Hf saturated zone is 3 m, and Rwie saturated zone is 7 m thick.

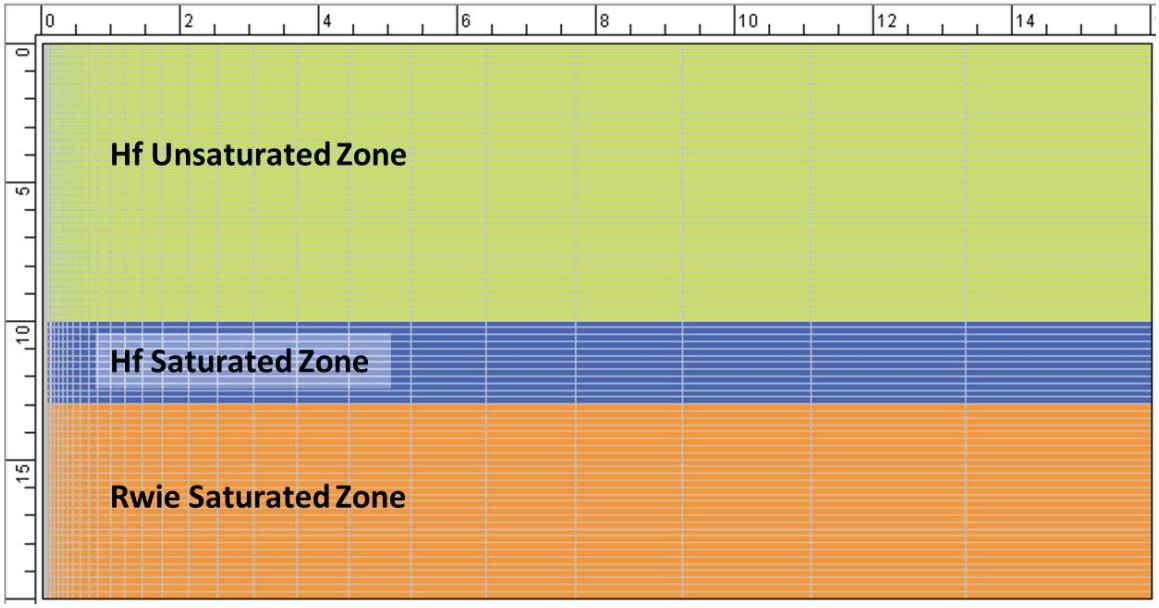

Figure 6-3. Distribution of Hydrogeologic Units

ECF-300FF5-19-0086 compiled textural hydraulic properties relevant to the Stage A and Stage B area hydrogeologic system and performed modeling of injection using STOMP model to evaluate large scale uranium contaminant transport. In order to remain consistent with the STOMP modeling, hydraulic (Table 6-8) and solute transport (Table 6-9) properties were adopted for their respective textural classes.

Table 6-8. 3-D Remedy Injection Model Textural Class Hydraulic Properties

HSU	Kzz/Khh [a]	Saturated Khh (m/day)	SS	Porosity	RMC	Alpha (m^{-1}) [b]	beta [b]
Hf_UZ	0.33	6.7	1.32E-4	0.174	0.0038	8.86	1.271
Hf_Aq	0.1	4E3	1.32E-4	0.174	0.0038	8.86	1.271
Ringold_Aq	0.1	40	1.32E-4	0.174	0.0038	8.86	1.271

a. Kzz and Khh are vertical and horizontal hydraulic conductivity, respectively.

b. van Genuchten parameters

HSU = hydrostratigraphic unit

RMC = residual moisture content

SS = specific storage

Table 6-9. 3-D Remedy Injection Model Textural Class Solute Transport Properties

HSU	Longitudinal Dispersivity (m)	Transverse Dispersivity (m)	Coefficient of Molecular Diffusion (m^2/day)
Hf_UZ	0.15	0.015	2E-5

Table 6-9. 3-D Remedy Injection Model Textural Class Solute Transport Properties

HSU	Longitudinal Dispersivity (m)	Transverse Dispersivity (m)	Coefficient of Molecular Diffusion (m^2/day)
Hf_Aq	1	0.1	2E-5
Ringold_Aq	1	0.1	2E-5

HSU = hydrostratigraphic unit

6.2.3 Boundary Conditions

Recharge periods are used to define changes in boundary conditions (e.g., periods of remedy injections and when no injections are occurring) over specified lengths of time. This model assumes a start time of midnight prior to injections and includes two periods of 8 hour (0.33 day) PRZ injections occurring during periods 2 and 4, and two 8 hour (0.33 day) LVZ injections during approximately similar start/end times of a typical workday (8 am to 4 pm) occurring during periods 6 and 8. Between injections, 16 hour (0.66 day) periods are included to represent inactive injection periods occurring overnight. A final period of 10 days is included at the end of the fourth injection to see near term evolution of chemistries after remedy implementation. The complete set of nine recharge periods and corresponding criteria are outlined in Table 6-10.

Table 6-10. Three-Dimensional Remedy Injection Model Recharge Periods

Number	Period Length (day)	Initial TS [a] (day)	TS Multiplier	Max. TS (day)	Min. TS (day)	TS Red. Factor	Max Head Change (m)	SS Head Criterion [b] (m)	Max Ponding Height (m)
1	0.33[c]	0.001	1.1	0.1	1e-5	0.1	0.1	1e-4	0
2	0.33	1e-5	1.1	0.001	1e-8	0.1	0.1	1e-4	0
3	0.66	1e-5	1.1	0.001	1e-8	0.1	0.1	1e-4	0
4	0.33	1e-5	1.1	0.001	1e-8	0.1	0.1	1e-4	0
5	0.66	1e-5	1.1	0.001	1e-8	0.1	0.1	1e-4	0
6	0.33	1e-7	1.1	0.001	1e-9	0.1	1	1e-4	0
7	0.66	1e-6	1.1	0.001	1e-8	0.1	0.1	1e-4	0
8	0.33	1e-6	1.1	0.001	1e-8	0.1	0.1	1e-4	0
9	10	1e-6	1.1	0.1	1e-8	0.1	0.1	1e-4	0

a. TS: Time Step in days

b. SS: Steady-State

c. Assuming the simulation starts at midnight, 8 hours (0.33 days) of initial run time is needed prior to injections starting at 8 am.

The surface flux applied in the 3-D remedy injection model was derived using lysimeter drainage analysis at the south caisson located in the Buried Waste Test Facility of the north 300 Area from July 1985 to

June 1993 (PNL-10285, *Estimated Recharge Rates at the Hanford Site*). An average recharge rate of 5.54 cm/year, or 1.51e-4 m/day, was recorded over the eight-year period. Because the model is set in radial coordinates, the surface recharge is designated as a volumetric flux into the domain with units of $[L^3]/[T]$. The volumetric flux at the surface boundary is defined by the following equation:

$$Q_{surface} = q_{recharge}(\pi)r^2 \quad \textbf{(Eq. 6-2)}$$

such that the radius (r, in m) is equal to the domain width of 16 m and recharge rate ($q_{recharge}$) is 1.51e-4 m/day. The resulting surface volumetric flux is 0.1211 m^3/day. This surface flux rate is applied to the top boundary for all nine recharge periods (Figure 6-4).

Because the 3-D remedy injection model is set in radial coordinates, natural groundwater flow gradient cannot be incorporated in the model as all flow would radiate outward at variable velocities from the injection point. Instead, the water table is held at a constant elevation of 105 m, an equivalent to 10 m depth from the surface (assigned as -10m due to model convention in Figure 6-4 for all recharge periods). An additional 2-D model is described in Section 6.2.6 to evaluate the short-term impacts of groundwater flow on contaminant concentrations in the aquifer.

Remedy injection solutions for the PRZ and LVZ were assigned an injection rate of 46 gpm (250 m^3/day) during their respective recharge periods (Figure 6-4). A supplemental no action case (NAC) was run using the same recharge periods outlined in Table 6-10 with no flow boundaries assigned at both PRZ and LVZ screens throughout the simulation duration.

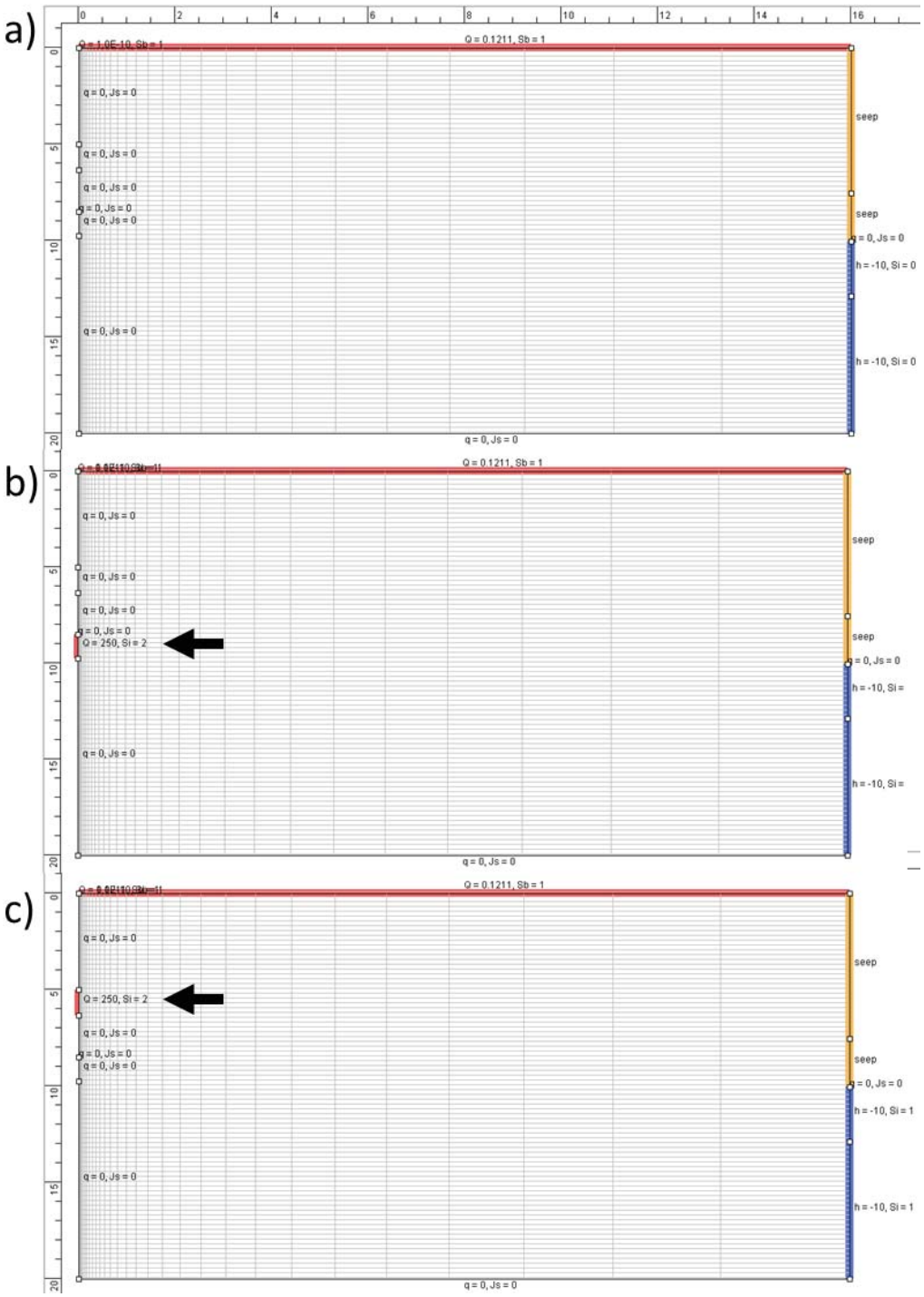

Figure 6-4. Boundary Conditions for a) Initial Conditions and Non-Injection, b) PRZ Injection, and c) LVZ Injection Periods

An initial pressure head was assigned to the model domain as an abstraction from the corresponding STOMP model regime (ECF-300FF5-19-0086). Pressure head values and elevations assigned are shown in Figure 6-5.

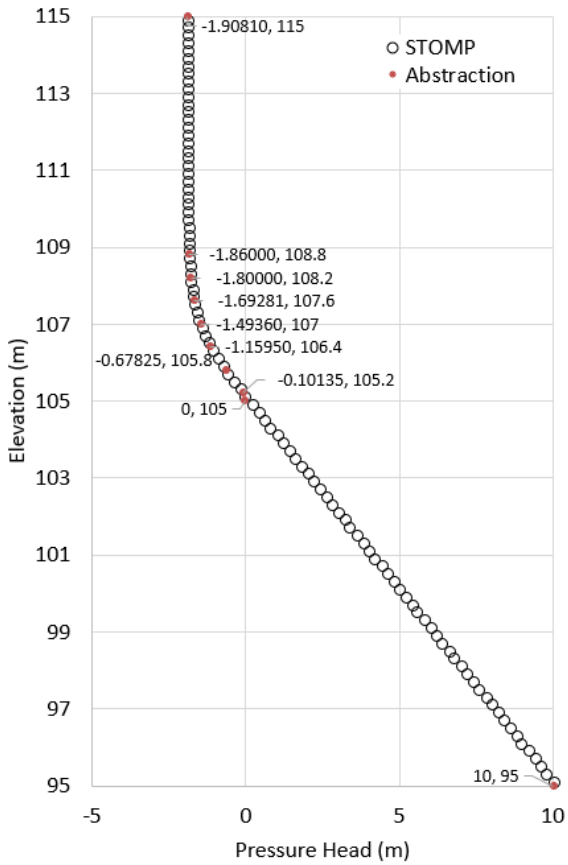

Figure 6-5. Initial Pressure Head STOMP Abstraction

6.2.4 Development of PHREEQC Reactive Transport Parameters

This section describes the compilation of reactive transport parameters and cards used in the PHREEQC input file for 3-D Remedy Injection Modeling including:

- Aqueous uranium and phosphate complex chemistry
- Relevant ion-exchange and surface complexation reactions
- Porewater and remedy injection solution compositions
- Reactive mineral assemblage
- Kinetic dissolution of calcite and mixed uranium-silicate-phosphate-carbonate solids

6.2.4.1 Supplementing the Existing Thermodynamic Database

A number of databases are provided with the VS2DRTI software. The llnl.dat database is derived from EQ 3/6 and Geochemist's Workbench databases using thermodynamic data compiled by the Lawrence Livermore National Laboratory. Though a range of uranium relevant reactions are already included in llnl.dat, the database is incomplete. Tables 6-11 through 6-13 provide inputs for aqueous species, mineral phases, and surface complexation reactions, respectively, and their original sources for database completeness. Though log K values are defined at 25°C, solution temperatures are assumed to be slightly lower (20°C).

Table 6-11. Aqueous Uranium and Phosphate Species

Equation	log K (25°C)	Source
$UO_2^{2+} + H_2O = UO_2OH^+ + H^+$	-5.25	a
$UO_2^{2+} + 2H_2O = UO_2(OH)_2 + 2H^+$	-12.15	a
$UO_2^{2+} + 3H_2O = UO_2(OH)_3^- + 3H^+$	-20.25	a
$UO_2^{2+} + 4H_2O = UO_2(OH)_4^{2-} + 4H^+$	-32.40	a
$2UO_2^{2+} + H_2O = (UO_2)_2OH^{3+} + H^+$	-2.70	a
$2UO_2^{2+} + 2H_2O = (UO_2)_2(OH)_2^{2+} + 2H^+$	-5.62	a
$3UO_2^{2+} + 4H_2O = (UO_2)_3(OH)_4^{2+} + 4H^+$	-11.90	a
$3UO_2^{2+} + 5H_2O = (UO_2)_3(OH)_5^+ + 5H^+$	-15.55	a
$3UO_2^{2+} + 7H_2O = (UO_2)_3(OH)_7^- + 7H^+$	-32.20	a
$4UO_2^{2+} + 7H_2O = (UO_2)_4(OH)_7^+ + 7H^+$	-21.90	a
$UO_2^{2+} + CO_3^{2-} = UO_2CO_3$	9.94	a
$UO_2^{2+} + 2CO_3^{2-} = UO_2(CO_3)_2^{2-}$	16.61	a
$UO_2^{2+} + 3CO_3^{2-} = UO_2(CO_3)_3^{4-}$	21.84	a
$3UO_2^{2+} + 6CO_3^{2-} = (UO_2)_3(CO_3)_6^{6-}$	54.0	a
$2UO_2^{2+} + CO_3^{2-} + 3H_2O = (UO_2)_2CO_3(OH)_3^- + 3H^+$	-0.855	a
$3UO_2^{2+} + CO_3^{2-} + 3H_2O = (UO_2)_3O(OH)_2HCO_3^+ + 3H^+$	0.655	a
$11UO_2^{2+} + 6CO_3^{2-} + 12H_2O = (UO_2)_{11}(CO_3)_6(OH)_{12}^{2-} + 12H^+$	36.43	a
$2Ca^{2+} + UO_2^{2+} + 3CO_3^{2-} = Ca_2UO_2(CO_3)_3$	30.70	b
$Ca^{2+} + UO_2^{2+} + 3CO_3^{2-} = CaUO_2(CO_3)_3^{2-}$	27.18	b
$Mg+2 + UO_2^{2+} + CO_3^{2-} = MgUO_2(CO_3)_3^{2-}$	26.11	b
$UO_2^{2+} + NO_3^- = UO_2NO_3^+$	0.30	a
$Ca^{2+} + HPO_4^{2-} = CaHPO_4$	2.740	c

Table 6-11. Aqueous Uranium and Phosphate Species

Equation	log K (25°C)	Source
$Na^{+} + HPO4^{2-} = NaPO4\text{-}2 + H^{+}$	-10.8918	c
$UO_2^{2+} + 2HPO_4^{2-} = UO_2(HPO_4)_2^{2-}$	18.344	a
$UO_2^{2+} + PO_4^{3-} = UO_2PO4^{-}$	13.23	d
$UO_2^{2+} + PO_4^{3-} + H^{+} = UO_2HPO_4$	19.59	d
$UO_2^{2+} + PO_4^{3-} + 2H^{+} = UO_2H_2PO_4^{+}$	22.82	d
$UO_2^{2+} + PO_4^{3-} + 3H^{+} = UO_2H_3PO_4^{2+}$	22.46	d
$UO_2^{2+} + 2PO_4^{3-} + 4H^{+} = UO_2(H_2PO_4)_2$	44.04	d
$UO_2^{2+} + 2PO_4^{3-} + 5H^{+} = UO_2(H_2PO_4)(H_3PO_4)^{+}$	45.05	d

a. Guillaumont et al., 2003, *Update on the Chemical Thermodynamics of Uranium, Neptunium, Plutonium, Americium and Technetium.*

b. Dong and Brooks, 2006, "Determination of the formation constants of ternary complexes of uranyl and carbonate with alkaline earth metal (Mg2+, Ca2+, Sr2+, and Ba2+) using anion exchange method."

c. Wolery and Jarek, 2003, *Software User's Manual, EQ3/6*.

d. Guillaumont and Mompean, 2003, *Update on the Chemical Thermodynamics of Uranium, Neptunium, Plutonium, Americium and Technetium*.

Table 6-12. Uranium Mineral Phases

Mineral	Equation	log K (25°C)*
Autunite	$Ca(UO_2)_2(PO_4)_2{:}3H_2O = Ca^{2+} + 2UO_2^{2+} + 2PO_4^{3-} + 3H_2O$	-48.36
Uranyl Hydrogen Phosphate	$UO_2HPO_4{:}3H_2O = UO_2^{2+} + HPO_4^{2-} + 3H_2O$	-13.17
Uranyl Orthophosphate	$(UO_2)_3(PO_4)_2{:}4H_2O = 3UO_2^{2+} + 2PO_4^{3-} + 4H_2O$	-49.36
Andersonite	$Na_2CaUO_2(CO_3)_3(H_2O)_6 = 2Na^{+} + Ca^{2+} + UO_2^{2+} + 3CO_3^{2-} + 6H_2O$	-37.5
Liebigite	$Ca_2UO_2(CO_3)_3(H_2O)_{10} = 2Ca^{2+} + UO_2^{2+} + 3CO_3^{2-} + 10H_2O$	-36.9
Chernikovite	$(UO_2)HPO_4(H_2O)_4 = UO_2^{2+} + HPO_4^{2-} + 4H_2O$	-22.73

* Gorman-Lewis et al., 2009, "Thermodynamic Properties of Autunite, Uranyl Hydrogen Phosphate, and Uranyl Orthophosphate from Solubility and Calorimetric Measurements."

Table 6-13. Surface Complexation Site Reactions

Equation [a]	log K (25°C)	Source
$HfssOH + H^+ = HfssOH_2^+$	7.35	b
$HfssOH = HfssO^- + H^+$	-9.17	b
$HfssOH + Ca^{2+} + H_2PO_4^- = HfssOCaHPO_4^- + 2H^+$	-6.44	b
$HfssOH + Ca^{2+} + H_2PO_4 = HfssOCaH_2PO_4 + H^+$	0.19	b
$HfssOH + UO_2^{2+} + 2CO_3^{2-} + H^+ = HfssOH_2UO_2(CO_3)_2^-$	29.15	b
$HfssOH + UO_2^{2+} + 3CO_3^{2-} + H^+ = HfssOH_2UO_2(CO_3)_3^{3-}$	36.28	b
$HfssOH + 2UO_2^{2+} + CO_3^{2-} + 3H_2O = HfssOH_2(UO_2)2CO_3(OH)_3 + 2H^+$	12.62	b
$HfssOH + CO_3^{2-} = HfssOHCO_3^{2-}$	4.78	c
$HfssOH + CO_3^{2-} + 2H^+ = HfssHCO_3 + H_2O$	20.3	c
$HfssOH + Ca^{2+} = HfssOCa^+ + H^+$	-5.85	d
$HfssOH + Mg^{2+} = HfssOMg^+ + H^+$	-4.6	d
$HfssOH + Mn^{2+} = HfssOMn^+ + H^+$	-3.5	d
$HfssOH + Ra^{2+} = HfssORa^+ + H^+$	-7.2	d
$HfssOH + UO_2^{2+} + H_2PO_4^- = HfssPO_4UO_2 + H_2O + H^+$	7.84	e

a. All surface complexation sites (Hfss) represent weak binding sites.

b. Turner and Sassman, 1996, "Approaches to Sorption Modeling for High-Level Waste Performance Assessment."

c. Appelo et al., 2002, "Surface complexation of ferrous iron and carbonate on ferrihydrite and the mobilization of arsenic."

d. Dzombak and Morel, 1990, *Surface Complexation Modeling: Hydrous Ferric Oxide*.

e. Romero-Gonzalez et al., 2007, "Surface complexation modeling of the effects of phosphate on uranium(VI) adsorption."

6.2.4.2 Porewater and Remedy Injection Solution Chemistry

Pre-remedy injection groundwater well monitoring and daily skid sampling data were used to define the initial porewater solution composition and remedy injection solutions, respectively. Groundwater monitoring data from August 27 and September 4, 2018, at well 399-1-17A (Figure 1-1) were averaged to define the initial porewater composition (Table 6-14). Daily skid measurements between September 4 and October 17, 2018, were averaged and used to define the remedy injection solution for both PRZ and LVZ

recharge periods (Table 6-14). Average river water measurements for magnesium and nitrate are reported as maximum skid constituent concentrations, though the values are likely much lower after injection solution mixing. The iron detection limit is listed as no iron was detected in both skid injection solution or river water. Figure 6-6 displays the relative concentrations of pre- and post-treatment solution constituents expressed in milliequivalents per kg water.

Table 6-14. Solution Card Chemistries

Constituent	Solution 1 [a]	Solution 2 [b]
Sodium (mg/L)	26.7	2605.76
Potassium (mg/L)	8.0	1769.39
Phosphorus (mg/L)	--	2769.09
pH	7.5	7.6
Calcium (mg/L)	53.1	17.64
Magnesium (mg/L)	12.6	4.55
Chloride (mg/L)	25.0	1.17
Bicarbonate (mg/L)	129.5	3666.90
Sulfate (mg/L)	58.5	28.46
Nitrate (mg/L)	31.9	0.48
Iron (mg/L)	0.05	--
Uranium (mg/L)	0.10	--

a. Background porewater chemistry

b. Remedy injection solution

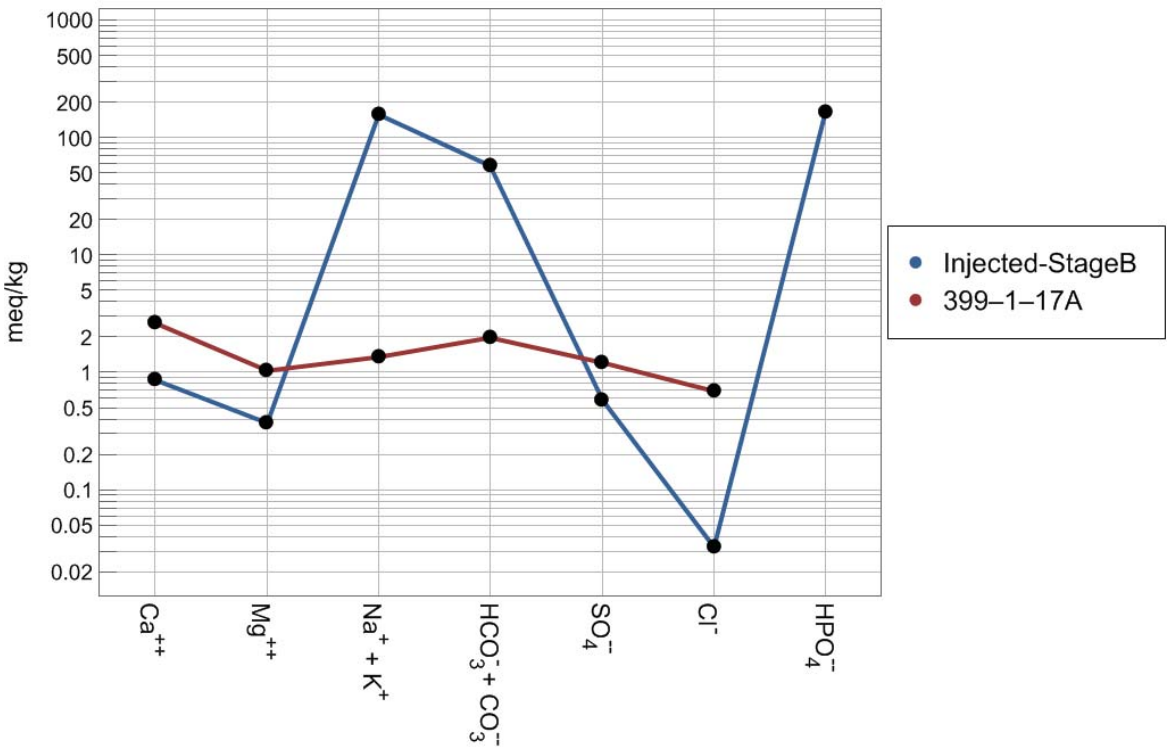

Figure 6-6. Schoeller Diagram of Injected Remedy and Porewater Solutions

6.2.4.3 Equilibrium Phase Mineral Assemblage

Minerals in equilibrium with the background pore water, reactive surface sites and available cation exchange sites are defined by the Equilibrium Phase, Surface, and Exchange cards in PHREEQC, respectively. A generalized mineral assemblage of quartz, potassium-feldspar, and goethite are in excess and considered in contact with atmospheric oxygen as there are no confining layers in the geologic framework (Section 4.1.1). Select uranium-carbonate and uranium-phosphate bearing minerals autunite, uranyl hydrogen phosphate, uranyl orthophosphate, liebigite, andersonite, and chernikovite are included as the most thermodynamically favorable minerals to precipitate during the simulation (initial moles of minerals set to 0). Similarly, phosphate and carbonate minerals hydroxylapatite, whitlockite, and siderite were included due to the high phosphate and carbonate added to the system during the injections, representing mineral precipitate coatings which have the potential to decrease uranium mobility in the vadose zone. It is worth noting that the minerals defined in the Equilibrium Phase card immediately precipitate or dissolve when conditions are favorable with no kinetic constraints. This is not an indication of what is in the sediments initially, but what may be thermodynamically favored at a given point in time and space.

Sequential extraction results for iron concentrations in pre-treatment samples were used to calculate the initial amount of reactive surface sites in the model. An average iron content of 5e-4 g/g was used, subsequently assuming 10% of the iron content represents reactive hydrous ferric oxide (HFO), the mineral assemblage with which the surface complexation reactions are defined.

Clay mineral interstitial reactive sites can bind and exchange cations with the surrounding solution. Previous characterization of the 300 Area determined total surface calcium available ranging from 0.9 to 1.5 meq/100g (PNNL-21733). Particle size distribution analysis indicated lower clay content than previously reported in PNNL-21733 of 3-6% volume fraction (PNNL-29650). Approximately 1% volume

fraction was determined for clay fraction when assuming a clay size of <0.004 mm using the Wentworth scale. A cation exchange capacity of 1 meq/100g sediment and 1% clay content weight fraction were used to define an exchanger concentration of 1.26e-3 eq/L.

6.2.4.4 Kinetic Mineral Dissolution and Precipitation

The precipitation and dissolution of calcite and bulk release of uranium are kinetically mediated in the model implementation. The focus of 3-D Remedy Injection modeling is on calcium-phosphate interaction and uranium sequestration during and following the injections. So, the dissolution kinetics associated with these reactions were evaluated specifically while holding all background minerals and other potential reactions under equilibrium. PHREEQC allows for the defining kinetic rates by the use of the Kinetics card which names each kinetic rate and Rates card which specifies the equations defining each kinetic rate.

Calcite dissolution and precipitation is defined by the rate expression first developed by Plummer et al., 1978, "The kinetics of calcite dissolution in CO2-water systems at 5 to 60 °C and 0.0 to 1.0 atm CO_2," dependent on pH, the partial pressure of carbon dioxide (CO_2), and temperature. The forward rate reaction, R_f, is shown in Equation 6-3:

$$R_f = k_1[H^+] + k_2[CO_{2(aq)}] + k_3[H_2O] \quad \textbf{(Eq. 6-3)}$$

Such that k_1, k_2, and k_3 are first order rate constants dependent on temperature and R_f has units of $[mol/cm^2/s]$ (Plummer et al., 1978). The overall rate ($R_{calcite}$, $[mol/L/s]$) is defined by Equation 6-4:

$$R_{calcite} = \left(\frac{A}{V}\right) R_f[1 - 10^{\left(\frac{2}{3}SI_{calcite}\right)}] \quad \textbf{(Eq. 6-4)}$$

where:

A: area $[cm^2]$

V: volume $[L]$

$SI_{calcite}$: saturation index of calcite $[dimensionless]$.

The calcite saturation index ($SI_{calcite}$) is calculated as log10 of the ion activity product divided by equilibrium constant of calcite. When greater than 1, the system is considered saturated and calcite is thermodynamically favored to precipitate. When less than one, the system is undersaturated with respect to calcite.

Bulk kinetic release rates of uranium where phosphate is not and is present representing pre-injection and post-injection scenarios, respectively, is implemented in a single Kinetics and Rates card pair (Kinetics 1 and Rates "U_Sorption", Appendix D) in PHREEQC using Equation 4-4 as outlined in Section 4.2.1. A simple if-then statement is included where the pre-injection bulk uranium kinetic release rate is applied when hydrogen phosphate (HPO_4^{2-}) is less than 1e4 mol or the post-injection bulk uranium kinetic release rate will be applied when HPO_4^{2-} is greater than 1e4 mol for any given grid node in space and time. PHREEQC requires a mineral formula when designating kinetic rates. Uranophane was assigned in the Kinetics 1 card, though any uranium mineral could be chosen. As discussed in Section 4.2, the change from initial conditions uranium solid phase to post-treatment uranium incorporated and sorbed to calcium phosphate phases is considered instantaneous once the phosphate threshold is met.

Kinetic rate parameters for both calcite and uranium solid phases are outlined in Table 6-15.

The initial molar amount of calcite is based on the sum of weak and strong acid extractions of calcium from sequential extraction results outlined in Section 4.1.5.2. A total of approximately 400 µg/g calcium has an equivalent calcite concentration of about 1e-3 g/g. The resulting calcite concentration does not include calcium available in extraction 4 and was thus doubled to account for this discrepancy. 1000-hour carbonate batch extraction uranium data generally define the amount of uranium available for release from sediments. The average labile uranium concentration from 1000-hr batch carbonate extraction pre-treatment samples was used as the initial amount of available uranium solid reservoir for bulk kinetic release in the system. The forward rate (α_f) and distribution coefficient (K_d) values used are the average of all pre-treatment one-dimensional column leach kinetic rate parameter estimation results. To account for the impact of injection on uranium sorption behavior, a K_d multiplier of 10 is included when HPO_4^{2-} concentrations (the dominant aqueous phosphate species in the system) exceed a threshold greater than 1e-4 mol/L (background levels are much lower than this value) representing an approximate ten-fold reduction in uranium leachability based on comparing flow-through column test results between pre-treatment to post-treatment sample pairs.

Table 6-15. Mineral Kinetic Parameters

Parameter	Value	Unit
Calcite		
Initial amount of calcite	2000	µg/g
Specific surface area of calcite [a]	1.67e5	cm^2/mol
Exponent factor [a]	0.6	-
Generic Uranium-Silicate		
Initial amount of mineral	20	µg/g
Forward rate (α_f)	3.87e-2	1/hr
Distribution coefficient (Kd)	7.41e-3	L/g
Kd multiplier	10	-
Solids (bulk density/porosity) [b]	1.03e4	g/L

a. Plummer et al., 1978, "The kinetics of calcite dissolution in CO2-water systems at 5 to 60 °C and 0.0 to 1.0 atm CO_2."

b. Bulk density of 1800 kg/m^3 and porosity of 0.174.

6.2.5 Chemistry Domain Assignment

Chemistry domains can be assigned for specific solution chemistries, equilibrium phases, exchange phases, surface phases, gas phases, solid solutions, and kinetic releases defined in the corresponding PHREEQC input file. A given Solution, Equilibrium Phase, Exchange, Surface, Gas, Solid Solution, and Kinetic PHREEQC card is assigned a number which can be read by VS2DRTI. The chemistry classes defined for this 3-D remedy injection simulation is shown in Table 6-16 with extents shown in Figure 6-7. Boundary conditions also allow for defining the solution chemistry for which applied at that boundary location. Remedy injection solution is identified as "2" while background porewater chemistry solution is "1" as shown in Table 6-16 and Figure 6-4. Two separate chemistry domains are used to represent the vadose zone where kinetic dissolution of calcite and bulk uranium release occurs, while the saturated zone

does not include kinetics. The assumption being that groundwater flow over time has driven these reactive minerals to negligible concentrations. Aquifer studies conducted by PNNL-16435, *Limited Field Investigation Report for Uranium Contamination in the 300-FF-5 Operable Unit at the 300 Area, Hanford Site, Washington*, indicate dissolved uranium contamination limited to the upper unconfined aquifer though no indication of solid phase uranium contamination was identified. Furthermore, no direct identification of calcite was found, though alkalinity and calcium concentrations were such that calculated saturation index values were in the range of 1.5 to 3 indicating oversaturation conditions with respect to calcite. Corresponding PHREEQC input file cards are described in Section 6.2.4 with the full file provided in Appendix D of this document.

Table 6-16. Three-Dimensional Remedy Injection Base Case Model Chemistry Classes [a]

Name	Solution	Equilibrium Phases	Exchange	Surface	Gas Phase	Solid Solution	Kinetics
Inactive [b]	-1	-1	-1	-1	-1	-1	-1
Initial Saturated Zone	1	1	1	1	-1	-1	-1
Injection Solution	2	-1	-1	-1	-1	-1	1
Initial Unsaturated Zone	1	1	1	1	-1	-1	1

a. A value of -1 is assigned for all deselect a card from the chemistry class.

b. Inactive class is used to define the domain extents.

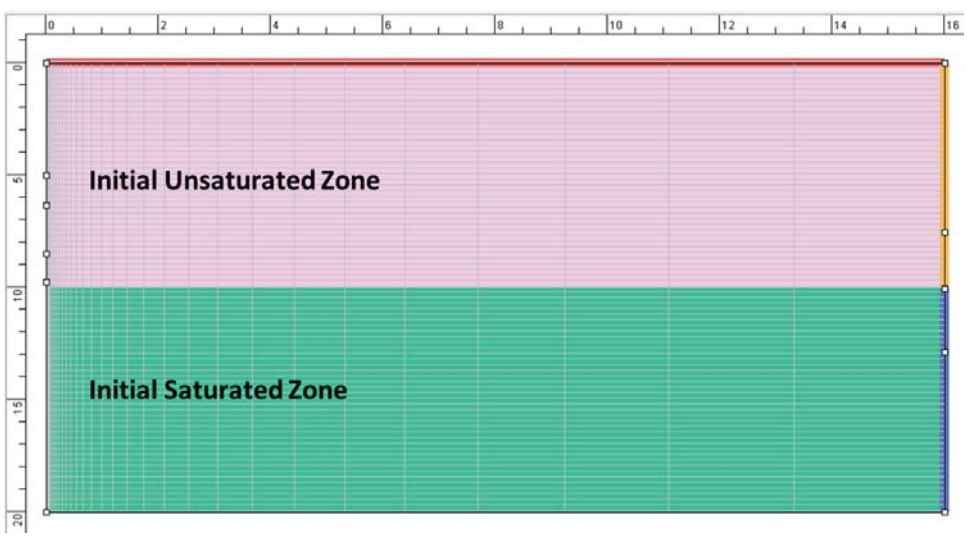

Figure 6-7. Distribution of Chemistry Classes

6.2.6 Sensitivity Analysis

Sensitivity analyses were conducted to evaluate the effectiveness of model components in representing observation data, the impact of groundwater flow on uranium transport, and the inclusion of unsaturated zone heterogeneity.

6.2.6.1 Evaluation of Model Components

Three model cases were conducted to evaluate the effectiveness in representing observation data by increasing the model complexity:

1) Kinetics mediated case (Case 1): The model setup is identical to the base case described above with the exclusion of all identified equilibrium phases and surface complexation reactions.

2) Kinetics mediated and calcium-phosphate precipitation case (Case 2): Similar to the kinetics mediated case with the inclusion of calcium-phosphate minerals hydroxyapatite and whitlockite.

3) Kinetics mediated, calcium-phosphate precipitation, and surface complexation reaction case (Case 3): The model setup is identical to the base case with the exclusion of all uranium-bearing mineral phases.

To run the models, changes to the PHREEQC input file were made (Table 6-17) for all three sensitivities in addition to the inactivation of the surface card in the chemistry class definition in VS2DRTI for cases 1 and 2 (Table 6-18).

Table 6-17. PHREEQC Input File Modifications

Excluded Component*	Case 1	Case 2	Case 3
hydroxyapatite	X		
whitlockite	X		
autunite	X	X	X
uranyl hydrogen phosphate	X	X	X
uranyl orthophosphate	X	X	X
liebigite	X	X	X
andersonite	X	X	X
chernikovite	X	X	X
Surface card	X	X	

* Exclusions made by including pound symbol (#) at the beginning of text string.

Table 6-18. Sensitivity Cases 1 and 2 Chemistry Classes [a]

Name	Solution	Equilibrium Phases	Exchange	Surface	Gas Phase	Solid Solution	Kinetics
Inactive [b]	-1	-1	-1	-1	-1	-1	-1
Initial Saturated Zone	1	1	1	-1	-1	-1	-1
Injection Solution	2	-1	-1	-1	-1	-1	1
Initial Unsaturated Zone	1	1	1	-1	-1	-1	1

a. A value of -1 is assigned for all deselect a card from the chemistry class.

b. Inactive class is used to define the domain extents.

6.2.6.2 Impact of Groundwater Flow using 2-D Model

In order to evaluate the impact of groundwater flow during remedy solution injections within the aquifer, a two-dimensional model was developed allowing for flow across the domain. The following sections discuss the model domain and boundary conditions. The textural class, initial pressure head and chemistry class designations do not change from the 3-D remedy injection model. Also, the same PHREEQC input file was retained for this effort (see Section 6.2.4 for discussion and Appendix D for the file). The time units used between the 3-D Remedy Injection model and 2-D Groundwater Flow model changed from days to hours, respectively. As a result, a minor edit to the RATES card time unit conversion from 8640 to 360 representing 0.1 day and 0.1 hour timesteps, respectively.

The basic model setup includes assigning all units in terms of meters, hours, grams, and Joules with respect to length time, mass, and energy. Simulating solute transport is selected to allow for two-dimensional injection modeling with reactive transport. Flow options are comprised of pressure head contour assignment to specify the initial hydraulic conditions, upstream weighting for computing relative intercell hydraulic conductivity, and van Genuchten functions for hydraulic flow. Transport calculations are centered in space and backward in time. Table 6-19 outlines the model solver options and corresponding values.

Table 6-19. Two-Dimensional Groundwater Model Solver Options

Parameter	Value
Relaxation Parameter	0.7
Minimum iterations per time step	2
Maximum iterations per time step	1000
Maximum number of time steps	50,000,000
Closure criteria for head	0.1
Closure criterion for concentration	0.001

Model Domain

The 2-D VS2DRTI model domain has been selected in such a way that there is adequate coverage of a single generalized injection well both horizontally to capture the maximum horizontal saturation and vertically to incorporate both Hf and Rwie relevant saturated units.

The total domain dimensions of 50 m (164 ft) horizontally and 20 m (65.6 ft) vertically were found sufficient to capture horizontal contaminant mobility in the vadose zone (Figure 6-8). A height of 0.2 m (0.66 ft) was used for the vertical cell discretization. Horizontal discretization was uniform for 5 m in either direction using a 0.2 m spacing then successively increasing in width by a factor of 1.2 such that a minimum cell width of 0.28 m (0.92 ft) was located nearest the line source (shown as red square in Figure 6-8) and 3.56 m (11.68 ft) at the domain edges. A total of 8,000 nodes centered in each grid cell are used in calculations for the simulation.

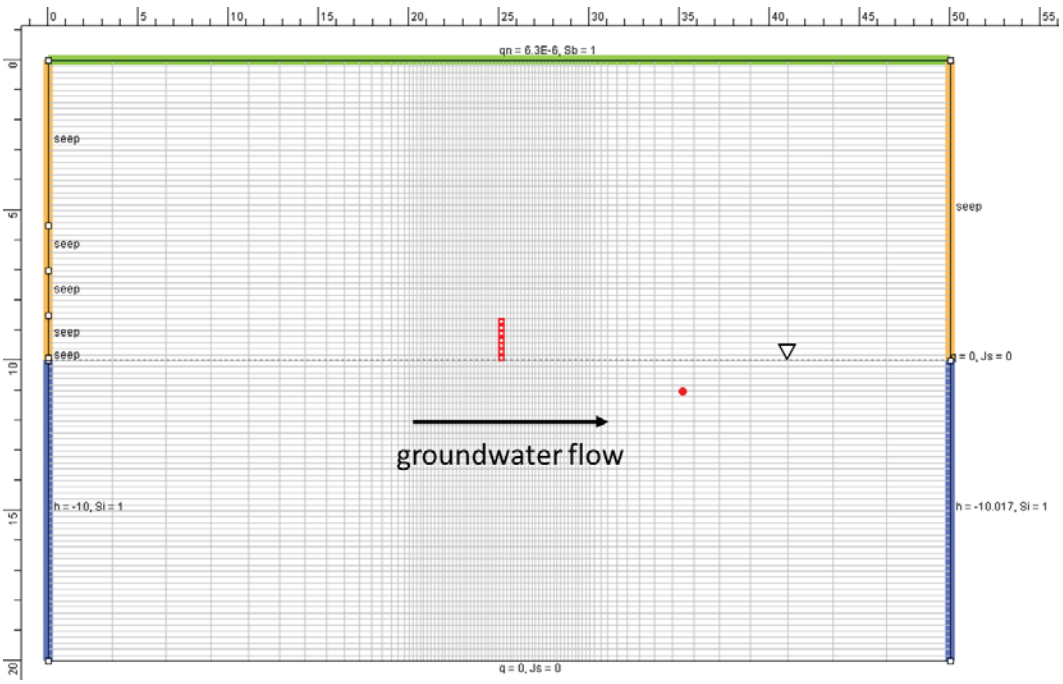

Figure 6-8. Two-Dimensional Remedy Injection Groundwater Model Domain

Boundary Conditions

Recharge periods are used to define changes in boundary conditions (e.g., periods of remedy injections and when no injections are occurring) over specified lengths of time. This model assumes a start time of midnight prior to injections and includes two periods of 8 hour PRZ injections during approximately similar start/end times of a typical workday (8 am to 4 pm). Between injections, a 16 hour period is included to represent inactive injection period occurring overnight. A final period of 10 days is included at the end of the second injection to see near term evolution of chemistries after remedy implementation. The complete set of five recharge periods and corresponding criteria are outlined in Table 6-20.

Table 6-20. Two-Dimensional Remedy Injection Groundwater Model Recharge Periods

Number	Period Length	Initial TS [a]	TS Multiplier	Max. TS	Min. TS	TS Red. Factor	Max Head Change	SS Head Criterion [b]	Max Ponding Height
1	8 [c]	0.001	1.1	0.5	1e-3	0.1	0.1	1e-4	0
2	8	0.001	1.1	0.1	1e-6	0.1	1	1e-4	0
3	16	1e-4	1.1	0.2	1e-6	0.1	0.5	1e-4	0
4	8	0.001	1.1	0.1	1e-4	0.1	0.5	1e-4	0
5	240	0.001	1.1	0.2	1e-6	0.1	0.5	1e-4	0

a. TS: Time Step in hours

b. SS: Steady-State

c. Assuming the simulation starts at midnight, 8 hours of initial run time are needed prior to injections starting at 8 am.

The surface flux applied in the 2-D remedy injection groundwater model was derived using lysimeter drainage analysis at the south caisson located in the Buried Waste Test Facility of the north 300 Area from July 1985 to June 1993 (PNL-10285). An average recharge rate of 5.54 cm/year, or 6.3e-6 m/hour, was recorded over the eight-year period. This surface flux rate is applied to the top boundary for all five recharge periods (Figure 6-8).

Remedy injection solutions for the PRZ were assigned an injection rate of 50 gpm (11.34 m^3/hour) during their respective recharge periods. Implementation of the injection zone is done by line source in the center of the model domain at elevations 105 m to 106.3 m (Figure 6-8). The injection rate was further reduced using the estimated diameter of injection influence of 6 m (see Section 7.2.1 for additional details). Finally, a total of seven nodes were used to define the line source, each having an assigned rate of 0.27 m^3/hr which occur during the 2nd and 4th recharge periods.

Two hydraulic head boundaries were assigned to induce groundwater flow through the domain. A water table gradient of 3.4e-4 m/m is determined by trend surface analysis using data from February 2018 (DOE/RL-2018-66). In assigning the left domain boundary at -10 m (105 m elevation) based on the origin location at the top left of the domain and having a 50 m domain width, the right domain boundary is 0.017 lower. The resulting right boundary hydraulic head is -10.017 m or 104.983 m elevation (Figure 6-8).

6.2.6.3 Impact of Textural Heterogeneity on Reactive Transport Modeling

A separate 3-D Heterogeneous Remedy Injection model was developed to evaluate the impact of varying unsaturated zone textures on geochemical evolution during simulated remedy injection. Variations in baseline bulk electrical conductivity in addition to maximum extents of elevated bulk electrical conductivity identified using ERT (Section 4.1.4) indicate lower permeability zones within the unsaturated zone. A single generalized low permeability zone was included in the base case 3-D Remedy Injection model as described below.

Fate and Transport Parameters

The highest baseline ERT bulk conductivity measurements were captured in Cluster 1 (Figure 4-7), suggesting horizontal regions of low permeability. Elevations above the LVZ injection are primarily associated with backfill material that is not being modeled in our injection systems. An additional 1 to

2 m thick low permeability zone is indicated between elevations of 106 to 108 m. Further evidence is shown in the maximum changes of bulk electrical conductivity shown in Figure 4-8, such that the least amount of change was observed between 106 to 108 m elevation post-treatment. Zones exhibiting less change in bulk electrical conductivity indicate less remedy solution present post injections.

To simulate the observed heterogeneity in the unsaturated zone, a single 1 m thick Hanford formation silt zone was included in the 3-D Remedy Injection model (Figure 6-9). Corresponding flow and solute transport properties for the low-permeability zone are included in Table 6-21 and Table 6-22, respectively. All remaining parameters were unchanged from the base case 3-D Remedy Injection model.

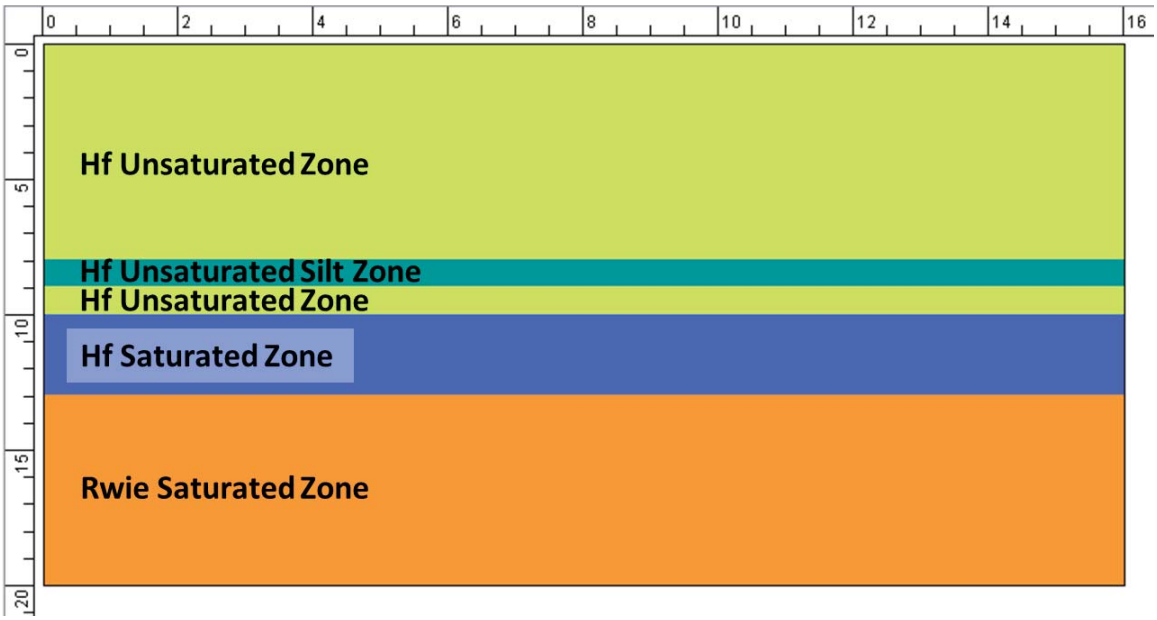

Figure 6-9. Distribution of Hydrogeologic Units in the 3-D Heterogeneous Remedy Injection Model

Table 6-21. 3-D Heterogeneous Remedy Injection Model Textural Class Flow Properties

HSU	Kzz/Khh	Sat Khh (m/day)	SS	Porosity	RMC	Alpha (m^{-1})*	Beta*
Hf_UZ	0.33	6.7	1.32E-4	0.174	0.0038	8.86	1.271
Hf_UZ_silt	0.33	0.12	1.32E-4	0.399	0.054	0.63	1.83
Hf_Aq	0.1	4E3	1.32E-4	0.174	0.0038	8.86	1.271
Ringold_Aq	0.1	40	1.32E-4	0.174	0.0038	8.86	1.271

* van Genuchten parameters

HSU = hydrostratigraphic unit

RMC = residual moisture content

SS = specific storage

Table 6-22. 3-D Heterogeneous Remedy Injection Model Textural Class Solute Properties

HSU	Longitudinal Dispersivity (m)	Transverse Dispersivity (m)	Coefficient of Molecular Diffusion (m^2/day)
Hf_UZ	0.15	0.015	2E-5
Hf_UZ_silt	0.05	0.005	2E-5
Hf_Aq	1	0.1	2E-5
Ringold_Aq	1	0.1	2E-5

HSU = hydrostratigraphic unit

6.3 Supplemental Thermodynamic Geochemical Assessment

VS2DRTI modeling results were qualitatively compared to thermodynamic geochemical modeling conducted using GWB. Three programs were used for developing figures for this ECF: the GSS program which stores tabular geochemical data and has the ability to display information in a range of diagrams; SpecE8 which calculations species distributions and activities in aqueous solutions; and Act2 with the ability to calculate phase stability diagrams.

Remedy injection and porewater solution chemistries outlined in Table 6-14 were input into GSS, allowing for plotting of the Schoeller diagram provided in Figure 6-6. Similarly, solutions 1 and 2 from Table 6-14 were individually input into SpecE8 files in order to calculate the species distributions. Two modifications were made to the porewater input including 1) the hydrogen phosphate concentration being suppressed to 1e-6 mg/L as phosphorus and 2) uranyl ion (UO_2^{2+}) selected as the dominant uranium aqueous species. Results from the two SpecE8 files provide log activities for each chemical constituent relevant to the two individual aqueous solutions. The SpecE8 remedy injection solution results were then used as a corresponding input to the Act2 program (Table 6-23) with the uranyl carbonate [$UO_2(CO_3)_2^{2-}$] input supplemented by the porewater SpecE8 results. The thermo.com.V8.R6+ GWB database was used as an equivalent database to the llnl.dat PHREEQC file in order to develop phase diagrams for VS2DRTI results comparisons. Slight modification was made to the GWB database to add the uranium mineral phases autunite and andersonite (Table 6-12). Two phase diagrams were produced to provide insight on the relevant mineral phases with and without uranium present in solution. In the case of thermodynamically favorable mineral phases without uranium present, dolomite phases were suppressed due to mineral formation typically under long term diagenesis occurring beyond the timeframe simulated by models in this ECF.

Table 6-23. Act2 Inputs

Aqueous Species	log activity *
Ca^{2+}	-4.462
pH	4 to 9
HPO_4^{2-}/HCO_3^-	-10 to 10
HCO_3^-	-1.041

Table 6-23. Act2 Inputs

Aqueous Species	log activity *
Ca^{2+}	-4.462
pH	4 to 9
HPO_4^{2-}/HCO_3^-	-10 to 10
Cl^-	-4.637
Na^+	-1.177
K^+	-1.56
Mg^{2+}	-4.927
SO_4^{2-}	-4.184
$UO_2(CO_3)_2^{2-}$	-6.724
Temperature	25°C
Pressure	1.13 r

* All injection solution SpecE8 results used with the exception of $UO_2(CO_3)_2^{2-}$

7 Results

7.1 One-Dimensional Column Leaching Simulation Results

Simulated aqueous bromide and uranium concentrations from the one-dimensional column leaching simulation were compiled from the lower most node to compare with experimental data (Figure 6-1). Figure 7-1 shows history match results for representative pretreatment and post-treatment samples G21 and G113, respectively. Simulated results for both sample bromide breakthrough curve comparisons have strong matches with experimental data providing confidence in the model setup. Differences in measured column leaching bromide concentrations and simulated results are likely due to initially unsaturated conditions during experiments which in turn reduces the effective porosity than would be expected.

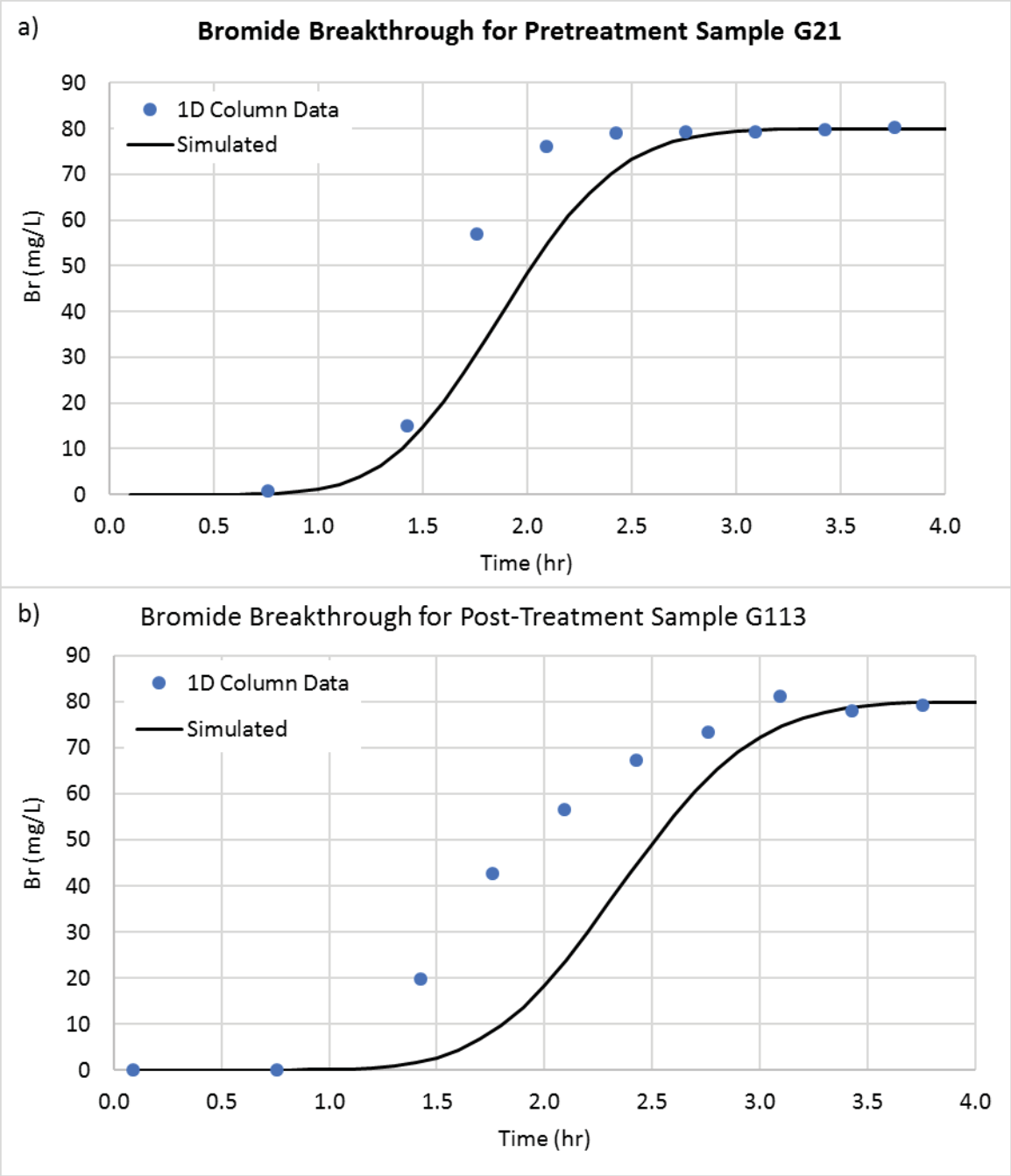

Figure 7-1. Bromide Result History Comparison for a) Pretreatment Sample G21, and b) Post-Treatment Sample G113

Experimental effluent aqueous uranium concentrations were compared to simulated model results in Figure 7-2. Gaps in sample collection from 4 to 54 hours and 69 to 150 hours represent two stop flow events where effluent was not collected. Results show the timestep assignment is independent of the time unit conversion of hours (as defined in VS2DRTI) to seconds (as required by PHREEQC Rates card) applied to Eq. 4-3 when fully implemented in the PHREEQC input file (Figure 7-2). Simulation comparisons for both samples match experimental data well providing confidence in the PHREEQC uranium kinetic release rate implementation. Experimentally derived release rates during stop-flow events

for pre-treatment sample G21 are in good agreement with simulated release rates at 0.94 mg/L/day and 3.32 mg/L/day, respectively, for the first stop-flow event and 0.28 mg/L/day and 3.19 mg/L/day, respectively, for the second stop-flow event. Comparison of release rates for the post-treatment sample G113 against simulated results are in less agreement with values of -1.45e-4 mg/L/day and 0.052 mg/L/day, respectively, for the first stop-flow event and -9.1e-5 mg/L/day and 0.052 mg/L/day, respectively, for the second stop-flow event. Simulated release rates are used due to being consistently higher than the corresponding experimentally derived rates and thus conservative in representing the release of uranium.

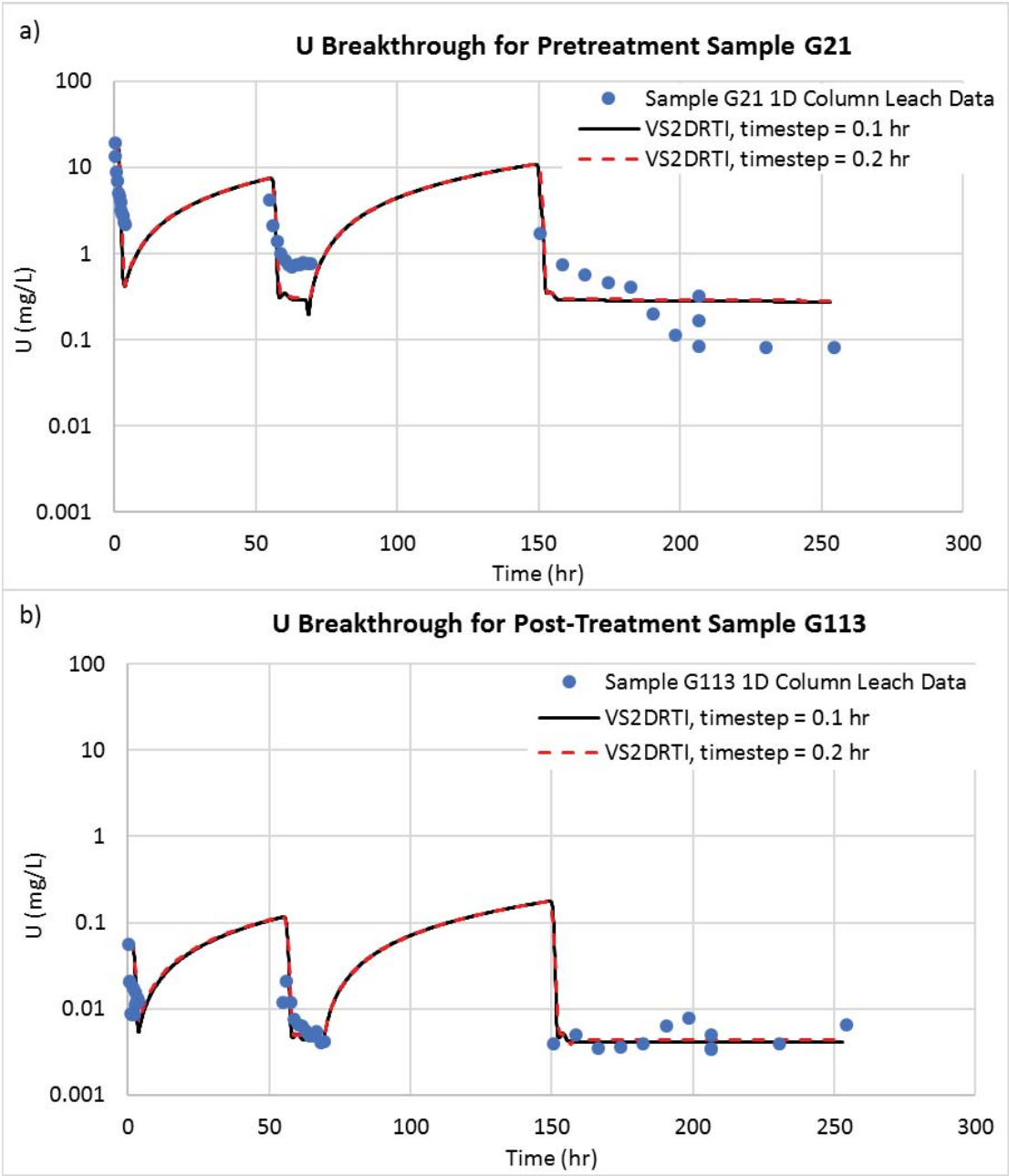

Figure 7-2. Uranium Result History Comparison for a) Pretreatment Sample G21, and b) Post-Treatment Sample G113

One-dimensional uranium kinetic release parameters were compared between previously derived values from ECF-300FF5-11-0151 and those calculated from Stage B EAA characterization data for use in 3-D remedy injection modeling. Results between the two simulation parameter sets are in good agreement with each other for both pretreatment and post-treatment scenarios (Figure 7-3). In general, previously derived forward rate and distribution coefficient values produce slightly lower uranium concentrations when compared to recently derived values during the simulation period. Both parameter sets fall within the range of estimated parameter uncertainty and are valid in estimating kinetic uranium release.

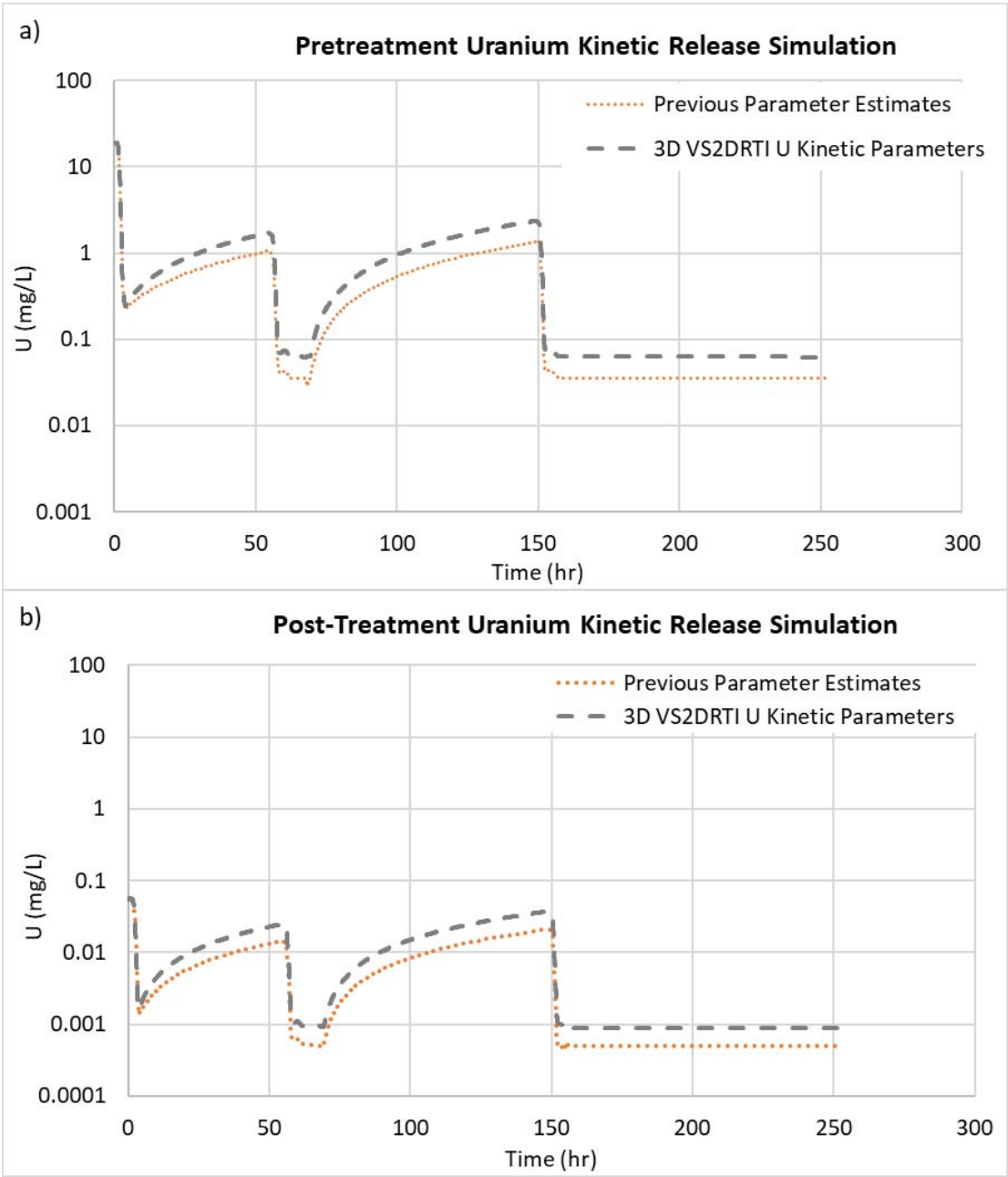

Figure 7-3. Uranium Kinetic Release Parameter Comparison between a) Pretreatment, and b) Post-Treatment Simulations

7.2 Three-Dimensional Remedy Injection Model Results

This section discusses results from the 3-D Remedy Injection model and supporting 2-D groundwater and 3-D heterogeneous models.

7.2.1 Remedy Injection Flow Field

Flow field results from the 3-D Remedy Injection model show extensive mounding of solution above the groundwater table as a result of remedy injections into the PRZ and LVZ. Aqueous saturation results are presented at 0, 1, 2, 3, and 4 day time periods (Figure 7-4). Increases in saturation are observed from approximately 5 m horizontally and 3 m vertically above the water table after two successive injection periods to the PRZ (Figure 7-4c), though the greatest saturation (values >0.9) extends approximately 3 m horizontally and 1 m vertically above the water table after. Little change was observed to the horizontal extent after the remaining two LVZ injection periods reaching approximately 6 m, though the vertical extent did reach approximately 7 m above the water table (Figure 7-4e). Saturations greater than 0.9 reached between 3 to 4 m horizontally and vertically above the water table.

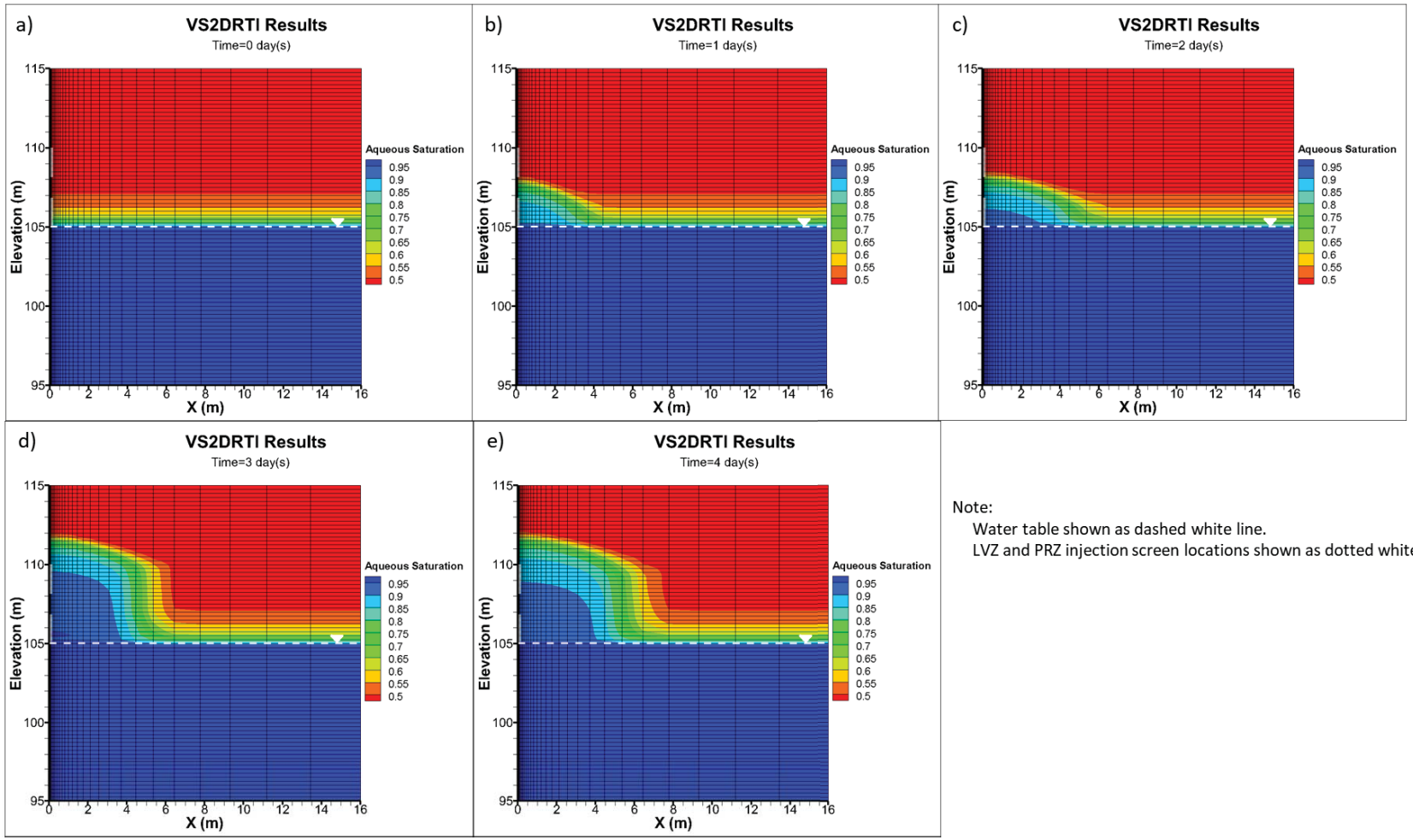

Note:
Water table shown as dashed white line.
LVZ and PRZ injection screen locations shown as dotted white lines.

Figure 7-4. 3-D Remedy Injection Model Aqueous Saturation Profiles a) Before Injections, b) After the First PRZ, c) Second PRZ, d) First LVZ, and e) Second LVZ Injection Periods

7.2.2 Geochemical Evolution

Evaluation of system geochemistry was conducted using observation nodes near the injection sites to compare constituent evolution over time (Figure 7-5) in addition to two-dimensional plots showing spatial variability at a single point in time.

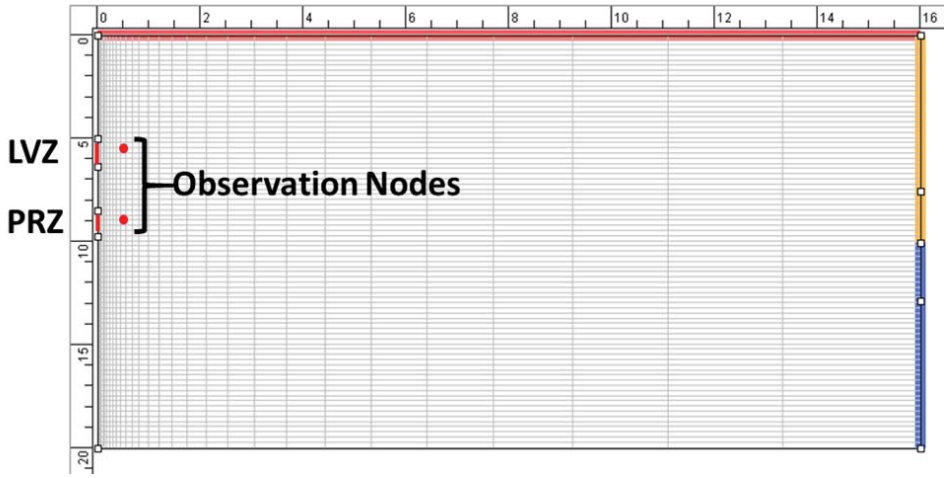

Figure 7-5. Observation Node Locations Used for Timeseries Plots

Timeseries plots for major system aqueous constituents including HPO_4^{2-}, uranium, calcium, sodium, bicarbonate, and pH are shown in Figure 7-6 near the LVZ and PRZ injection screens. A phosphorus species timeseries plot near the PRZ injection screen is included in Figure 7-7 showing HPO_4^- as the dominant species over a range of pH values during injections. A single 100-fold increase in sodium occurs at the first instance of injection for a respective PRZ and LVZ period from 10^{-3} M to 10^{-1} M. Uranium and calcium show a sharp decrease in concentration at the onset of the first respective injection while bicarbonate and phosphate increase. Between injection periods, pH, uranium and bicarbonate concentrations increase while calcium and phosphate concentrations decrease. Increases in both bicarbonate and uranium are consistent with kinetic dissolution of calcite and generic uranium-silicate, respectively while decreasing phosphate concentrations indicate phosphate group mineral precipitation. Furthermore, bicarbonate could be added as a result of the injection solution itself (Table 6-14). Changes in pH range from 7.6 during times of injection (matching the injection solution pH) and increasing to 8.9 between injection periods. After all remedy injections are completed (approximately at day 5), all constituents level off with no observed changes.

Changes in dominant cation exchange sites are shown in Figure 7-8. Prior to injections, calcium occupies a majority of the exchange sites in the vadose zone. With the influx of high sodium and potassium concentrations into the system with the injection of the remedy solution (Table 6-14), calcium is displaced into solution as calcium bound exchange sites decrease nearly 1000-fold from 10^{-3} M to 10^{-7} M. Sodium and potassium bound exchange sites subsequently increase nearly 100-fold from 10^{-5} M to 10^{-3} M.

Mineral composition timeseries plots are compiled in Figure 7-9. The uranium solid phase representing the total amount of uranium defined by either pre-treatment or post-treatment bulk kinetic release rates (see Section 6.2.4.4 for additional details) is shown to be in excess throughout the simulation with little observable change. Calcite decreases with time during all four remedy injection periods in the PRZ and last two injection periods in LVZ. Uranium bearing mineral phases liebigite ($Ca_2UO_2(CO_3)_3(H_2O)_{10}$), chernikovite ($(UO_2)HPO_4(H_2O)_4$), and andersonite ($Na_2CaUO_2(CO_3)_3(H_2O)_6$) are thermodynamically favorable at different times during the simulation. Liebigite precipitation is only found early in the simulation, with increasing amount prior to remedy injections in both the PRZ (first remedy injection)

and LVZ (third remedy injection). Chernikovite is observed briefly between the second and third remedy injection periods near the PRZ injection screen. Andersonite is most favorable after all four remedy injections (beginning on day five), increasing 100-fold in amount over time from approximately 10^{-8} mol to 10^{-6} mol. Hydroxylapatite ($Ca_5(OH)(PO_4)_3$) precipitation occurs at the onset of injections (first and third injections in the PRZ and LVZ, respectively) with amounts in excess of 10^{-3} mol and increasing to approximately 10^{-2} mol. The excess of calcium in pore waters due to displacement from exchange sites and calcite dissolution in addition to phosphate from remedy solution injection create favorable conditions for hydroxylapatite. It is worth noting that the simulation indicates that hydroxylapatite reaches saturation and precipitation is favorable. Mineral precipitation and dissolution for all minerals modeled is assumed instantaneous with the exception of calcite and generic uranium-silicate.

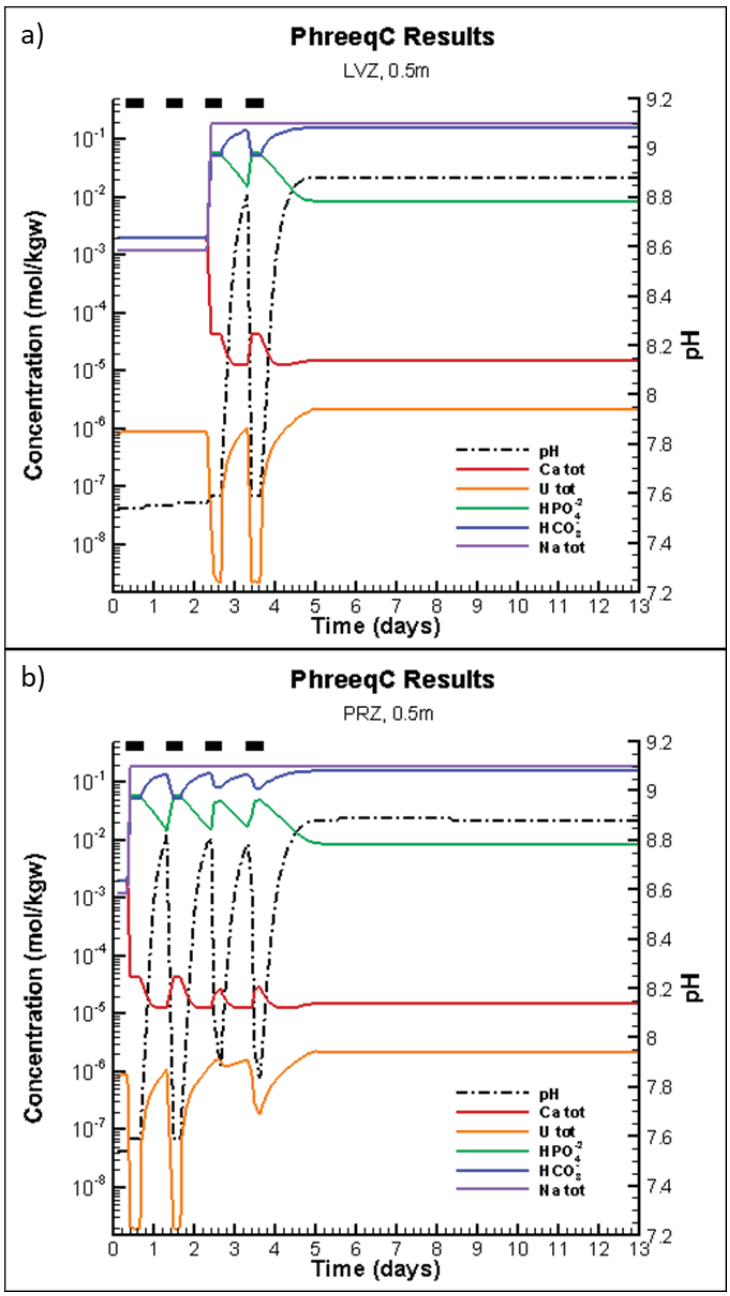

Figure 7-6. 3-D Remedy Injection Model Geochemical Evolution Timeseries Plots for a) 0.5 m Distance from LVZ Injection Screen, and b) 0.5 m Distance from PRZ Injection Screen with Injection Periods Indicated by Black Bars

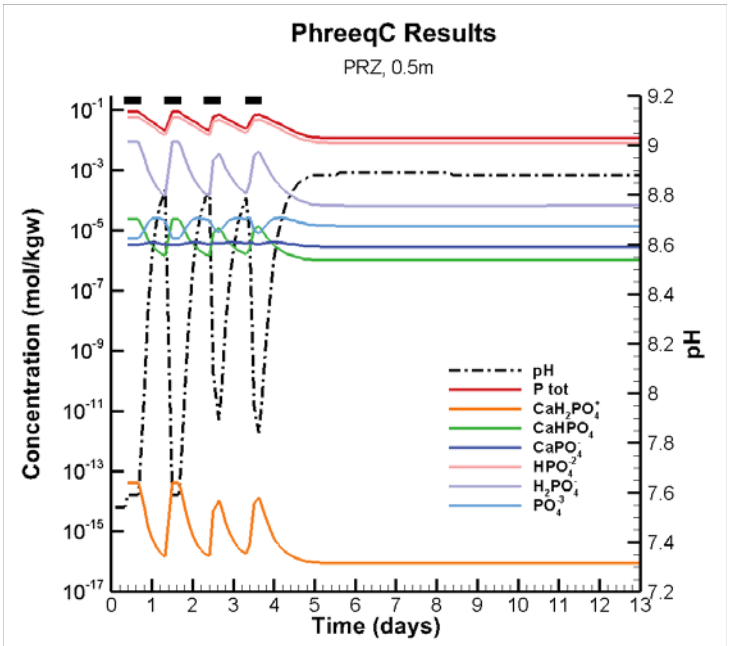

Figure 7-7. 3-D Remedy Injection Model Geochemical Evolution Timeseries Plots for Phosphorus Species 0.5 m Distance from PRZ Injection Screen with Injection Periods Indicated by Black Bars

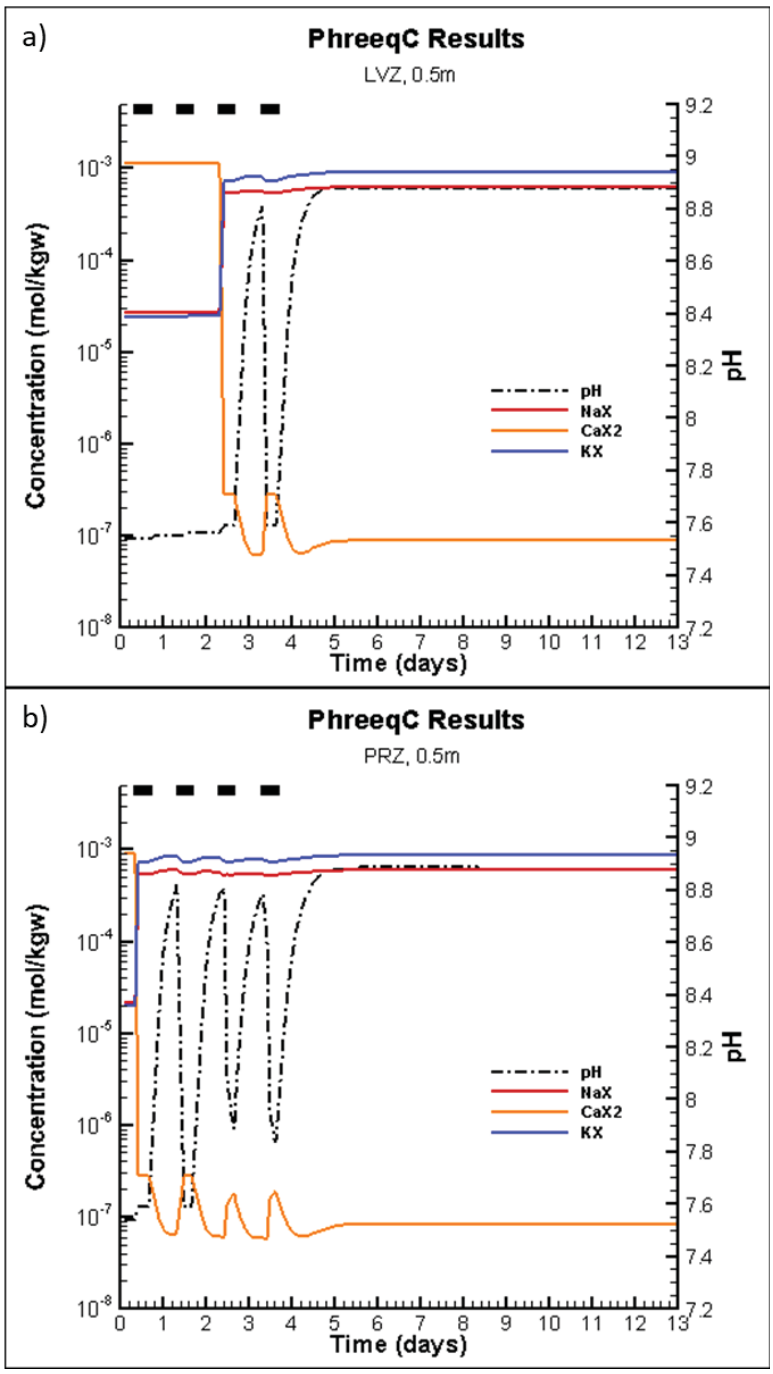

Figure 7-8. 3-D Remedy Injection Model Cation Exchange Site Timeseries Plots for a) 0.5 m Distance from LVZ Injection Screen, and b) 0.5 m Distance from PRZ Injection Screen with Injection Periods Indicated by Black Bars

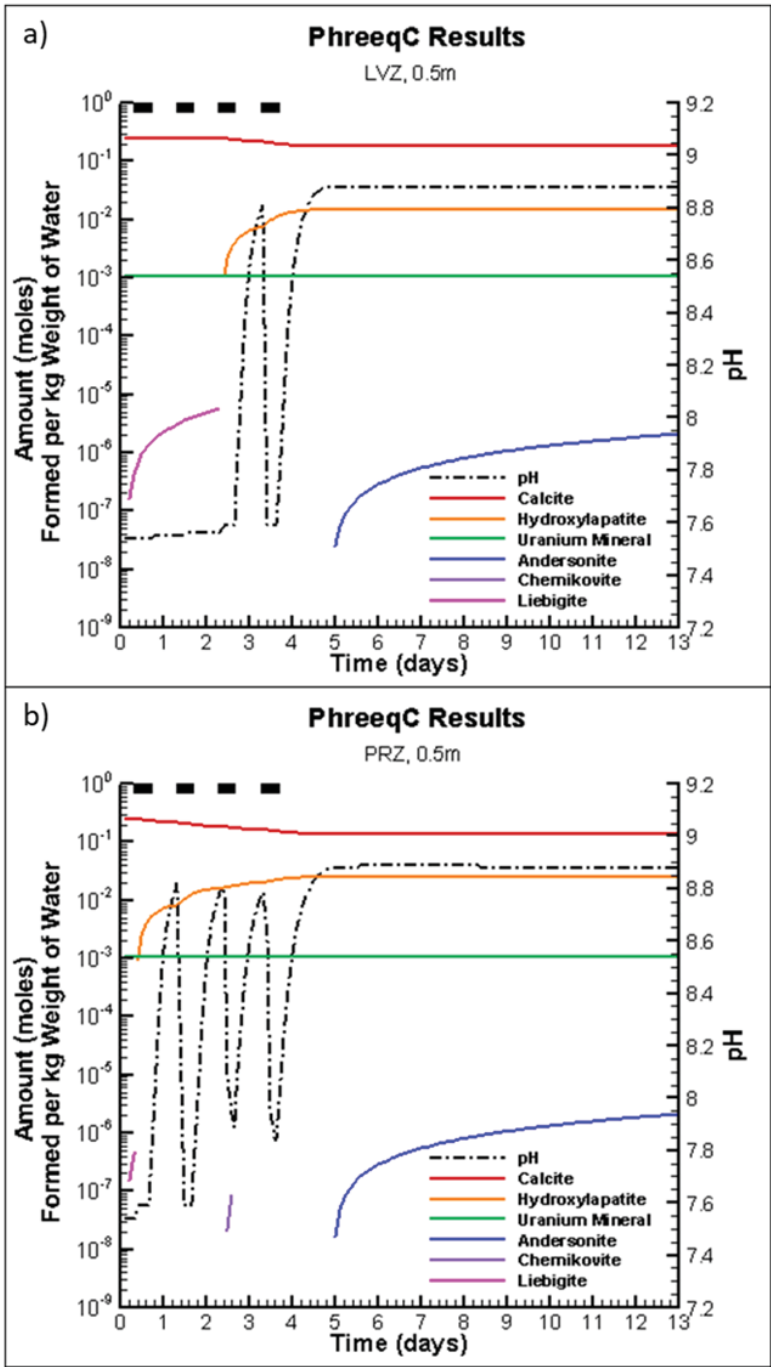

Figure 7-9. 3-D Remedy Injection Model Mineral Timeseries Plots for a) 0.5 m Distance from LVZ Injection Screen, and b) 0.5 m Distance from PRZ Injection Screen with Injection Periods Indicated by Black Bars

3-D Remedy Injection modeling results were compared to mineral phase diagrams generated using GWB (Figure 7-10) to provide model confidence. The logarithmic molar ratio of hydrogen phosphate to bicarbonate (Log HPO_4/HCO_3) represent the relative amount of phosphate to bicarbonate in the system such that high phosphate concentrations relative to bicarbonate produces positive values while greater bicarbonate concentrations relative to phosphate produces negative values. Log HPO_4/HCO_3 values range from 0.05 during injections to -1.3 after all remedy injection periods. As discussed in Figure 7-9, both hydroxylapatite and andersonite precipitate during 3-D Remedy Injection simulation, corroborated by

thermodynamically favorable non-uranium-phase mineral diagram and uranium-phase mineral diagrams produced by GWB (Figure 7-10b and d, respectively).

Dissolution behavior of the generic uranium-silicate mineral phase was compared between the 3-D Remedy Injection model and NAC scenario 2 m laterally from the PRZ injection screen (Figure 7-11). In the NAC scenario (without any injection or active remediation), a linear decrease is observed throughout the simulation. When comparing to the 3-D Remedy Injection model results, the amount of generic uranium-mineral decreases at the same rate as the NAC early in the simulation and diverges during the first remedy injection period. Over time, more generic uranium-silicate is present in the 3-D Remedy Injection model relative to the NAC scenario indicating less aqueous uranium release over time as a result of remedy injections.

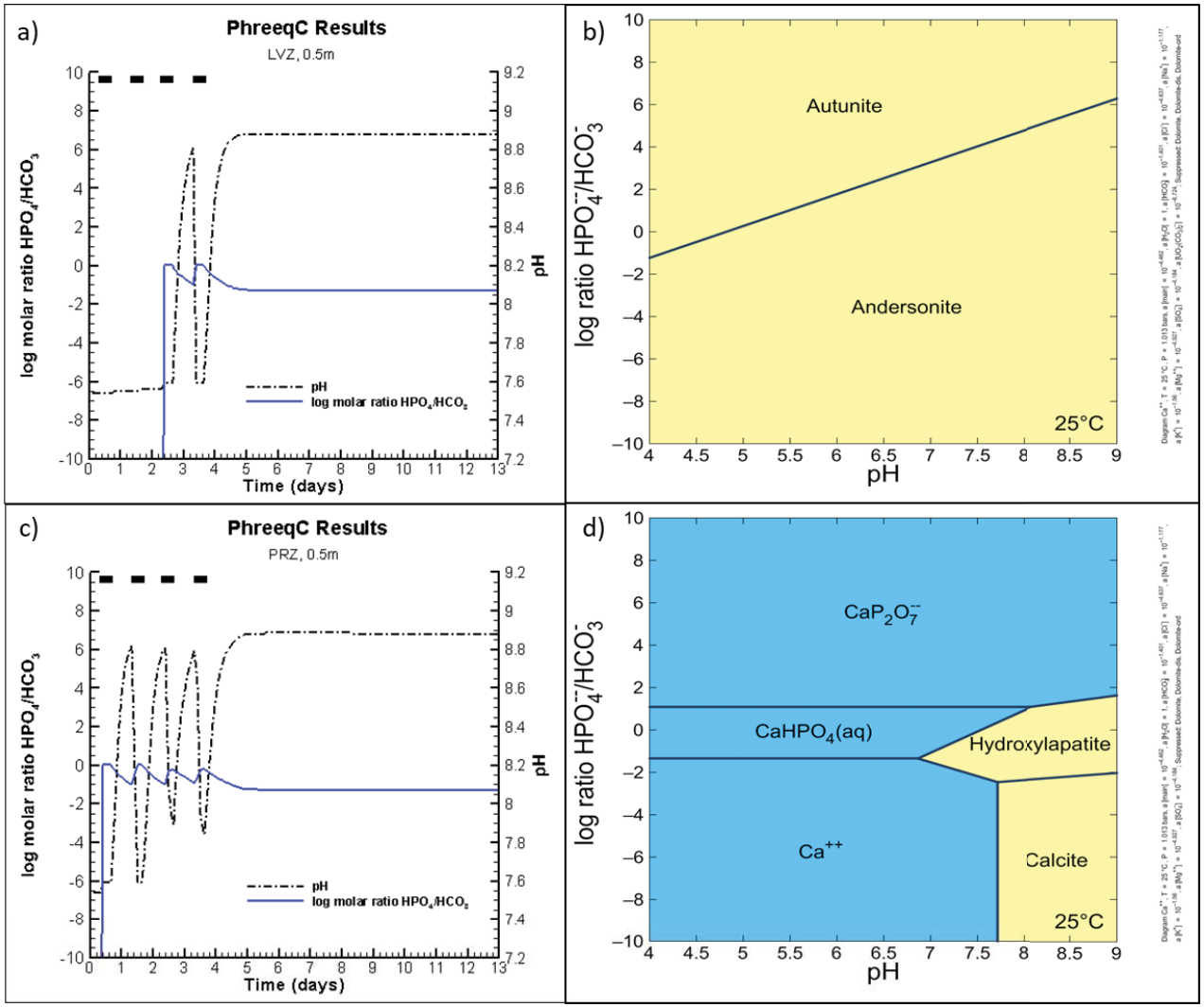

Figure 7-10. 3-D Remedy Injection Model log Molar Ratio HPO4/HCO3 and pH Timeseries Plots (Left) for 0.5 m Distance from a) LVZ Injection Screen, and c) PRZ Injection Screen with Injection Periods Indicated by Black Bars and Phase Diagrams (Right) b) with Uranium, and d) without Uranium

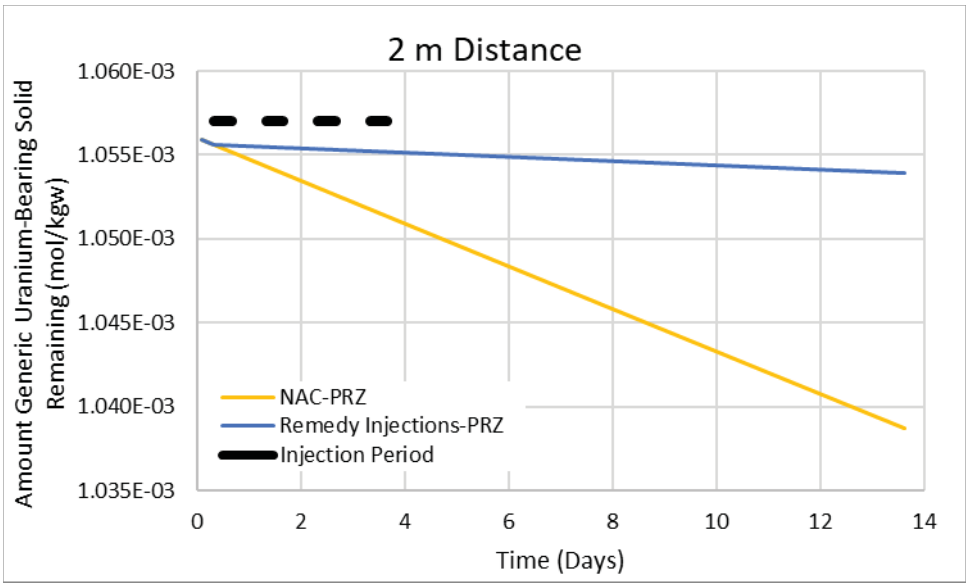

Figure 7-11. Comparison of Remaining Amount of Generic Uranium-Bearing Solid per kg Water between Simulated 3-D Remedy Injection Model and No Action Case (NAC)

Two-dimensional plots from the 3-D Remedy Injection Model are presented at 0, 1, 2, 3, and 4 day time periods for phosphate shown as HPO_4^{2-}, uranium solid phase available for bulk kinetic release, total aqueous uranium, pH, calcite, and hydroxylapatite to evaluate constituent extents (Figures 7-12 through 7-17, respectively).

Changes in phosphate molar concentration and extent is shown in Figure 7-12. Phosphate extents mirror increases in aqueous saturation due to remedy injections in the vadose zone with greatest extents of 5 m horizontally and 3 m vertically above the water table after both PRZ injections and approximately 6 m horizontally and vertically above the water table after both LVZ injection periods. Groundwater phosphate concentrations rapidly increase during the injection periods and remain primarily in the saturated Hf unit. Horizontal groundwater migration is likely due to solution displacement during the injection periods as no flow gradient is imposed in the aquifer in the 3-D VS2DRTI radial setup.

Kinetic dissolution of a uranium solid is shown in Figure 7-13. As described in earlier sections, kinetic mineral dissolution was only assigned to the unsaturated portion of the model domain with conditional pre-treatment and post-treatment rates based on the presence of phosphate. As phosphate concentrations increase due to remedy solution injections, the dissolution rate of uranium mineral decreases. Differences in dissolution rates are shown by minor changes in total uranium mineral moles present (Figure 7-13b-e). For example, after two periods of PRZ injections, approximately 1.0557e-3 moles of uranium mineral is present (per kg of water) near the injection screen as compared to 1.0533e-3 moles (per kg of water) present throughout the rest of the model domain (Figure 7-13c). This is consistent with the conceptual model where less aqueous uranium in leached, or conversely more uranium mineral is sequestered, where remedy solution is injected. Similarly, more uranium mineral is present near the LVZ screen after both remedy injection periods as compared to the remainder of the model domain (Figure 7-13e).

Aqueous uranium concentrations show an increased reaction front as a result of remedy solution injections (Figure 7-14). As high concentrations of phosphate and bicarbonate enter the system via remedy solution injection, uranium bound by reactive surface complexes are released into the porewater solution. This is shown by increased aqueous uranium concentrations at the furthest edge of solution front, with decreasing concentrations near the injection sites.

The system pH is largely controlled by calcite dissolution. High concentrations of bicarbonate entering the system as a result of remedy solution injection results in calcite dissolution (Figure 7-15). After both PRZ injection periods, calcite nearest the injection screen decreased to approximately 1.8e-1 moles as compared to 2.52e-1 moles (per kg of water) throughout the rest of the unsaturated model domain. Calcite dissolved further after the remaining two LVZ injection periods decreasing to approximately 1.3e-1 moles (per kg of water) nearest the PRZ injection screen. Corresponding pH values ranged dramatically throughout the model domain with the greatest increases of 8.8 collocated with decreasing amounts of calcite (Figure 7-16). Furthermore, simulated unsaturated domain pH values of 8.8 to 7.5 are in agreement with measured 1-D column leach experiment pH values (Section 4.1.5.3).

Modeled 3-D remedy solution injections indicate favorable conditions for sustained hydroxylapatite formation (Figure 7-17). Approximately 1.36e-2 moles (per kg of water) of hydroxylapatite formed within 3 m horizontally and 2 m vertically above the water table after both PRZ injection periods (Figure 7-17c). Greater amounts of hydroxylapatite formed after both LVZ injections with a maximum amount of 2.5e-2 moles nearest the PRZ injection screens. Amounts greater than 1.36e-2 moles (per kg of water) were shown from 4 m horizontally and 6 m vertically above the water table (Figure 7-17e). As stated earlier the simulation indicates when hydroxylapatite reaches saturation and precipitation is favorable. No kinetic limits were imposed on mineral precipitation or dissolution for all minerals modeled with the exception of calcite and generic uranium-silicate.

Similarly, the 3-D simulation indicates favorable conditions for sustained andersonite ($Na_2CaUO_2(CO_3)_3(H_2O)_6$) formation (Figure 7-18). Approximately 3e-6 moles of andersonite formed with the outermost reaction band after both PRZ injection periods (Figure 7-18c). Greater amounts of andersonite formed after both LVZ injections with a maximum of 7.5e-6 moles (per kg of water) (Figure 7-18e). As stated earlier the simulation indicates when andersonite reaches saturation and precipitation is favorable. No kinetic limits were imposed on mineral precipitation or dissolution for all minerals modeled with the exception of calcite and generic uranium-silicate.

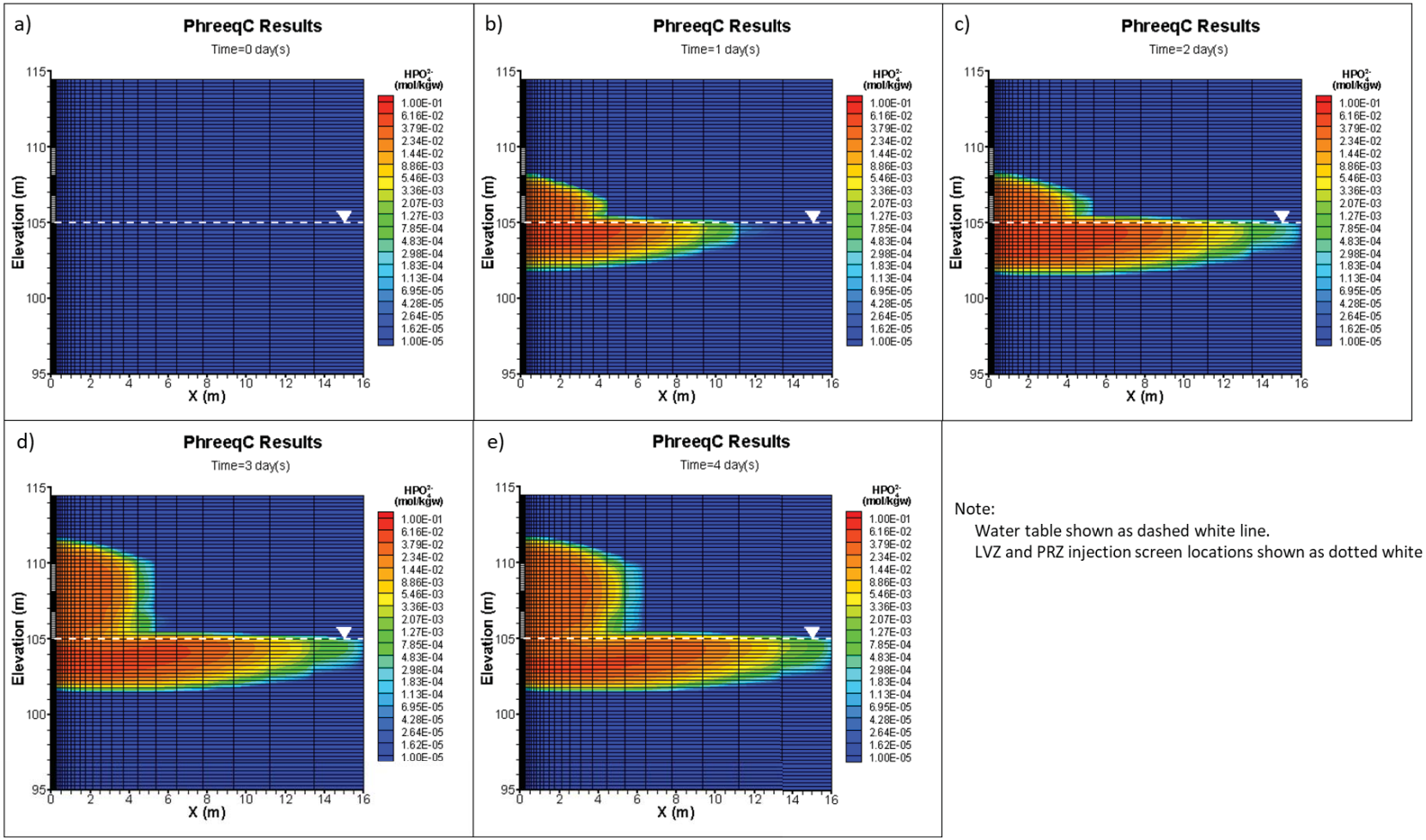

Note:
Water table shown as dashed white line.
LVZ and PRZ injection screen locations shown as dotted white lines.

Figure 7-12. 3-D Remedy Injection Model HPO_4^{2-} Profile a) Before Injections, b) After the First PRZ, c) Second PRZ, d) First LVZ, and e) Second LVZ Injection Periods

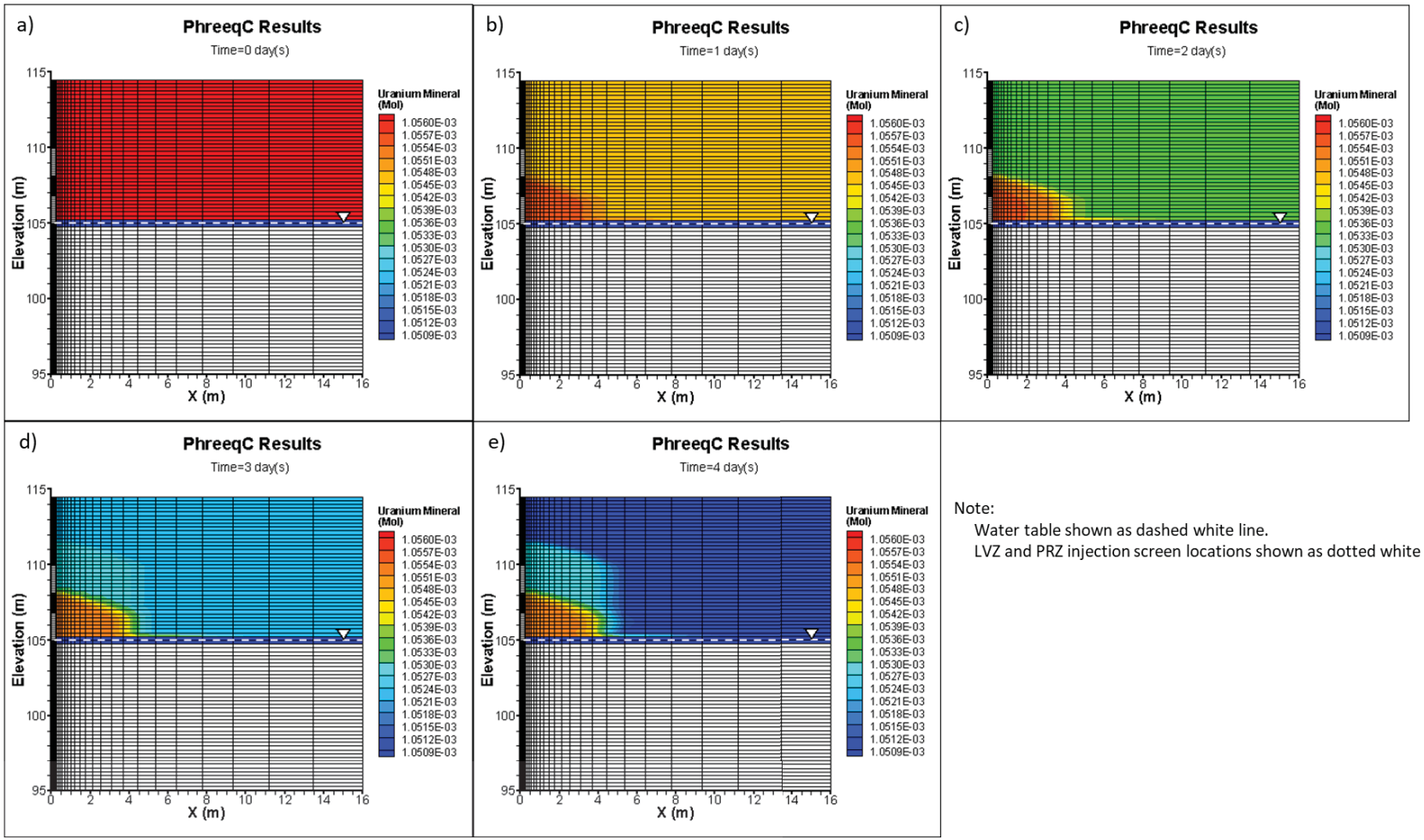

Note:
Water table shown as dashed white line.
LVZ and PRZ injection screen locations shown as dotted white lines.

Figure 7-13. 3-D Remedy Injection Model Generalized Uranium-Bearing Solid Profile a) Before Injections, b) After the First PRZ, c) Second PRZ, d) First LVZ, and e) Second LVZ Injection Periods

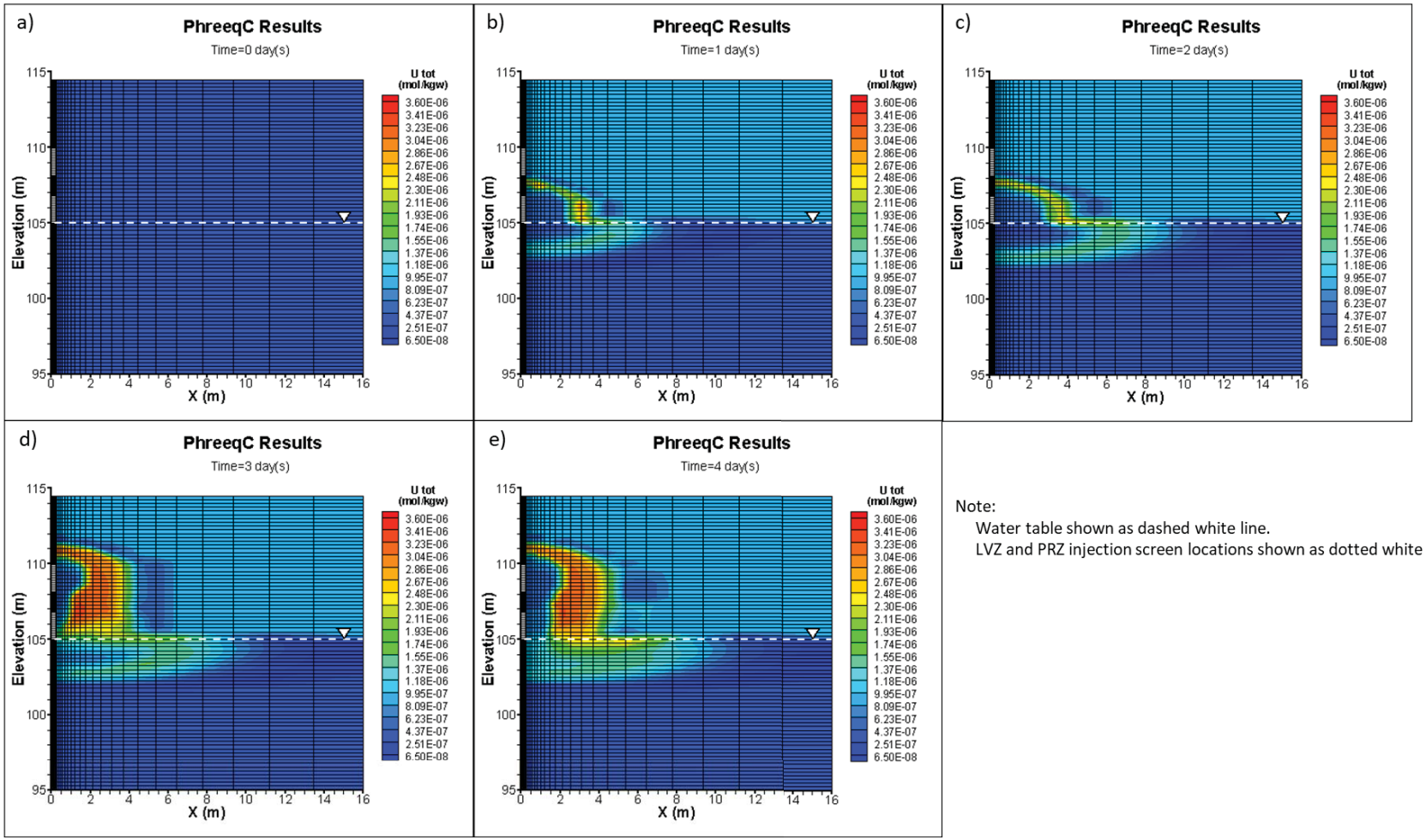

Note:
Water table shown as dashed white line.
LVZ and PRZ injection screen locations shown as dotted white lines.

Figure 7-14. 3-D Remedy Injection Model Total Aqueous Uranium Profile a) Before Injections, b) After the First PRZ, c) Second PRZ, d) First LVZ, and e) Second LVZ Injection Periods

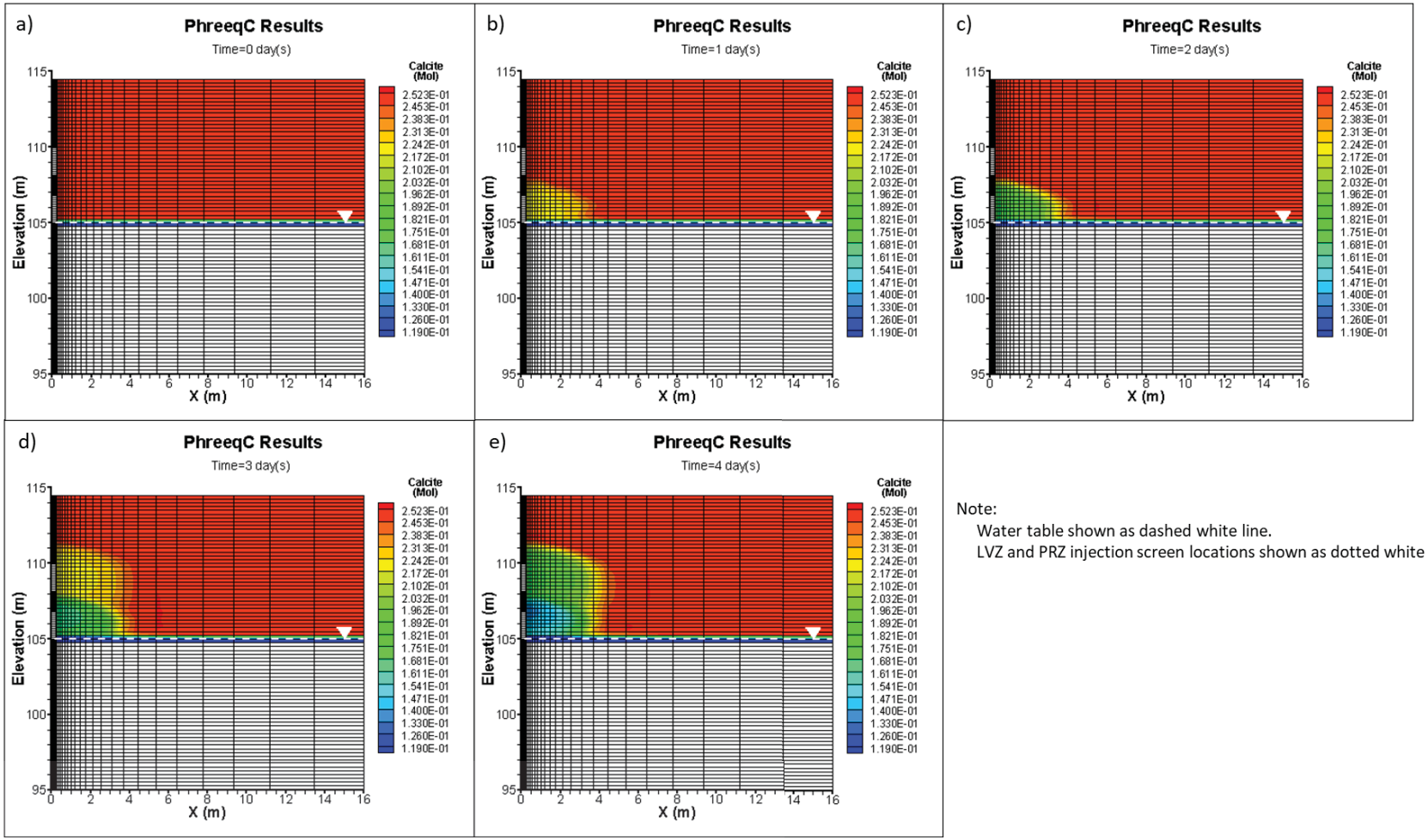

Note:
Water table shown as dashed white line.
LVZ and PRZ injection screen locations shown as dotted white lines.

Figure 7-15. 3-D Remedy Injection Model Calcite Profile a) Before Injections, b) After the First PRZ, c) Second PRZ, d) First LVZ, and e) Second LVZ Injection Periods

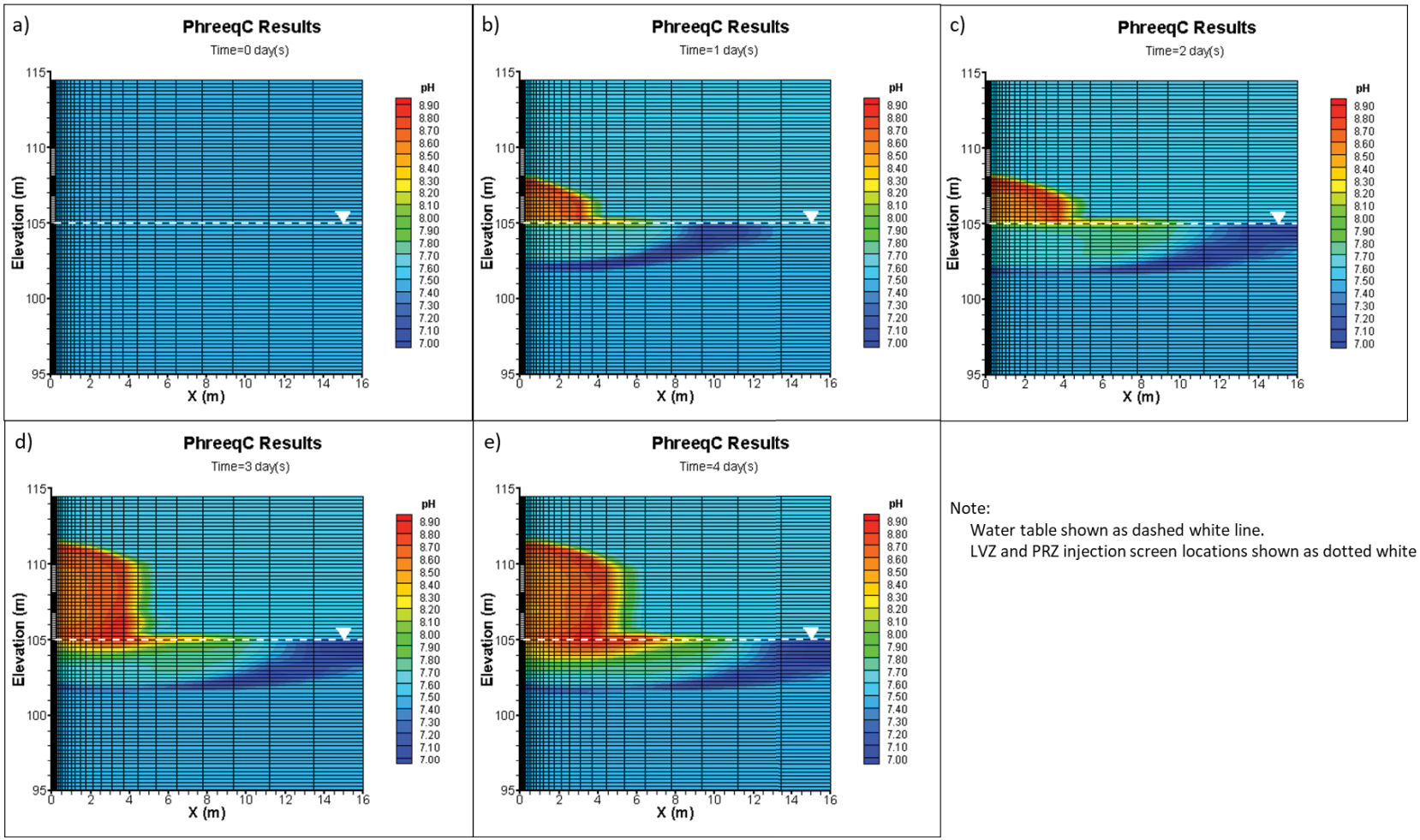

Note:
Water table shown as dashed white line.
LVZ and PRZ injection screen locations shown as dotted white lines.

Figure 7-16. 3-D Remedy Injection Model pH Profile a) Before Injections, b) After the First PRZ, c) Second PRZ, d) First LVZ, and e) Second LVZ Injection Periods

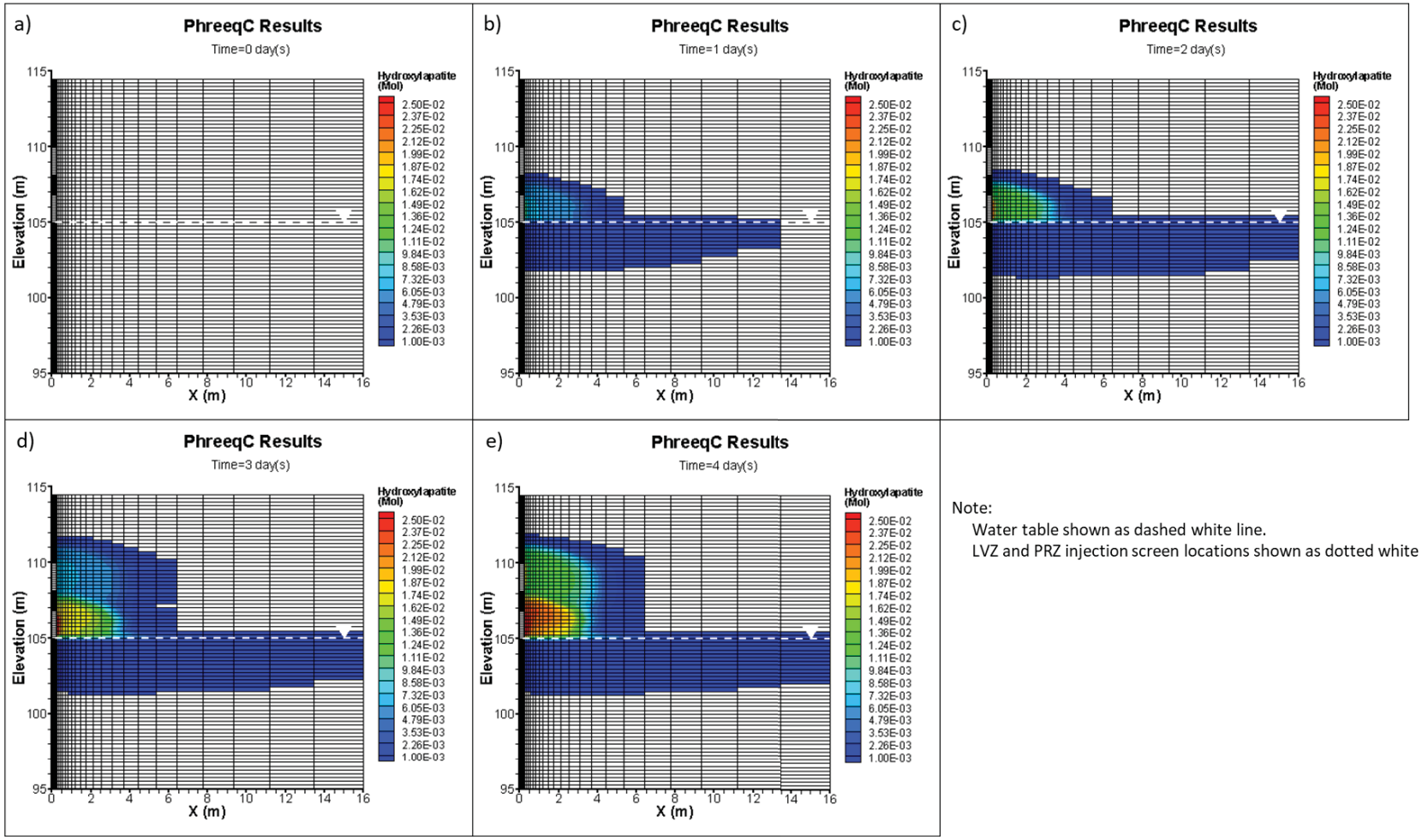

Note:
Water table shown as dashed white line.
LVZ and PRZ injection screen locations shown as dotted white lines.

Figure 7-17. 3-D Remedy Injection Model Hydroxylapatite Profile a) Before Injections, b) After the First PRZ, c) Second PRZ, d) First LVZ, and e) Second LVZ Injection Periods

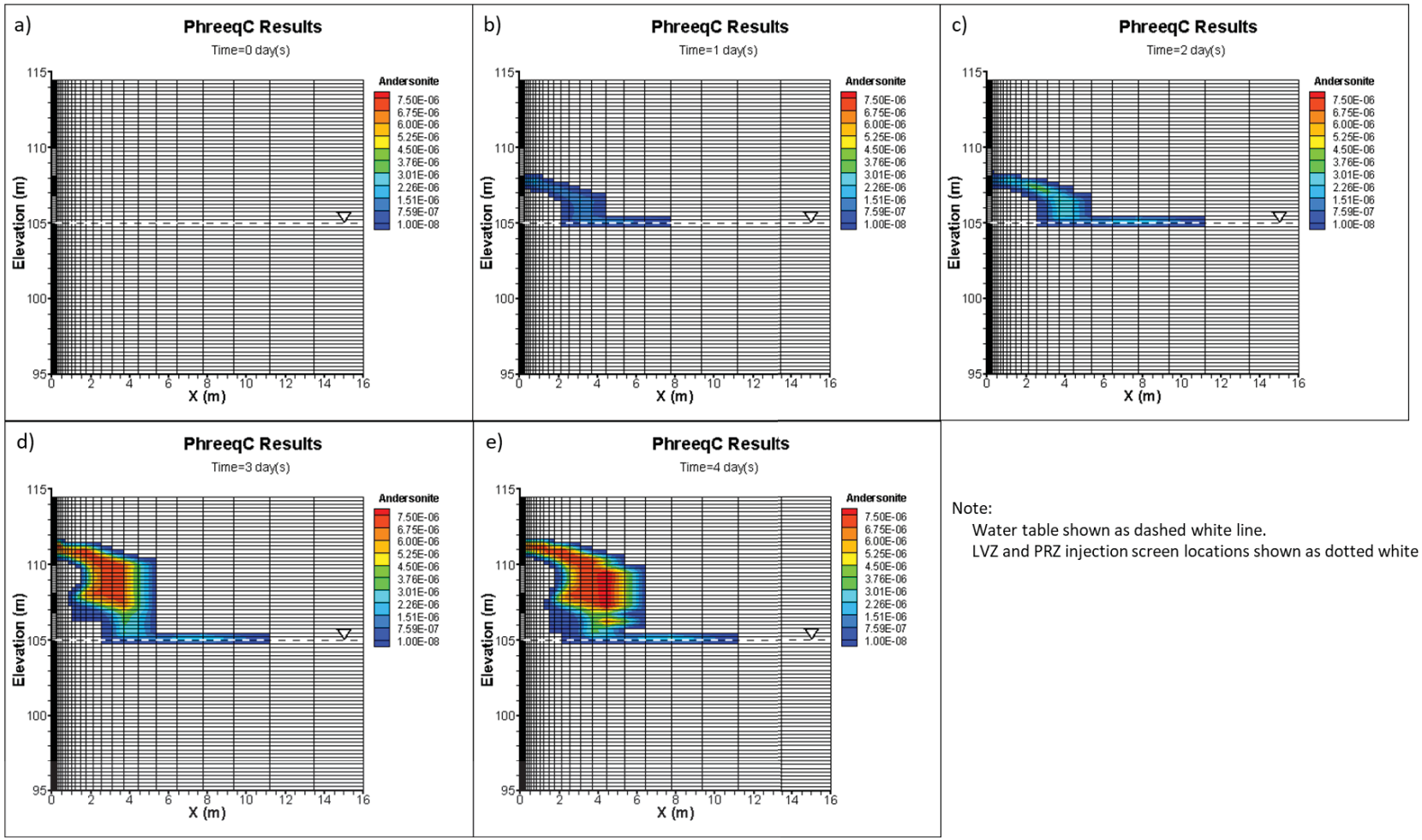

Note:
Water table shown as dashed white line.
LVZ and PRZ injection screen locations shown as dotted white lines.

Figure 7-18. 3-D Remedy Injection Model Andersonite Profile a) Before Injections, b) After the First PRZ, c) Second PRZ, d) First LVZ, and e) Second LVZ Injection Periods

7.2.3 Sensitivity Analysis

Discussion of all sensitivity case results are provided in the following section.

7.2.3.1 Evaluation of Model Components Results

Three model cases were conducted to evaluate the effectiveness in representing observation data by increasing the model complexity:

1) Kinetics mediated case (Case 1): The model setup is identical to the base case described above with the exclusion of all identified equilibrium phases and surface complexation reactions.

2) Kinetics mediated and calcium-phosphate precipitation case (Case 2): Similar to the kinetics mediated case with the inclusion of calcium-phosphate minerals hydroxyapatite and whitlockite.

3) Kinetics mediated, calcium-phosphate precipitation, and surface complexation reaction case (Case 3): The model setup is identical to the base case with the exclusion of all uranium-bearing mineral phases.

Timeseries plots for major system aqueous constituents including sodium, HPO_4^{2-}, bicarbonate, calcium, pH, and uranium are shown in Figure 7-19 near the PRZ injection screens for all three cases described above. A single 100-fold increase in sodium occurs at the first instance of injection from 10^{-3} M to 10^{-1} M for all three cases. In the absence of any mineral precipitation, both HPO_4^{2-} and bicarbonate increase from 1e-3 M to ~5e-2 M at the onset of the first injection for Case 1. Both HPO_4^{2-} and bicarbonate remain high with no changes in concentration for the remainder of the simulation. The constant simulated concentrations are inconsistent with the observed changes in phosphate to bicarbonate ratios during injection (Section 4.1.4.2). For Cases 1 and 2, calcium-phosphate minerals can precipitate resulting in concentration fluctuations between injections. Bicarbonate concentrations result in higher concentrations of ~0.1 M while HPO_4^{2-} decreases to ~10^{-2} M after 13 days of simulation. Calcium concentrations show little change for Case 1 with concentrations stabilizing at ~10^{-3} M. Both Cases 2 and 3, though, show a greater decrease in calcium concentration at the onset of injections with decreasing concentrations between injection periods. In Case 1, pH values remain constant at ~7.6, likely due to the exclusion of mineral precipitation from occurring. The resulting pH of 7.6 is largely inconsistent with post-injection 1-D column leaching sample pH measurement values typically greater than a pH of 8 (Figure 4-33). Cases 2 and 3 exhibit large fluctuations in pH from 7.6 to 8.8 between injection periods with the final pH remaining high at ~8.9 after 13 days of simulation, more consistent with measured values of post-treatment samples. For Case 1 and 2, uranium shows a sharp increase in concentration just prior to injections with a maximum concentration of ~10^{-5} M. Unlike the previous two cases, the uranium concentration in Case 3 has a dampened increase to ~10^{-6} M due to the incorporation of surface complexation reactions. During the remainder of the simulation period, all three cases act similarly in that uranium concentrations decrease during injections with gradual increases in between. After the fourth injection, uranium concentrations rebound to concentrations of ~10^{-5} M (~2,000 μg/L), much higher than observed uranium concentrations in post-injection 1-D column leaching experiments of 600 μg/L.

Saturation index timeseries plots are compiled in Figure 7-20 for all three cases. Because certain minerals were excluded from precipitating during the modeling sensitivities, tracking the saturation index in the system allows for direct comparisons between cases. For all minerals presented, a saturation index of zero or greater (positive) indicates thermodynamically favorable precipitation conditions. Hydroxylapatite ($Ca_5(OH)(PO_4)_3$) and whitlockite ($Ca_3(PO_4)_2$) indicate favorable conditions for precipitation for Case 1, though hydryoxylapatite is likely to out compete whitlockite. This is evident for Cases 2 and 3 where calcium-phosphate minerals can readily precipitate under favorable conditions. Hydroxylapatite remains at a saturation index of zero from the onset of the first injection indicating precipitation while whitlockite

remains below zero during the 13 day simulation period. Uranium bearing mineral phase chernikovite ($(UO_2)HPO_4(H_2O)_4$) is thermodynamically favorable after approximately 5 days of simulation for Case 1. Both Cases 2 and 3 indicate andersonite ($Na_2CaUO_2(CO_3)_3(H_2O)_6$) as the favorable uranium mineral phase to precipitate after 5 days of simulation.

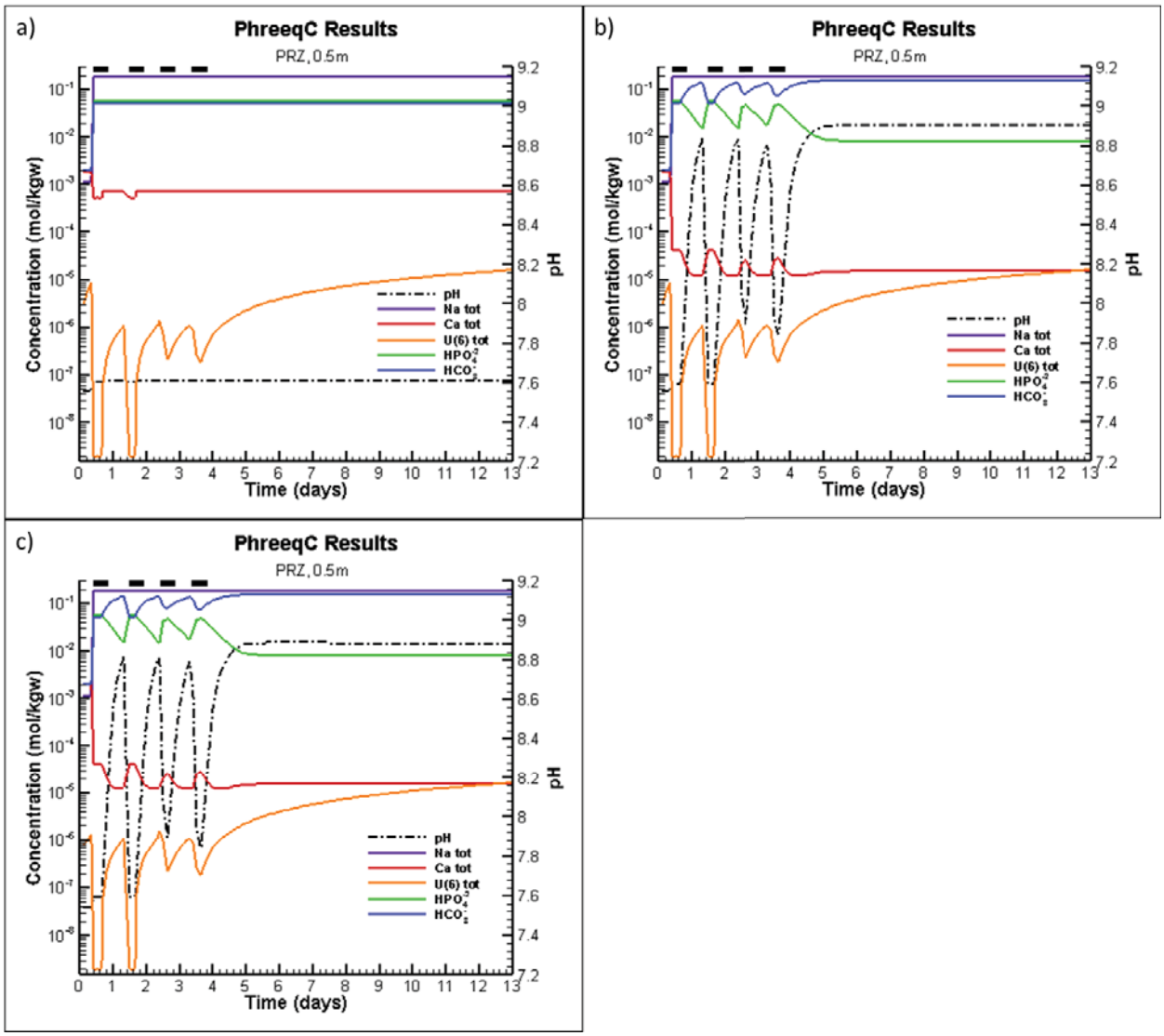

Figure 7-19. Model Component Sensitivity Case Geochemical Timeseries Plots for a) Case 1, b) Case 2, and c) Case 3 from PRZ Injection Screen with Injection Periods Indicated by Black Bars

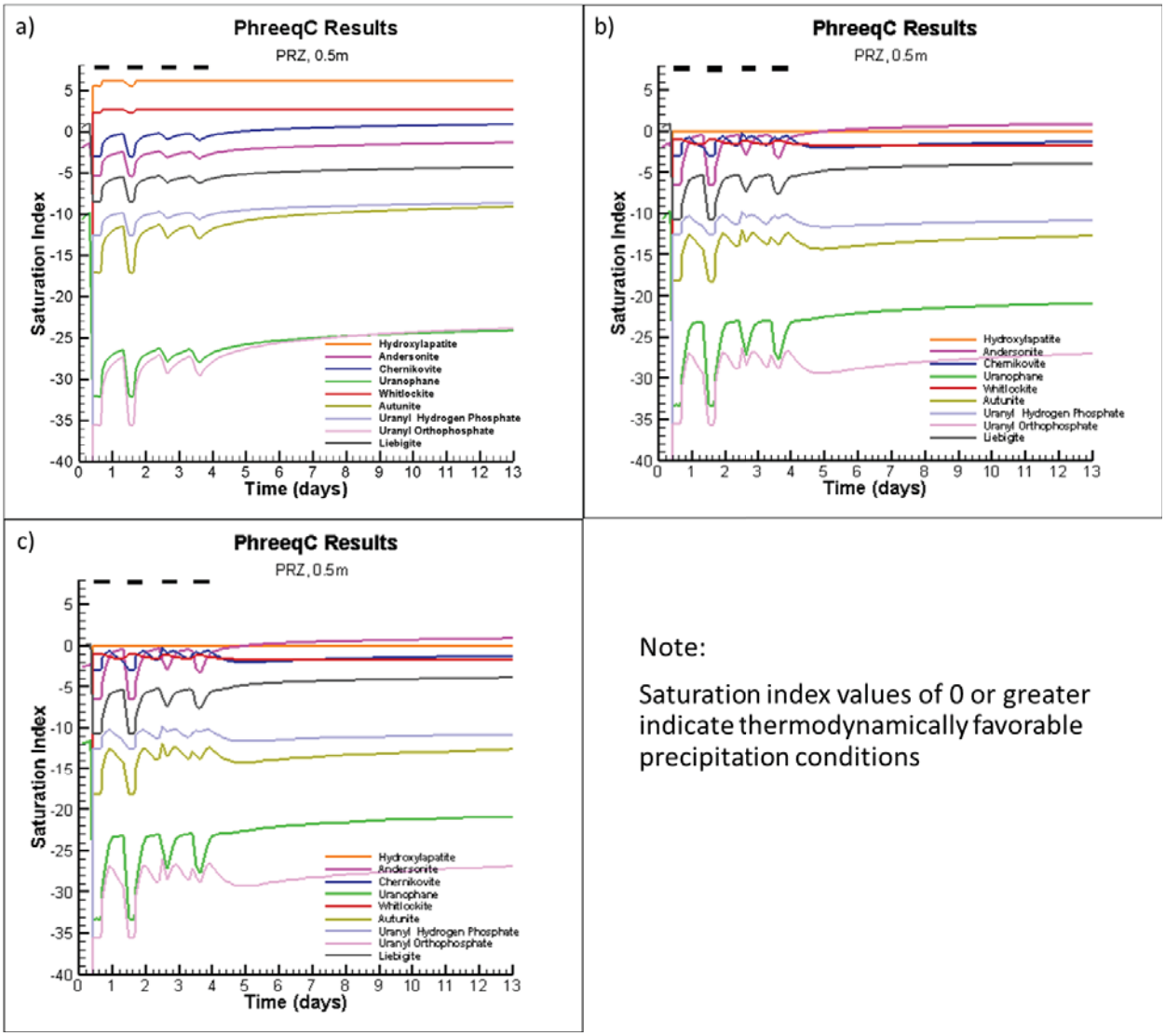

Figure 7-20. Model Component Sensitivity Case Saturation Index Timeseries Plots for a) Case 1, b) Case 2, and c) Case 3 from PRZ Injection Screen with Injection Periods Indicated by Black Bars

7.2.3.2 Two-Dimensional Remedy Injection Groundwater Model Results

A supplemental two-dimensional groundwater model was developed to evaluate the impact of groundwater flow on near-field geochemical evolution during and shortly after remedy injections. Groundwater velocity is calculated by the following:

$$v = \frac{KI}{n} \qquad \textbf{(Eq. 7-1)}$$

where:

v: groundwater velocity $[m/hr]$

K: horizontal hydraulic conductivity $[m/hr]$

I: horizontal hydraulic gradient $[m/m]$

n: porosity [−].

Simulated groundwater velocity prior to injections across the model domain within the saturated Hf unit at two elevations (104.9 and 102.9 m) were compared against target velocity value of 0.33 m/hr to provide confidence in model flow implementation (Figure 7-21). Simulated groundwater velocity is relatively constant across the model domain at an average of 0.35 m/hr and matches the target velocity.

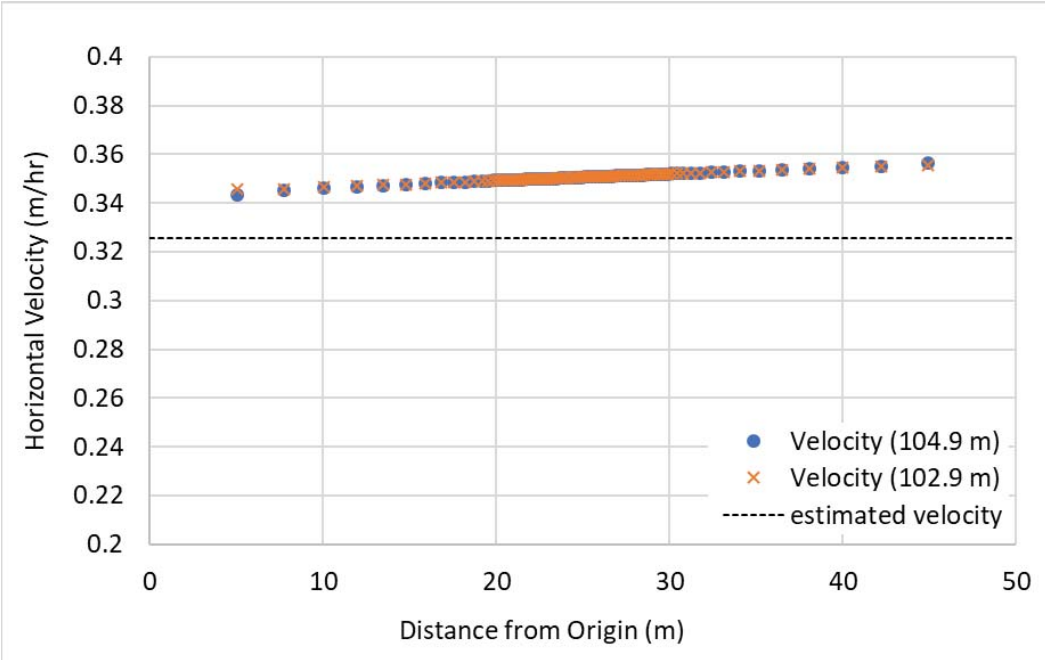

Figure 7-21. Horizontal Groundwater Velocity in 2-D Remedy Injection Groundwater Model

Geochemical evolution timeseries plots are presented for an observation node 10 m downgradient of the injection site and one meter below the water table (Figure 6-8). Aqueous concentrations for select constituents calcium, uranium, HPO_4^{2-}, bicarbonate, and sodium are shown in Figure 7-22. Concentrations in sodium, bicarbonate, and HPO_4^{2-} increased rapidly after the first injection period (within 1 day) to concentrations approximately 0.2 M, 0.1 M, and 0.03 M, respectively. Concentrations for all three constituents gradually decrease after day 3 to concentrations elevated prior to injections. Similarly, uranium concentrations increase to ~1e-6 M after the first remedy injection period, with a rapid decline after five days below concentrations prior to injections. Similar rapid increases and subsequent decreases in concentration were observed in groundwater monitoring wells surrounding the Stage B EAA for uranium and phosphate (Figure 4-9 through Figure 4-11). Conversely, calcium concentrations decrease nearly 100-fold from 10^{-3} M to 10^{-5} M, remaining low through the rest of the simulated period. Though groundwater monitoring data show a slow rebound in calcium concentration over the course of months after remedy injections occur, this simulation shows consistent results with near term monitoring results (Figure 4-15 through Figure 4-17). Rapid changes to pH are observed in the simulated data, fluctuating between 8.4 directly following the first injection and declining back to pH of 8. Measured pH values greater than 8 were not observed in monitoring data, likely due to uncertainty in the amount of calcite present in the vadose zone.

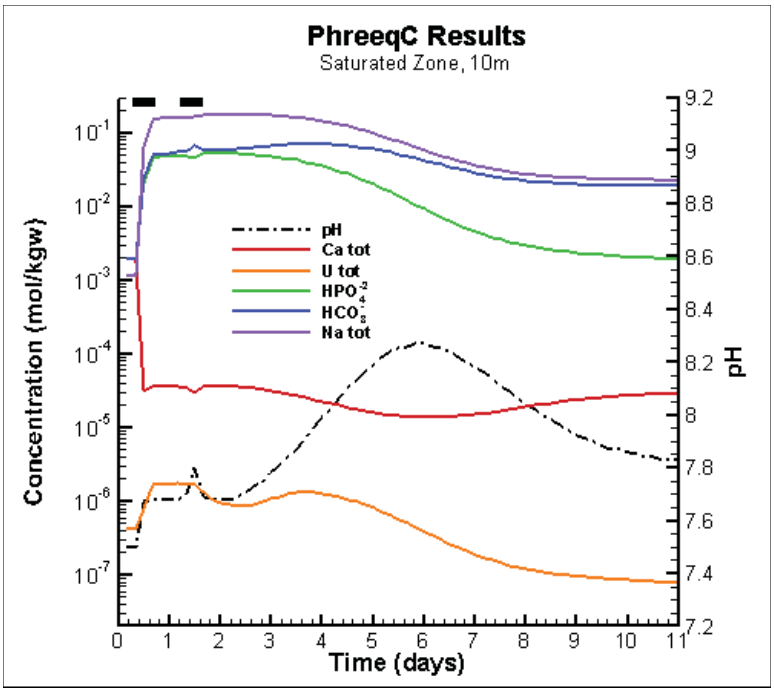

Figure 7-22. 2-D Remedy Injection Groundwater Flow Model Geochemical Evolution Timeseries Plots for 10 m Distance Downgradient from PRZ Injection Screen with Injection Periods Indicated by Black Bars

The molar ratio of phosphate to bicarbonate is presented in Figure 7-23. More phosphate is available relative to bicarbonate at higher molar ratios, providing more favorable conditions for uranium to phosphate interaction. An increase in phosphate to bicarbonate is observed, peaking just after a day of both remedy injection periods. Similar trends are observed in groundwater monitoring data directly following remedy injections (Figure 4-12 through Figure 4-14).

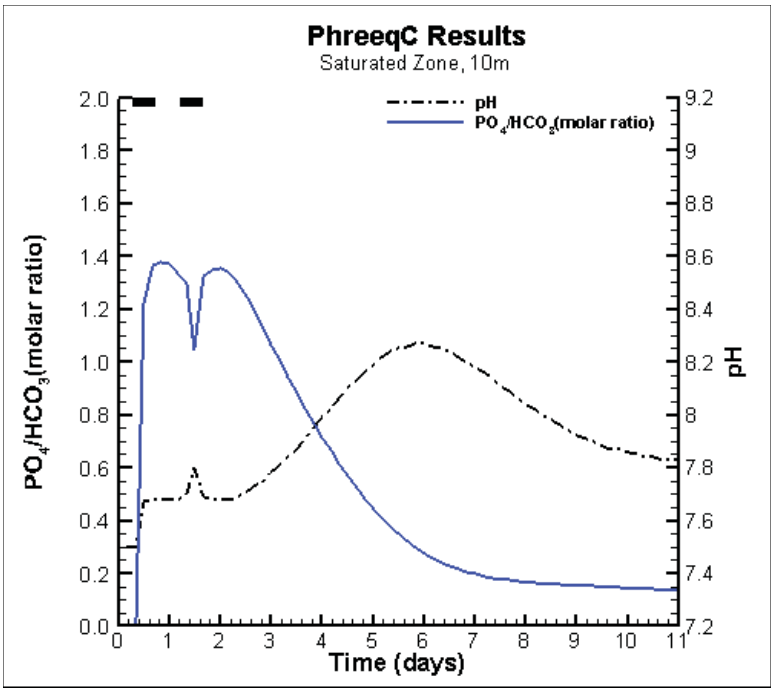

Figure 7-23. 2-D Remedy Injection Groundwater Flow Model Phosphate to Bicarbonate Indicator Timeseries Plots for 10 m Distance Downgradient from PRZ Injection Screen with Injection Periods Indicated by Black Bars

The ratio of calcium to sodium in milliequivalents is presented in Figure 7-24. A rapid decline is observed shortly after the onset of remedy injections from 3.3 to 1e-4, remaining low throughout the remainder of the simulation. This is reflective of the high concentration of sodium introduced to the system via remedy solution in combination with the concurrent decrease in calcium concentrations (Figure 7-24). A similar ratio trend is observed in groundwater monitoring wells within and downgradient of the Stage B EAA directly after remedy injections (Figure 4-21 through Figure 4-23).

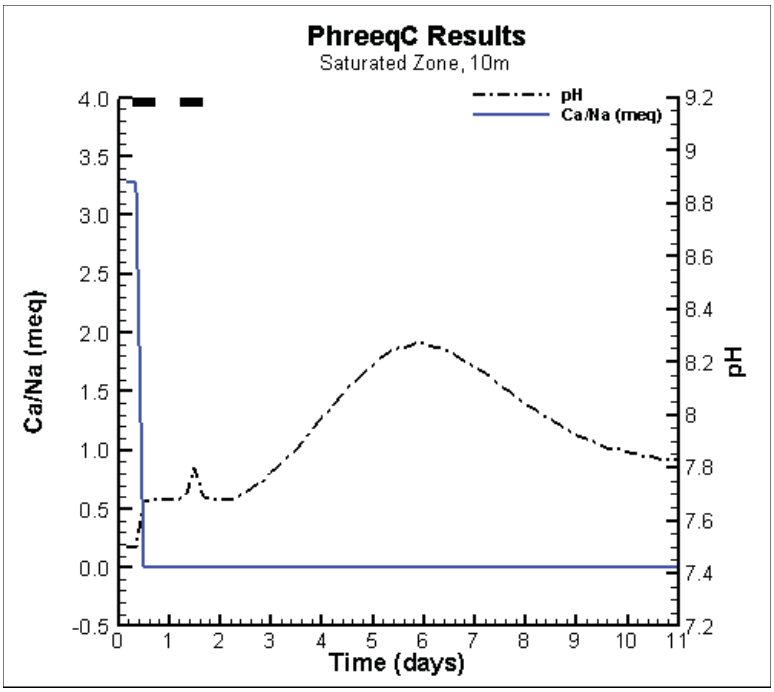

Figure 7-24. 2-D Remedy Injection Groundwater Flow Model Calcium to Sodium Ratio Indicator Timeseries Plots for 10 m Distance Downgradient from PRZ Injection Screen with Injection Periods Indicated by Black Bars

The observed increase and subsequent decrease in aqueous uranium concentration shown in Figure 7-25 is plotted in two-dimensions as snapshots in time in Figure 7-25. After the first PRZ injection, increases in uranium concentration are observed both upgradient (to the left) and downgradient (to the right) of the injection screen within the saturated Hf zone, truncated vertically by the top of the saturated Rwie (Figure 7-25b). The increase in both up and down gradient persists after the second PRZ injection (Figure 7-25c). After injections occur, groundwater flow prevails and removes the slight increase in aqueous uranium downgradient and out of the model domain within four days (Figure 7-25d). Finally, Figure 7-25e shows no remaining uranium plume in the groundwater near the injection screen. Furthermore, a lower aqueous uranium concentration is observed in the groundwater surrounding the injection screen when compared to the initial conditions.

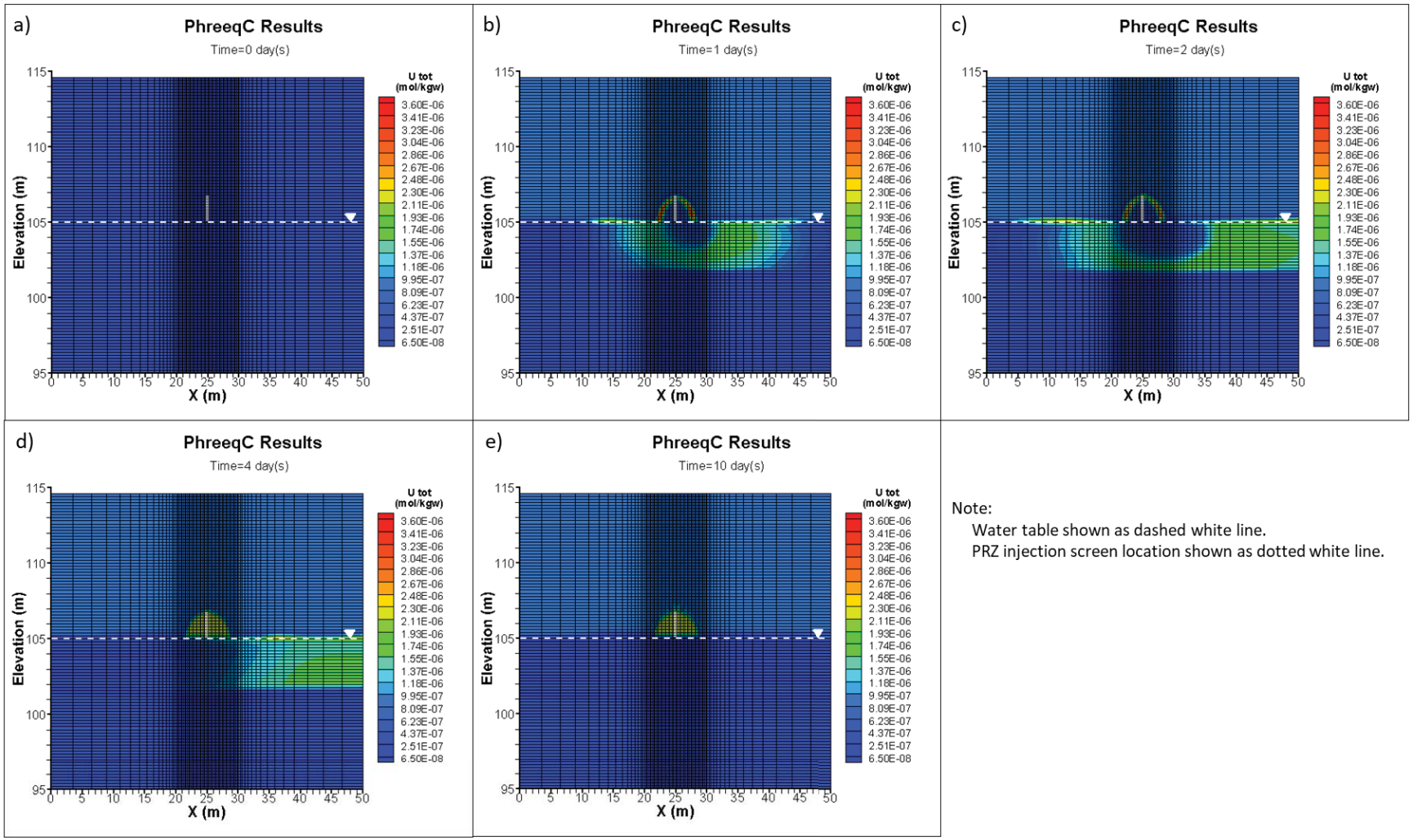

Figure 7-25. 2-D Groundwater Model Uranium Profile a) Before Injections, b) After the First PRZ Injection, c) After the Second PRZ Injection, d) 4 Days, and e) 10 Days

7.2.3.3 Textural Heterogeneity Modeling

This section discusses results from the 3-D Heterogeneous Remedy Injection model.

Remedy Injection Flow Field

Flow field results from the 3-D Heterogeneous Remedy Injection model show extensive mounding of solution above the groundwater table as a result of remedy injections into the PRZ and LVZ. Aqueous saturation results are presented at 0, 1, 2, 3, and 4 day time periods (Figure 7-26). Increases in saturation are observed from approximately 5 m horizontally within the Hanford formation silt (Hf m) after two successive injection periods to the PRZ (Figure 7-26c). The horizontal extent increased from 5 m to 11m within the Hf m after the remaining two LVZ injection periods. Significant increase in the vertical extent was observed, reaching an approximately elevation of 112 m (Figure 7-26e) with saturations greater than 0.9 between elevations 106 - 109 m.

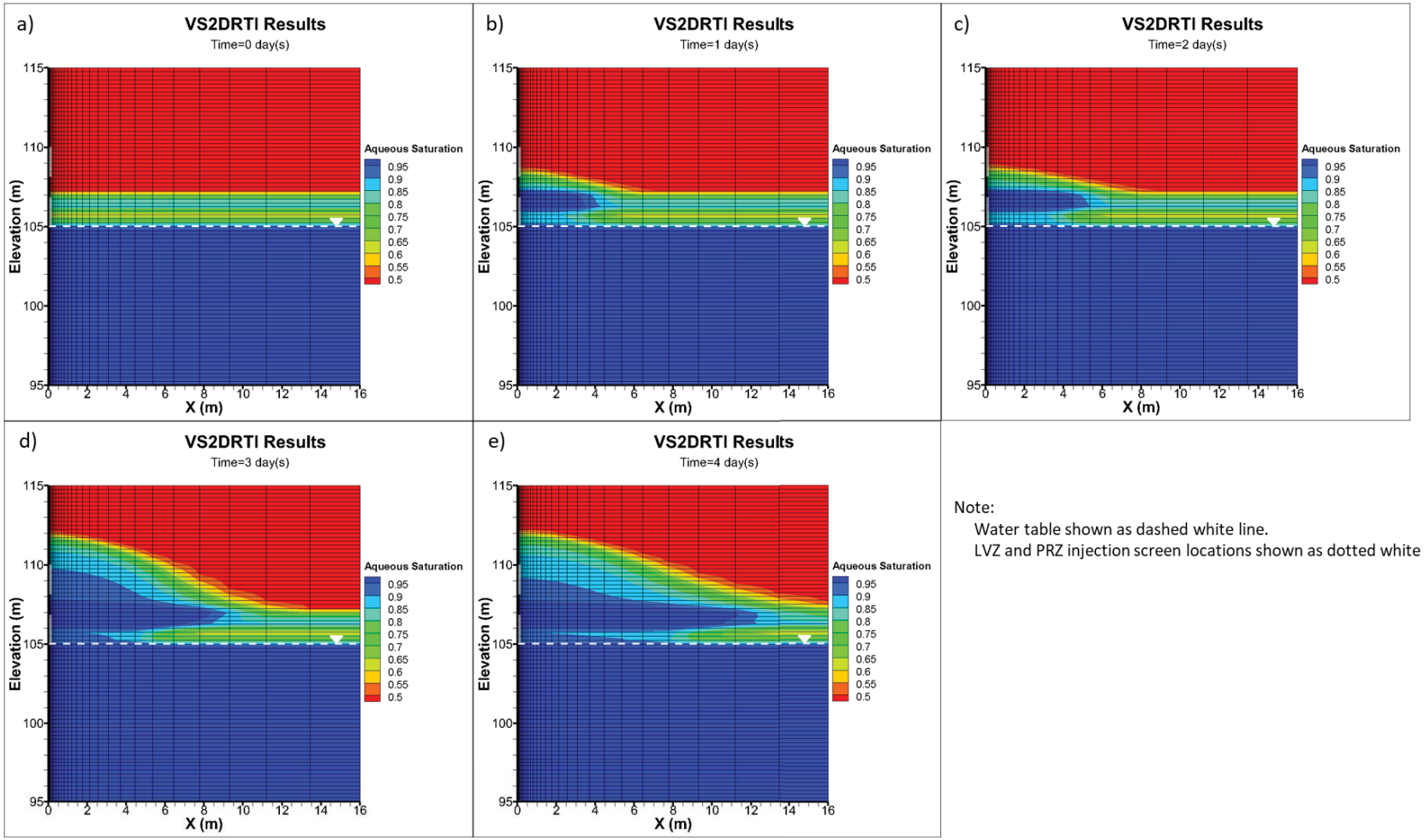

Note:
Water table shown as dashed white line.
LVZ and PRZ injection screen locations shown as dotted white lines.

Figure 7-26. 3-D Heterogeneous Remedy Injection Model Aqueous Saturation Profiles a) Before Injections, b) After the First PRZ, c) Second PRZ, d) First LVZ, and e) Second LVZ Injection Periods

Figure 7-27 shows the change in aqueous saturation after all four injection periods as defined by:

$$\Delta S = S_{t=4} - S_{t=0} \quad \textbf{(Eq. 7-2)}$$

where:

ΔS: Change in aqueous saturation

$S_{t=0}$: Aqueous saturation at time = 0 days

$S_{t=4}$: Aqueous saturation at time = 4 days

Though a direct comparison between the maximum change in bulk electrical conductivity and change in simulated aqueous saturation cannot be made (both pore fluid conductivity and saturation influence bulk electrical conductivity measurements), similarities in geometry between the two impacted regions is striking. Larger difference in bulk electrical conductivity is observed near the LVZ injection screen which tapers with distance, extending approximately 9 m horizontally from wells C9647 to C9693 (Figure 4-6). A similar horizontal extent of 9 to 12 m is observed in simulated change in aqueous saturation (Figure 7-27 right).

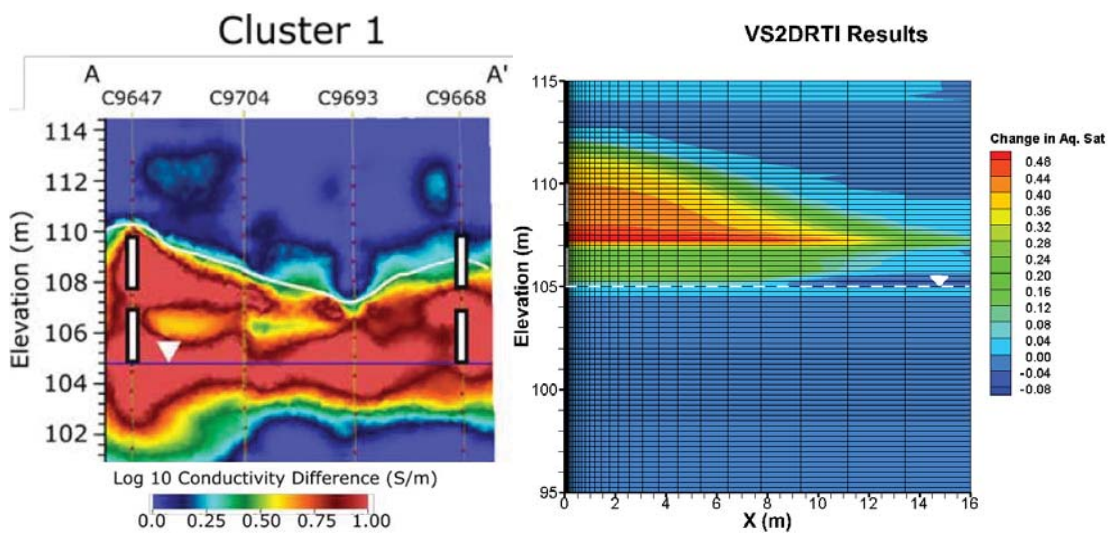

Figure 7-27. Maximum Change in Bulk Electrical Conductivity (Left) and Change in Aqueous Saturation between Days 0 and 4 for the 3-D Heterogeneous Remedy Injection Model (Right)

Geochemical Evolution

Evaluation of system geochemistry was conducted using observation nodes near the injection sites to compare constituent evolution over time (Figure 7-5) in addition to two-dimensional plots showing spatial variability at a single point in time.

Timeseries plots comparing results from the 3-D Remedy Injection model and 3-D Heterogeneous Remedy Injection model, hereinafter respectively referred to as the base case and heterogeneous models, for major system aqueous constituents including HPO_4^{2-}, uranium, calcium, sodium, bicarbonate, and pH are shown in Figure 7-28 near the LVZ and PRZ injection screens. No discernable changes are present between the heterogeneous model and base case model results near the LVZ injection screen (Figure 7-28a and b) with the exception of low concentrations (<1e-9 M) of phosphate observed during the second PRZ injection period in the heterogeneous model. Most differences are seen when comparing the results near the PRZ screen. Either a dampened or negligible effect is noticeable near the PRZ in the

heterogeneous model for all plotted constituents during LVZ injections (Figure 7-28c and d). This is likely due to the low permeability silt layer in the unsaturated zone restricting the LVZ injection solutions to higher elevations (shallower depths), taking longer to reach the LVZ observation node. Overall, no observable difference is shown between the base case and heterogeneous model end-state results after 13 days of simulation time for both observation node locations.

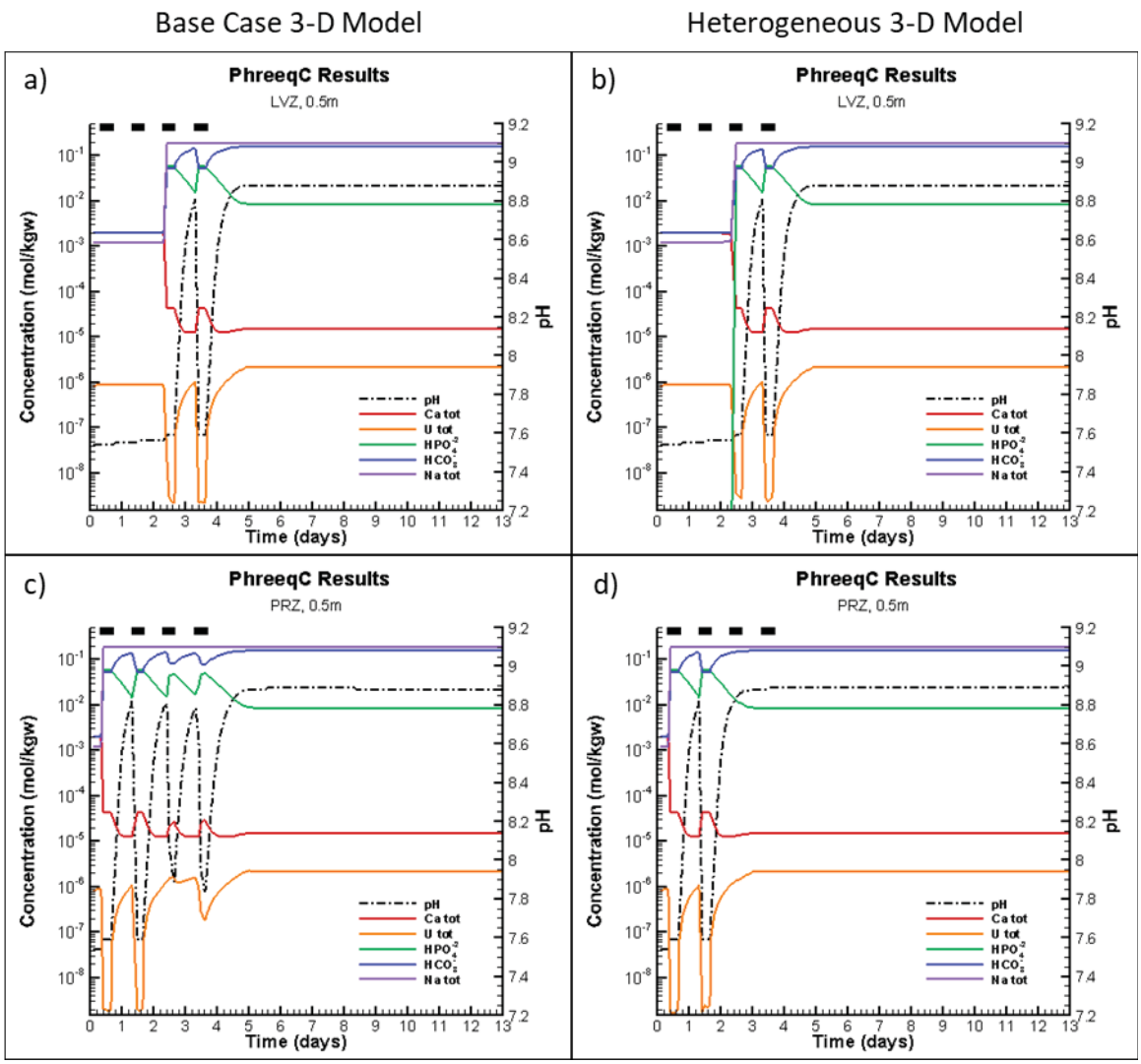

Figure 7-28. Comparison of Geochemical Evolution Timeseries Plots for Base Case 3-D Remedy Injection Model (Left) and 3-D Heterogeneous Remedy Injection Model (Right) with Injection Periods Indicated by Black Bars

Timeseries plots comparing results from the base case and heterogeneous models for minerals are shown in Figure 7-29 near the LVZ and PRZ injection screens. No discernable changes are present between the heterogeneous model and base case model results near the LVZ injection screen (Figure 7-29a and b). Most differences are seen when comparing the results near the PRZ screen. The three major differences are with the overall amount of hydroxylapatite precipitation being slightly less, slightly less dissolution of calcite, and earlier onset of andersonite precipitation in the heterogeneous model when compared to the base case model (Figure 7-28c and d). Overall, slight observable differences are shown between the base

case and heterogeneous model end-state results after 13 days of simulation time for both observation node locations for the amount of calcite and hydroxylapatite.

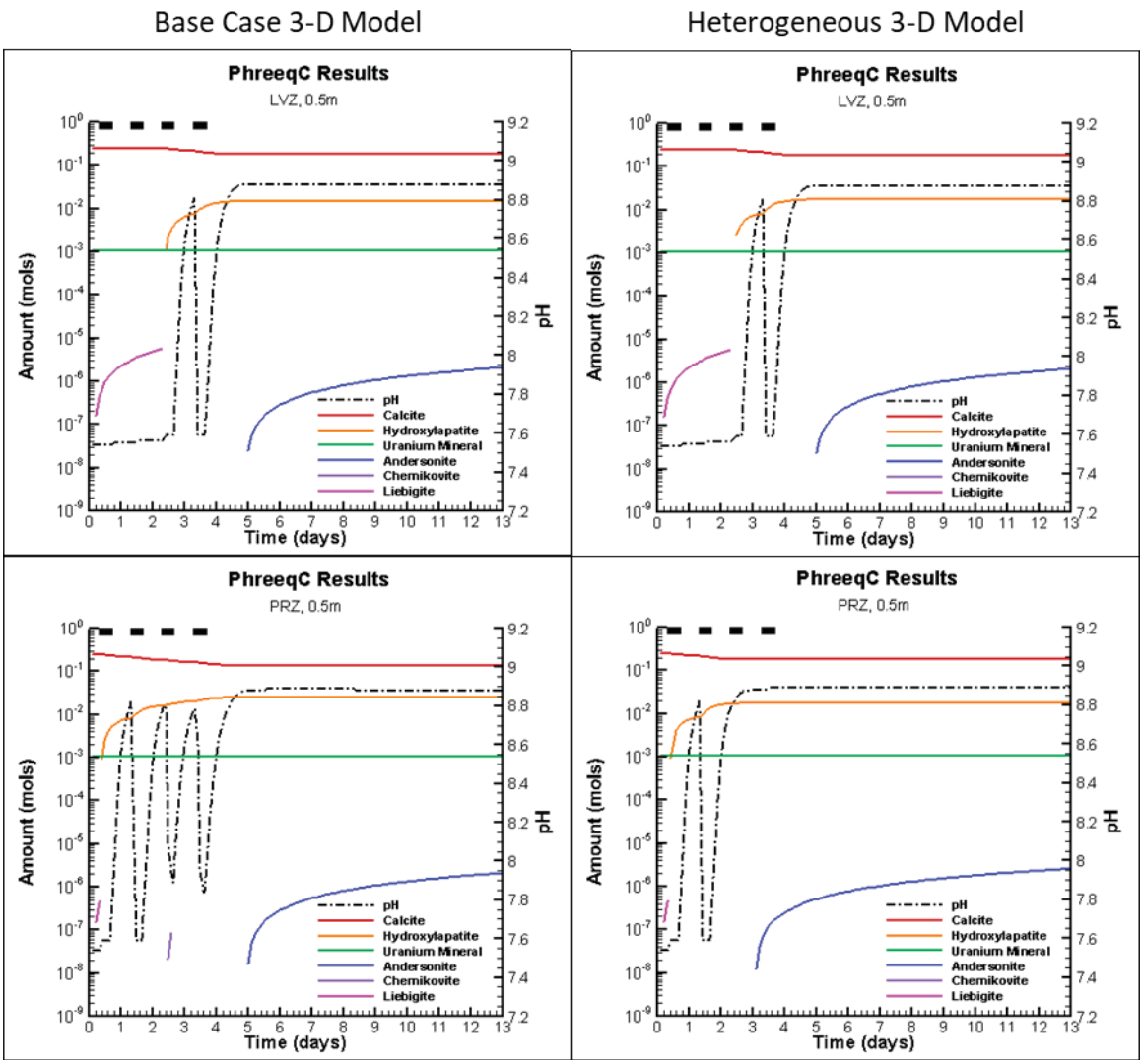

Figure 7-29. Comparison of Mineral Timeseries Plots for Base Case 3-D Remedy Injection Model (Left) and 3-D Heterogeneous Remedy Injection Model (Right) with Injection Periods Indicated by Black Bars

2-D single variable plots show the greatest differences in results between the base case and heterogeneous models. A greater horizontal extent of hydroxylapatite is shown from heterogeneous model results (Figure 7-30e) as compared to the base case model (Figure 7-17e) above 107 m elevation after all four injection periods. Similarly, a greater extent of andersonite formation is observed in the heterogeneous model (Figure 7-31e) as compared to the base case model (Figure 7-18e) for elevations above 107m after all four injection periods. Though the range of precipitation amounts remain similar between the two models, the horizontal extent increased dramatically to approximately 12 m in the heterogeneous model as compared to roughly 5 m in the base case model.

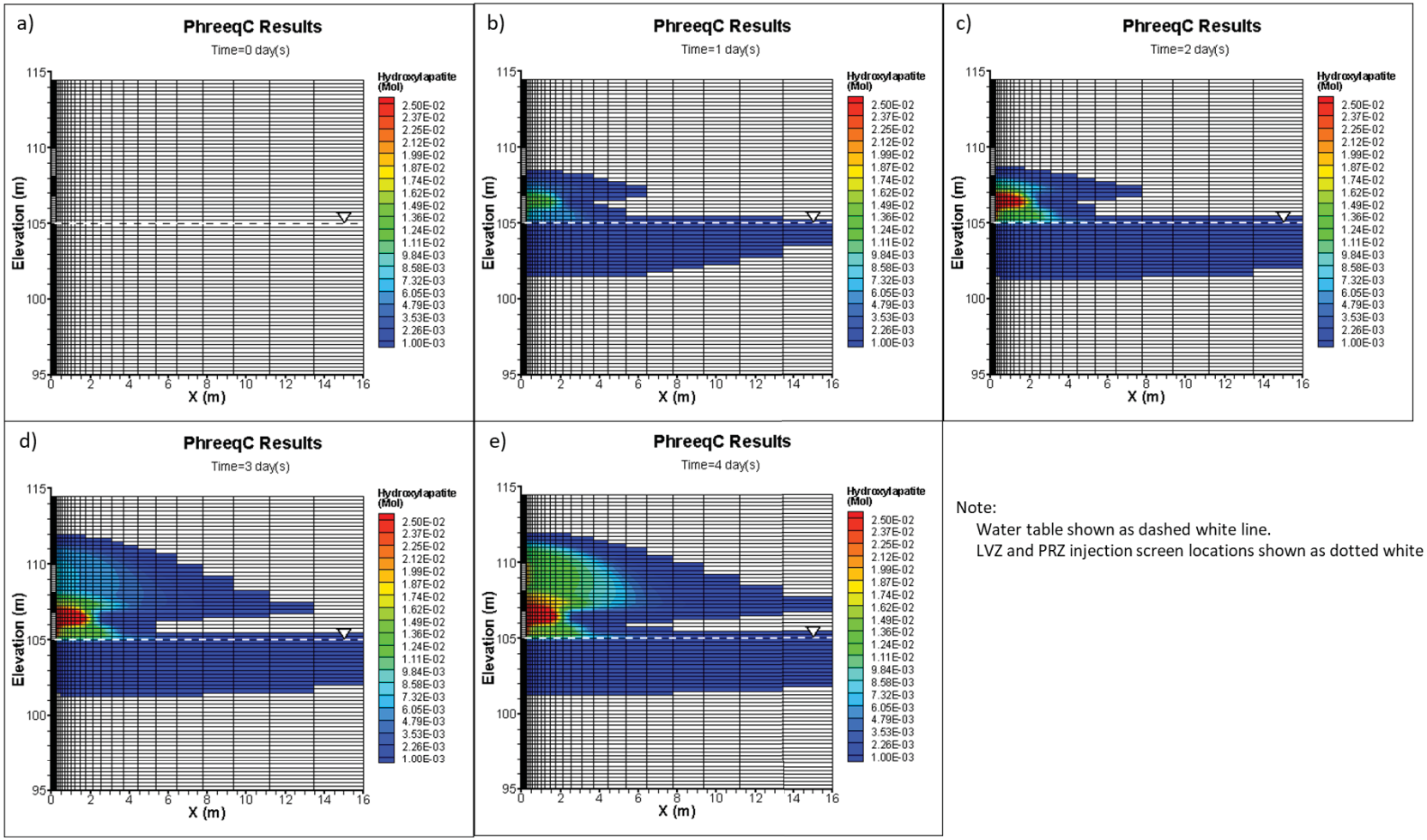

Note:
Water table shown as dashed white line.
LVZ and PRZ injection screen locations shown as dotted white lines.

Figure 7-30. 3-D Heterogeneous Remedy Injection Model Hydroxylapatite Profiles a) Before Injections, b) After the First PRZ, c) Second PRZ, d) First LVZ, and e) Second LVZ Injection Periods

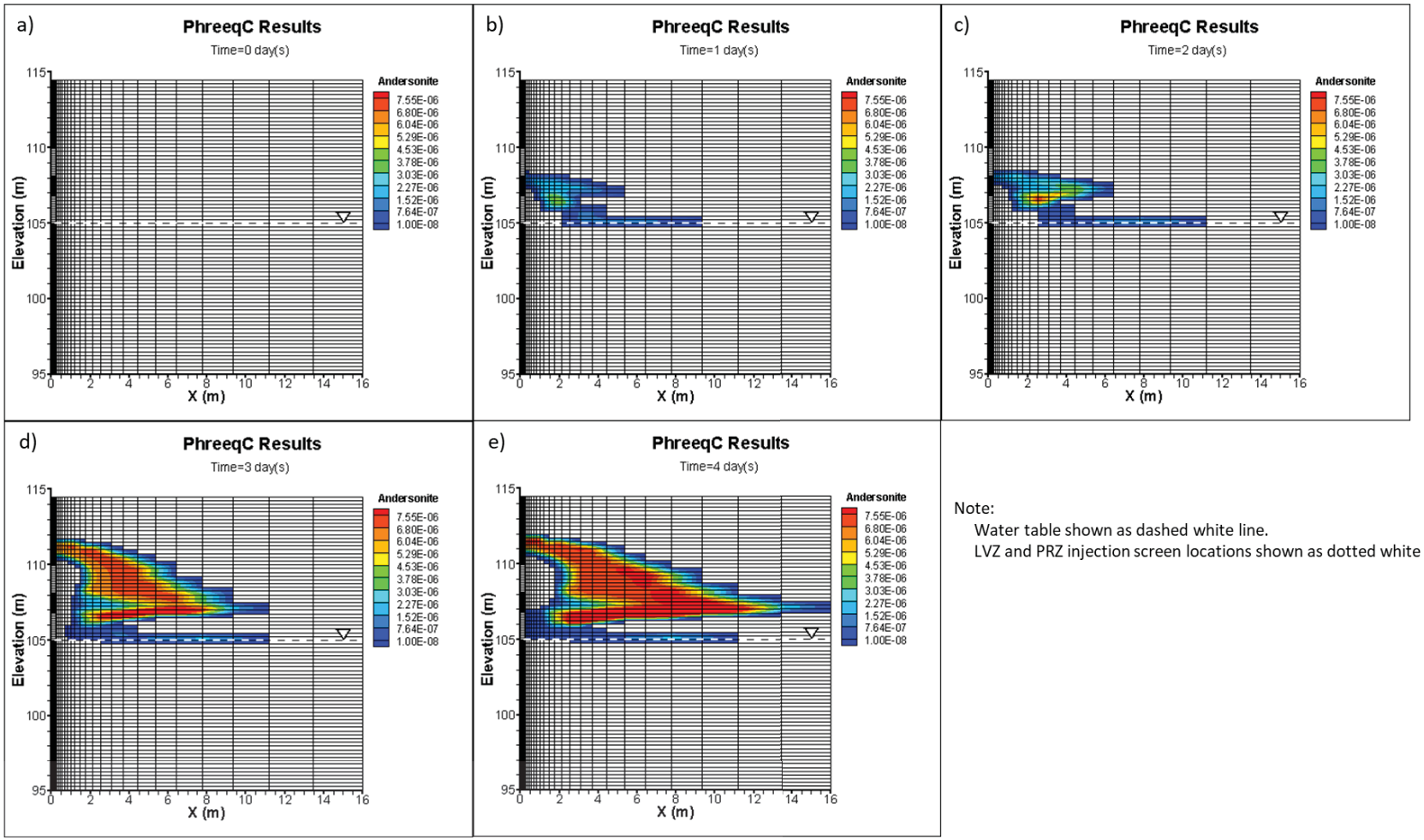

Note:
Water table shown as dashed white line.
LVZ and PRZ injection screen locations shown as dotted white lines.

Figure 7-31. 3-D Heterogeneous Remedy Injection Model Andersonite Profiles a) Before Injections, b) After the First PRZ, c) Second PRZ, d) First LVZ, and e) Second LVZ Injection Periods

8 Conclusions

Injections of high concentration polyphosphate solution to the PRZ and LVZ were conducted to reduce the labile fraction of uranium in sediments in the Stage B EAA footprint. This report summarizes geophysical imaging, groundwater data and soil characterization data gathered prior, during, and directly following remedy implementation time periods, synthesizing all relevant information to develop a conceptual understanding of geochemical interactions during and shortly after treatment.

The system is highly complex, relying on empirical data with no one clear modeling approach. This ECF chose a coupled reactive-transport and variably saturated flow modeling approach conducted to develop an understanding of the various subsurface reactions that lead to sequestration of uranium. Reactive transport modeling was conducted to match experimental data providing proof-of-concept implementation of kinetic release of uranium. Information gathered from geochemical evaluations of pre- and post-injection soil samples, sequential extractions, batch desorption and flow-through column leaching tests, mineral analysis, and groundwater monitoring were used to develop parameters and conceptual models for conducting fate and transport calculations. Aqueous uranium concentrations were reduced in groundwater monitoring wells directly following Stage B EAA remedy treatment with long term reduction observed indicating successful sequestration of uranium in situ. Short-term geochemical reactive transport modeling indicates favorable conditions for multiple mechanisms of uranium sequestration including adsorption of uranyl phases to reactive surface site, precipitation of uranium mineral phases (e.g., liebigite, chernikovite, and andersonite), and precipitation of hydroxylapatite which can incorporate uranium either by co-precipitation and/or by forming a coating around in-situ uranium minerals. The addition of silt zone representing textural heterogeneity in the unsaturated zone allowed for increased mineral formation in the unsaturated zone (i.e., enhanced sequestration).

This page intentionally left blank.

9 References

Appelo, C.A.J., Van der Weiden, M.J.J., Tournassat, C., and Charlet, L., 2002, "Surface complexation of ferrous iron and carbonate on ferrihydrite and the mobilization of arsenic," *Environ. Sci. & Technol.*, 36: 3096-3103.

Arai, Yuji, M.A. Marcus, N.Tamura, J.A. Davis, and J.M. Zachara, 2007, "Spectroscopic Evidence for Uranium Bearing Precipitates in Vadose Zone Sediments at the Hanford 300-Area Site," *Environ. Sci. Technol.,* 41:4633-4639.

CHPRC-01874, 2019, *The Geochemist's Workbench Integrated Software Management Plan: Version 12.0.4*, Rev. 3, CH2M HILL Plateau Remediation Company, Richland, Washington.

CHPRC-04166, 2019, *VS2DRTI Software Management Plan*, Rev. 0, CH2M HILL Plateau Remediation Company, Richland, Washington.

CHPRC-04167, 2019, *VS2DRTI Software Test Plan*, Rev. 0, CH2M HILL Plateau Remediation Company, Richland, Washington.

CHPRC-04168, 2019, *VS2DRTI Acceptance Test Report and Requirements Traceability Matrix*, Rev. 0, CH2M HILL Plateau Remediation Company, Richland, Washington.

DOE O 414.1D, 2011, *Quality Assurance*, U.S. Department of Energy, Washington, D.C. Available at: https://www.directives.doe.gov/directives-documents/400-series/0414.1-BOrder-d/@@images/file.

DOE/RL-2014-13-ADD2, 2015, *Remedial Design Report/Remedial Action Work Plan Addendum for the 300 Area Groundwater*, Rev. 0, CH2M HILL Plateau Remediation Company, Richland, Washington. Available at: https://pdw.hanford.gov/document/0081151H

DOE/RL-2014-42, 2015, *300-FF-5 Operable Unit Remedy Implementation Sampling and Analysis Plan*, Rev. 0, U.S. Department of Energy, Richland Operations Office, Richland, Washington. Available at: https://pdw.hanford.gov/document/0079669H.

DOE/RL-2014-42-ADD1, 2016, *300-FF-5 Operable Unit Remedy Implementation Sampling and Analysis Plan Addendum for Stage B Uranium Sequestration*, Rev. 0, U.S. Department of Energy, Richland Operations Office, Richland, Washington. Available at: https://pdw.hanford.gov/document/0071642H.

DOE/RL-2018-66, 2019, *Hanford Site Groundwater Monitoring Report for 2018*, Rev. 0, U.S. Department of Energy, Richland Operations Office, Richland, Washington. Available at: https://pdw.hanford.gov/document/AR-03138.

Dong, W., and S.C. Brooks, 2006, "Determination of the formation constants of ternary complexes of uranyl and carbonate with alkaline earth metal (Mg2+, Ca2+, Sr2+, and Ba2+) using anion exchange method," *Environ. Sci. Technol.*, 39, 4689-4695.

Dzombak., D.A., and F.M.M. Morel, 1990, *Surface Complexation Modeling: Hydrous Ferric Oxide*, New York.

ECF-300FF5-11-0151, 2012, *Groundwater Flow and Uranium Transport Modeling in Support of the 300 Area FF-5 RI/FS*, Rev. 3, CH2M HILL Plateau Remediation Company, Richland, Washington. Available at: https://pdw.hanford.gov/document/0078650H

ECF-300FF5-16-0087, 2016, *Determination of Vadose Zone Uranium Concentration Distribution Extents and Development of a Three-Dimensional Geologic Framework Model for the 300-FF-5 Operable Unit, Hanford, Washington*, Rev. 1, U.S. Department of Energy, Richland Operations Office, Richland, Washington.

ECF-300FF5-16-0091, 2016, *Uranium Transport Modeling in Support of the Stage A Enhanced Attenuation Remedy at 300-FF-5 Operable Unit*, Rev. 0, CH2M HILL Plateau Remediation Company, Richland, Washington. Available at: https://pdw.hanford.gov/document/AR-01154.

ECF-300FF5-19-0005, 2019, *Injection Volumes for 300-FF-5 Stage B Injections and Sampling*, Rev. 0, CH2M HILL Plateau Remediation Company, Richland, Washington. Available at: https://pdw.hanford.gov/document/AR-03056.

ECF-300FF5-19-0086, *STOMP Modeling in Support of Stage B Sequestration of Uranium at 300-FF-5 Operable Unit*, Rev. 0 pending, CH2M HILL Plateau Remediation Company, Richland, Washington.

EPA and DOE, 2013, *Hanford Site 300 Area Record of Decision for 300-FF-2 and 300-FF-5, and Record of Decision Amendment for 300-FF-1*, U.S. Environmental Protection Agency and U.S. Department of Energy, Richland, Washington. Available at: https://pdw.hanford.gov/document/0087180

Gorman-Lewis, D., Shvareva, T., Kubatok, K., Burns, P.C., Wellman, D.M., McNamara, B., Szymanowski, J., Navrotsky, A., and J.B. Fein, 2009, "Thermodynamic Properties of Autunite, Uranyl Hydrogen Phosphate, and Uranyl Orthophosphate from Solubility and Calorimetric Measurements," *Environ. Sci. Technol*., 43, 7416-7422.

Guillaumont, R., Fanghanel, T., Fuger, J., Grenthe, I., Neck, V., Palmer, D.A., and M.H. Rand, 2003, *Update on the Chemical Thermodynamics of Uranium, Neptunium, Plutonium, Americium and Technetium*, Elsevier and OECD Nucl. Energy Agency, Organ. For Econ. Co-op. and Dev., Amsterdam.

Guillaumont, R., and F.J. Mompean, 2003, *Update on the Chemical Thermodynamics of Uranium, Neptunium, Plutonium, Americium and Technetium*, Elsevier and OECD Nucl. Energy Agency, Organ. For Econ. Co-op. and Dev., Amsterdam.

Haile, S.S., 2013, "VS2DRT: Variable saturated two dimensional reactive transport modeling in the vadose zone," doctoral dissertation, *Freiberg Online Geoscience* 34: 1-152.

Healy, R.W., 1990, "Simulation of solute transport in variably saturated porous media with supplemental information on modifications to the U.S. Geological Survey's computer program VS2D," U.S. Geological Survey Water Resources Investigations Report 90-4025. Reston, Virginia: USGS.

Healy, R.W., and A.D. Ronan, 1996, "Documentation of computer program VS2DH for simulation of energy transport in variably saturated porous media: Modification of the U.S. Geological Survey's computer program VS2DT," U.S. Geological Survey Water Resources Investigation Report 96-4230. Reston, Virginia: USGS.

Healy, R.W., S.S. Haile, D.L. Parkhurst, and S.R. Charlton, 2018, "VS2DRTI: Simulating Heat and Reactive Solute Transport in Variably Saturated Porous Media," *Groundwater* 56: 810-815.

McKinley, JP, JM Zachara, J Wan, DE McCready, SM Heald, 2007, "Geochemical controls on contaminant uranium in vadose Hanford formation sediments at the 200 area and 300 area, Hanford site Washington," *Vadose Zone Journal* 6(4): 1004-1017.

Mehta, S., 2017, "Geochemical evaluation of uranium sequestration from field-scale infiltration and injection of polyphosphate solutions in contaminated Hanford sediments," *Applied Geochemistry* 84: 133-153.

Mehta, VS, F Mailot, Z Wang, JG Catalono, and DE Giammar, 2016, "Effect of reaction pathway on the extent and mechanism of uranium(VI) immobilization with calcium and phosphate," *Environmental Science and Technology* 50:3128-3136.

NAVD88, 1988, *North American Vertical Datum of 1988*, as revised, National Geodetic Survey, Federal Geodetic Control Committee, Silver Spring, Maryland. Available at: https://www.ngs.noaa.gov/datums/vertical/north-american-vertical-datum-1988.shtml.

Parkhurst and Wissmeier, 2015, "PhreeqcRM: A reaction module for transport simulators based on the geochemical model PHREEQC," *Advances in Water Resources* 83: 176-189.

Plummer, L.N., T.M.L.Wigley, and D.L. Parkhurst, 1978, "The kinetics of calcite dissolution in CO2-water systems at 5 to 60 °C and 0.0 to 1.0 atm CO_2," *Am. J. Sci.*, 278, 179-216.

PNL-10285, 1995, *Estimated Recharge Rates at the Hanford Site*, Pacific Northwest Laboratory, Richland, Washington. Available at: https://www.osti.gov/biblio/10122247-estimated-recharge-rates-hanford-site

PNNL-16435, 2007, *Limited Field Investigation Report for Uranium Contamination in the 300-FF-5 Operable Unit at the 300 Area, Hanford Site, Washington*, Pacific Northwest National Laboratory, Richland, WA. Available at: https://www.pnnl.gov/main/publications/external/technical_reports/PNNL-16435.pdf

PNNL-17031, 2007, *A Site-Wide Perspective on Uranium Geochemistry at the Hanford Site*, Pacific Northwest National Laboratory, Richland, WA. Available at: https://www.pnnl.gov/main/publications/external/technical_reports/PNNL-17031.pdf

PNNL-21733, 2012, *Use of Polyphosphate to Decrease Uranium Leaching in Hanford 300 Area Smear Zone Sediment*, Pacific Northwest National Laboratory, Richland, WA. Available at: https://www.pnnl.gov/main/publications/external/technical_reports/PNNL-21733.pdf

PNNL-28619, 2019, *Stage B Uranium Sequestration Amendment Delivery Monitoring Using Time-Lapse Electrical Resistivity Tomography*, Pacific Northwest National Laboratory, Richland, Washington.

PNNL-29650, 2020, *Evaluation of the Change in Uranium Mobility in Sediments from Hanford 300-FF-5 Stage B Polyphosphate Field Injection*, Pacific Northwest National Laboratory, Richland, Washington.

PRC-PRO-IRM-309, 2014, *Controlled Software Management*, Revision 5, Change 0, CH2M HILL Plateau Remediation Company, Richland, Washington.

Romero-Ganzalez, M.R., Cheng, T., Barnett, M.O., and E.E. Roden, 2007, "Surface complexation modeling of the effects of phosphate on uranium(VI) adsorption," *Radiochim. Acta*, 95, 251-259.

SGW-59455, 2016, *300-FF-5 Operable Unit Stage A Uranium Sequestration System Installation Report*, Rev. 0, CH2M HILL Plateau Remediation Company, Richland, Washington. Available at: https://pdw.hanford.gov/document/0077730H

SGW-60778, 2019, *300-FF-5 Operable Unit Stage B Uranium Sequestration System Installation Report*, Rev. 0, CH2M HILL Plateau Remediation Company, Richland, Washington. Available at: https://pdw.hanford.gov/document/0063871H

Turner, D.R. and Sassman, S.A., 1996 "Approaches to Sorption Modeling for High-Level Waste Performance Assessment," *J. Contam. Hydrol.,* 21: 311–332.

Wang, Z., J.M. Zachara, J.P. McKinley, and S.C. Smith, 2005, "Cryogenic laser induced U(VI) fluorescence studies of a U(VI) substituted natural calcite: Implications to U(VI) speciation in contaminated Hanford sediments," *Environ. Sci. Technol.*, 39, 2651-2659.

WHC-EP-0500, 1991, *Geology and Hydrology of the 300 Area and Vicinity, Hanford Site, South-Central Washington*, Westinghouse Hanford Company, Richland, Washington. Available at: https://pdw.hanford.gov/document/E0017495.

WHC-MR-0440, 1993, *Multiple Missions: The 300 Area in Hanford Site History*, Westinghouse Hanford Company, Richland, WA. Available at: https://pdw.hanford.gov/document/E0033041

Wolery, T.W., and R.L. Jarek, 2003, *Software User's Manual, EQ3/6*, Version 8.0, Sandia National Laboratories, Albuquerque, New Mexico.

Appendix A

Monitoring Data for the Stage B EAA Extended Well Network

This page intentionally left blank.

A1 Monitoring Network

Groundwater monitoring data for the Stage B EAA monitoring network (Figure A-1) is presented in this appendix.

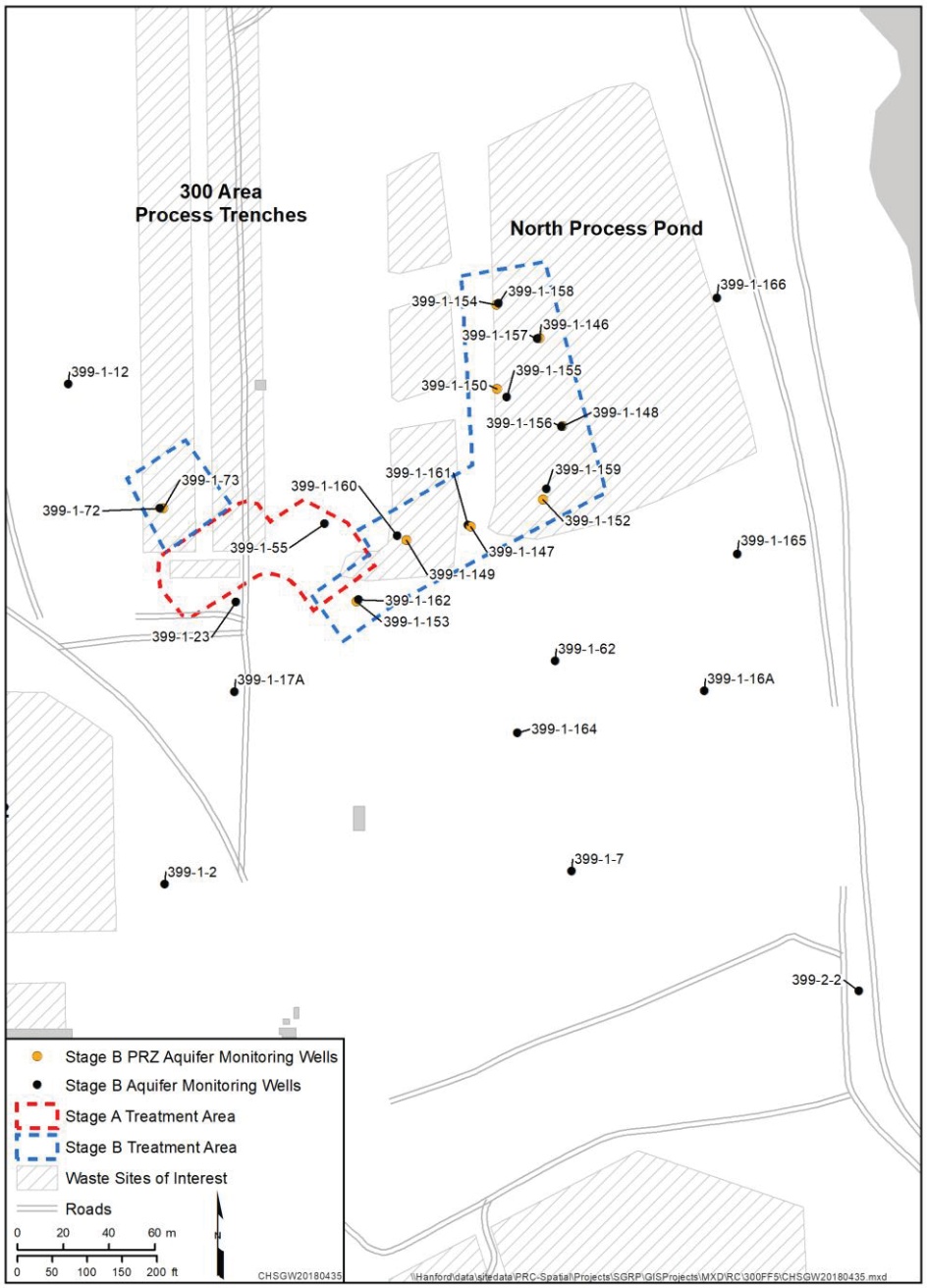

Figure A-1. 300 Area Industrial Complex and the Stage A and Stage B Enhanced Attenuation Areas

A2 Uranium Concentration Compared to Phosphate Concentration

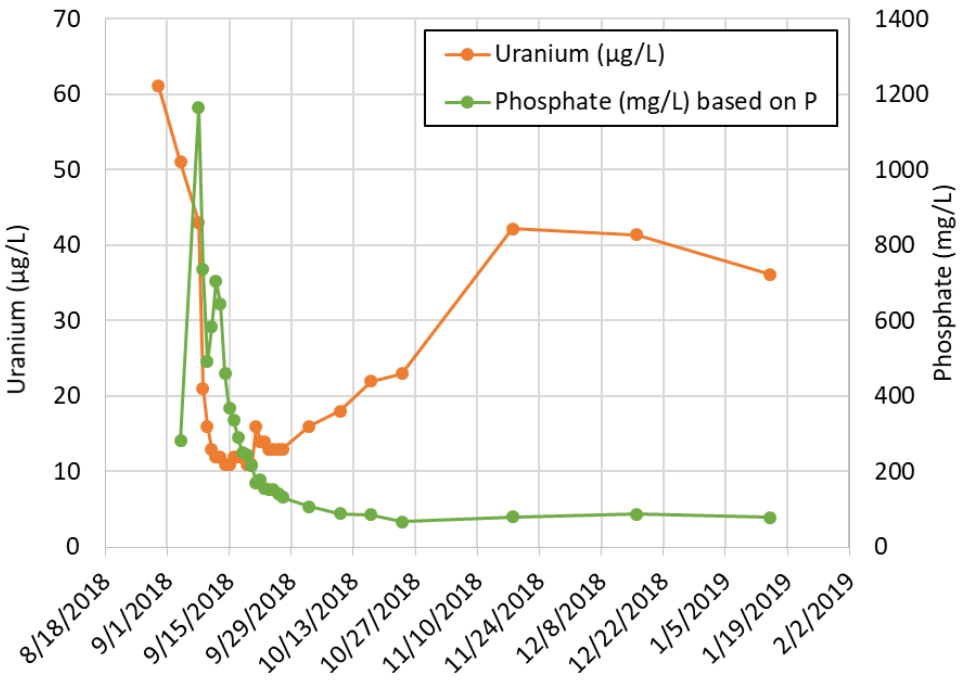

Figure A-2. Comparison of Uranium to Phosphate for Well 399-1-162

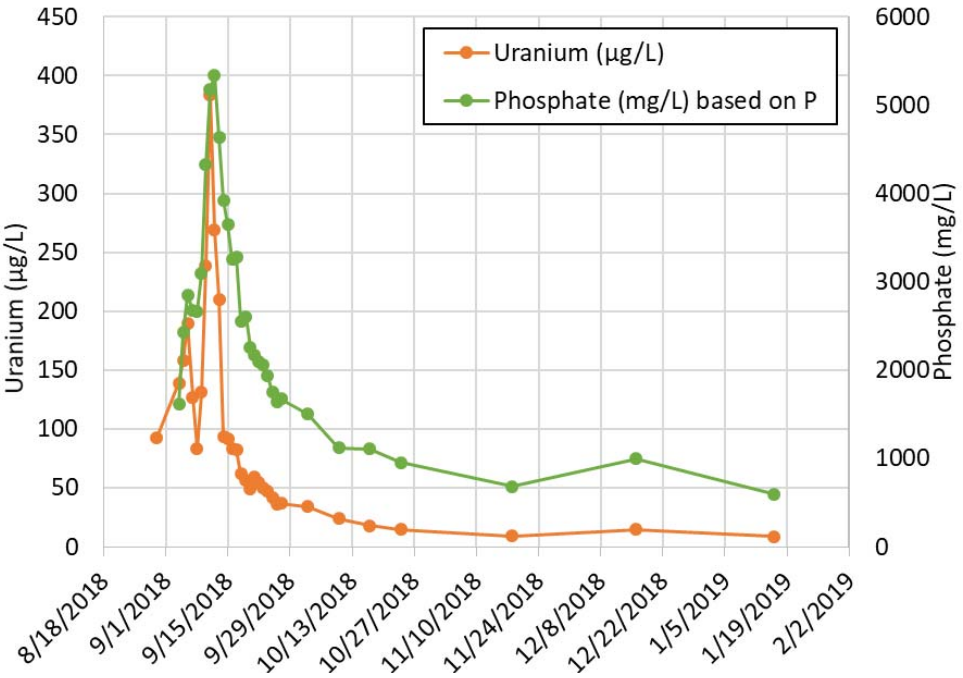

Figure A-3. Comparison of Uranium to Phosphate for Well 399-1-160

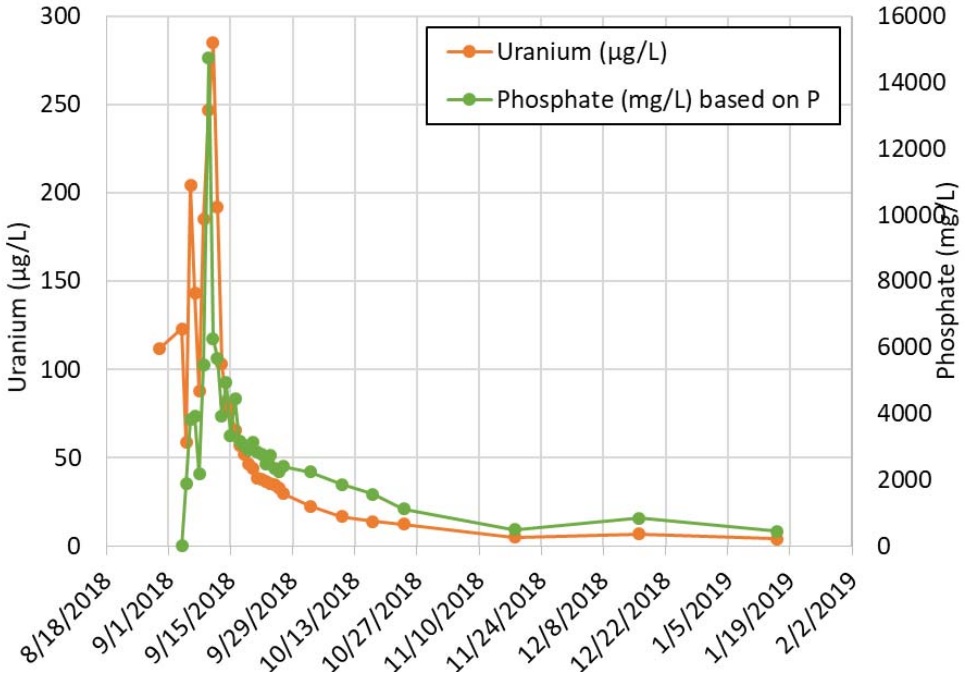

Figure A-4. Comparison of Uranium to Phosphate for Well 399-1-161

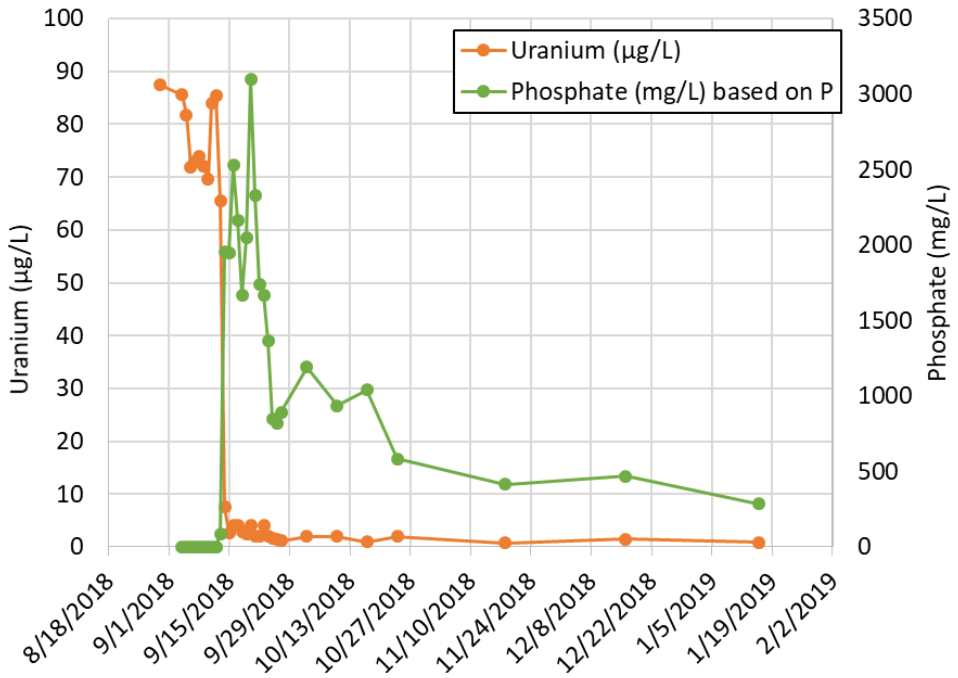

Figure A-5. Comparison of Uranium to Phosphate for Well 399-1-156

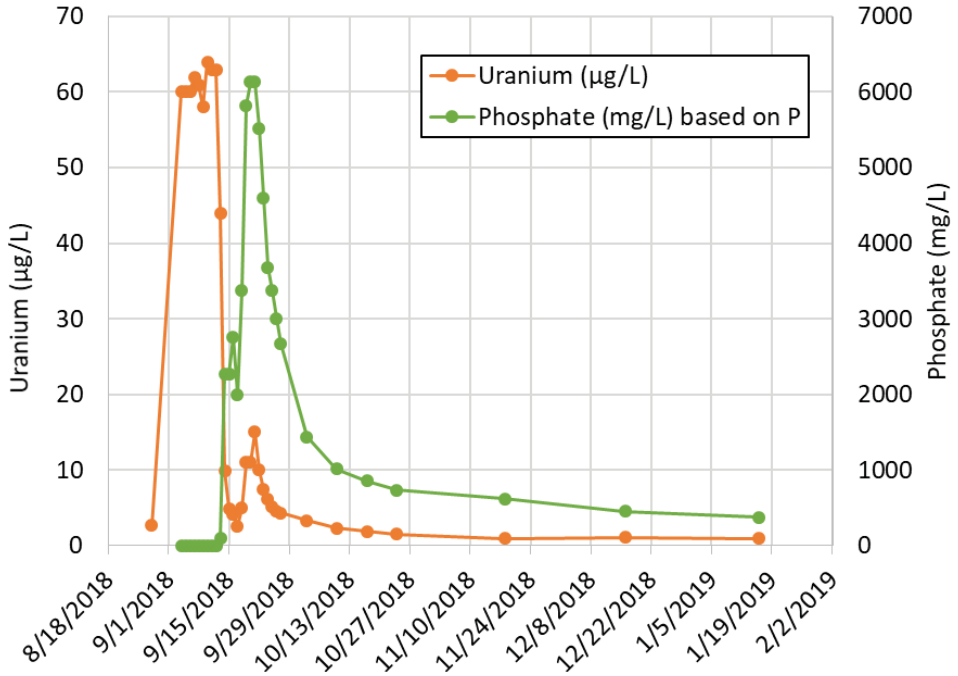

Figure A-6. Comparison of Uranium to Phosphate for Well 399-1-155

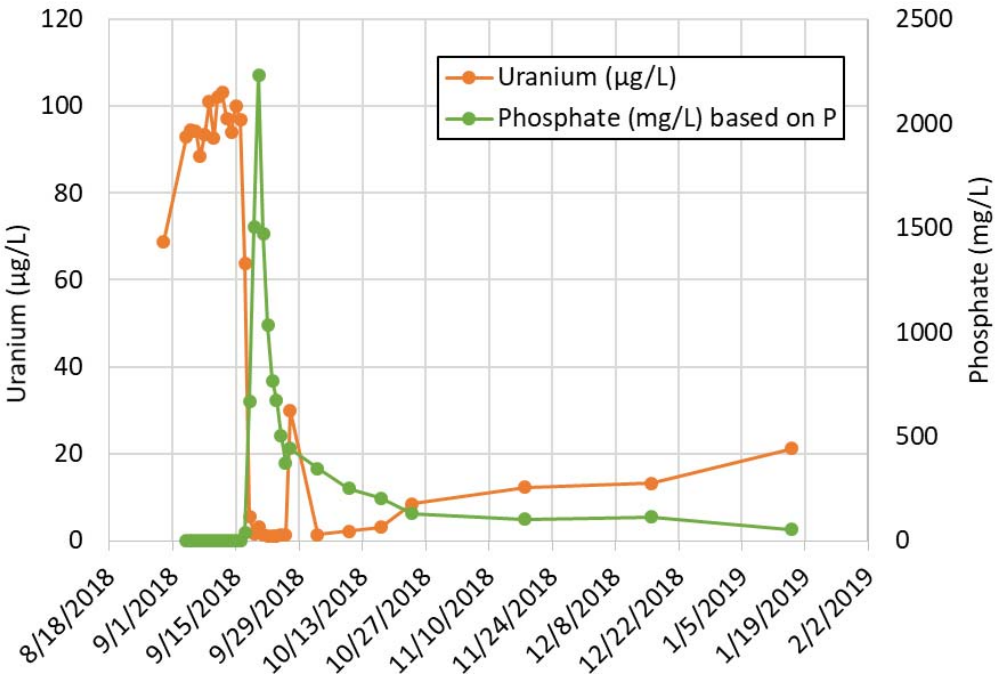

Figure A-7. Comparison of Uranium to Phosphate for Well 399-1-157

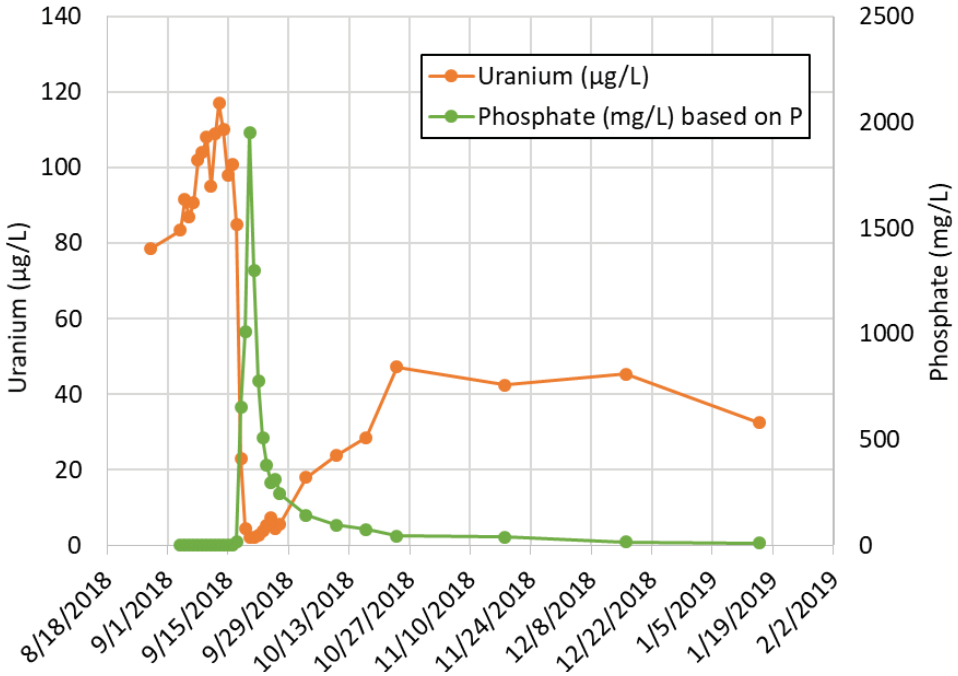

Figure A-8. Comparison of Uranium to Phosphate for Well 399-1-158

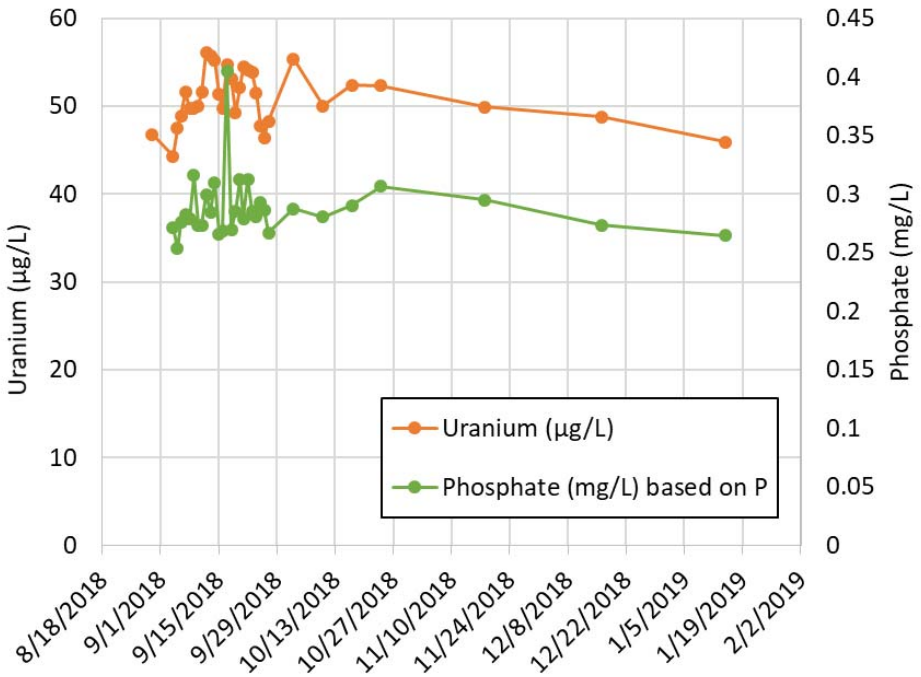

Figure A-9. Comparison of Uranium to Phosphate for Well 399-1-166

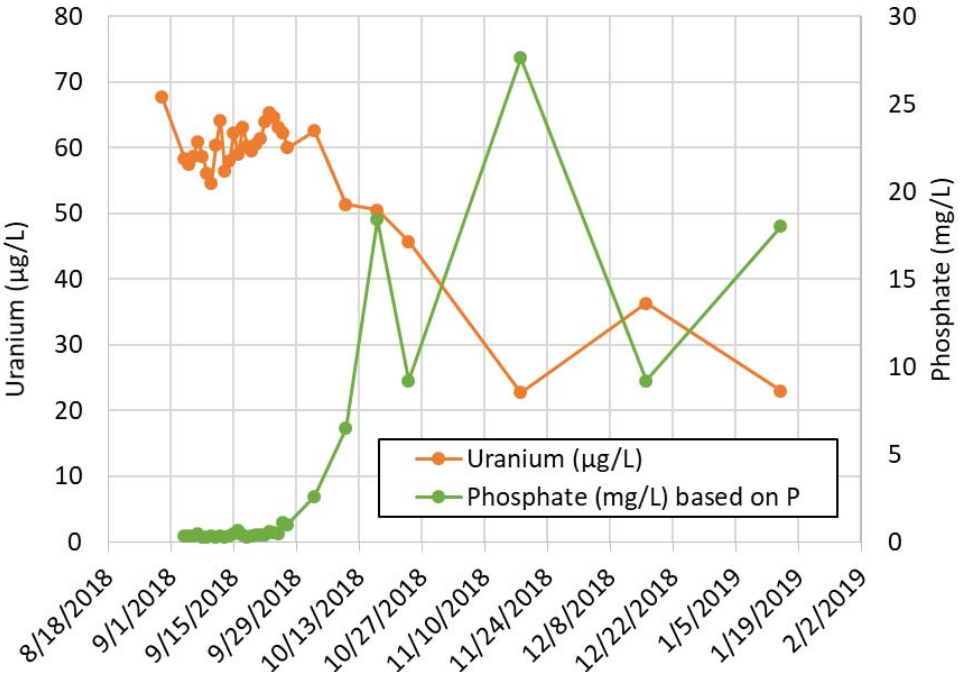

Figure A-10. Comparison of Uranium to Phosphate for Well 399-1-165

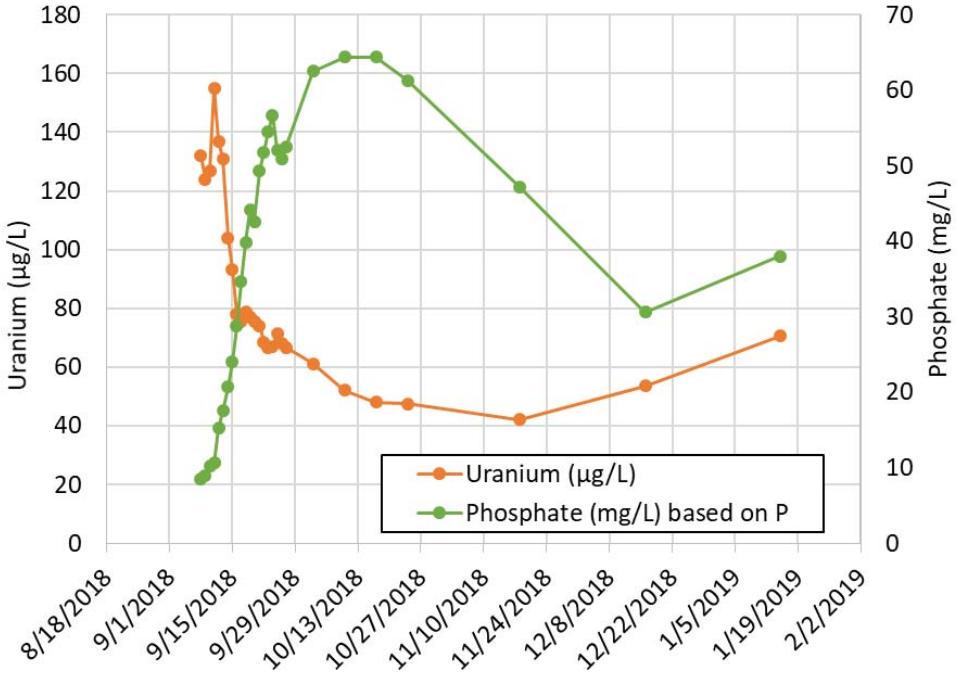

Figure A-11. Comparison of Uranium to Phosphate for Well 399-1-164

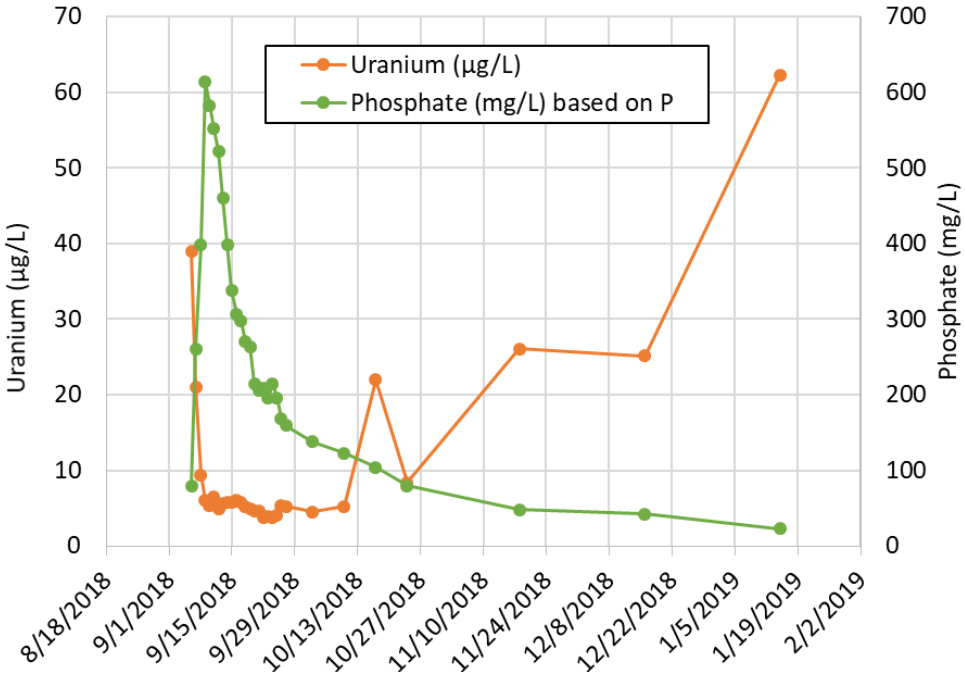

Figure A-12. Comparison of Uranium to Phosphate for Well 399-1-23

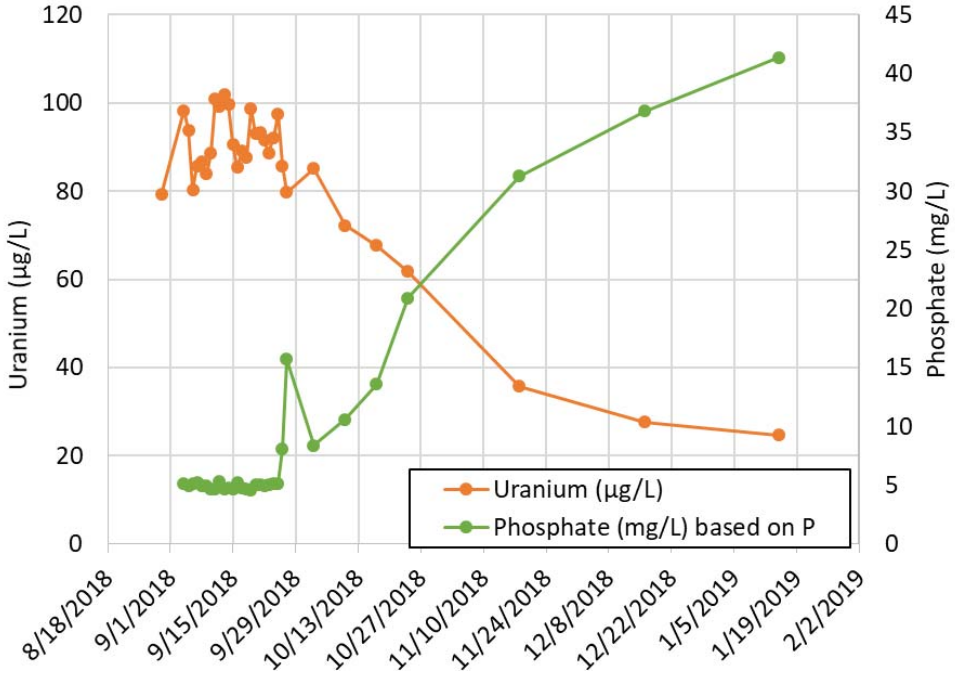

Figure A-13. Comparison of Uranium to Phosphate for Well 399-1-7

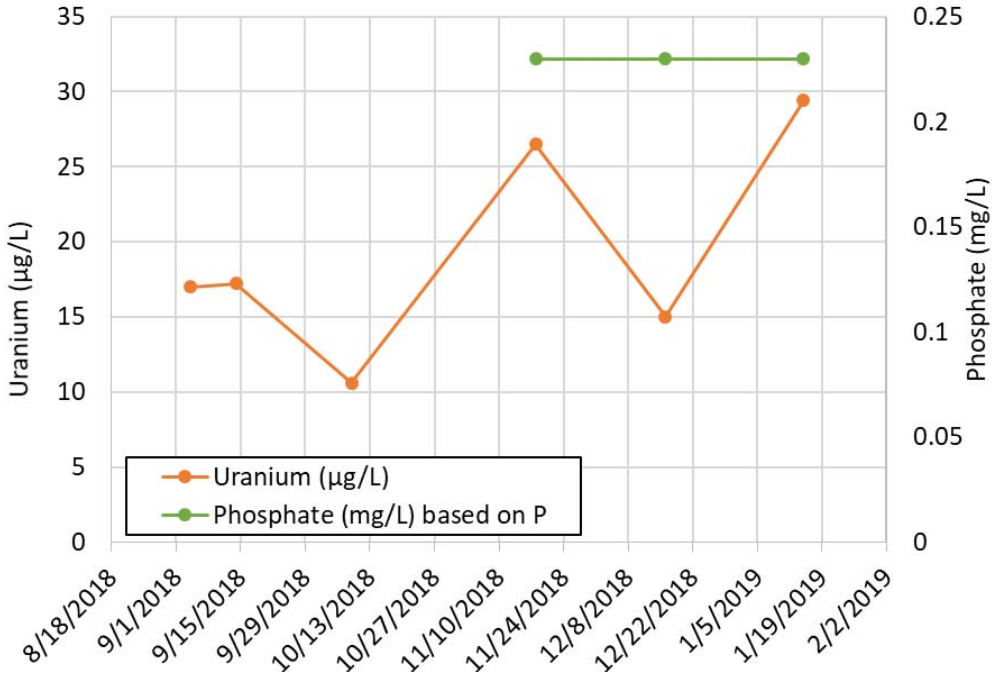

Figure A-14. Comparison of Uranium to Phosphate for Well 399-1-12

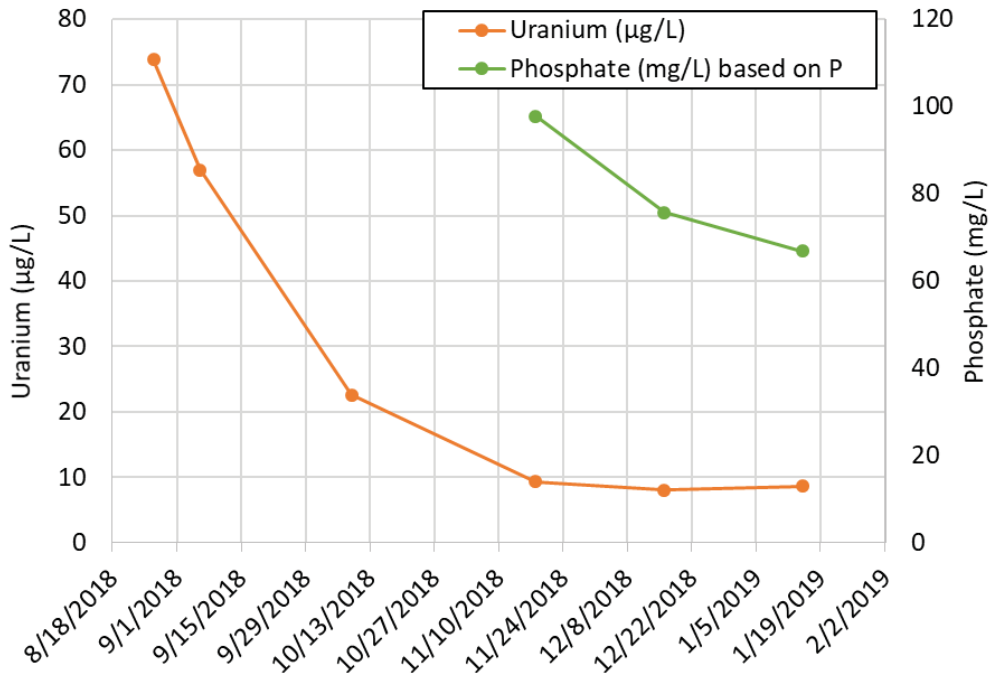

Figure A-15. Comparison of Uranium to Phosphate for Well 399-1-16A

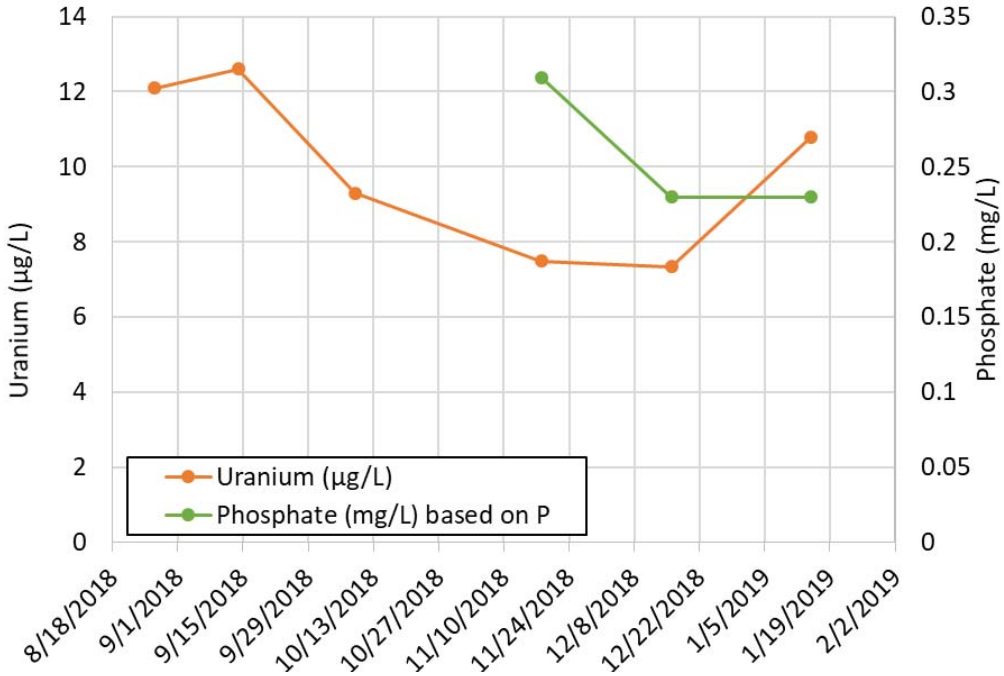

Figure A-16. Comparison of Uranium to Phosphate for Well 399-1-2

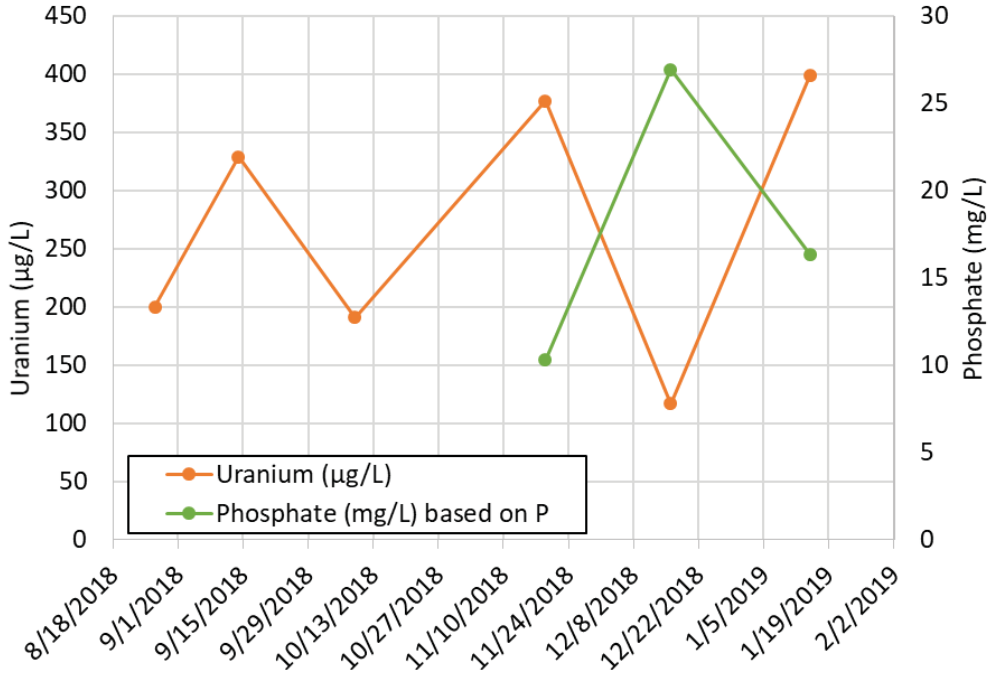

Figure A-17. Comparison of Uranium to Phosphate for Well 399-1-55

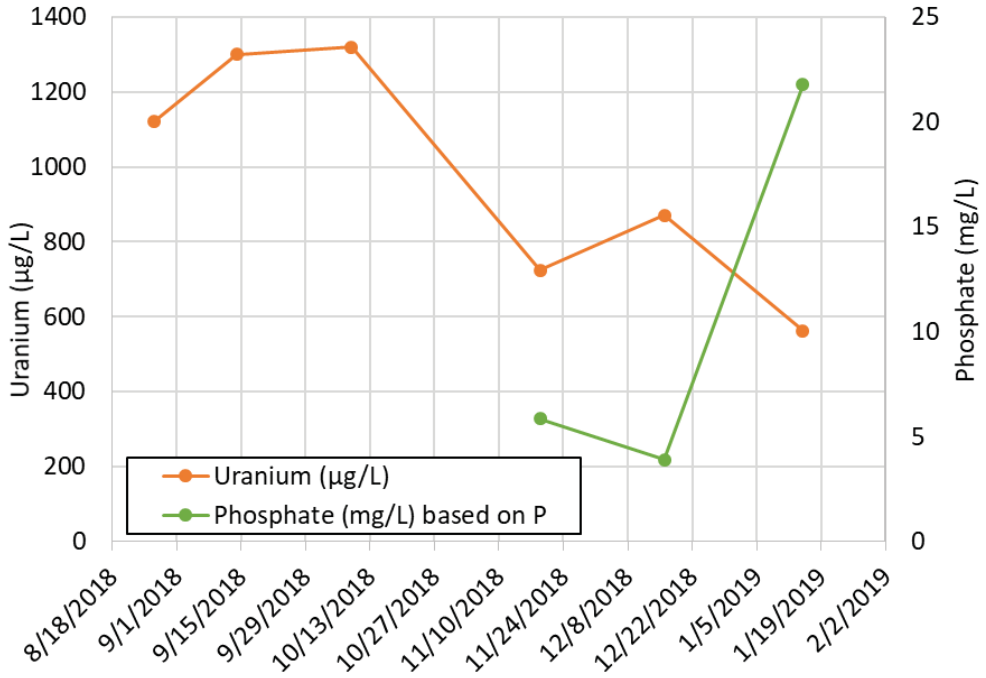

Figure A-18. Comparison of Uranium to Phosphate for Well 399-1-62

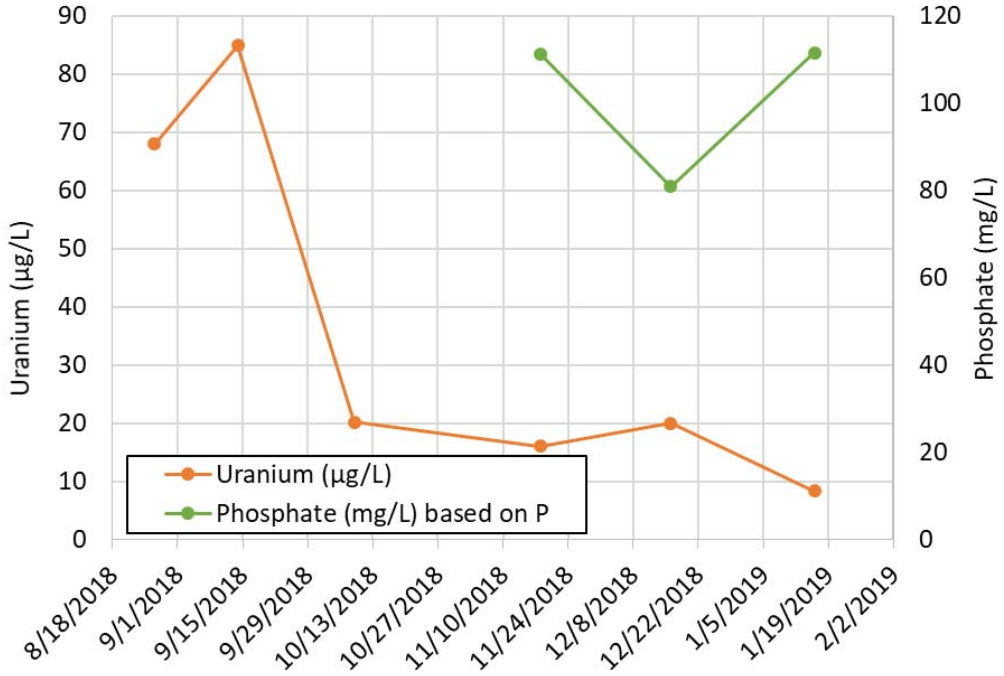

Figure A-19. Comparison of Uranium to Phosphate for Well 399-2-2

A3 Phosphate to Bicarbonate Ratio Compared to Calcium Concentration

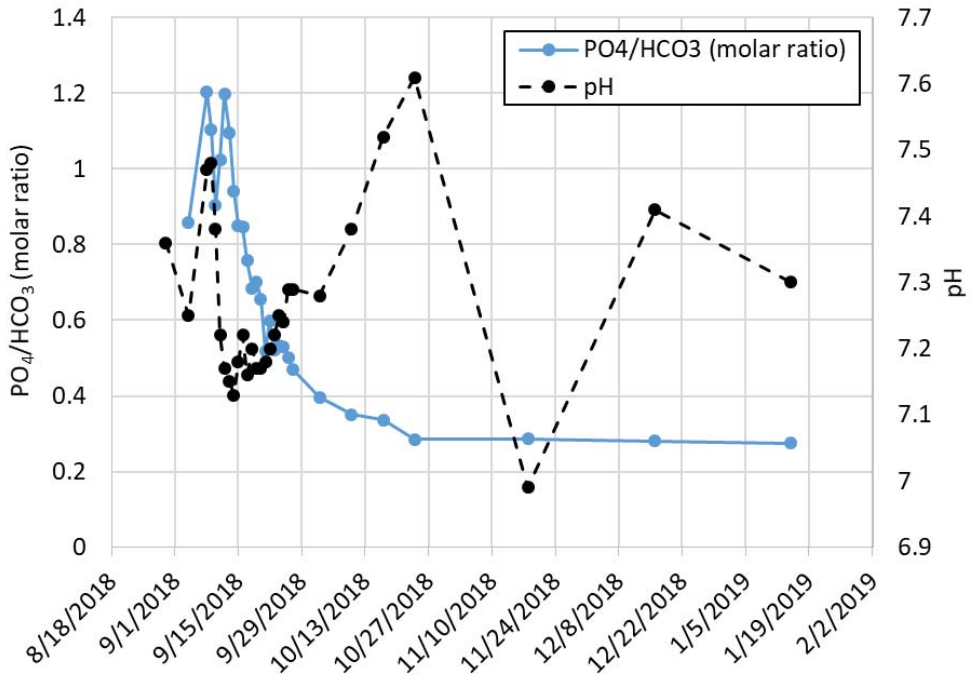

Figure A-20. Comparison of Phosphate to Bicarbonate Molar Ratio to pH for Well 399-1-162

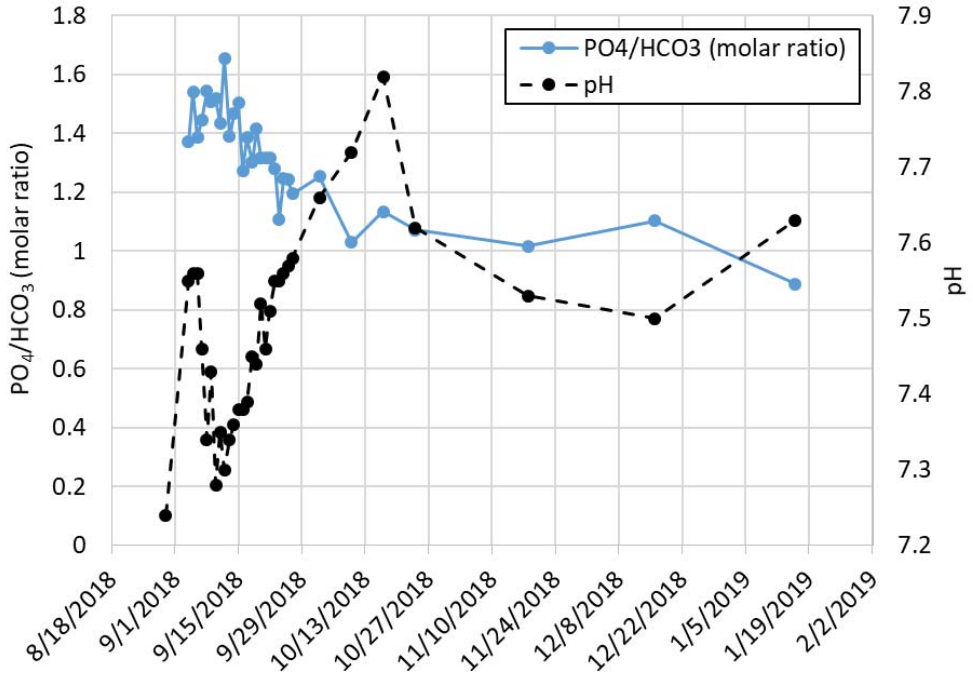

Figure A-21. Comparison of Phosphate to Bicarbonate Molar Ratio to pH for Well 399-1-160

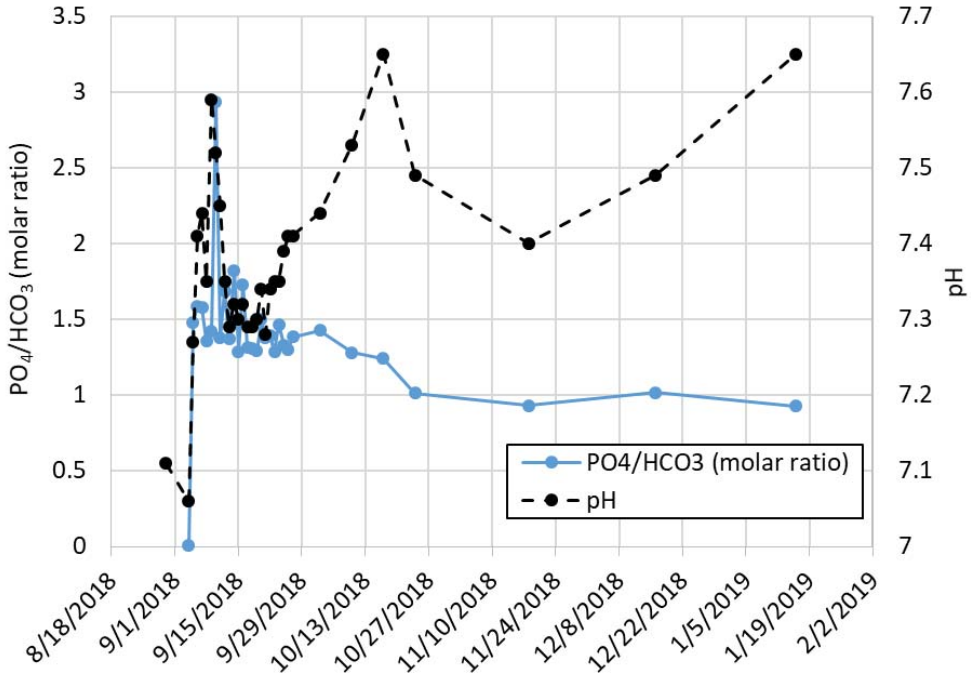

Figure A-22. Comparison of Phosphate to Bicarbonate Molar Ratio to pH for Well 399-1-161

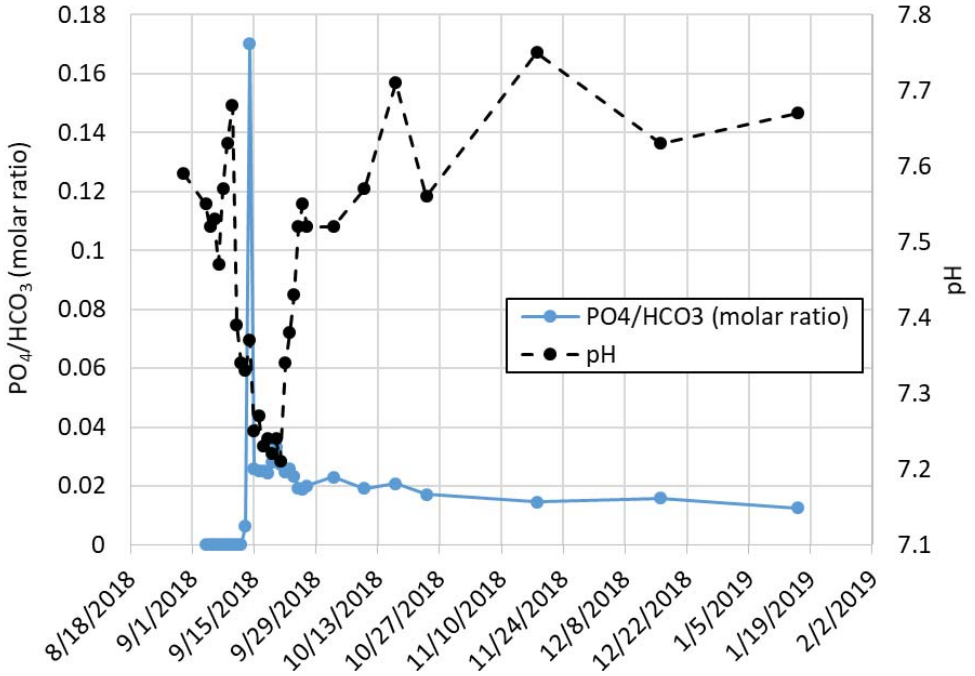

Figure A-23. Comparison of Phosphate to Bicarbonate Molar Ratio to pH for Well 399-1-156

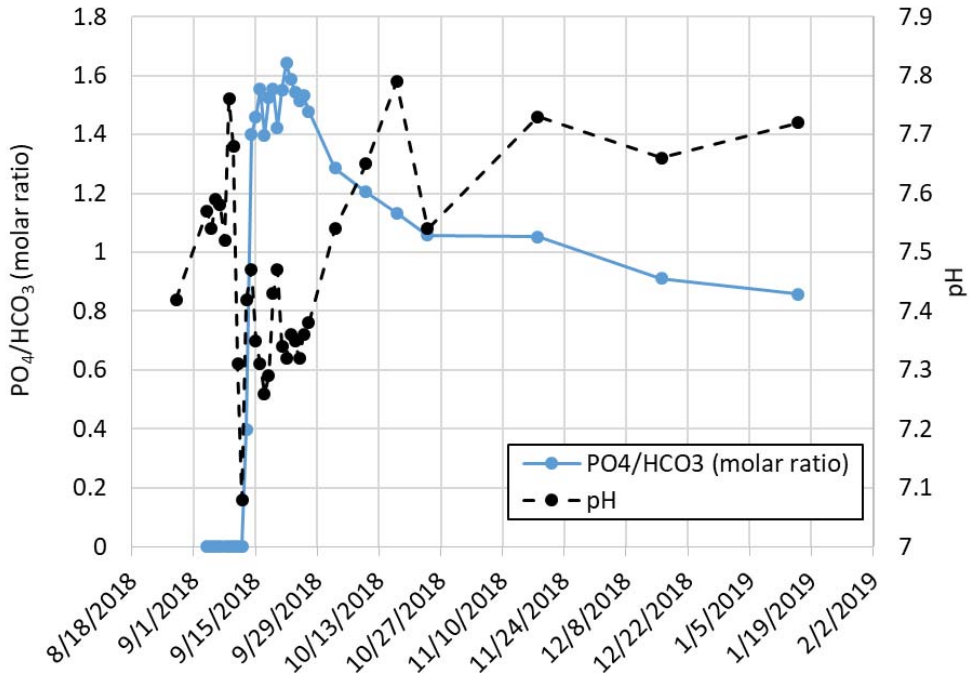

Figure A-24. Comparison of Phosphate to Bicarbonate Molar Ratio to pH for Well 399-1-155

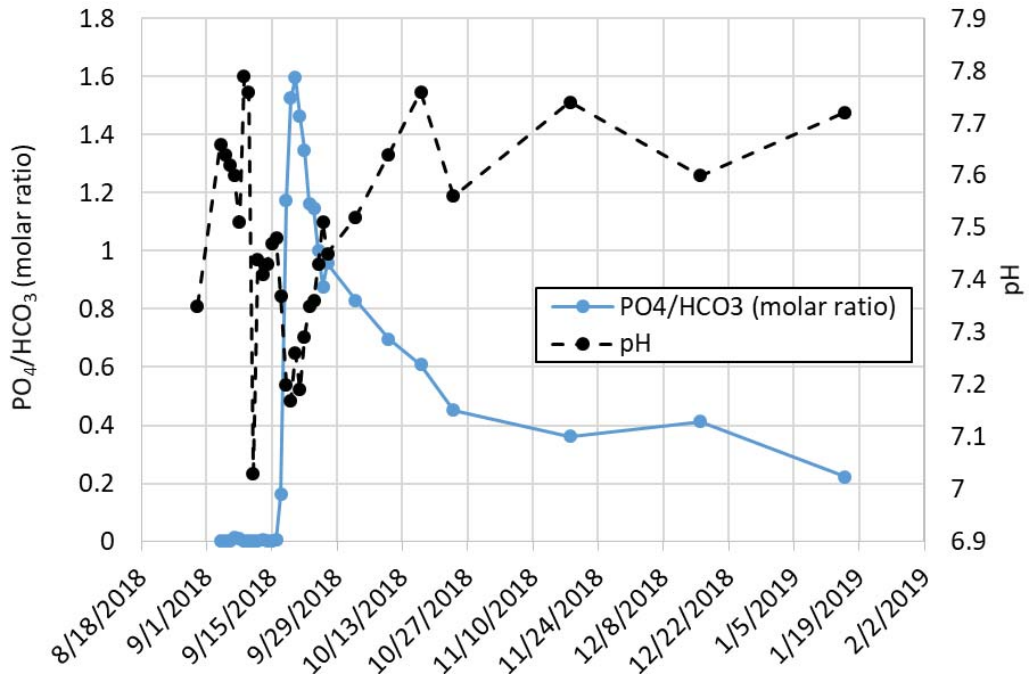

Figure A-25. Comparison of Phosphate to Bicarbonate Molar Ratio to pH for Well 399-1-157

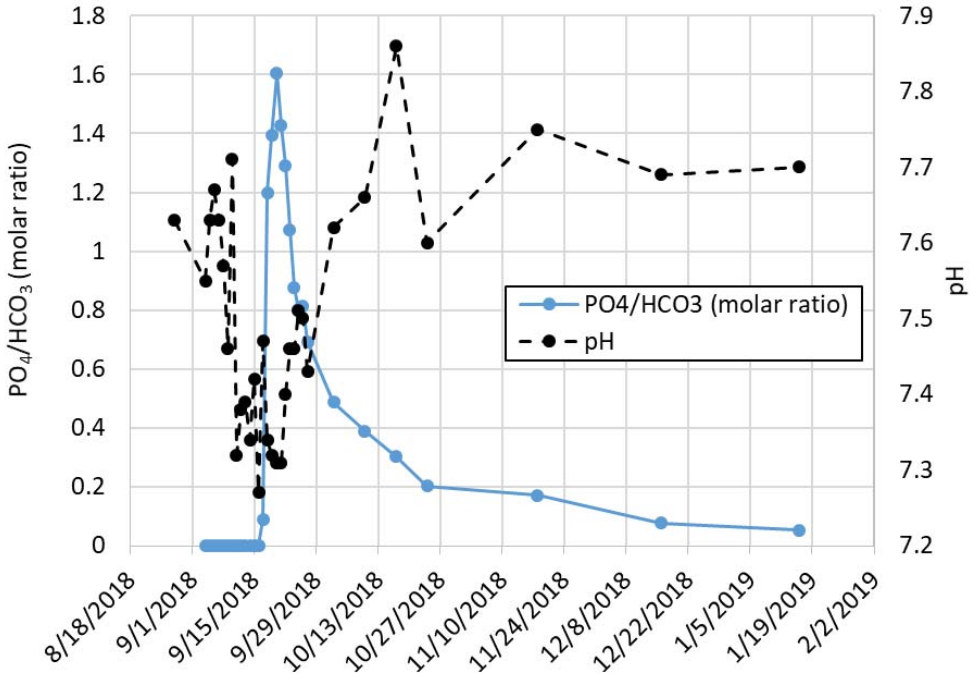

Figure A-26. Comparison of Phosphate to Bicarbonate Molar Ratio to pH for Well 399-1-158

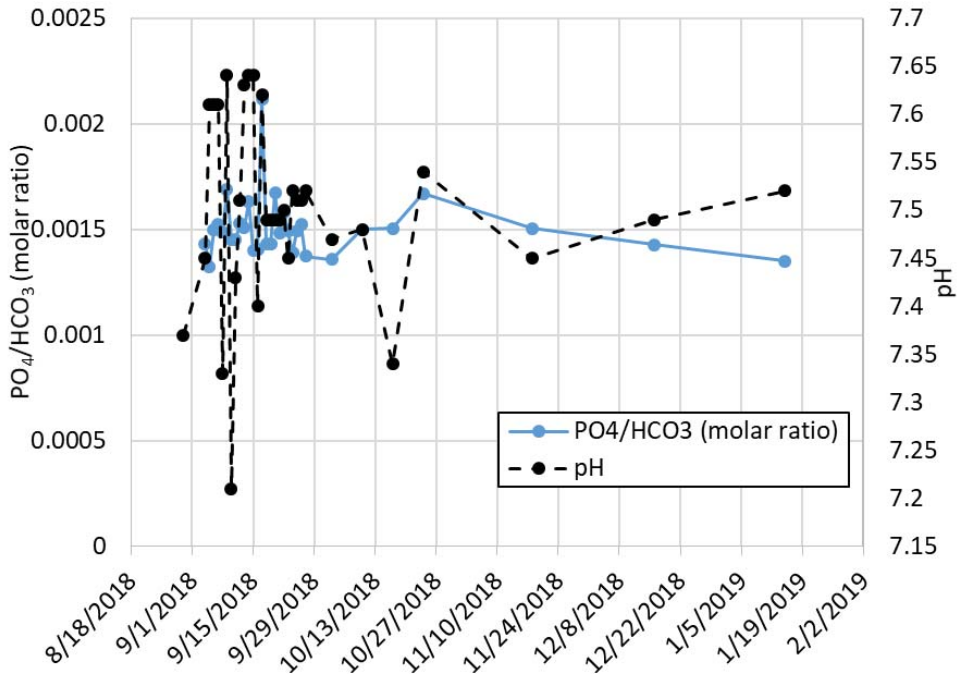

Figure A-27. Comparison of Phosphate to Bicarbonate Molar Ratio to pH for Well 399-1-166

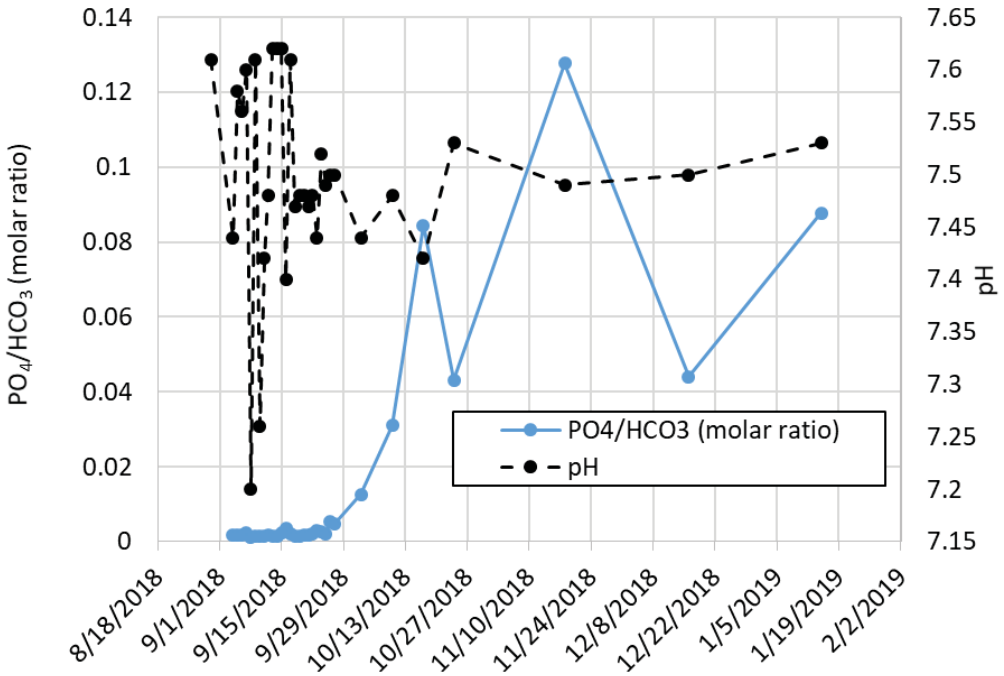

Figure A-28. Comparison of Phosphate to Bicarbonate Molar Ratio to pH for Well 399-1-165

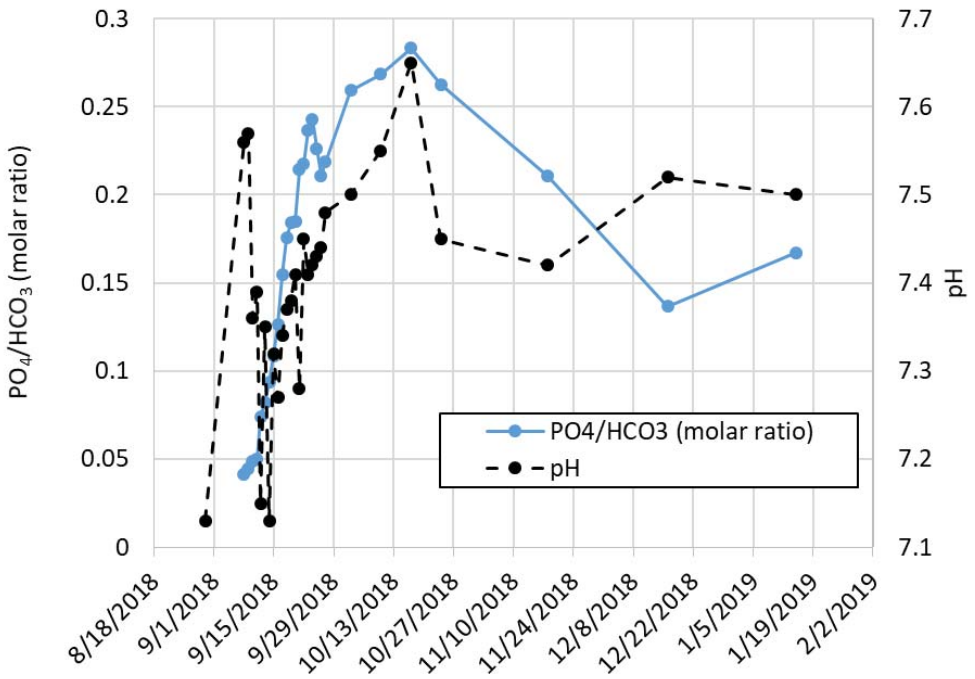

Figure A-29. Comparison of Phosphate to Bicarbonate Molar Ratio to pH for Well 399-1-164

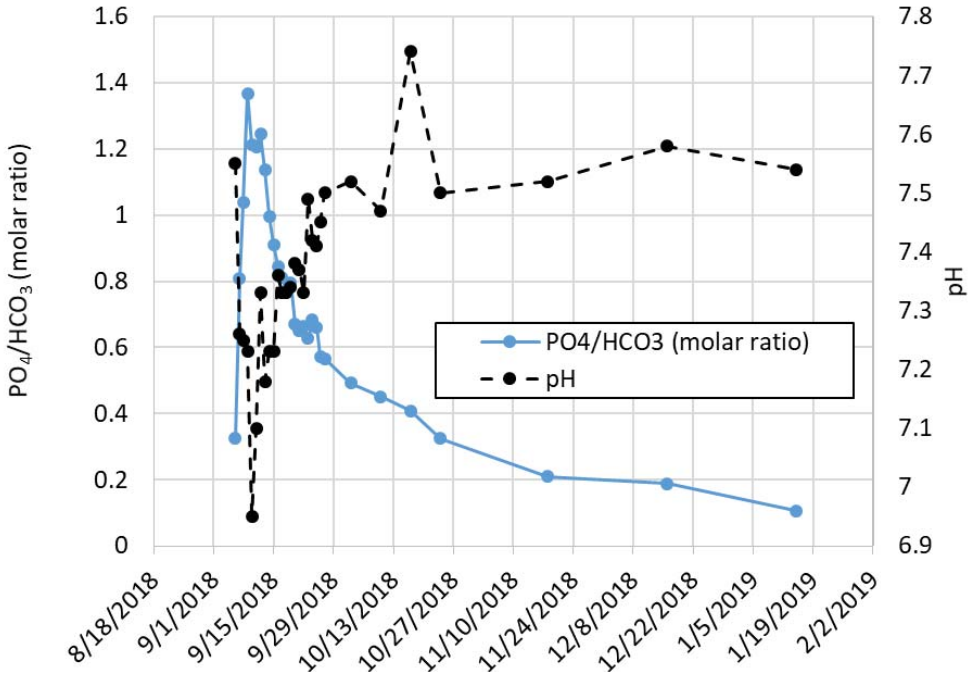

Figure A-30. Comparison of Phosphate to Bicarbonate Molar Ratio to pH for Well 399-1-23

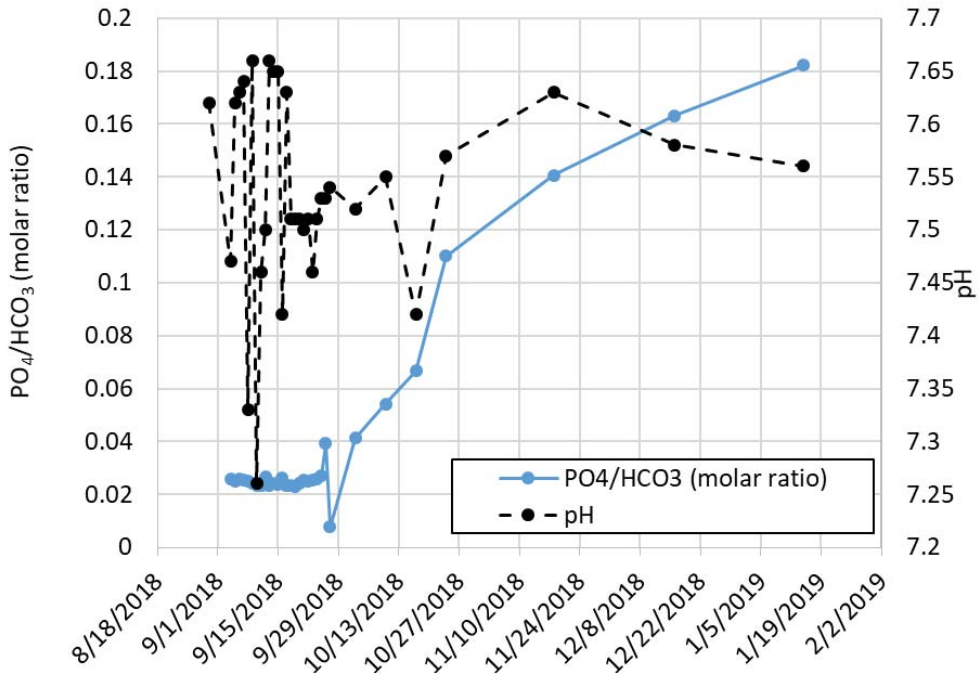

Figure A-31. Comparison of Phosphate to Bicarbonate Molar Ratio to pH for Well 399-1-7

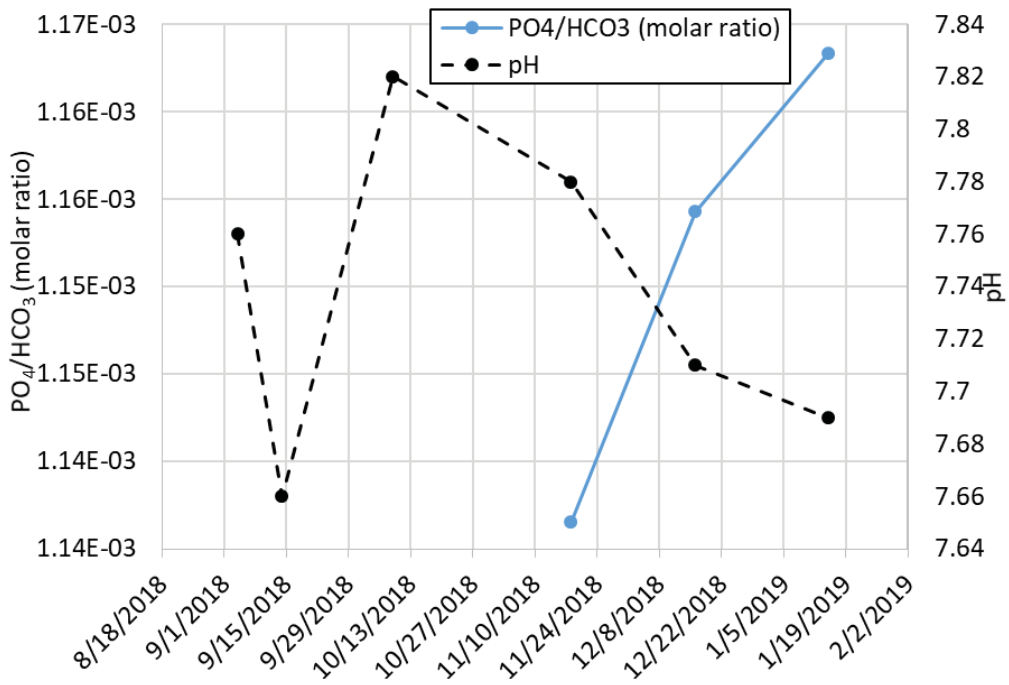

Figure A-32. Comparison of Phosphate to Bicarbonate Molar Ratio to pH for Well 399-1-12

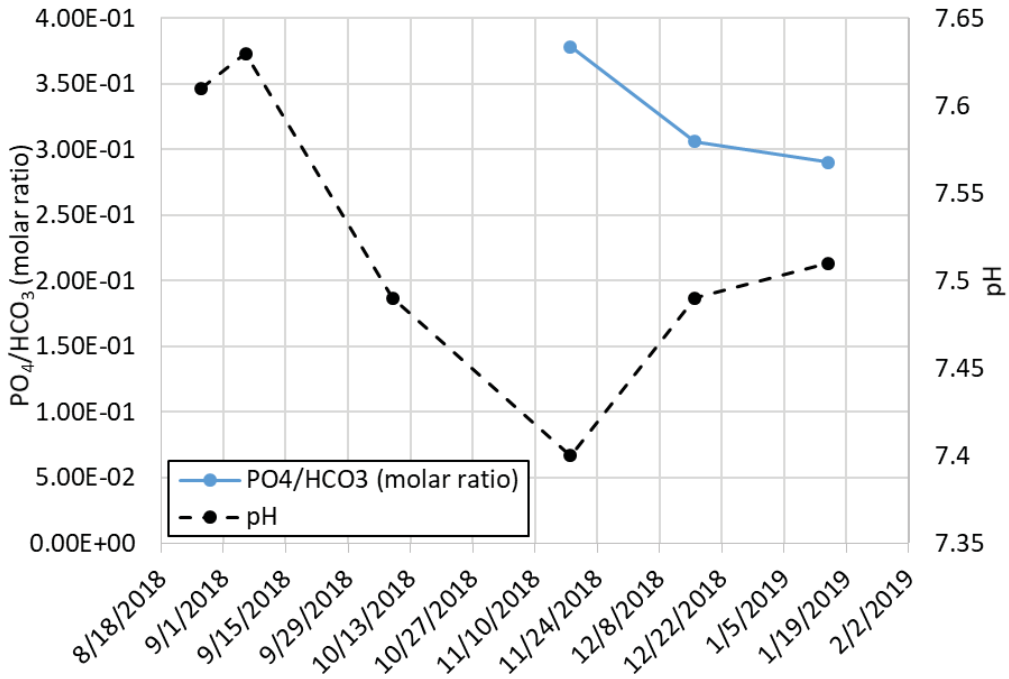

Figure A-33. Comparison of Phosphate to Bicarbonate Molar Ratio to pH for Well 399-1-16A

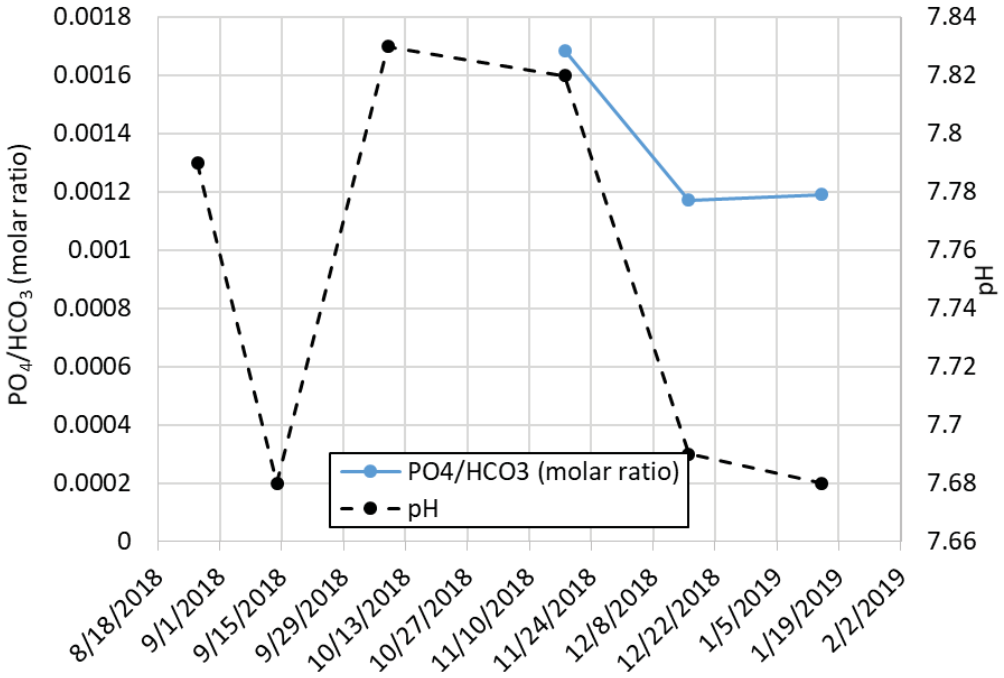

Figure A-34. Comparison of Phosphate to Bicarbonate Molar Ratio to pH for Well 399-1-2

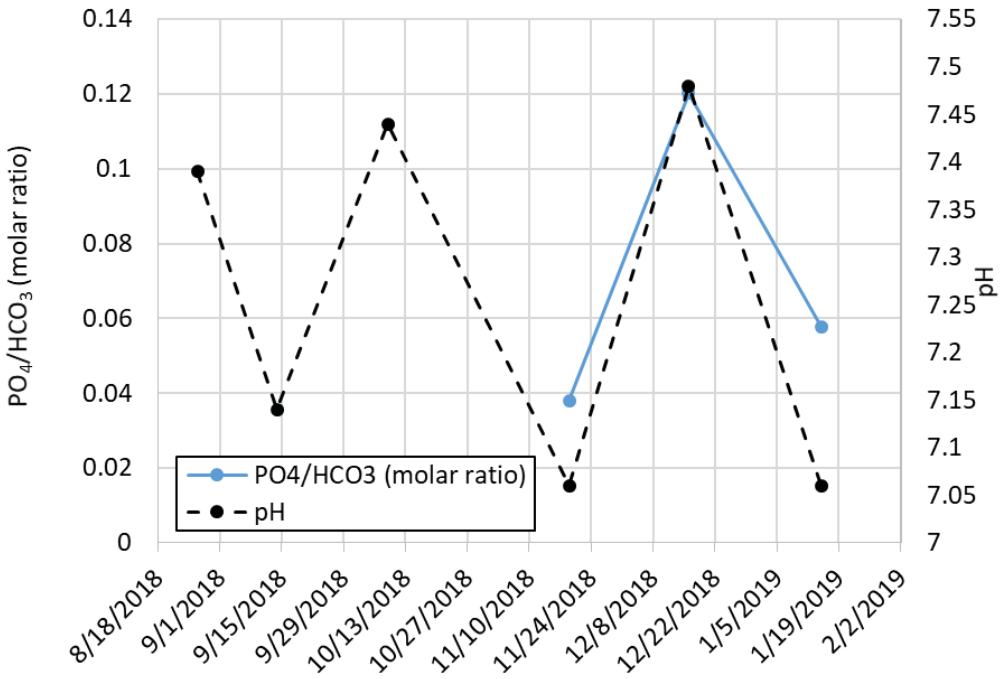

Figure A-35. Comparison of Phosphate to Bicarbonate Molar Ratio to pH for Well 399-1-55

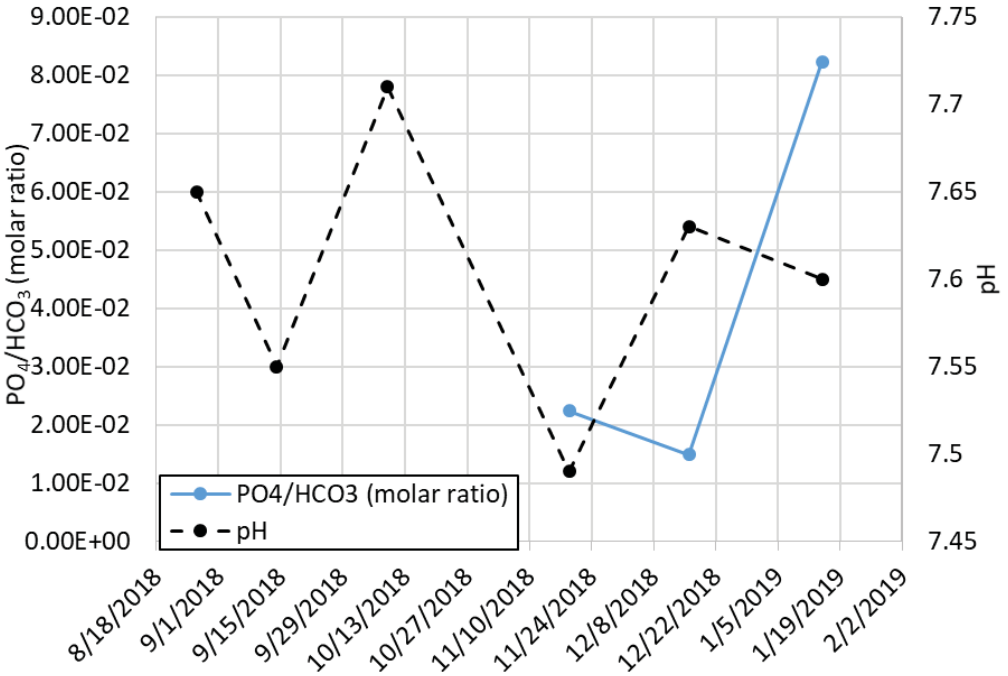

Figure A-36. Comparison of Phosphate to Bicarbonate Molar Ratio to pH for Well 399-1-62

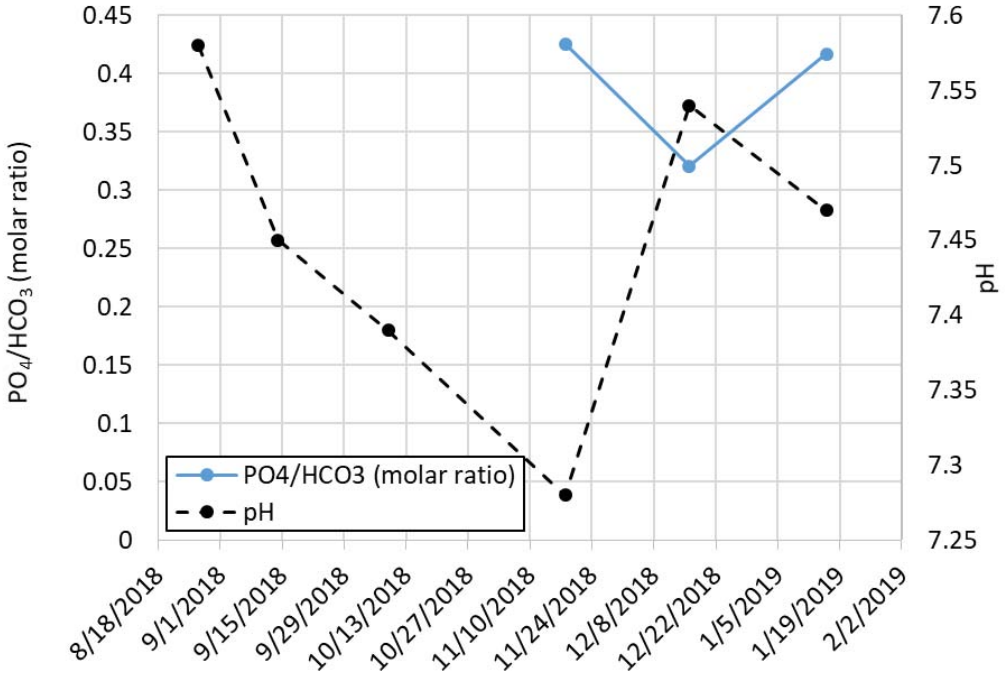

Figure A-37. Comparison of Phosphate to Bicarbonate Molar Ratio to pH for Well 399-2-2

A4 Uranium Concentration Compared to Calcium Concentration

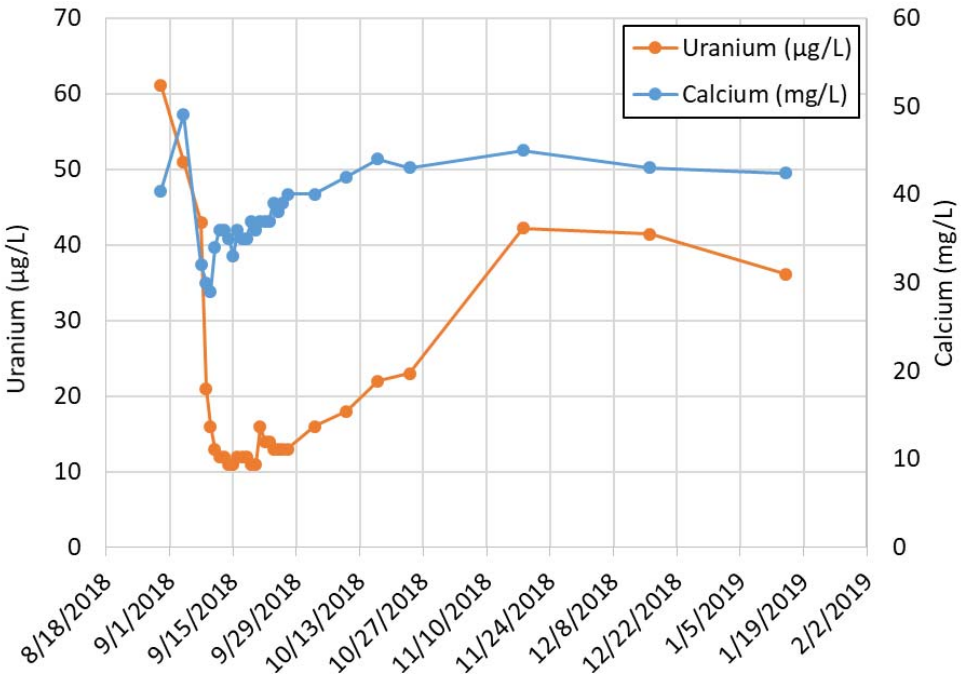

Figure A-38. Comparison of Uranium to Calcium for Well 399-1-162

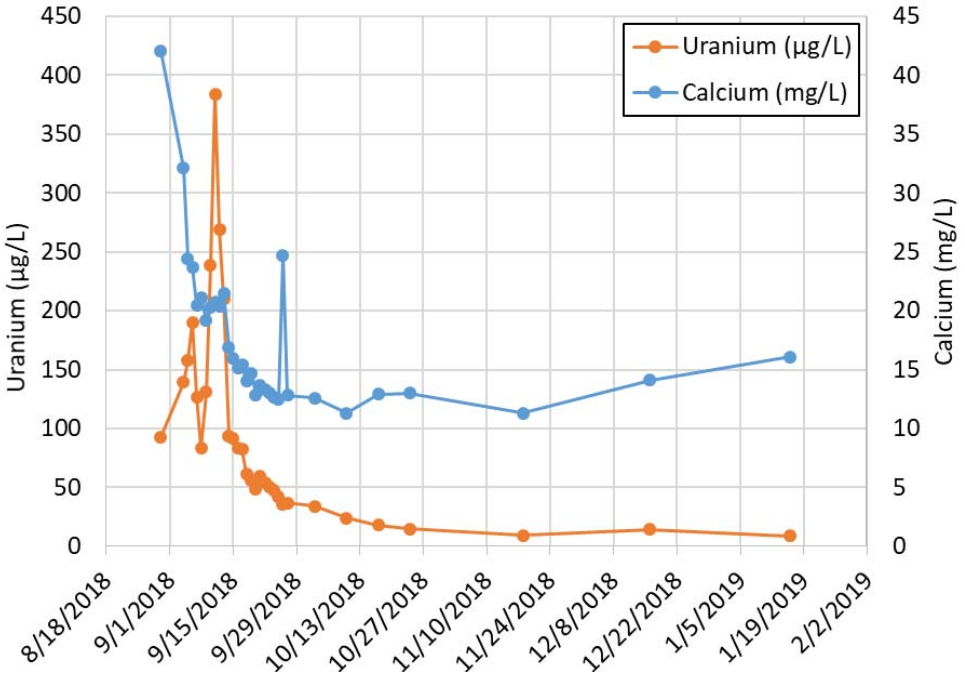

Figure A-39. Comparison of Uranium to Calcium for Well 399-1-160

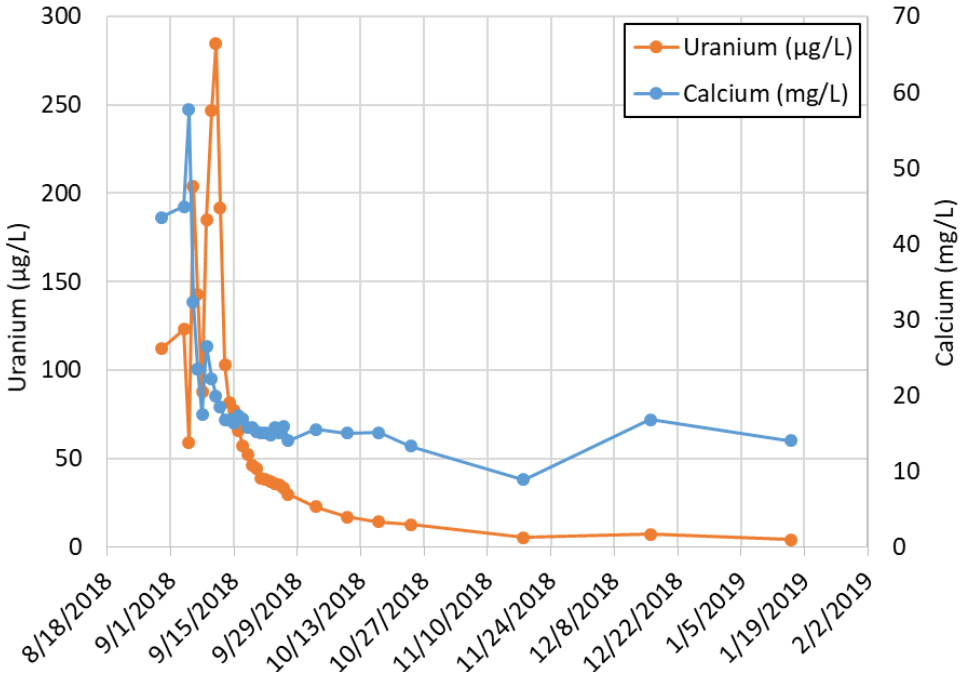

Figure A-40. Comparison of Uranium to Calcium for Well 399-1-161

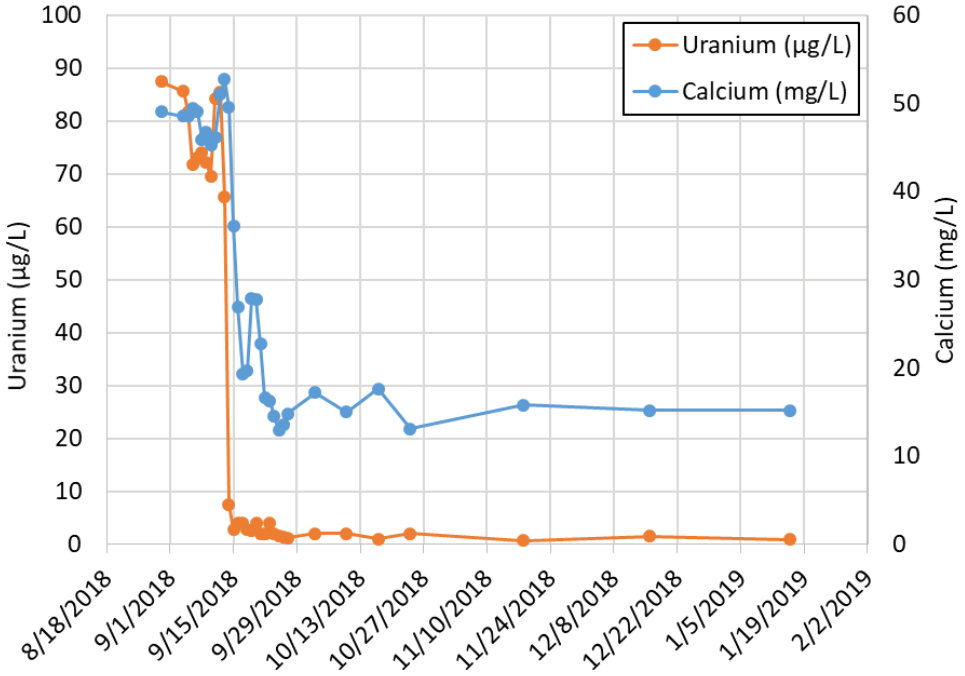

Figure A-41. Comparison of Uranium to Calcium for Well 399-1-156

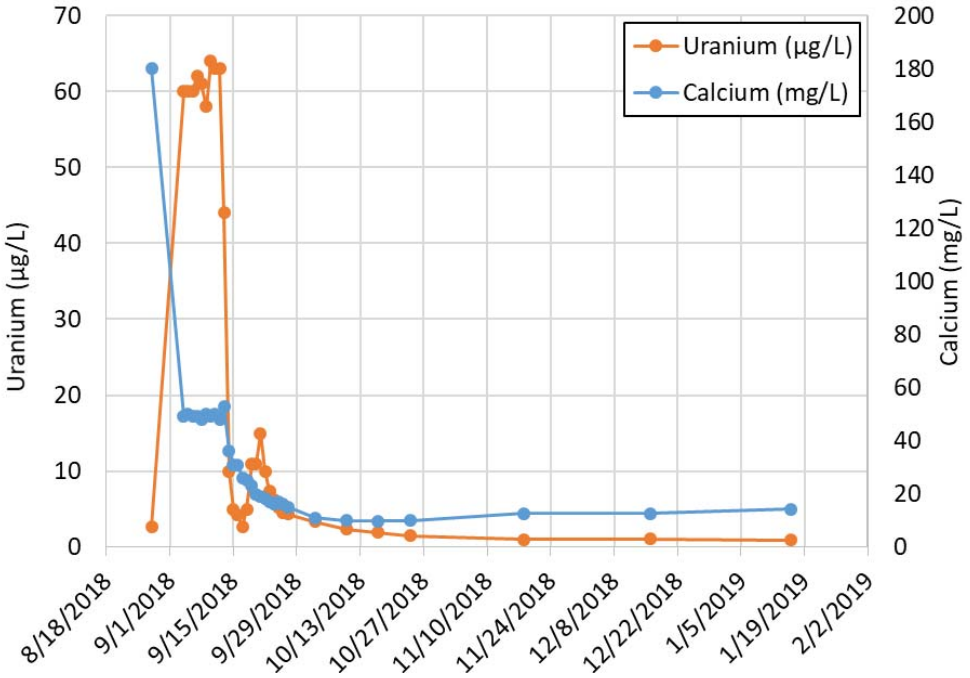

Figure A-42. Comparison of Uranium to Calcium for Well 399-1-155

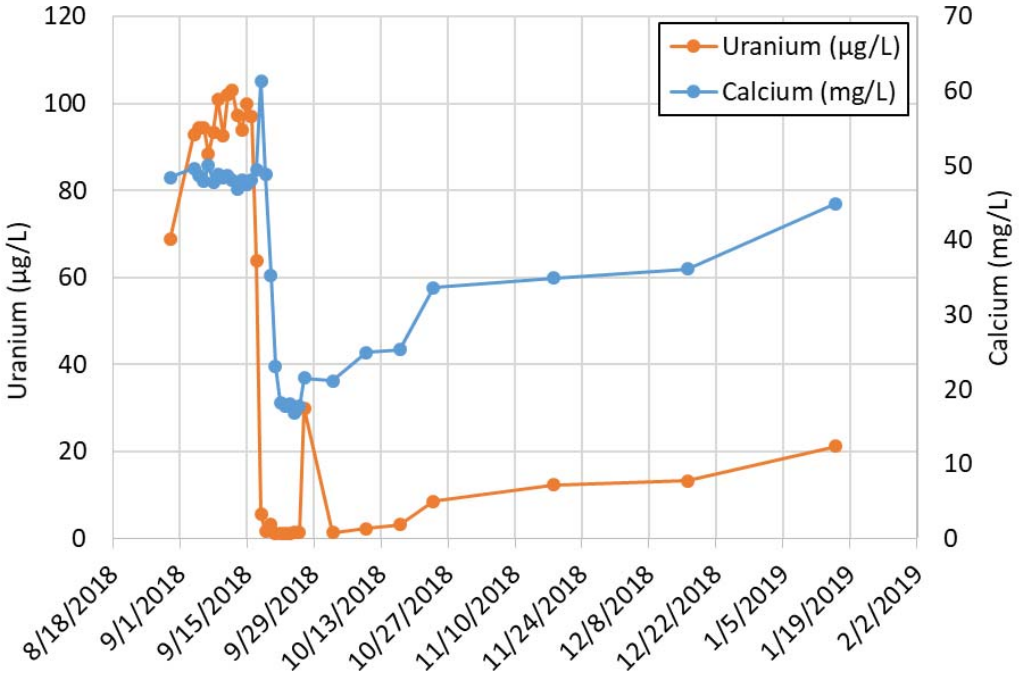

Figure A-43. Comparison of Uranium to Calcium for Well 399-1-157

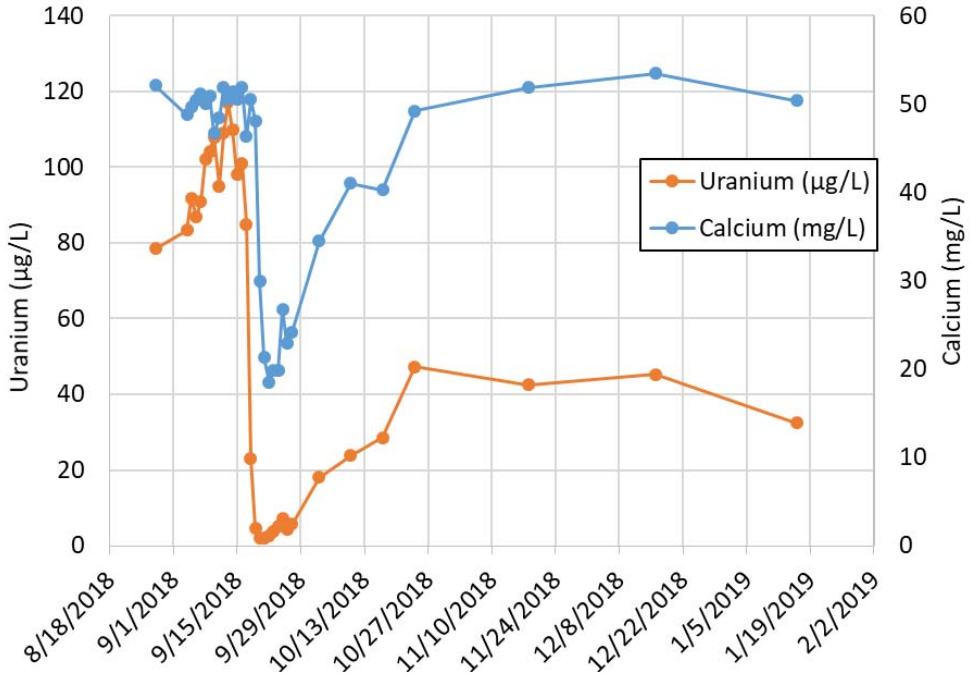

Figure A-44. Comparison of Uranium to Calcium for Well 399-1-158

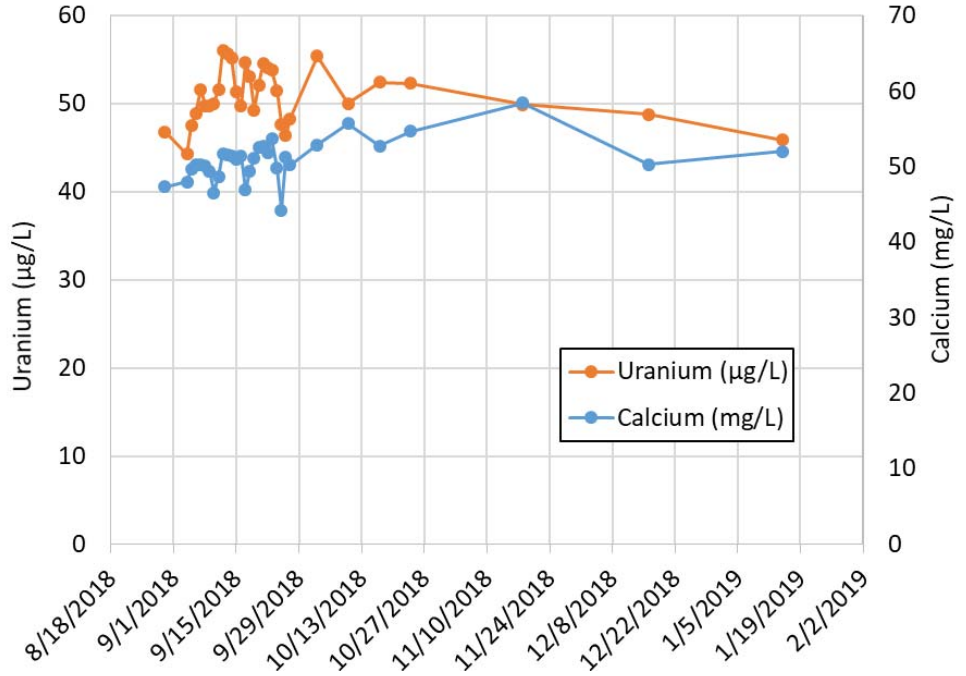

Figure A-45. Comparison of Uranium to Calcium for Well 399-1-166

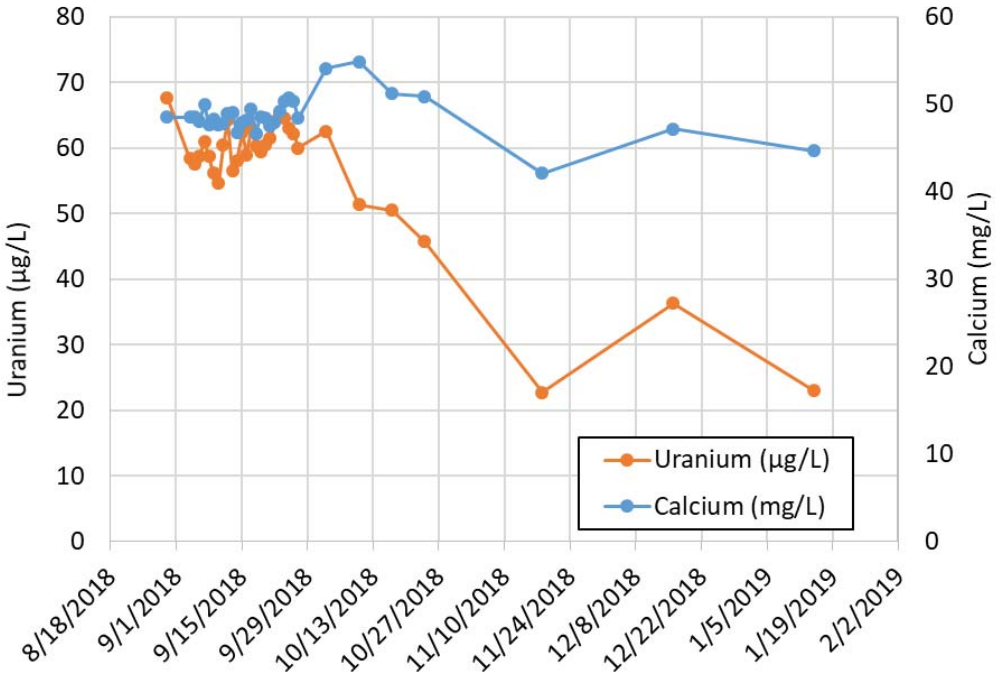

Figure A-46. Comparison of Uranium to Calcium for Well 399-1-165

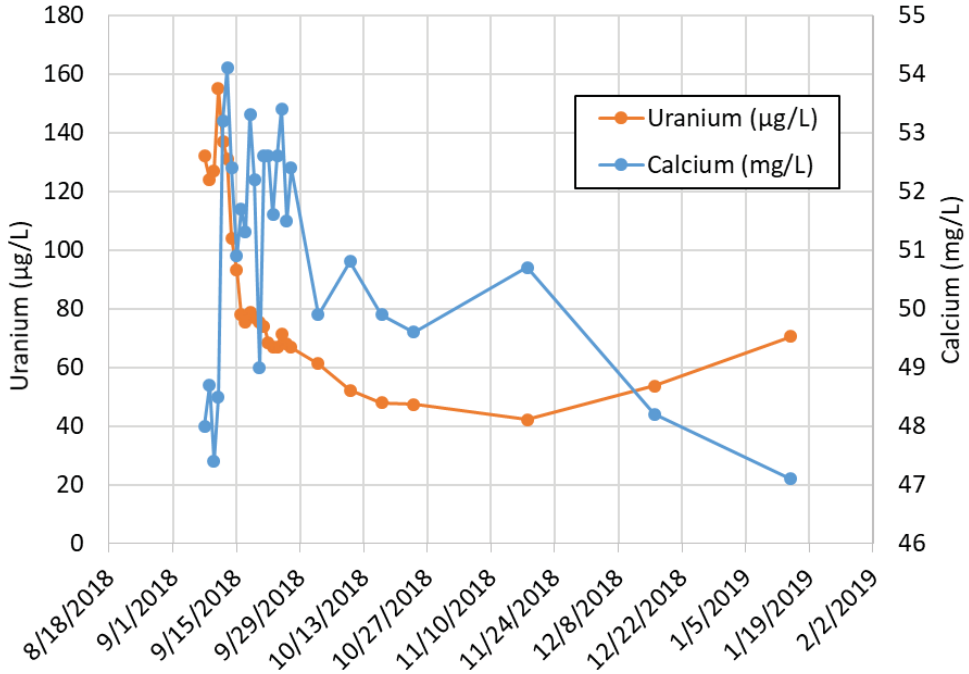

Figure A-47. Comparison of Uranium to Calcium for Well 399-1-164

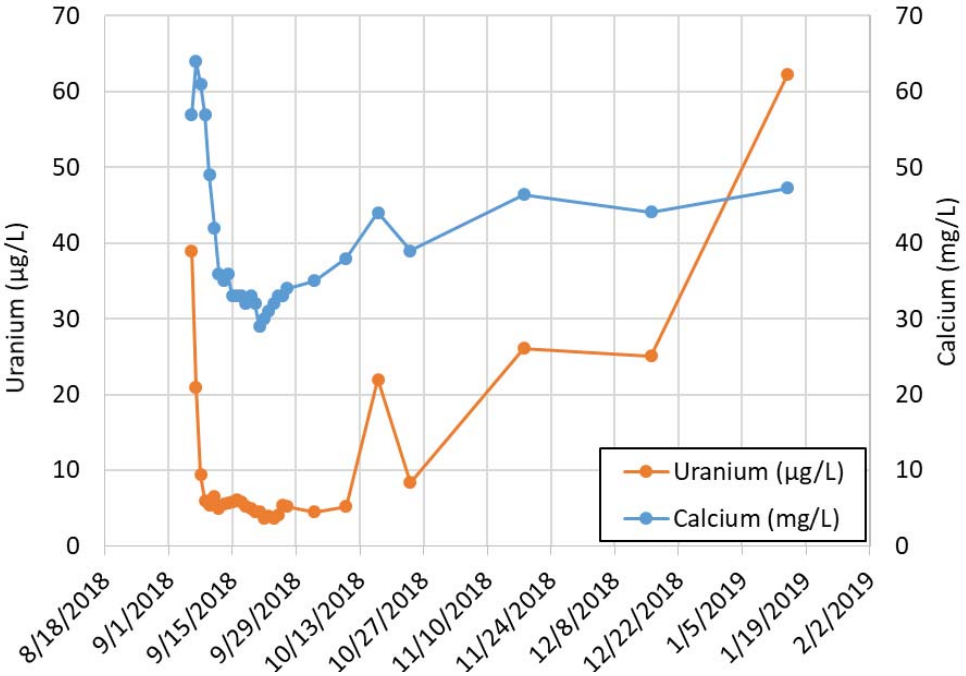

Figure A-48. Comparison of Uranium to Calcium for Well 399-1-23

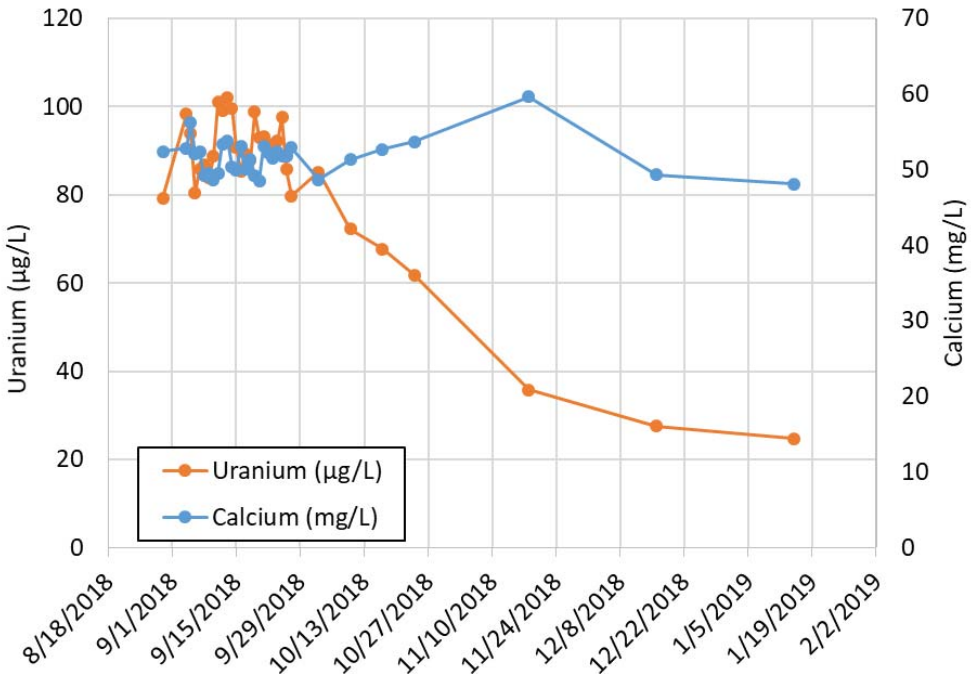

Figure A-49. Comparison of Uranium to Calcium for Well 399-1-7

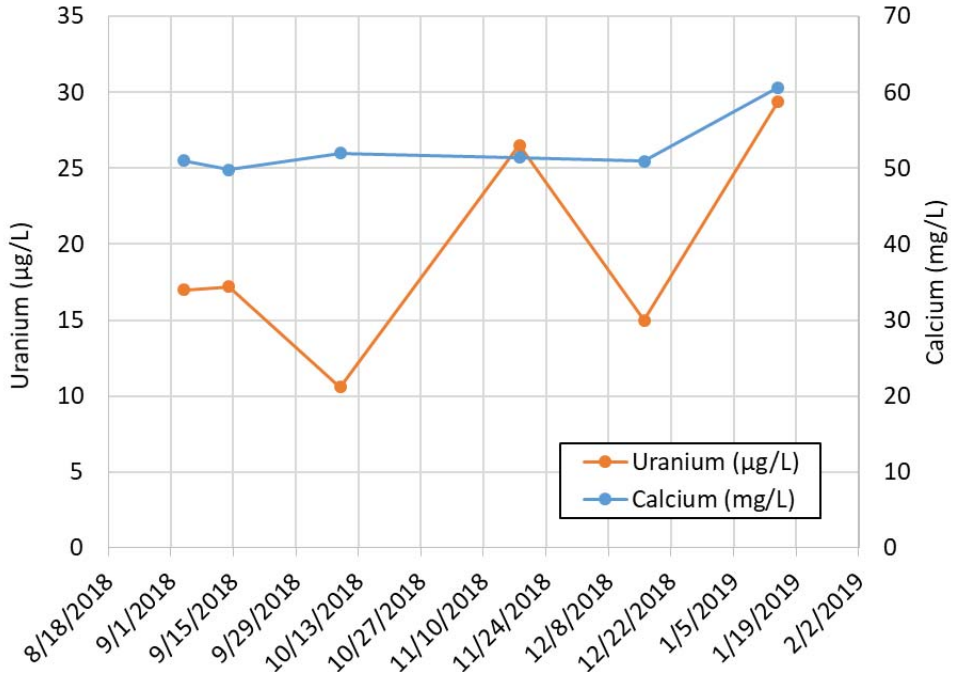

Figure A-50. Comparison of Uranium to Calcium for Well 399-1-12

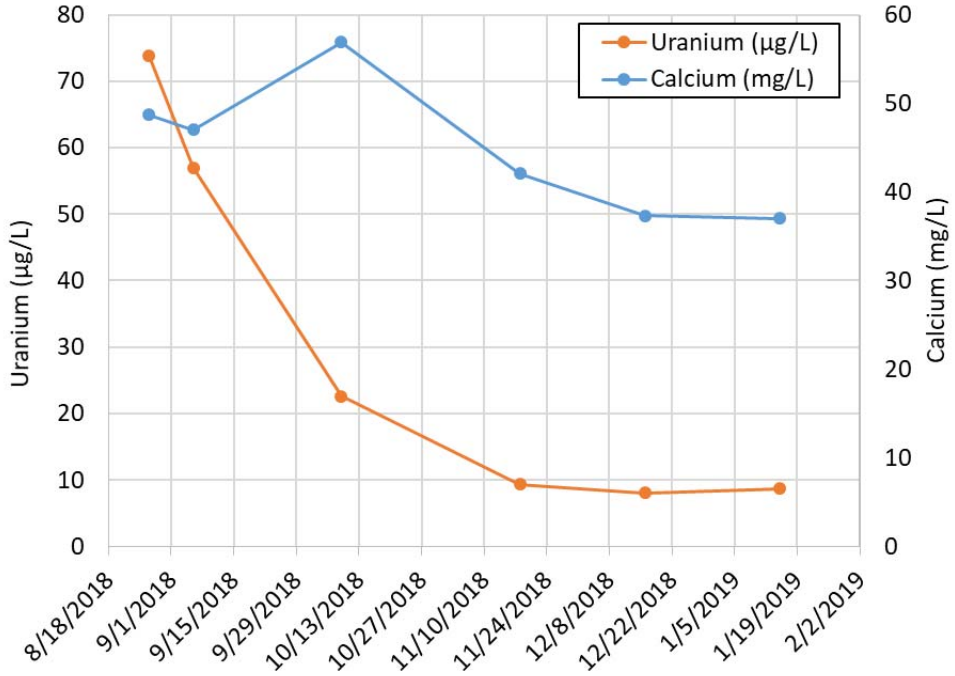

Figure A-51. Comparison of Uranium to Calcium for Well 399-1-16A

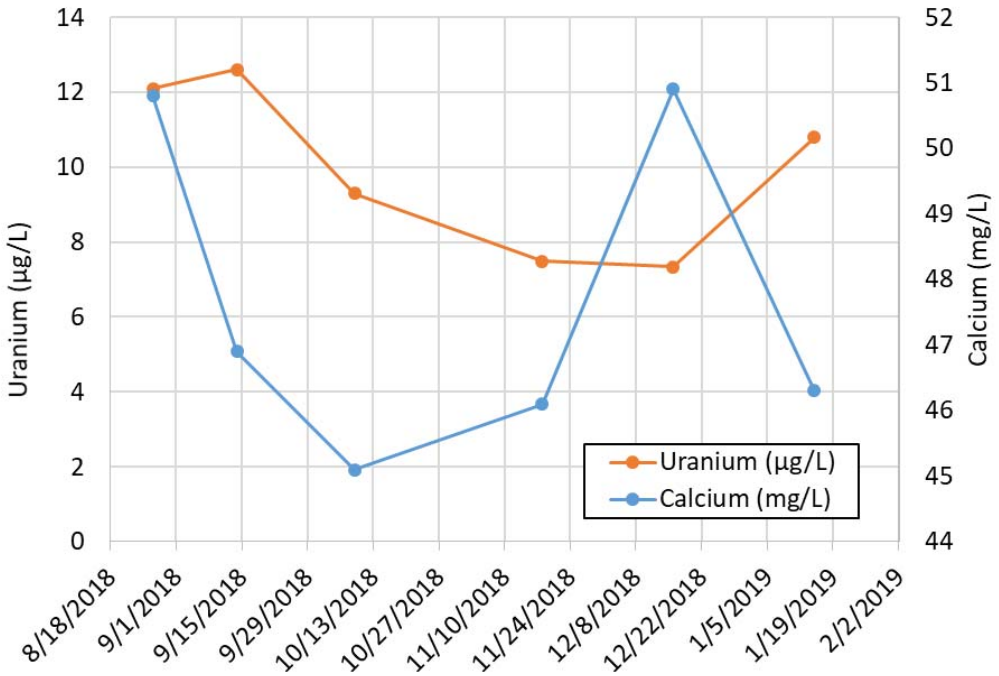

Figure A-52. Comparison of Uranium to Calcium for Well 399-1-2

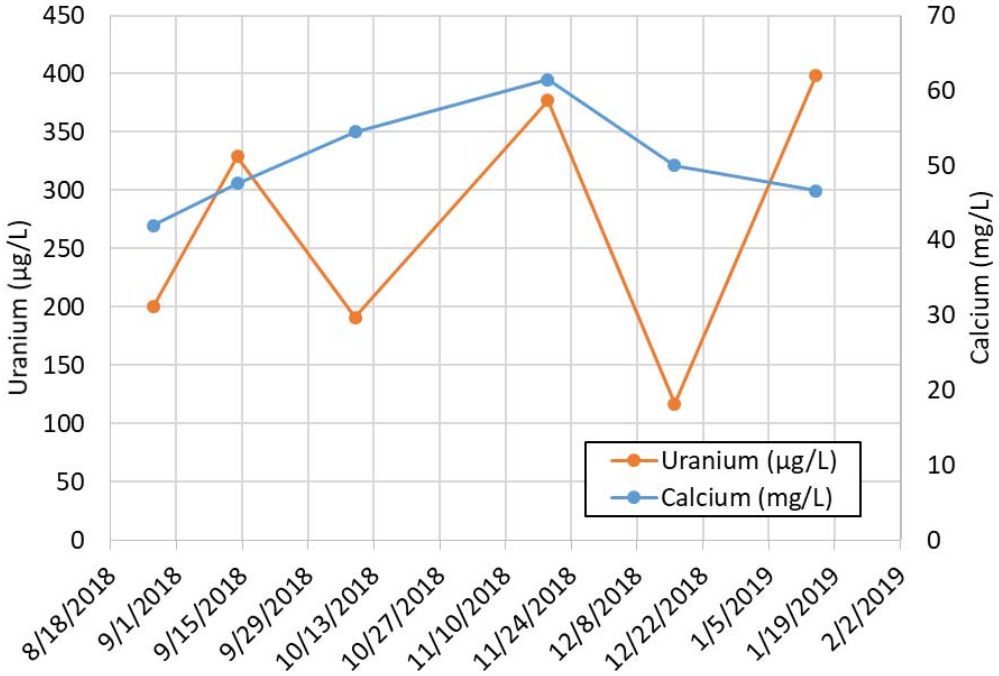

Figure A-53. Comparison of Uranium to Calcium for Well 399-1-55

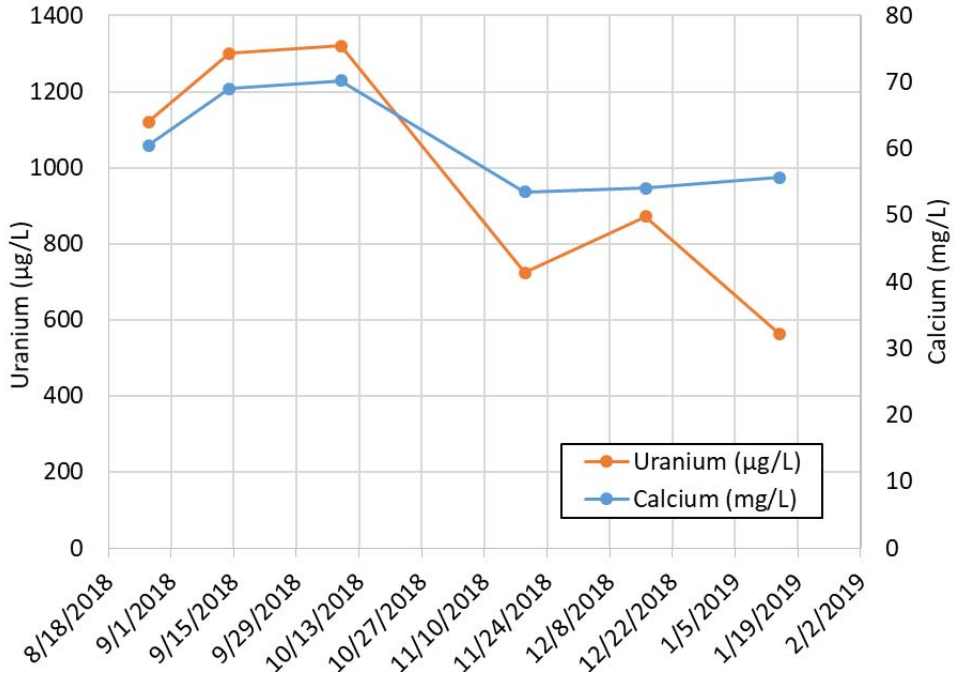

Figure A-54. Comparison of Uranium to Calcium for Well 399-1-62

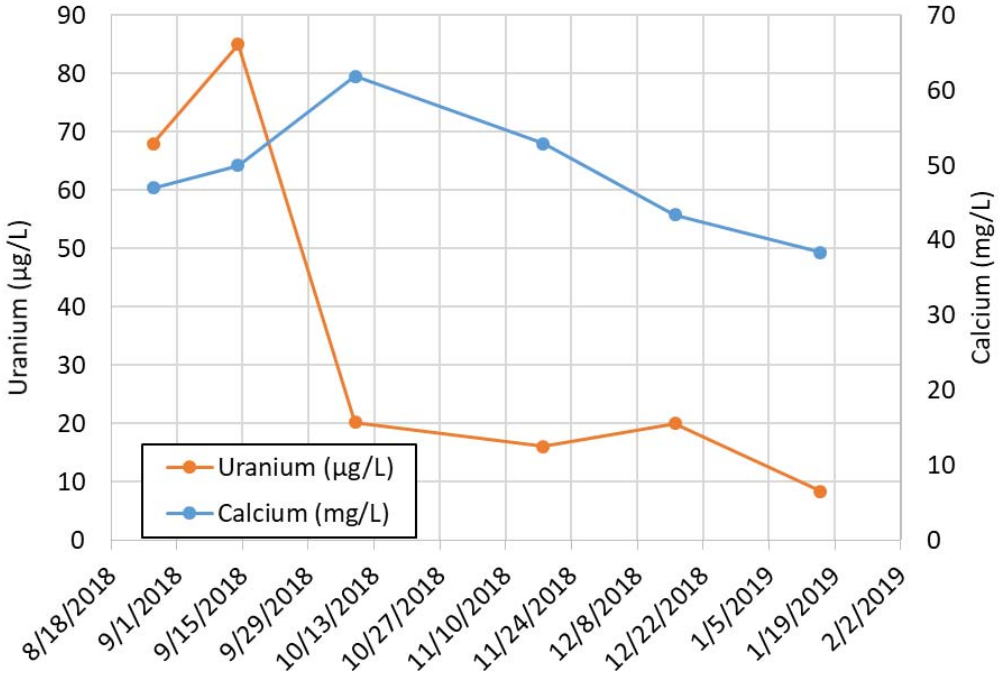

Figure A-55. Comparison of Uranium to Calcium for Well 399-2-2

A5 Calcium Concentration Compared to Phosphate Concentration

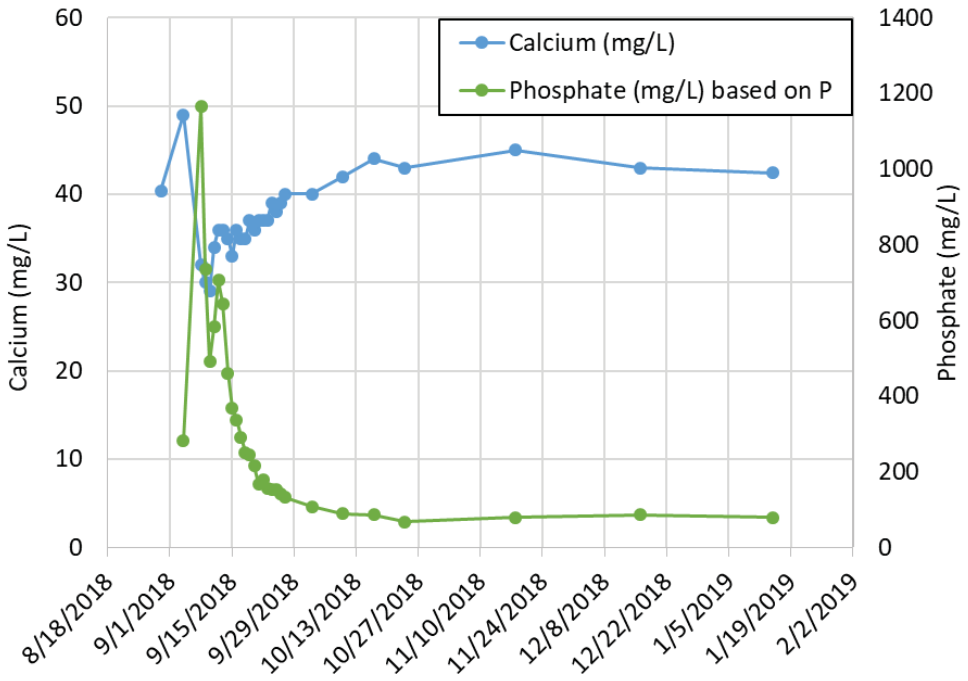

Figure A-56. Comparison of Calcium to Phosphate for Well 399-1-162

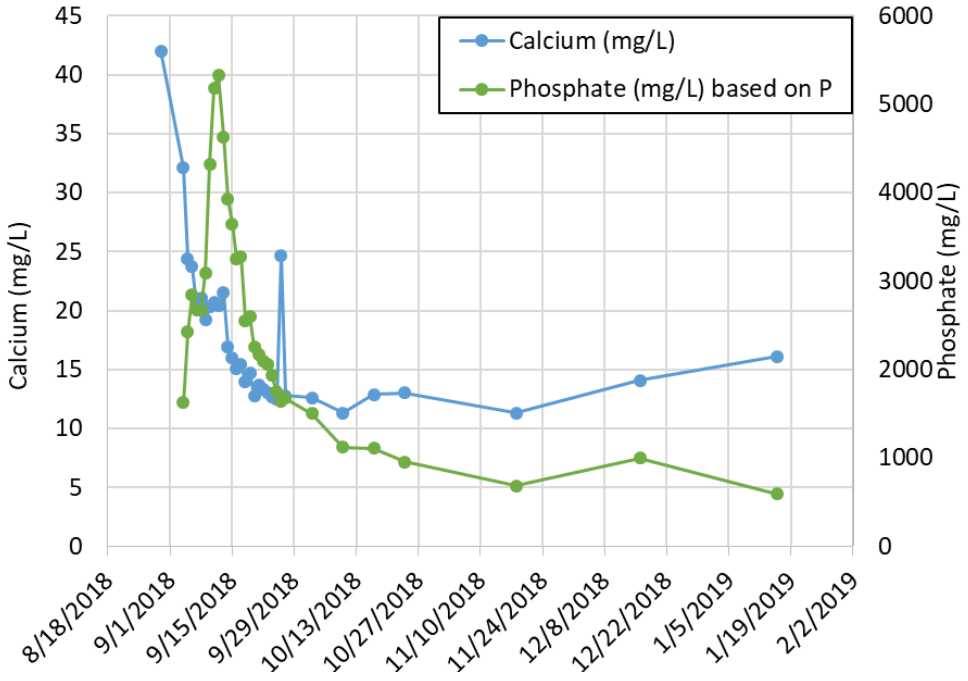

Figure A-57. Comparison of Calcium to Phosphate for Well 399-1-160

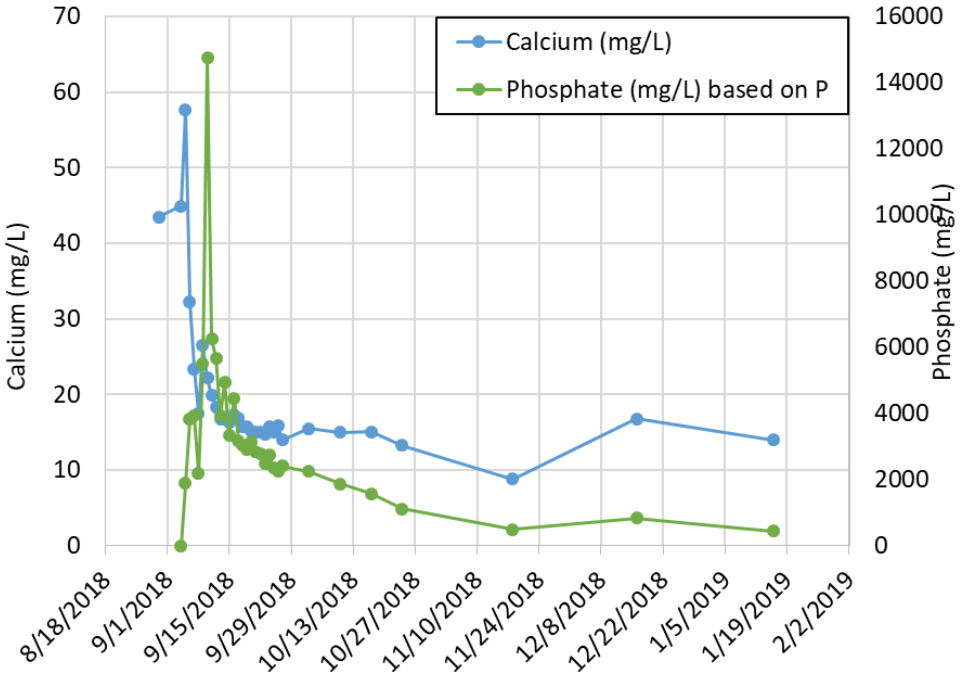

Figure A-58. Comparison of Calcium to Phosphate for Well 399-1-161

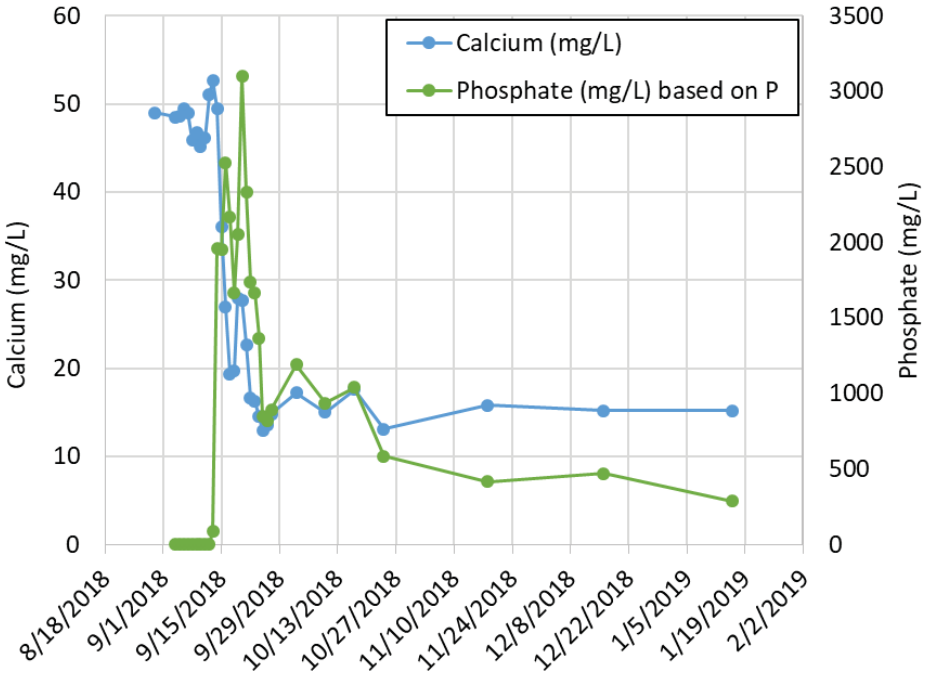

Figure A-59. Comparison of Calcium to Phosphate for Well 399-1-156

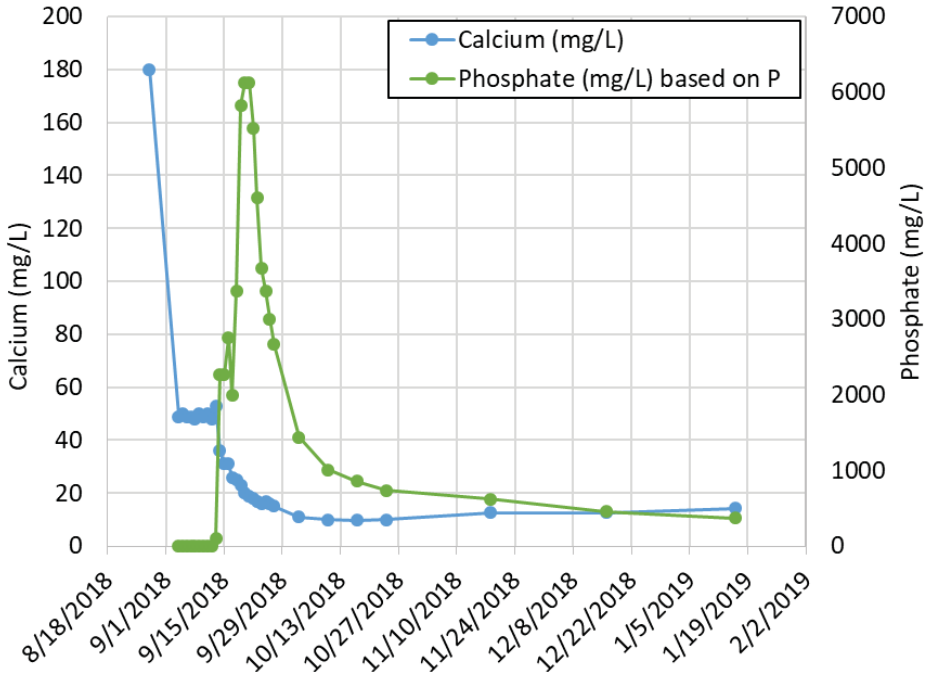

Figure A-60. Comparison of Calcium to Phosphate for Well 399-1-155

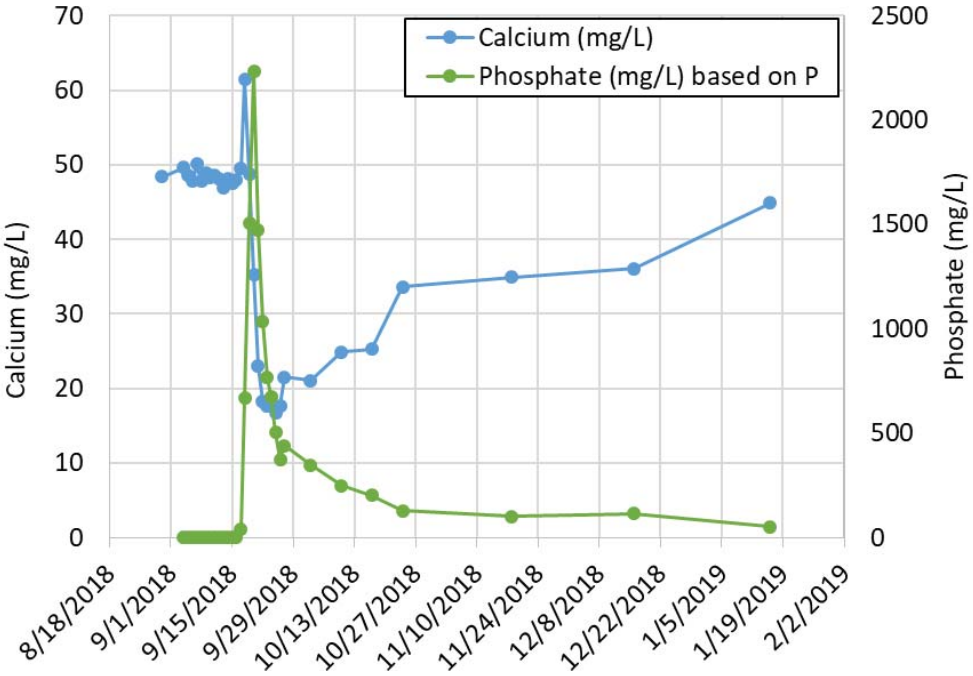

Figure A-61. Comparison of Calcium to Phosphate for Well 399-1-157

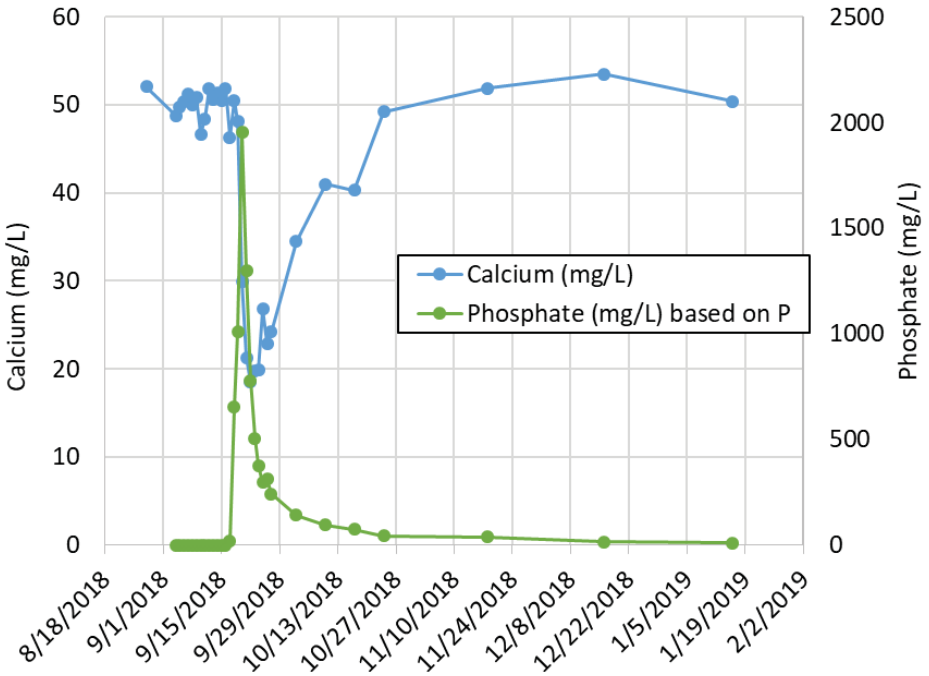

Figure A-62. Comparison of Calcium to Phosphate for Well 399-1-158

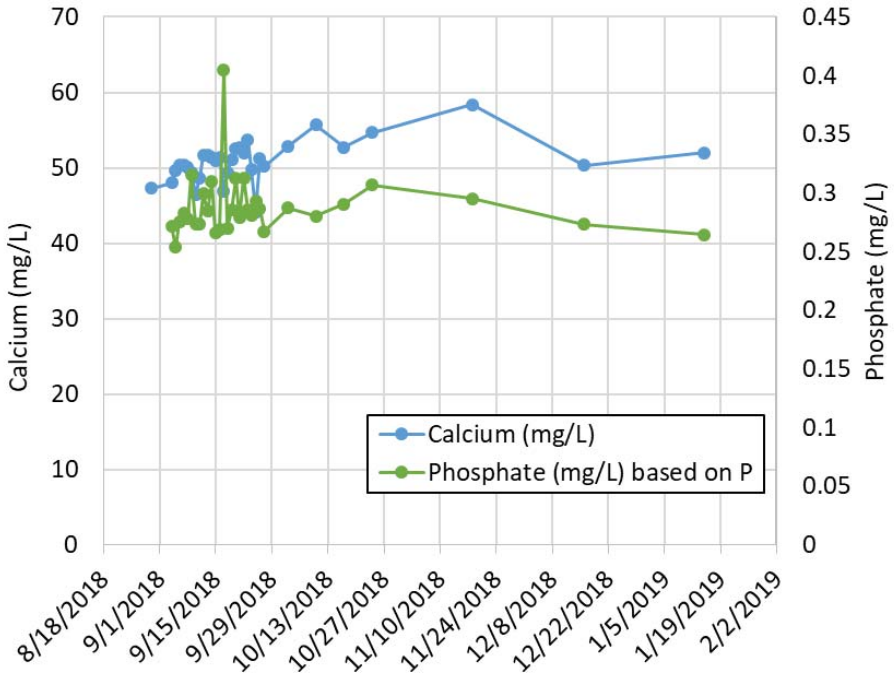

Figure A-63. Comparison of Calcium to Phosphate for Well 399-1-166

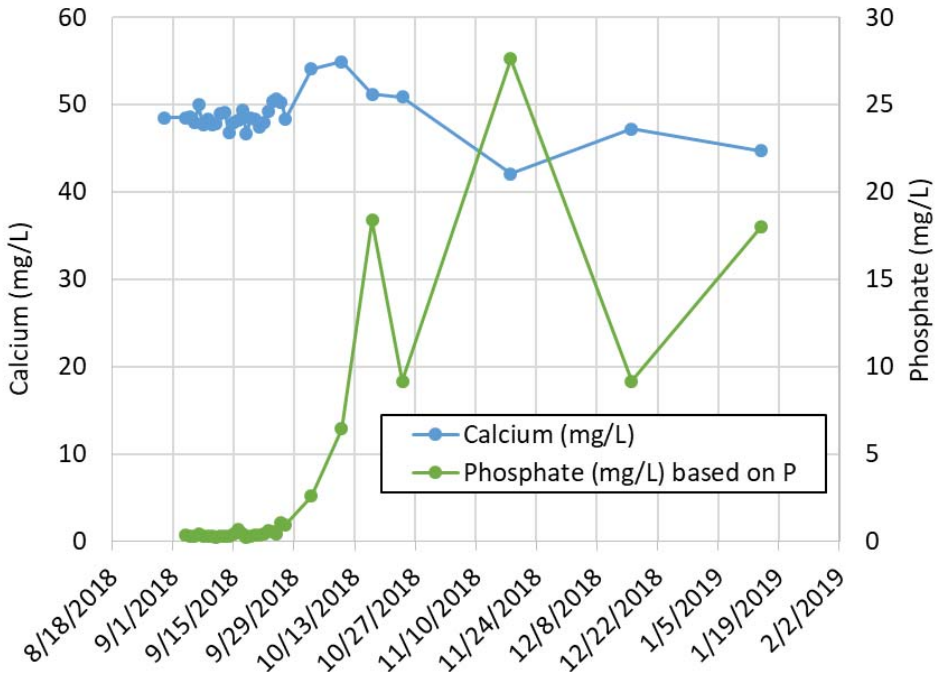

Figure A-64. Comparison of Calcium to Phosphate for Well 399-1-165

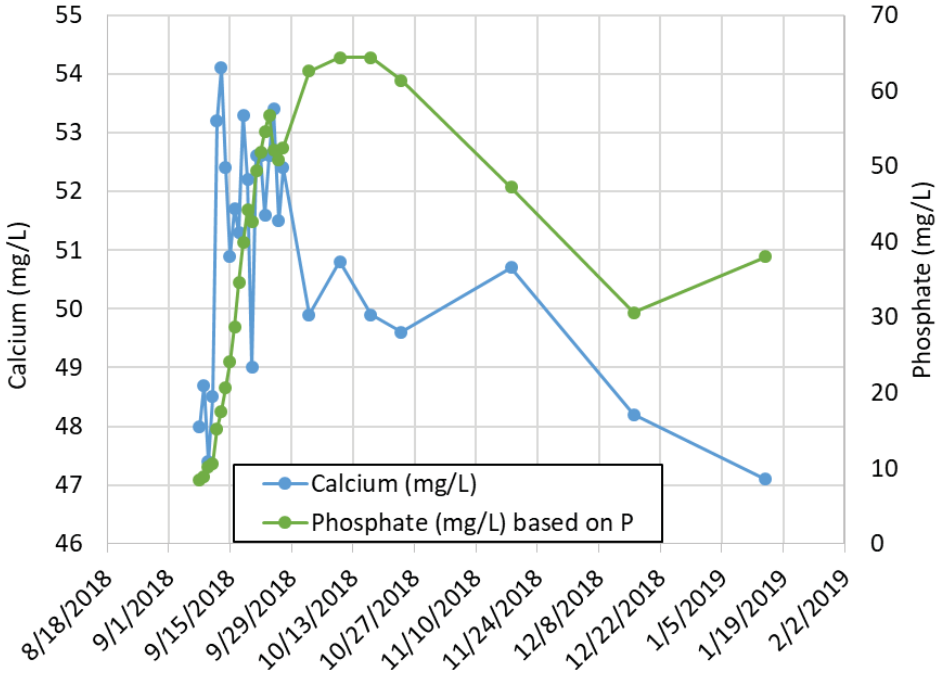

Figure A-65. Comparison of Calcium to Phosphate for Well 399-1-164

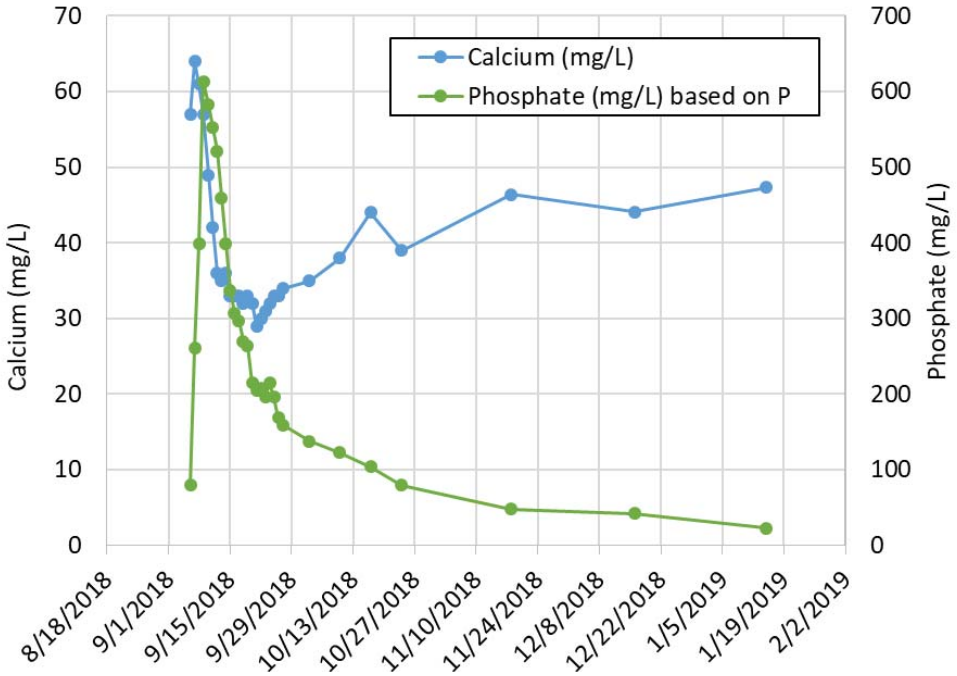

Figure A-66. Comparison of Calcium to Phosphate for Well 399-1-23

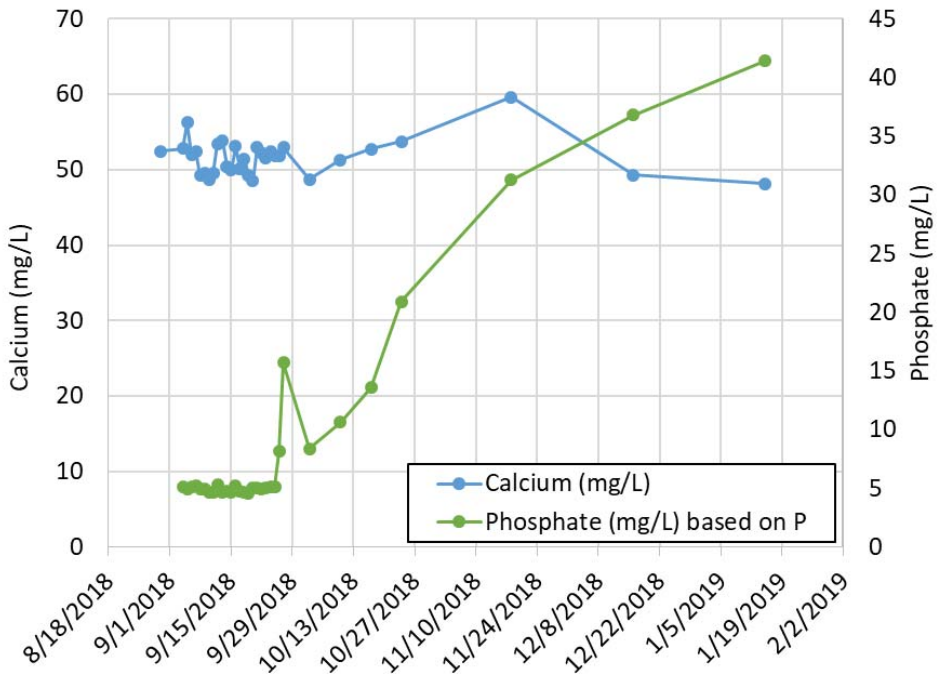

Figure A-67. Comparison of Calcium to Phosphate for Well 399-1-7

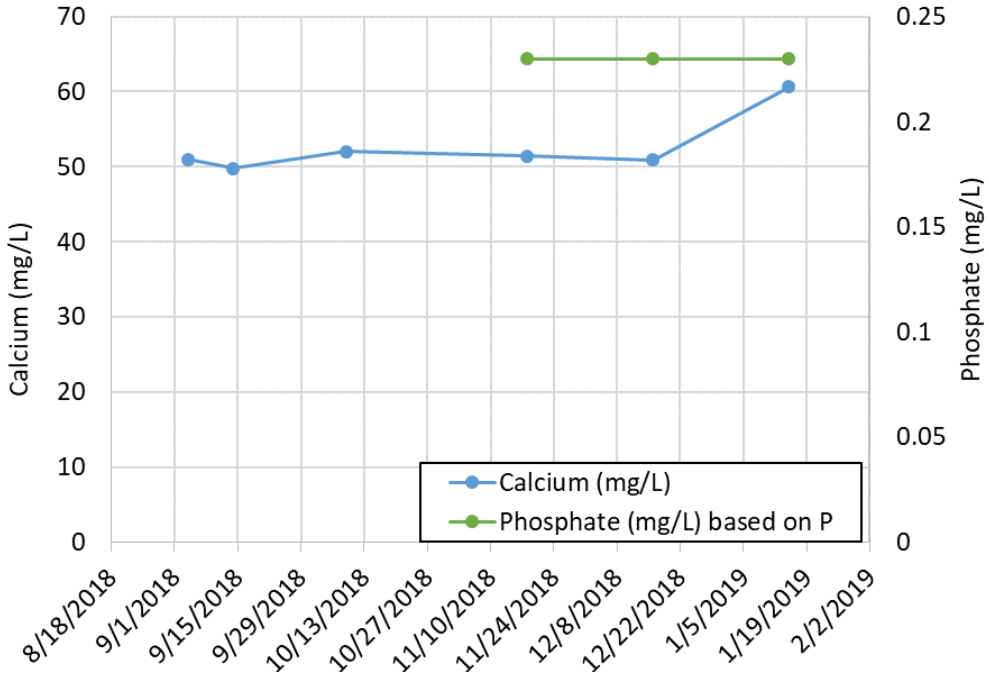

Figure A-68. Comparison of Calcium to Phosphate for Well 399-1-12

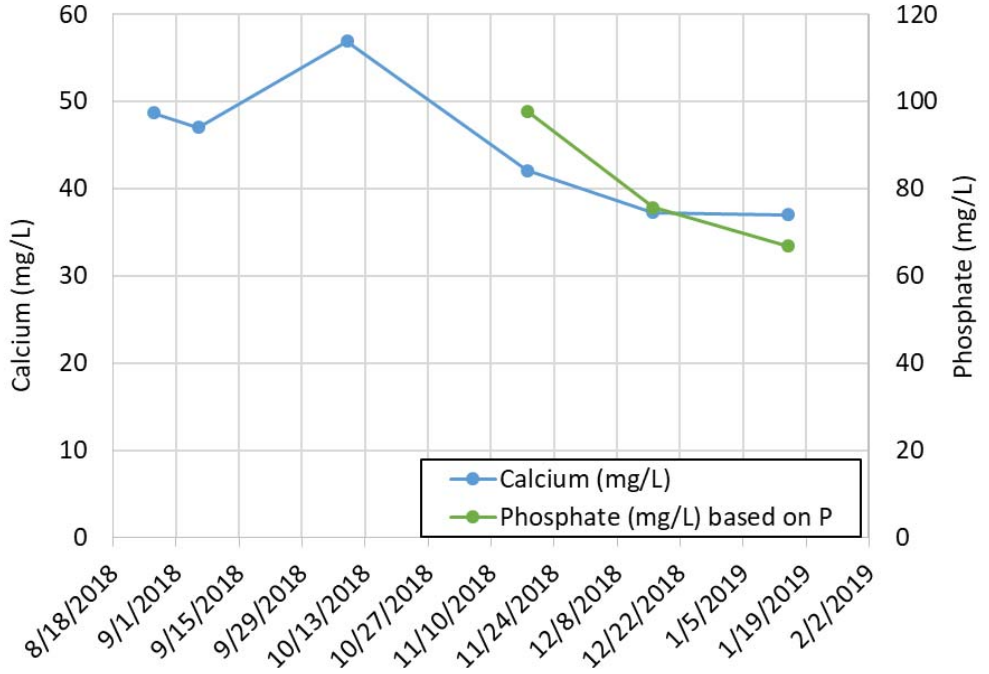

Figure A-69. Comparison of Calcium to Phosphate for Well 399-1-16A

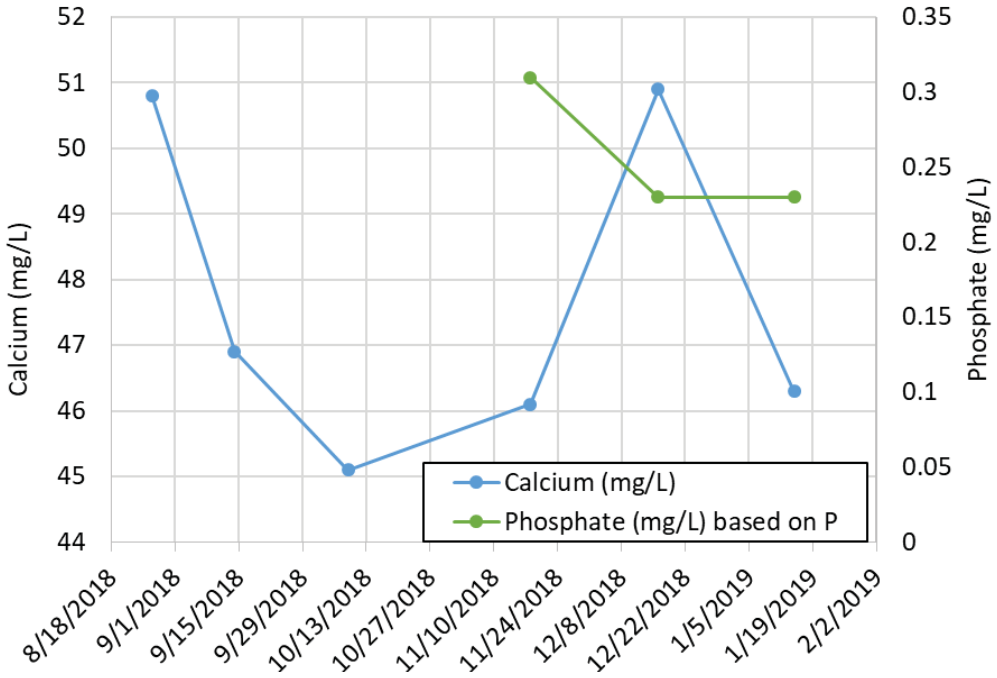

Figure A-70. Comparison of Calcium to Phosphate for Well 399-1-2

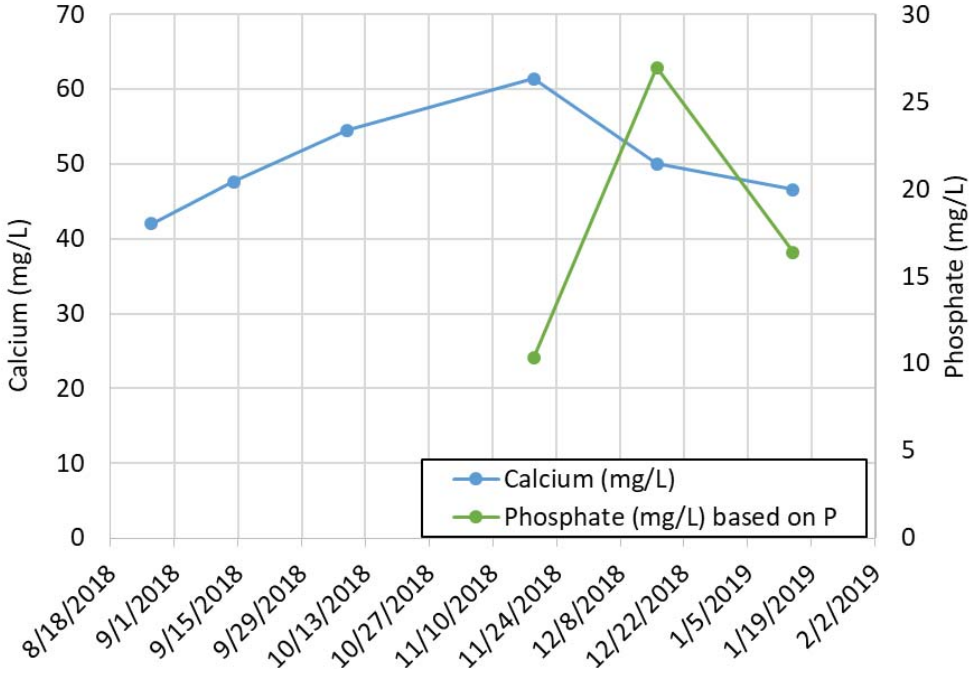

Figure A-71. Comparison of Calcium to Phosphate for Well 399-1-55

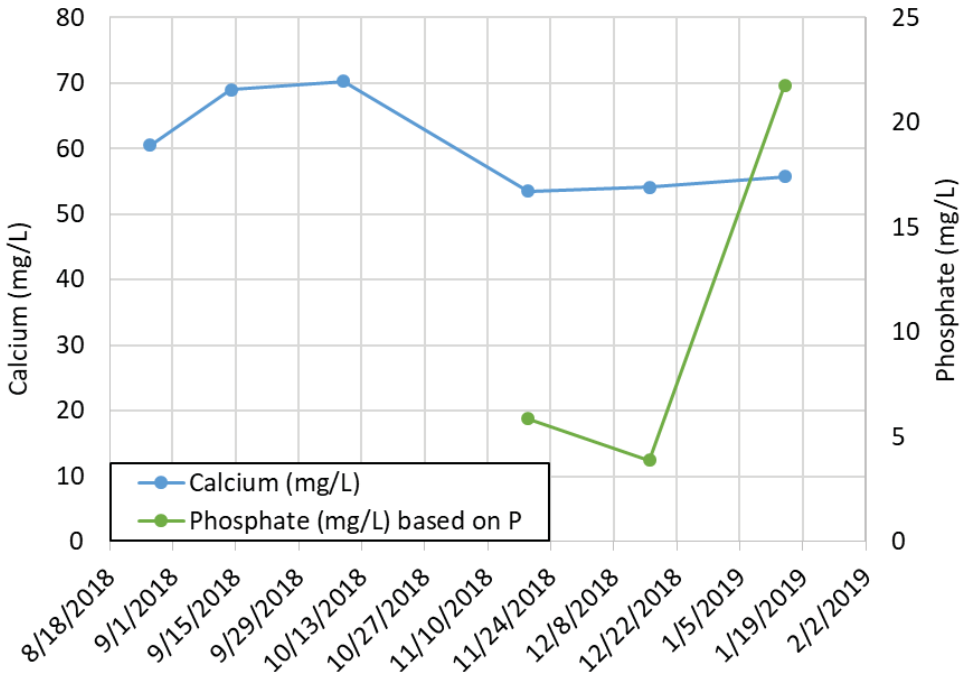

Figure A-72. Comparison of Calcium to Phosphate for Well 399-1-62

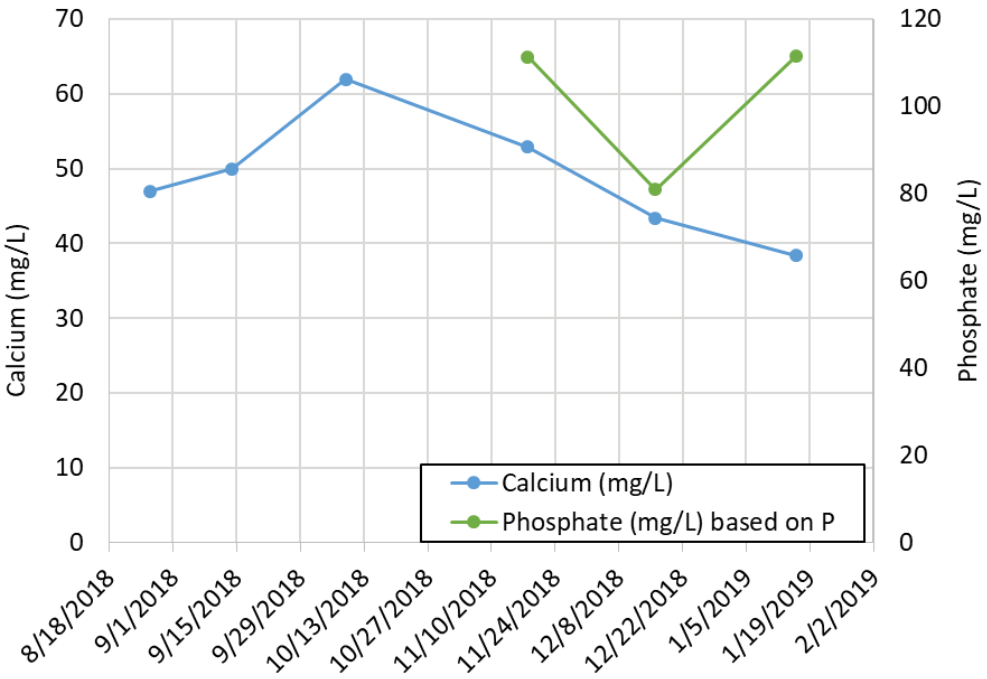

Figure A-73. Comparison of Calcium to Phosphate for Well 399-2-2

A6 Calcium to Sodium Ratio Compared to pH

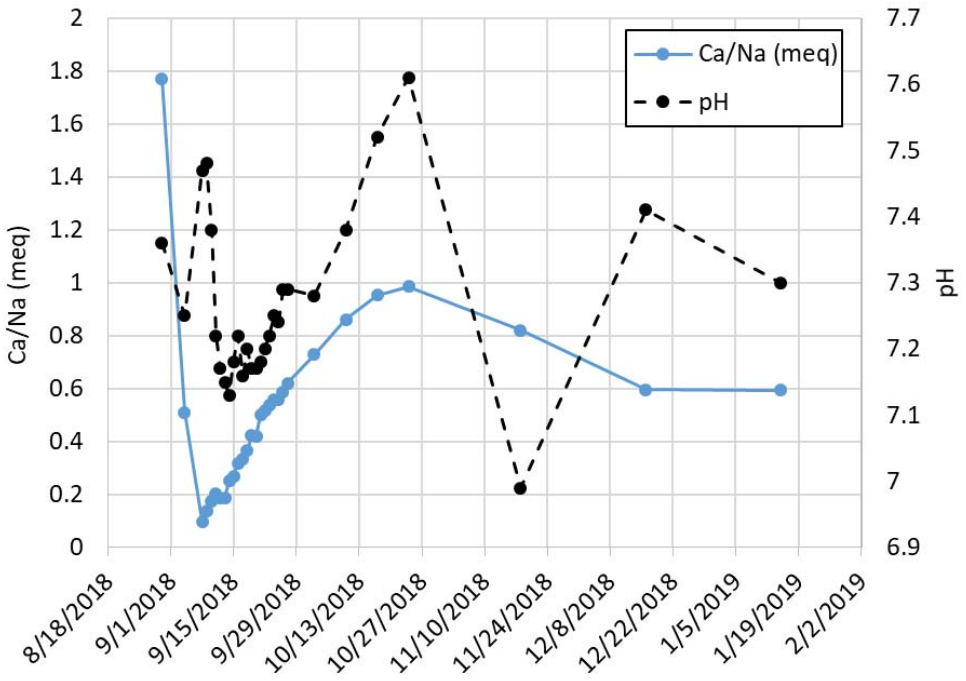

Figure A-74. Comparison of Calcium to Sodium Ratio to pH for Well 399-1-162

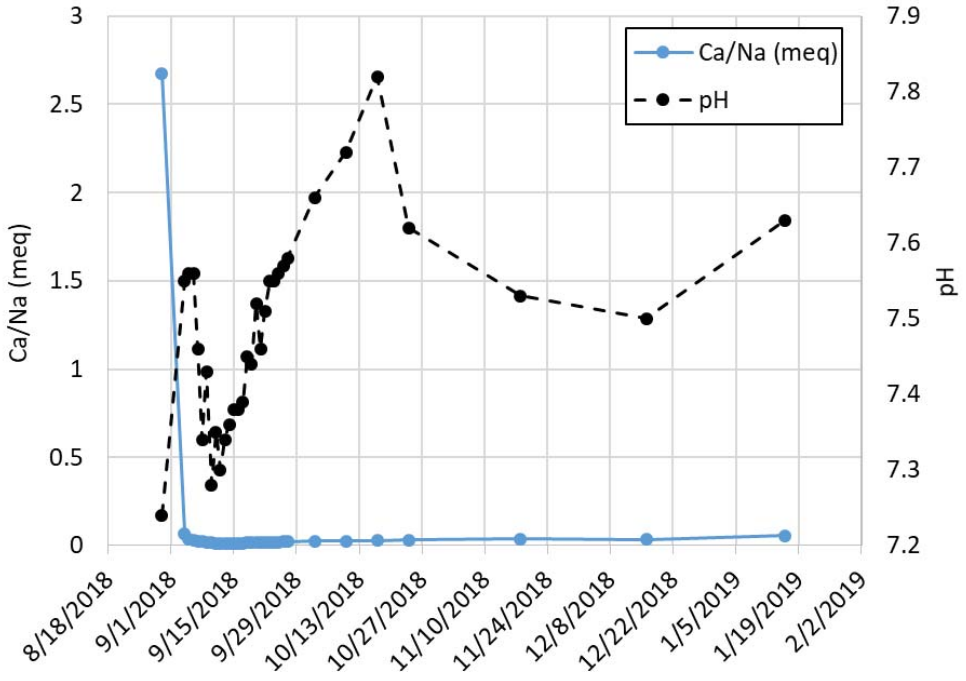

Figure A-75. Comparison of Calcium to Sodium Ratio to pH for Well 399-1-160

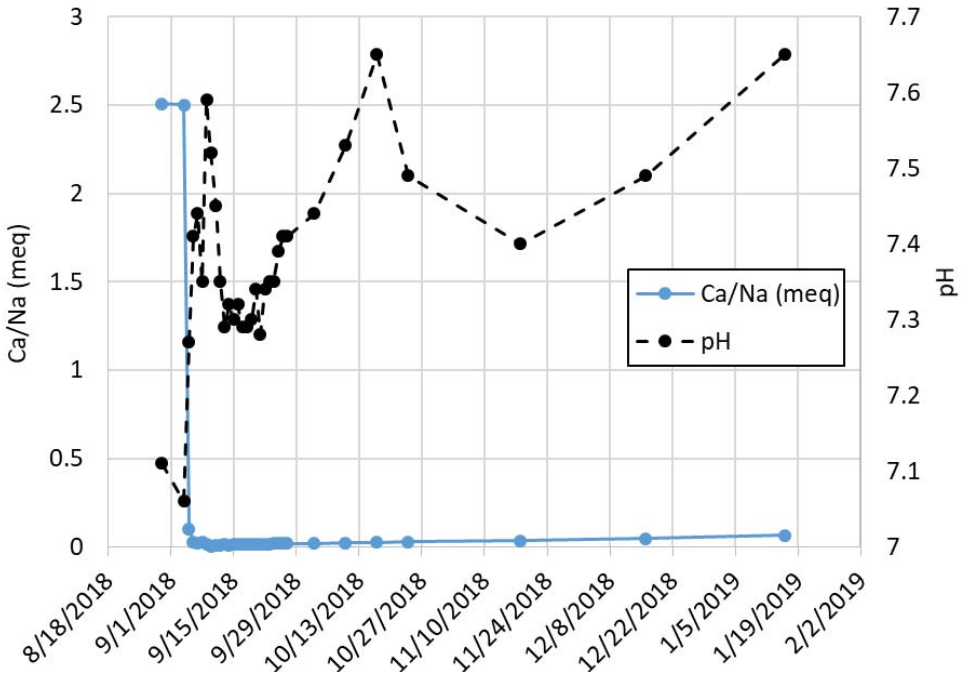

Figure A-76. Comparison of Calcium to Sodium Ratio to pH for Well 399-1-161

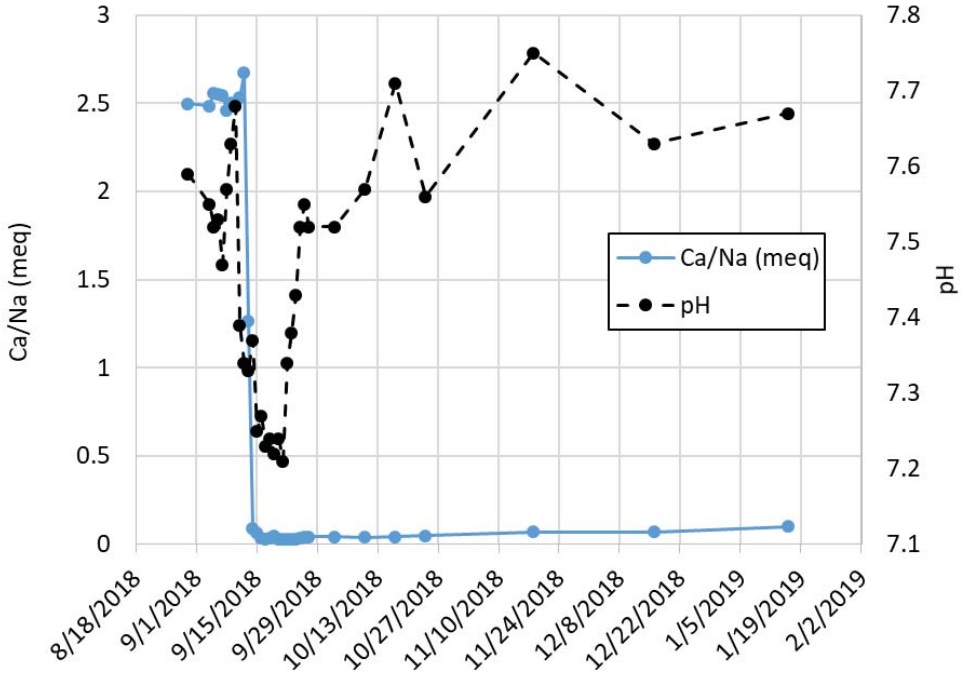

Figure A-77. Comparison of Calcium to Sodium Ratio to pH for Well 399-1-156

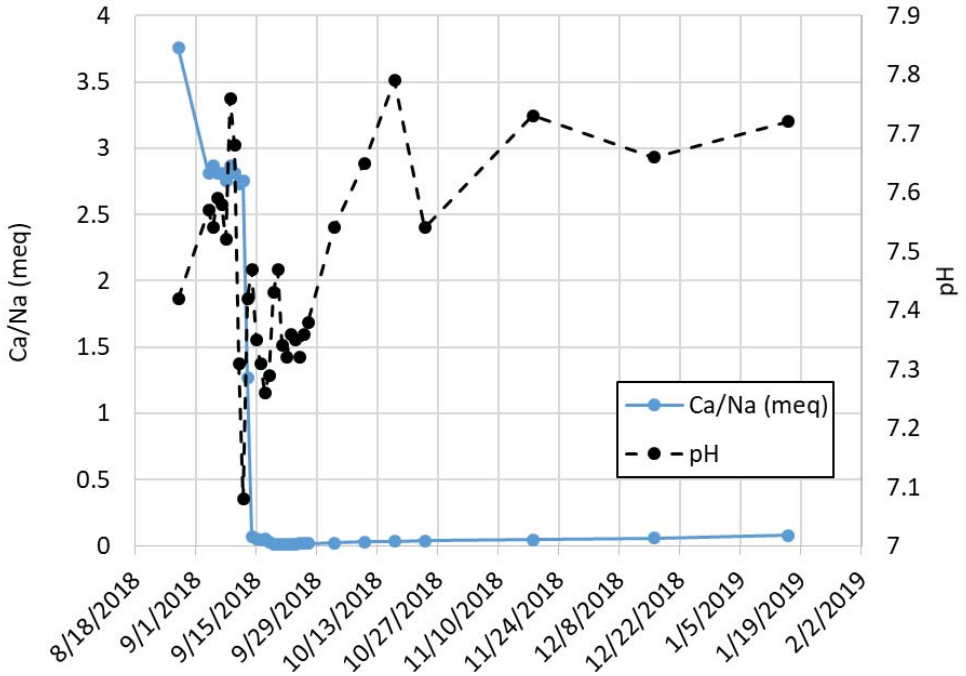

Figure A-78. Comparison of Calcium to Sodium Ratio to pH for Well 399-1-155

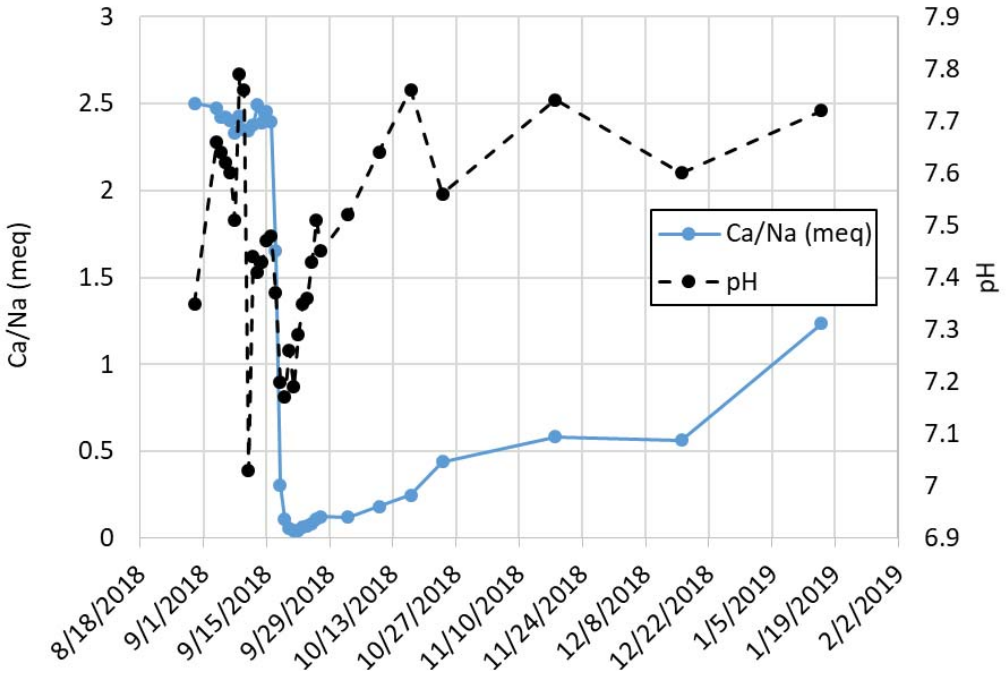

Figure A-79. Comparison of Calcium to Sodium Ratio to pH for Well 399-1-157

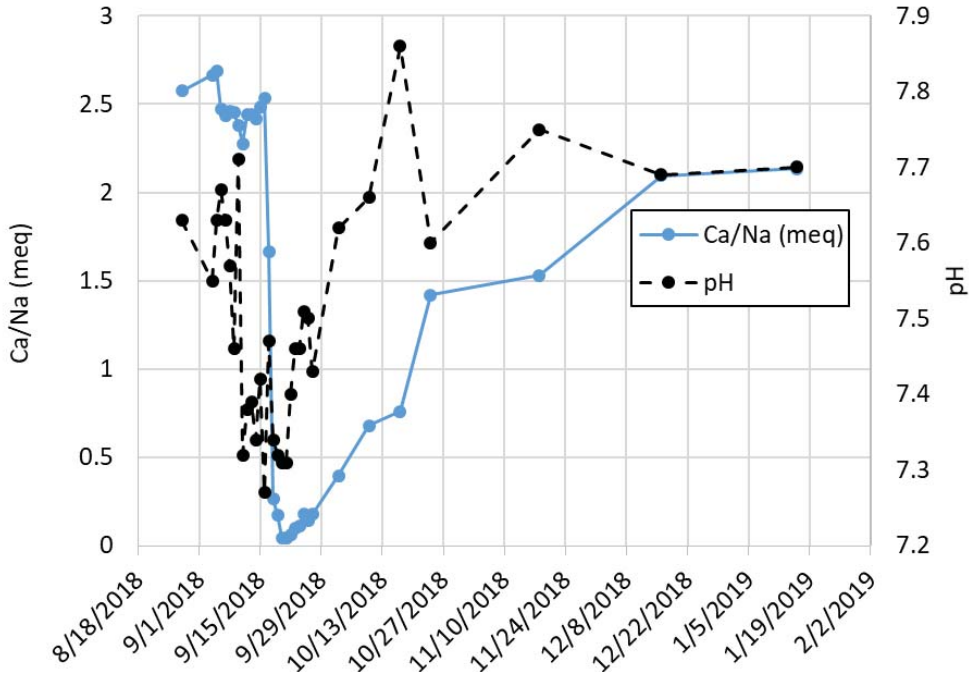

Figure A-80. Comparison of Calcium to Sodium Ratio to pH for Well 399-1-158

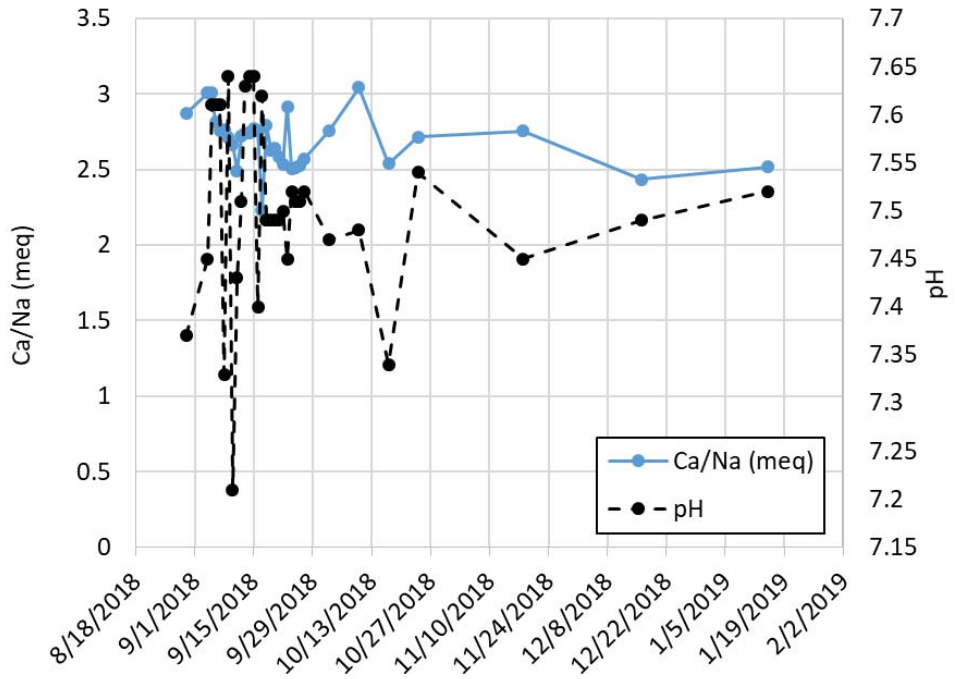

Figure A-81. Comparison of Calcium to Sodium Ratio to pH for Well 399-1-166

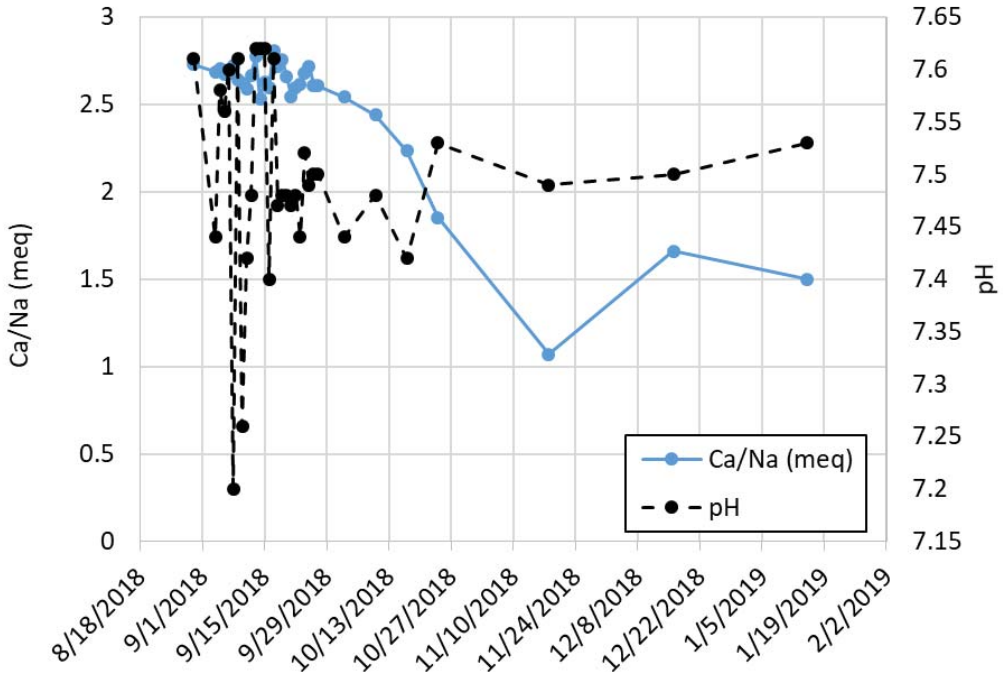

Figure A-82. Comparison of Calcium to Sodium Ratio to pH for Well 399-1-165

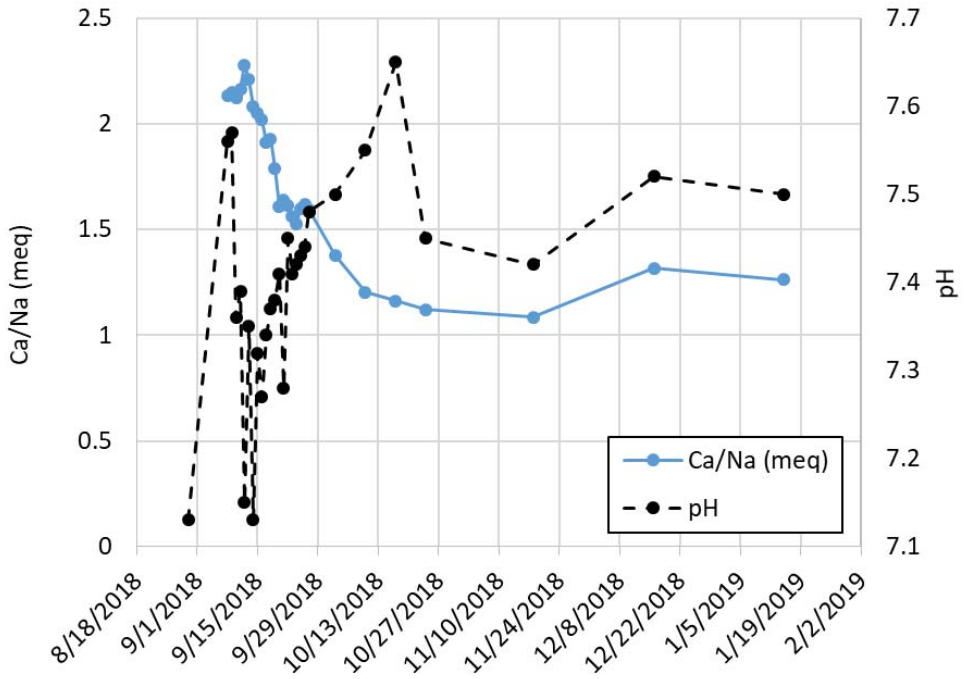

Figure A-83. Comparison of Calcium to Sodium Ratio to pH for Well 399-1-164

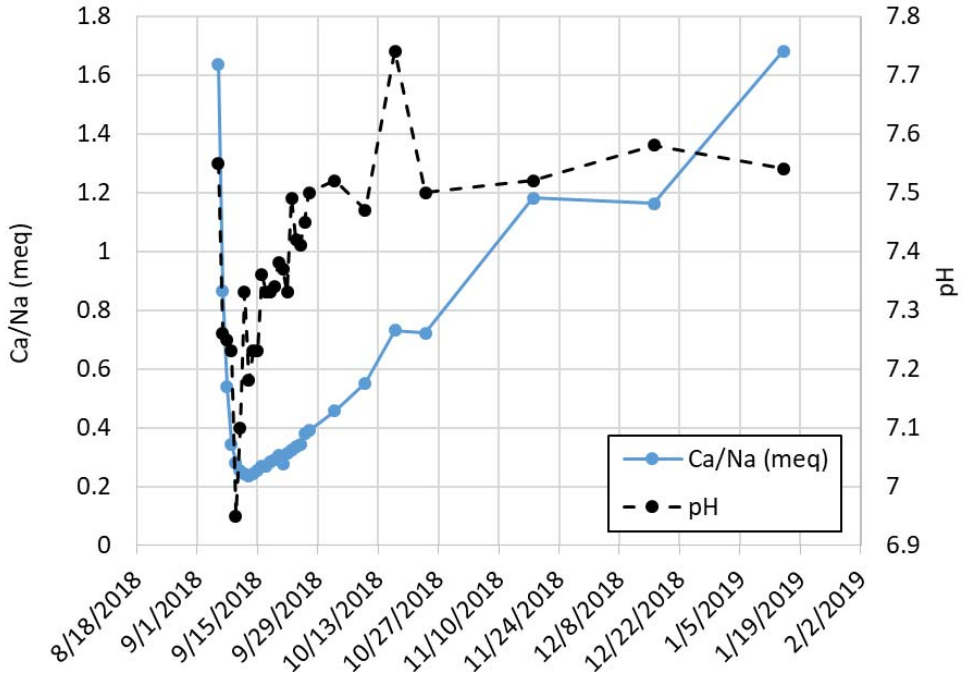

Figure A-84. Comparison of Calcium to Sodium Ratio to pH for Well 399-1-23

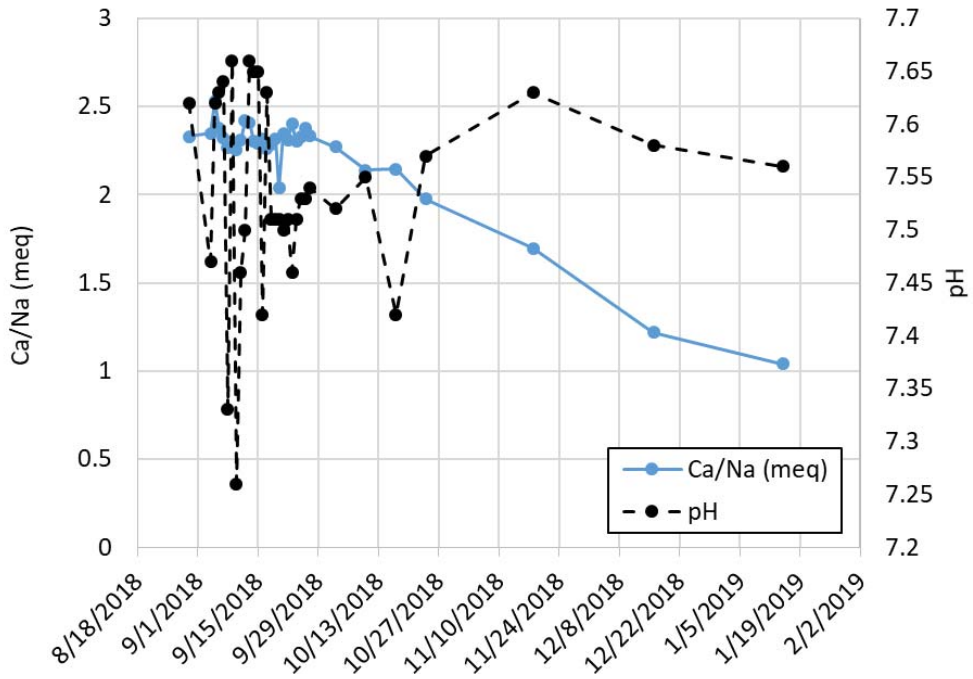

Figure A-85. Comparison of Calcium to Sodium Ratio to pH for Well 399-1-7

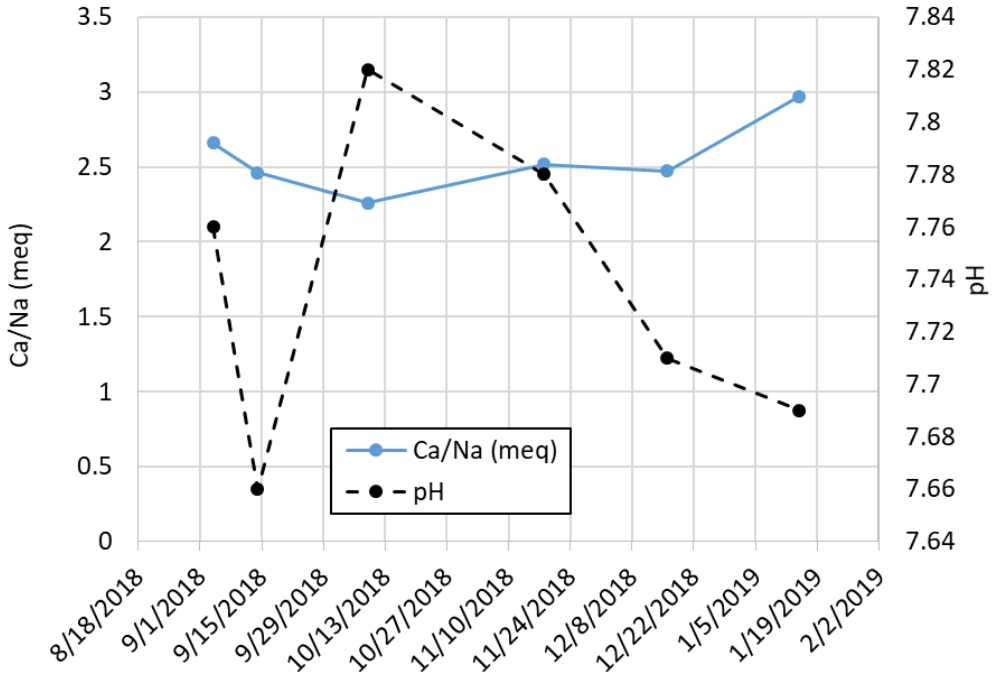

Figure A-86. Comparison of Calcium to Sodium Ratio to pH for Well 399-1-12

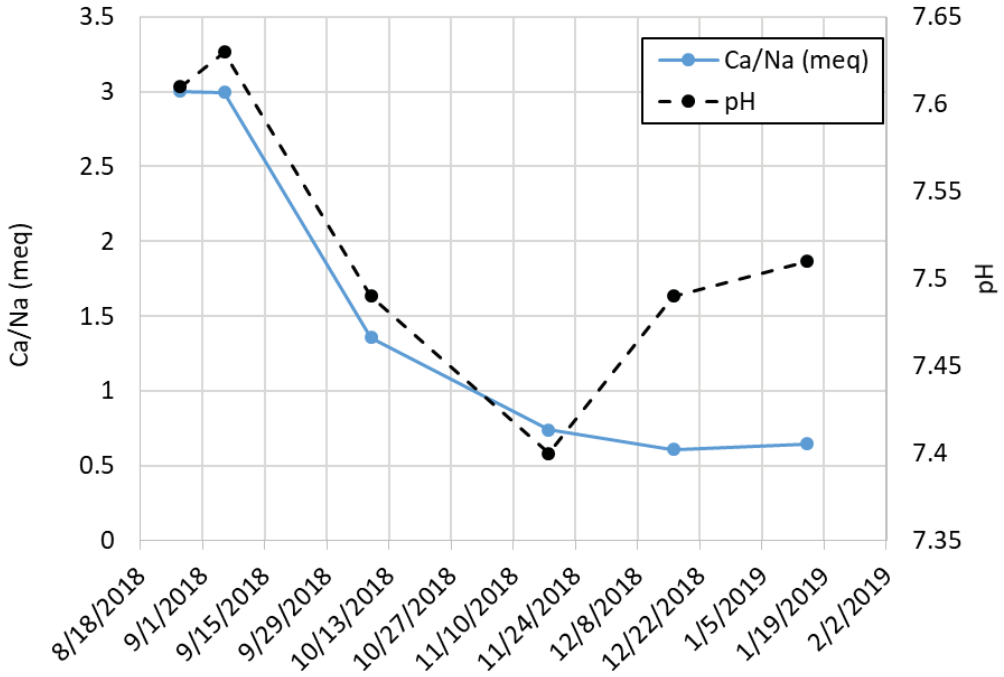

Figure A-87. Comparison of Calcium to Sodium Ratio to pH for Well 399-1-16A

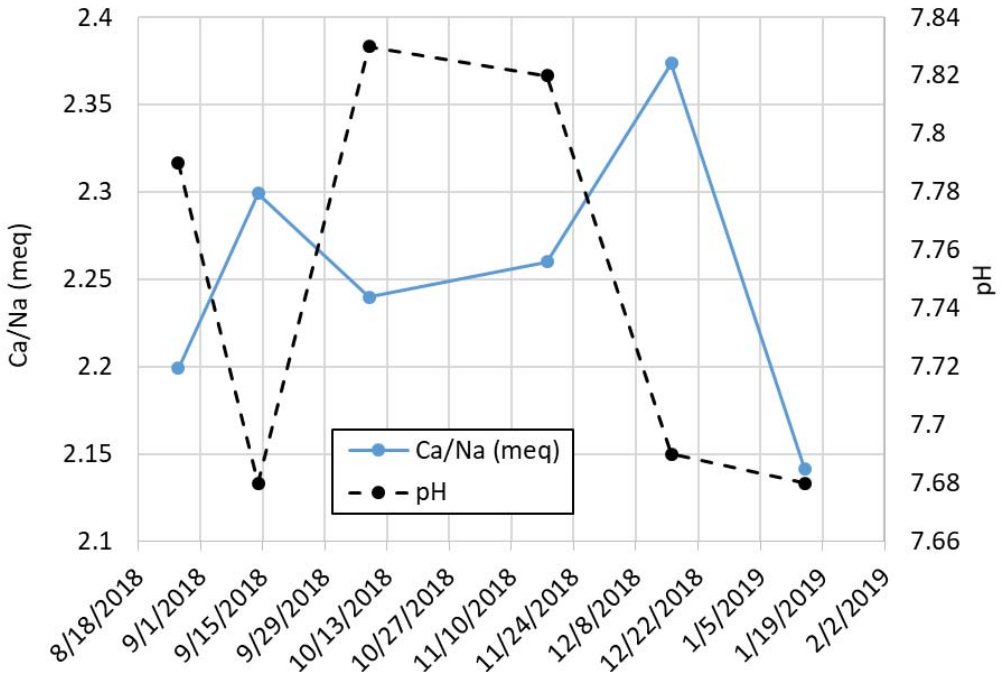

Figure A-88. Comparison of Calcium to Sodium Ratio to pH for Well 399-1-2

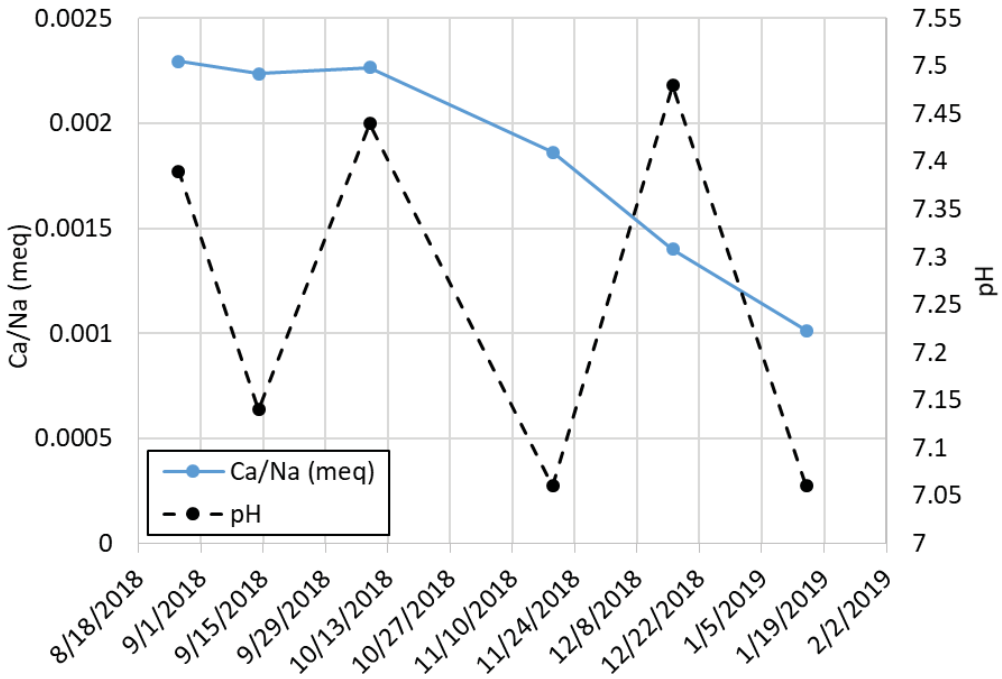

Figure A-89. Comparison of Calcium to Sodium Ratio to pH for Well 399-1-55

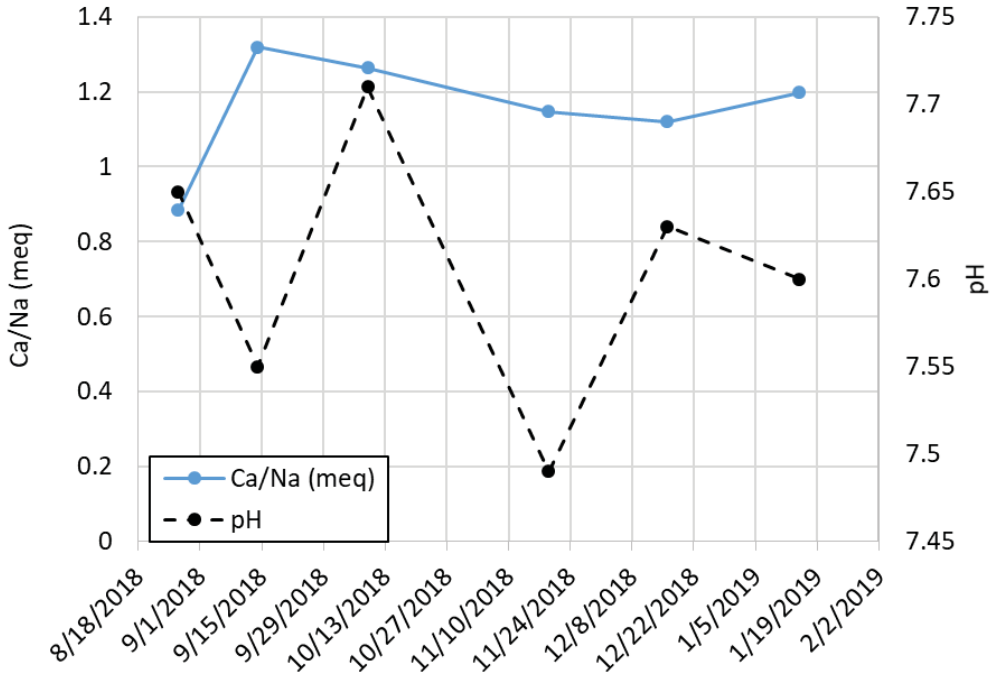

Figure A-90. Comparison of Calcium to Sodium Ratio to pH for Well 399-1-62

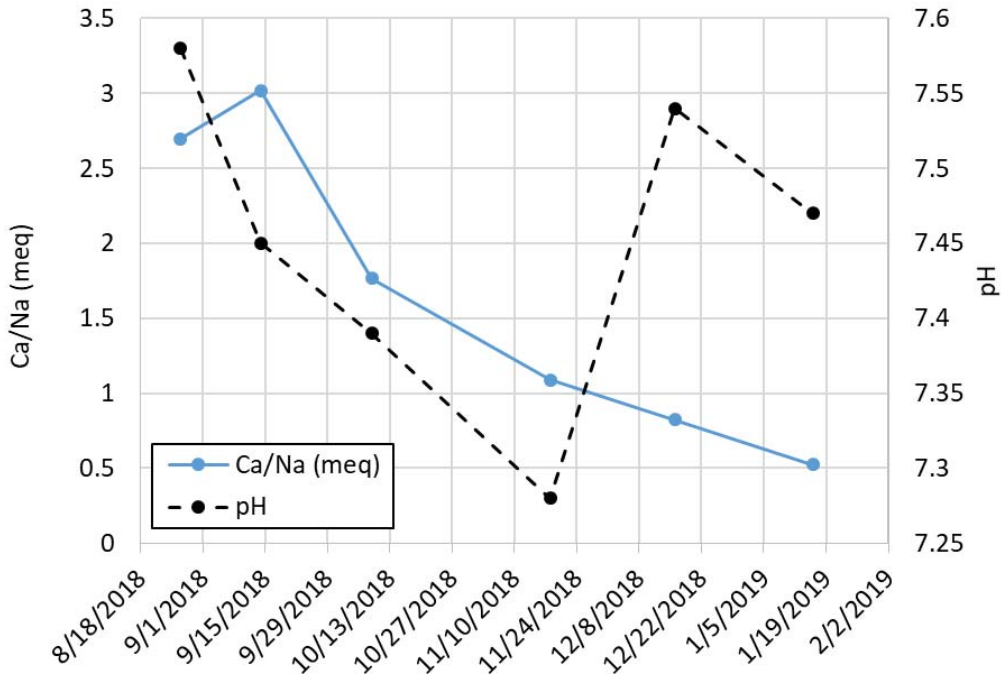

Figure A-91. Comparison of Calcium to Sodium Ratio to pH for Well 399-1-62

Appendix B

Additional Evaluations

This page intentionally left blank.

B1 Single Factor ANOVA Test

Single-factor ANOVA analysis was conducted to compare the effect of remedy injections on phosphorus and uranium soil concentrations in pre-/post-injection populations, separately. Soil sample data were compiled from eight pre- and nine post-injection boreholes in the Stage B EAA (Table B-1). The ANOVA test requires data to be normally distributed, have homogeneity of variances, and are independent observations. Empirical cumulative distribution plots showing uranium soil concentration data (log normalized) and phosphorus soil concentration data are provided in Figure B-1 and corresponding Q-Q plots in Figure B-2. Additional descriptive statistics on pre-and post-injection samples are provided in Table B-2.

Table B-1. Soil Characterization Samples from Pre-treatment and Post-treatment Boreholes

Pre-treatment				Post-treatment			
Borehole	HEIS #	Constituent	Sample (mg/kg)	Borehole	HEIS #	Constituent	Sample (mg/kg)
C9646	B38B36	uranium	48.9	C9728	B3P2J5	uranium	5.42
C9646	B38B39	uranium	70.3	C9728	B3P2J9	uranium	1.62
C9646	B38B42	uranium	20.7	C9728	B3P2K3	uranium	1.31
C9646	B38B45	uranium	39.9	C9728	B3P2K7	uranium	62.8
C9646	B38B48	uranium	32.5	C9728	B3P425	uranium	62.1
C9646	B38B51	uranium	6.83	C9728	B3P2L1	uranium	114
C9647	B38B66	uranium	26.5	C9729	B3P2L5	uranium	13.1
C9647	B38B72	uranium	85.4	C9729	B3P2L9	uranium	113
C9647	B38B75	uranium	7.35	C9729	B3P2M3	uranium	56.4
C9647	B38B78	uranium	11.3	C9729	B3P2M7	uranium	9.13
C9647	B38B81	uranium	13.7	C9729	B3P431	uranium	23.3
C9647	B38B84	uranium	7.09	C9729	B3P2N1	uranium	20
C9667	B388M2	uranium	16.2	C9729	B3P4F6[b]	uranium	158
C9667	B388M8	uranium	23.6	C9730	B3P2N5	uranium	10.9
C9667	B388M5	uranium	65.4	C9730	B3P2N9	uranium	24.4
C9667	B388N7	uranium	36.5	C9730	B3P2P3	uranium	11.5
C9667	B388N1	uranium	63.2	C9730	B3P2P7	uranium	12.3
C9667	B388P0	uranium	14.1	C9730	B3P437	uranium	22.1
C9673	B388X4	uranium	24.4	C9730	B3P2R1	uranium	16.9
C9673	B388X1	uranium	15.5	C9731	B3P2R5	uranium	33

Table B-1. Soil Characterization Samples from Pre-treatment and Post-treatment Boreholes

Pre-treatment				Post-treatment			
Borehole	HEIS #	Constituent	Sample (mg/kg)	Borehole	HEIS #	Constituent	Sample (mg/kg)
C9673	B388W8	uranium	16.3	C9731	B3P2R9	uranium	63.1
C9673	B388W5	uranium	3.85	C9731	B3P2T3	uranium	45.8
C9673	B388W2	uranium	6.54	C9731	B3P2T7	uranium	9.31
C9673	B388X7	uranium	51.6	C9731	B3P443	uranium	24
C9677	B38914	uranium	23.7	C9731	B3P2V1	uranium	22.1
C9677	B38917	uranium	25	C9732	B3P2V5	uranium	13.6
C9677	B38902	uranium	78.9	C9732	B3P2V9	uranium	5.11
C9677	B38908	uranium	39.1	C9732	B3P2W3	uranium	6.1
C9677	B38911	uranium	69.1	C9732	B3P2W7	uranium	11.2
C9677	B38920	uranium	1.05	C9732	B3P449	uranium	4.19
C9681	B38977	uranium	30.1	C9732	B3P2X1	uranium	4.82
C9681	B38971	uranium	6.9	C9733	B3P2X5	uranium	12.6
C9681	B38968	uranium	0.608	C9733	B3P2X9	uranium	7.68
C9681	B38965	uranium	0.914	C9733	B3P2Y3	uranium	22.3
C9681	B38962	uranium	0.438	C9733	B3P2Y7	uranium	15.4
C9681	B38980	uranium	3.74	C9733	B3P455	uranium	6.13
C9683	B389K7	uranium	7.47	C9733	B3P301	uranium	7.35
C9683	B389K4	uranium	9.38	C9734	B3P305	uranium	34.9
C9683	B389K1	uranium	11.1	C9734	B3P309	uranium	15.1
C9683	B389J8	uranium	9.88	C9734	B3P313	uranium	24.4
C9683	B389J5	uranium	23.3	C9734	B3P317	uranium	14
C9683	B389L0	uranium	4.12	C9734	B3P461	uranium	25.4
C9694[a]	B389V6	uranium	1.27	C9734	B3P321	uranium	23.9
C9694[a]	B389R5	uranium	3.87	C9735	B3P325	uranium	26.8
C9694[a]	B389R8	uranium	3.75	C9735	B3P329	uranium	70.6
C9694[a]	B389V3	uranium	2.9	C9735	B3P333	uranium	54.2
C9694[a]	B389T4	uranium	5.08	C9735	B3P337	uranium	7.68
C9694[a]	B389T7	uranium	3.53	C9735	B3P467	uranium	31.2

Table B-1. Soil Characterization Samples from Pre-treatment and Post-treatment Boreholes

Pre-treatment				Post-treatment			
Borehole	HEIS #	Constituent	Sample (mg/kg)	Borehole	HEIS #	Constituent	Sample (mg/kg)
C9694[a]	B389V0	uranium	2.68	C9735	B3P341	uranium	13.5
C9646	B38B36	phosphorus	904	C9735	B3P4K2[b]	uranium	175
C9646	B38B39	phosphorus	882	C9736	B3P345	uranium	2.26
C9646	B38B42	phosphorus	1120	C9736	B3P349	uranium	9.54
C9646	B38B45	phosphorus	1460	C9736	B3P353	uranium	10.7
C9646	B38B48	phosphorus	947	C9736	B3P357	uranium	1.7
C9646	B38B51	phosphorus	1170	C9736	B3P473	uranium	2.39
C9647	B38B66	phosphorus	1480	C9736	B3P361	uranium	2.11
C9647	B38B72	phosphorus	1460	C9736	B3P2J5	uranium	5.42
C9647	B38B75	phosphorus	1470	C9736	B3P2J9	uranium	1.62
C9647	B38B78	phosphorus	1310	C9728	B3P2J6	phosphorus	1280
C9647	B38B81	phosphorus	1110	C9728	B3P2K0	phosphorus	1160
C9647	B38B84	phosphorus	1370	C9728	B3P2K4	phosphorus	1230
C9667	B388M2	phosphorus	992	C9728	B3P2K8	phosphorus	1590
C9667	B388M5	phosphorus	848	C9728	B3P2L2	phosphorus	2270
C9667	B388M8	phosphorus	811	C9728	B3P426	phosphorus	1790
C9667	B388N1	phosphorus	798	C9729	B3P4F7[b]	phosphorus	1380
C9667	B388N7	phosphorus	1090	C9729	B3P2L6	phosphorus	1630
C9667	B388P0	phosphorus	1250	C9729	B3P2M0	phosphorus	2000
C9673	B388W2	phosphorus	372	C9729	B3P2M4	phosphorus	2020
C9673	B388W5	phosphorus	1270	C9729	B3P2M8	phosphorus	2310
C9673	B388W8	phosphorus	909	C9729	B3P2N2	phosphorus	1820
C9673	B388X1	phosphorus	1400	C9729	B3P432	phosphorus	1470
C9673	B388X4	phosphorus	1320	C9730	B3P2N6	phosphorus	1140
C9673	B388X7	phosphorus	1400	C9730	B3P2P0	phosphorus	1880
C9677	B38914	phosphorus	1640	C9730	B3P2P4	phosphorus	1590
C9677	B38902	phosphorus	1060	C9730	B3P2P8	phosphorus	1370
C9677	B38908	phosphorus	1090	C9730	B3P2R2	phosphorus	1740

Table B-1. Soil Characterization Samples from Pre-treatment and Post-treatment Boreholes

Pre-treatment				Post-treatment			
Borehole	HEIS #	Constituent	Sample (mg/kg)	Borehole	HEIS #	Constituent	Sample (mg/kg)
C9677	B38911	phosphorus	1280	C9730	B3P438	phosphorus	1360
C9677	B38917	phosphorus	1530	C9731	B3P2R6	phosphorus	1320
C9677	B38920	phosphorus	1240	C9731	B3P2T0	phosphorus	2150
C9681	B38962	phosphorus	1040	C9731	B3P2T3[b]	phosphorus	1860
C9681	B38965	phosphorus	868	C9731	B3P2T8	phosphorus	2320
C9681	B38968	phosphorus	961	C9731	B3P2V2	phosphorus	1850
C9681	B38971	phosphorus	1990	C9731	B3P444	phosphorus	1780
C9681	B38977	phosphorus	935	C9732	B3P2V6[b]	phosphorus	1310
C9681	B38980	phosphorus	2410	C9732	B3P2W0	phosphorus	2180
C9683	B389J5	phosphorus	927	C9732	B3P2W4	phosphorus	1090
C9683	B389J8	phosphorus	1740	C9732	B3P2W8	phosphorus	1070
C9683	B389K1	phosphorus	1010	C9732	B3P2X2	phosphorus	1330
C9683	B389K4	phosphorus	1530	C9732	B3P450	phosphorus	1650
C9683	B389K7	phosphorus	843	C9733	B3P2X6	phosphorus	1330
C9683	B389L0	phosphorus	1150	C9733	B3P2Y0	phosphorus	1800
C9694[a]	B389R5	phosphorus	1080	C9733	B3P2Y4	phosphorus	1510
C9694[a]	B389V6	phosphorus	938	C9733	B3P2Y8	phosphorus	1980
C9694[a]	B389V0	phosphorus	903	C9733	B3P302	phosphorus	1630
C9694[a]	B389R8	phosphorus	973	C9733	B3P456	phosphorus	1310
C9694[a]	B389T4	phosphorus	1040	C9734	B3P306	phosphorus	2440
C9694[a]	B389V3	phosphorus	1080	C9734	B3P310	phosphorus	2210
C9694[a]	B389T7	phosphorus	1460	C9734	B3P314	phosphorus	2570
				C9734	B3P318	phosphorus	2390
				C9734	B3P322	phosphorus	2470
				C9734	B3P462	phosphorus	2180
				C9735	B3P4K1[b]	phosphorus	1150
				C9735	B3P326	phosphorus	1340
				C9735	B3P330	phosphorus	1560

Table B-1. Soil Characterization Samples from Pre-treatment and Post-treatment Boreholes

Pre-treatment				Post-treatment			
Borehole	**HEIS #**	**Constituent**	**Sample (mg/kg)**	**Borehole**	**HEIS #**	**Constituent**	**Sample (mg/kg)**
				C9735	B3P334	phosphorus	1120
				C9735	B3P338	phosphorus	1580
				C9735	B3P468	phosphorus	1280
				C9735	B3P342	phosphorus	1060
				C9736	B3P346	phosphorus	1120
				C9736	B3P350	phosphorus	1760
				C9736	B3P354	phosphorus	2110
				C9736	B3P358	phosphorus	1930
				C9736	B3P362	phosphorus	1070
				C9736	B3P474	phosphorus	1490

a. Borehole C9694 samples listed as Miscellaneous Materials in HEIS

b. Shallow sample ignored in analysis

HEIS = Hanford Environmental Information System

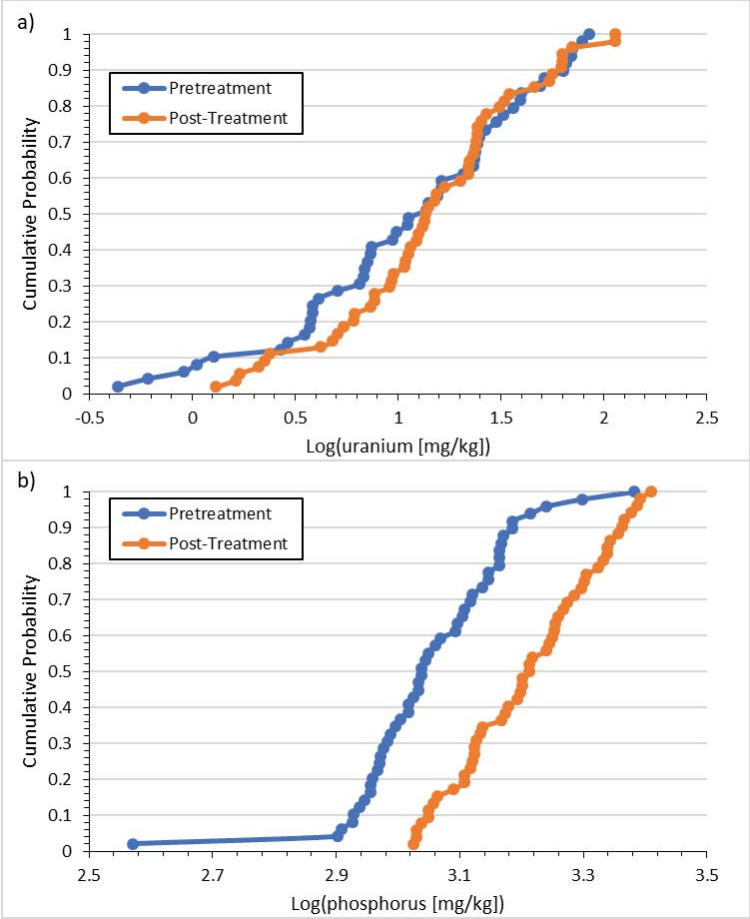

Figure B-1. Pre-treatment and Post-Treatment Empirical Cumulative Distribution Functions for a) Log Uranium, and b) Log Phosphorus Soil Concentrations

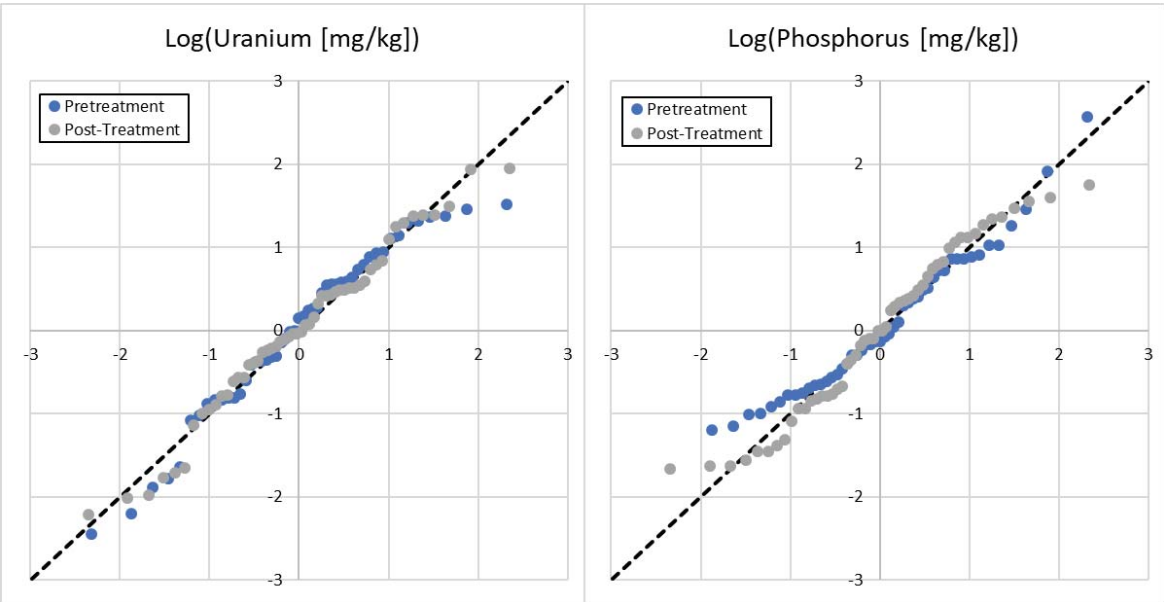

Figure B-2. Pre-treatment and Post-Treatment Q-Q Plots for a) Log Uranium, and b) Log Phosphorus Soil Concentrations

Table B-2. Soil Characterization Sample Descriptive Statistics for Pre- and Post-Treatment Samples

Statistic	Pre-treatment	Post-Treatment
Mean	21.95	23.42
Standard Error	3.29	3.42
Median	13.7	13.8
Mode	N/A	24.4
Standard Deviation	23.00	25.12
Sample Variance	529.20	631.16
Kurtosis	0.809	4.70
Skewness	1.324	2.096
Range	84.96	112.69
Minimum	0.438	1.31
Maximum	85.4	114
Sum	1075.54	1264.45
Count	49	54

B2 Thermodynamic Modeling of Uranium Mineral Solubility

Modeling was conducted using PHREEQC to determine the aqueous uranium concentration when pre- and post-treatment solutions were equilibrated with a single uranium mineral phase. Uranophane was chosen to represent a pre-treatment uranium mineral phase while andersonite and autunite are anticipated end state mineral phases post-treatment. PHREEQC was run using either the pre- or post-treatment solution (Table B-3) in equilibrium with a single mineral phase (uranophane, andersonite, or autunite). The resulting total aqueous uranium concentration is shown in Figure B-3.

When allowed to equilibrate with pre-injection solutions, uranophane, andersonite, and autunite result in sequentially decreasing aqueous uranium concentrations. In contrast, when in equilibrium with post-injection solutions, andersonite exhibits the lowest uranium concentration relative to autunite and uranophane.

Table B-3. Solution Chemistries for Pre- and Post-Treatment Porewaters

Constituent (mg/L)	Pre-treatment [a]	Post-Treatment [b]
Sodium	26.7	112.3
Potassium	8.0	8.7

Table B-3. Solution Chemistries for Pre- and Post-Treatment Porewaters

Constituent (mg/L)	Pre-treatment [a]	Post-Treatment [b]
Phosphorus	1.5	75.3
pH	7.5	7.3
Calcium	53.1	51.5
Magnesium	12.6	13.1
Chloride	25.0	24.0
Bi-Carbonate Alkalinity	129.5	198.0
Sulfate	58.5	57.3
Nitrate	31.9	28.6
Iron	0.05	0.13
Uranium	0.10	0.0045

a. Average values of samples measured from 8/27/18 and 9/4/18

b. Average values of samples measured 9/21/18, 9/22/18, and 9/23/18

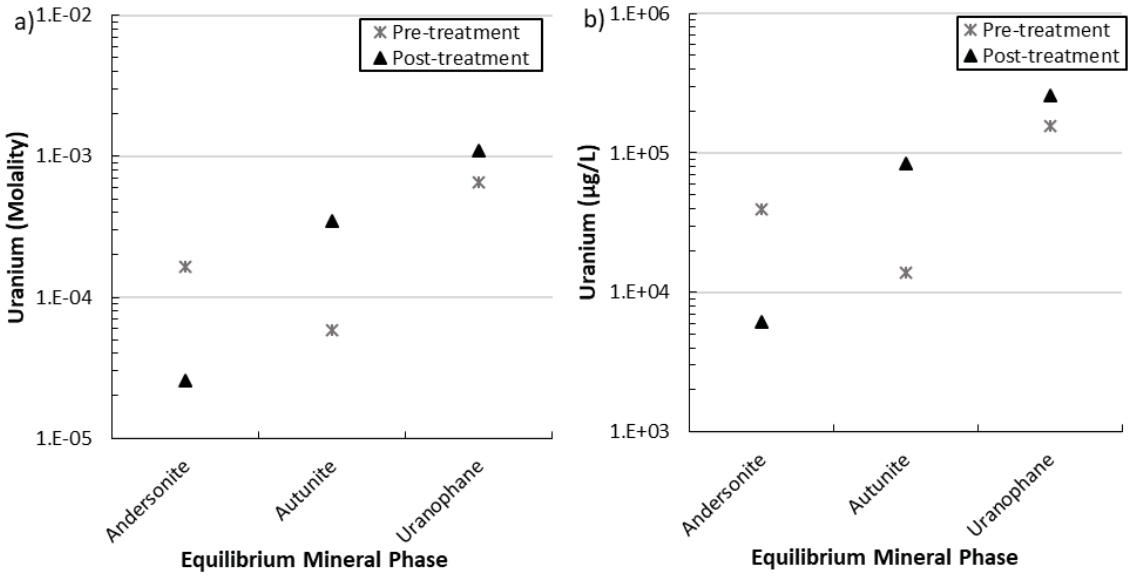

Figure B-3. Aqueous Uranium Concentration Results for Pre- and Post-Treatment Scenarios in a) Molality, and b) µg/L

Appendix C

One-Dimensional Column Leaching Simulation PHREEQC Input Files

This page intentionally left blank.

C1 Pretreatment G21.pqi

```
#Title: 1D Column Leach Test Comparison for Stage B EAA (Sample G21)
#
# Use llnl.dat
SOLUTION_SPECIES
#Taken from MINTEQ database
(http://www2.lwr.kth.se/English/OurSoftware/vminteq/), Wolery and Jarek
(2003), Guillaumount et al. (2003) and Dong and Brooks (2006)
#Discussed by Liu et al. (2008)

SOLUTION 1 Column Solution
-density 0.99704
-units mg/L
pH 7.5
Br      0
U(6)      19000 ug/l
C(4)      128
Ca        53 charge
Cl        25
Fe        0.03
K         8
Mg        12.6
N(5)      32
Na        26.7
O(0)      8 O2(g)      -0.68
S(6)      59
END

SOLUTION 2 Artificial Groundwater
-density 0.99704
-units mg/L
pH    8.0
Br    80
U(6)  0
C(4)  128
Ca    53 charge
Cl    13
S(6)  41
END

SOLUTION 3 Artificial Groundwater no Br
-density 0.99704
-units mg/L
pH    8.0
Br    0
U(6)  0
C(4)  128
Ca    53 charge
Cl    13
S(6)  41
END

KINETICS 1
   U_Sorption
  -formula  Uranophane
```

```
  -m0   5.907e-4 # see G21_Model_Parameter_Value_Calc_300FF5.xlsx for
determining this value. moles of uranium per Liter of water; porosity
corrected

  -m  5.907e-4

RATES
  U_Sorption
  -start
10 kf = 3.77e-2  #forward reaction rate constant in 1/hr
20 kd = 1.5e-3  # in units of L/g
30 kd_Mult = 10 #Kd multiplier to increase the Kd following HPO4 delivery
40 solids = 5.028e3 #solid to water volume in g/L; bulk density over porosity
50 IF (M <= 0) then GOTO 90
60 IF (MOL("HPO4-2") <= 1E-4) THEN rate = -(1/3600)* kf *(MOL("U(6)") -
(M/solids)/kd)
70 IF (MOL("HPO4-2") > 1E-4) THEN rate = -(1/3600)* kf *(MOL("U(6)") -
(M/solids)/(kd*kd_Mult))
80 moles = rate * TIME  * 360 #mutliplied by 360 seconds which is same as 0.1
hr timestep
90 SAVE moles
  -end
END

SELECTED_OUTPUT 1
    -file                 selected_output_1.sel
    -reset                false
    -totals               Br U(6)
    -kinetic_reactants    U_Sorption
END
```

C2 Post-Treatment G113.pqi

```
#Title: 1D Column Leach Test Comparison for Stage B EAA (Sample G113)
#
# Use llnl.dat
SOLUTION_SPECIES
#Taken from MINTEQ database
(http://www2.lwr.kth.se/English/OurSoftware/vminteq/), Wolery and Jarek
(2003), Guillaumount et al. (2003) and Dong and Brooks (2006)
#Discussed by Liu et al. (2008)

SOLUTION 1 Column Solution
-density 0.99704
-units mg/L
pH 7.5
Br      0
U(6)      55.5 ug/l
C(4)      128
Ca        53 charge
Cl        25
Fe        0.03
K         8
Mg        12.6
N(5)      32
Na        26.7
O(0)      8 O2(g)      -0.68
S(6)      59
END

SOLUTION 2 Artificial Groundwater
-density 0.99704
-units mg/L
pH    8.0
Br    80
U(6)  0
C(4)  128
Ca    53 charge
Cl    13
S(6)  41
END

SOLUTION 3 Artificial Groundwater no Br
-density 0.99704
-units mg/L
pH    8.0
Br    0
U(6)  0
C(4)  128
Ca    53 charge
Cl    13
S(6)  41
END

KINETICS 1
   U_Sorption
  -formula  Uranophane
```

```
  -m0   9.109e-5 # moles of uranium per Liter of water; 20 ug/g, porosity
corrected
  -m    9.109e-5

RATES
  U_Sorption
  -start
10 kf = 2.47E-1  #forward reaction rate constant in 1/hr
20 kd = 0.1  # in units of L/g
30 kd_Mult = 10 #Kd multiplier to increase the Kd following HPO4 delivery
40 solids = 4.933e3 #solid to water volume in g/L; bulk density over porosity
50 IF (M <= 0) then GOTO 90
60 IF (MOL("HPO4-2") <= 1E-4) THEN rate = -(1/3600)* kf *(MOL("U(6)") -
(M/solids)/kd)
70 IF (MOL("HPO4-2") > 1E-4) THEN rate = -(1/3600)* kf *(MOL("U(6)") -
(M/solids)/(kd*kd_Mult))
80 moles = rate * TIME  * 360 #mutliplied by 360 seconds which is same as 0.1
hr timestep
90 SAVE moles
  -end
  -end
END

SELECTED_OUTPUT 1
    -file                 selected_output_1.sel
    -reset                false
    -totals               Br U(6)
    -kinetic_reactants    U_Sorption
END
```

Appendix D

Remedy Injection Modeling PHREEQC Input File StageB.pqi

This page intentionally left blank.

```
#Surface Complexation Constants Taken from Turner and Sassman (1996) and Wang
et al. (2001)
#Only single site (weak sites) sorption is considered

SURFACE_MASTER_SPECIES
        Hfss  HfssOH

SURFACE_SPECIES
        HfssOH = HfssOH
        log_k  0.0

        HfssOH  + H+ = HfssOH2+
        log_k  7.35    # = pKa1,int

        HfssOH = HfssO- + H+
        log_k  -9.17   # = -pKa2,int

SURFACE_SPECIES
#-----------------Calcium/phosphate Surface Species--------------------------
----------
#1
      HfssOH + Ca+2 + H2PO4- = HfssOCaHPO4- + 2H+
        log_k  -6.44

#2
      HfssOH + Ca+2 + H2PO4- = HfssOCaH2PO4 + H+
        log_k  0.19


#-----------------Uranium Surface Species-----------------------------------
#1
      HfssOH + UO2+2 +2CO3-2 + H+ = HfssOH2UO2(CO3)2-
        log_k  29.15

#2
      HfssOH + UO2+2 +3CO3-2 + H+ = HfssOH2UO2(CO3)3-3
        log_k  36.28

#3
      HfssOH + 2UO2+2 + CO3-2 + 3H2O = HfssOH2(UO2)2CO3(OH)3 + 2H+
        log_k  12.62

# Ramero-Gonzalez et al. (2007)
#4
      HfssOH + UO2+2 + H2PO4- = HfssPO4UO2 + H2O + H+
        log_k  7.84

#----------------Carbonate Surface Species----------------------------------
---
# Taken from Appelo et al., ES&T 2002, p. 3097
# ---------------------------------------------
#   Carbonate

#1
      HfssOH + CO3-2 = HfssOHCO3-2
        log_k   4.78
```

```
#2
      HfssOH + CO3-2 + 2H+ = HfssHCO3 + H2O
         log_k   20.3

#----------------Other Cations Surface Species-------------------------------
-------
# Taken from Dzombak and Morel (1990) for the Weak sites
# Properties of Ba2+ are applied to Ra2+ due to chemical similiarities
# -------------------------------------------

      HfssOH + Ca+2 = HfssOCa+ + H+
            log_k   -5.85

      HfssOH + Mg+2 = HfssOMg+ + H+
            log_k   -4.6

      HfssOH + Mn+2 = HfssOMn+ + H+
            log_k   -3.5

      HfssOH + Ra+2 = HfssORa+ + H+
            log_k   -7.2

SOLUTION_SPECIES
#Taken from MINTEQ database
(http://www2.lwr.kth.se/English/OurSoftware/vminteq/), Wolery and Jarek
(2003), Guillaumount et al. (2003) and Dong and Brooks (2006)
#Discussed by Liu et al. (2008)

      UO2+2 = UO2+2
            log_k       0.0
            -gamma    4.50   0.0410

        UO2+2 + H2O = UO2OH+ + H+
            log_k       -5.25

        UO2+2 + 2H2O = UO2(OH)2 + 2H+
            log_k       -12.15

        UO2+2 + 3H2O = UO2(OH)3- + 3H+
            log_k       -20.25

        UO2+2 + 4H2O = UO2(OH)4-2 + 4H+
            log_k       -32.40

        2UO2+2 + H2O = (UO2)2OH+3 + H+
            log_k       -2.70

        2UO2+2 + 2H2O = (UO2)2(OH)2+2 + 2H+
            log_k       -5.62

        3UO2+2 + 4H2O = (UO2)3(OH)4+2 + 4H+
            log_k       -11.90

        3UO2+2 + 5H2O = (UO2)3(OH)5+ + 5H+
            log_k       -15.55

        3UO2+2 + 7H2O = (UO2)3(OH)7- + 7H+
```

```
    log_k       -32.20

4UO2+2 + 7H2O = (UO2)4(OH)7+ + 7H+
    log_k       -21.90

UO2+2 + CO3-2 = UO2CO3
    log_k       9.94

UO2+2 + 2CO3-2 = UO2(CO3)2-2
    log_k       16.61

UO2+2 + 3CO3-2 = UO2(CO3)3-4
    log_k       21.84

3UO2+2 + 6CO3-2 = (UO2)3(CO3)6-6
    log_k       54.0

2UO2+2 + CO3-2 + 3H2O = (UO2)2CO3(OH)3- + 3H+
    log_k       -0.855

3UO2+2 + CO3-2 + 3H2O = (UO2)3O(OH)2HCO3+ + 3H+
    log_k       0.655

11UO2+2 + 6CO3-2 + 12H2O = (UO2)11(CO3)6(OH)12-2 + 12H+
    log_k       36.43

2Ca+2 + UO2+2 + 3CO3-2 = Ca2UO2(CO3)3
    log_k       30.70

Ca+2 + UO2+2 + 3CO3-2 = CaUO2(CO3)3-2
    log_k       27.18

Mg+2 + UO2+2 + 3CO3-2 = MgUO2(CO3)3-2
    log_k       26.11

UO2+2 + NO3- = UO2NO3+
    log_k       0.30

3UO2+2 + 6CO3-2 = (UO2)3(CO3)6-6
    log_k       54

Ca+2 + HPO4-2 = CaHPO4
    log_k       2.740

Na+ + HPO4-2 = NaPO4-2 + H+
    log_k -10.8918

UO2+2 + 2HPO4-2 = UO2(HPO4)2-2
    log_k 18.344

UO2+2 + PO4-3 = UO2PO4-
    log_k 13.23

UO2+2 + PO4-3 + H+ = UO2HPO4
    log_k 19.59

UO2+2 + PO4-3 + 2H+ = UO2H2PO4+
```

```
            log_k 22.82

        UO2+2 + PO4-3 + 3H+ = UO2H3PO4+2
            log_k 22.46

        UO2+2 + 2PO4-3 + 4H+ = UO2(H2PO4)2
            log_k 44.04

        UO2+2 + 2PO4-3 + 5H+ = UO2(H2PO4)(H3PO4)+
            log_k 45.05

PHASES
#Gorman-Lewis, 2009
Autunite
      Ca(UO2)2(PO4)2:3H2O = Ca+2 + 2UO2+2 + 2PO4-3 + 3H2O
      log_k       -48.36

Uranyl_Hydrogen_Phosphate
      UO2HPO4:3H2O = UO2+2 + HPO4-2 + 3H2O
      log_k       -13.17

Uranyl_Orthophosphate
      (UO2)3(PO4)2:4H2O = 3UO2+2 + 2PO4-3 + 4H2O
      log_k       -49.36

Andersonite
      Na2CaUO2(CO3)3(H2O)6 = 2Na+ + Ca+2 + UO2+2 +3CO3-2 + 6H2O
      log_k       -37.5

Liebigite
      Ca2UO2(CO3)3(H2O)10 = 2Ca+2 + UO2+2 + 3CO3-2 + 10H2O
      log_k       -36.9

Chernikovite
      (UO2)HPO4(H2O)4 = UO2+2 + HPO4-2 + 4H2O
      log_k       -22.73

SOLUTION 1 Initial solution #average values from 8/27/18 and 9/4/18 at 399-1-
17A
    temp      20
    pH        7.5
    pe        4
    redox     pe
    units     mg/kgw
    density   1
    C(4)      129.5
    Ca        53.1 charge
    Cl        25
    Fe        0.05
    K         8
    Mg        12.6
    N(5)      31.9
    Na        26.7
    O(0)      1 O2(g)      -0.68
    S(6)      58.5
    U         0.1
    -water    1 # kg
```

```
END

EXCHANGE 1
X 0.00126

-equil 1
END

EQUILIBRIUM_PHASES 1
    Goethite  0 17.4
    K-feldspar 0 17.4
    O2(g)     -0.68 17.4
    Quartz    0 17.4
    Hydroxylapatite 0 0
    Whitlockite 0 0
    Autunite 0 0
    Uranyl_Hydrogen_Phosphate 0 0
    Uranyl_Orthophosphate 0 0
    Liebigite 0 0
    Andersonite 0 0
    Chernikovite 0 0
    Siderite 0 0
END

SURFACE 1
    -equilibrate with solution 1
    -sites DENSITY
    HfssOH     4      250       0.63

#Based on HFO site density of 4 sites per nm2; specific surface area of 250
m2/g; and mass solid (HFO) to
#water ratio is about 0.63 g/L assuming effective porosity of 0.174; 0.0005
weight fraction based on average sum of ext 3,4,5.
#This calculation assumes that HFO (amorphous iron content) is approximately
10% of total iron content
END

KINETICS 1
  Calcite
  -m0    1.45     # moles of calcite per Liter of water; ~2000 ug/g, porosity
corrected
  -m     1.45
  -parms 1.67e5   0.6  # cm^2/mol calcite, exp factor

   U_Sorption
  -formula  Uranophane
  -m0   6.07e-3 # moles of uranium per Liter of water; 20 ug/g, porosity
corrected
  -m    6.07e-3

RATES
  Calcite
   -start
1   REM   PARM(1) = specific surface area of calcite, cm^2/mol calcite
2   REM   PARM(2) = exponent for M/M0
```

```
10  si_cc = SI("Calcite")
20  IF (M <= 0  and si_cc < 0) THEN GOTO 200
30  k1 = 10^(0.198 - 444.0 / TK )
40  k2 = 10^(2.84 - 2177.0 /TK )
50  IF TC <= 25 THEN k3 = 10^(-5.86 - 317.0 / TK)
60  IF TC > 25 THEN k3 = 10^(-1.1 - 1737.0 / TK )
80  IF M0 > 0 THEN area = PARM(1)*M0*(M/M0)^PARM(2) ELSE area = PARM(1)*M
110 rate = area * (k1 * ACT("H+") + k2 * ACT("CO2") + k3 * ACT("H2O"))
120 rate = rate * (1 - 10^(2/3*si_cc))
130 moles = rate * 0.001 * TIME *8640 # convert from mmol to mol, multiplied
by 8640 seconds which is same as 0.1 day timestep NOTE: this changes to 360
for 0.1 hour timestep in 2D Groundwater model
200 SAVE moles
   -end

  U_Sorption
  -start
10 kf = 3.87e-2  #forward reaction rate constant in 1/hr
20 kd = 7.41e-3  # in units of L/g
30 kd_Mult = 10 #Kd multiplier to increase the Kd following HPO4 delivery
40 solids = 1.03e4 #solid to water volume in g/L; bulk density (1800 kg/m3)
over porosity (0.174)
50 IF (M <= 0) then GOTO 90
60 IF (MOL("HPO4-2") <= 1E-4) THEN rate = -(1/3600)* kf *(MOL("U(6)") -
(M/solids)/kd)
70 IF (MOL("HPO4-2") > 1E-4) THEN rate = -(1/3600)* kf *(MOL("U(6)") -
(M/solids)/(kd*kd_Mult))
80 moles = rate * TIME * 8640 #multiplied by 8640 seconds which is same as
0.1 day timestep NOTE: this changes to 360 for 0.1 hour timestep in 2D
Groundwater model
90 SAVE moles
  -end

SOLUTION 2 Injected solution #Daily skid measurements averaged from 9/4/18 to
10/17/18
    temp      20
    pH        7.6
    pe        4
    redox     pe
    units     mg/kgw
    density   1.017
    Br        100
    C(4)      3666.9
    Ca        17.64
    Cl        1.17
    K         1769.39
    Mg        4.55
    N(5)      0.48
    Na        2605.76 charge
    P         2769.09
    S(6)      28.46
    U         0
    -water    1 # kg
END

SELECTED_OUTPUT 1
    -file                 selected_output_1.sel
```

```
    -reset                false
    -pH                   true
    -alkalinity           true
    -ionic_strength       true
    -water                true
    -charge_balance       true
    -totals               Na  Ca  K  P  Cl  Br  Mg
                          Fe(2)  Fe(3)  U(6)
    -molalities           NaX  CaX2  KX  FeH2PO4+
                          FeH2PO4+2  FeHPO4  FeHPO4+  CaH2PO4+
                          CaHPO4  CaHCO3+  CaPO4-  Ca2UO2(CO3)3
                          HPO4-2  Ca+2  H2PO4-  PO4-3  Fe+2  HCO3-
                                      HfssOH2UO2(CO3)3-3
    -activities           H+
    -equilibrium_phases   K-feldspar  Goethite  Calcite Aragonite
                          Quartz  Kaolinite  Hematite  Hydroxylapatite
                          Whitlockite  Autunite  Uranyl_Hydrogen_Phosphate
Uranyl_Orthophosphate
                                      Liebigite  Andersonite  Chernikovite
Siderite Uranophane

   -saturation_indices    Calcite Hydroxylapatite Andersonite Chernikovite
Uranophane

   -kinetic_reactants     Calcite U_Sorption
END
USER_PUNCH
-headings Kinetic time

10 PUNCH SIM_TIME
20 PUNCH TIME
END
```

This page intentionally left blank.

Appendix E

Software Installation and Checkout Forms

This page intentionally left blank.

CHPRC SOFTWARE INSTALLATION AND CHECKOUT FORM

Software Owner Instructions:
Complete Fields 1-13, then run test cases in Field 14. Compare test case results listed in Field 15 to corresponding Test Report outputs. If results are the same, sign and date Field 19. If not, resolve differences and repeat above steps.

Software Subject Matter Expert Instructions:
Assign test personnel. Approve the installation of the code by signing and dating Field 21, then maintain form as part of the software support documentation.

GENERAL INFORMATION:

1. Software Name: VS2DRTI Software Version No.: 1.4

EXECUTABLE INFORMATION:

2. Executable Name (include path):

   C:\Program Files\USGS\vs2drti-1.4.0\bin\vs2drti.exe

3. Executable Size (bytes): 88,000

COMPILATION INFORMATION:

4. Hardware System (i.e., property number or ID):

   Vendor supplied

5. Operating System (include version number):

   Vendor supplied

INSTALLATION AND CHECKOUT INFORMATION:

6. Hardware System (i.e., property number or ID):

   INTERA-00873

7. Operating System (include version number):

   Windows 10 Pro version 1607

8. Open Problem Report? (●) No ( ) Yes PR/CR No.

TEST CASE INFORMATION:

9. Directory/Path:

   S:\PSC\CHPRC.C003.HANOFF\Rel.033\EAA Study Evaluation-Stage B\VS2DRTI Modeling\QA tests

10. Procedure(s):

    per CHPRC-04167 Rev 0, VS2DRTI Software Test Plan

11. Libraries:

    phreeqc.dat

12. Input Files:

    per CHPRC-04167 Rev 0, VS2DRTI Software Test Plan

13. Output Files:

    per CHPRC-04167 Rev 0, VS2DRTI Software Test Plan

14. Test Cases:

    TC-1 and TC-2

15. Test Case Results:

    Match expected results as presented in CHPRC-04167, VS2DRTI Software Test Plan

16. Test Performed By: Ryan Nell

17. Test Results: (●) Satisfactory, Accepted for Use ( ) Unsatisfactory

18. Disposition (include HISI update):

    Accepted; Authorized User added to HISI Entry 4582.

Page 1 of 2 A-6005-149 (REV 0)

CHPRC SOFTWARE INSTALLATION AND CHECKOUT FORM (continued)

1. Software Name: VS2DRTI — Software Version No.: 1.4

Prepared By:

19.	William E. Nichols	7 NOV 2019
Software Owner (Signature)	Print	Date

20. Test Personnel:

	Ryan M. Nell	11/7/19
Sign	Print	Date
Sign	Print	Date
Sign	Print	Date

Approved By:

21.	Not Required (CHPRC-04142)	
Software SME (Signature)	Print	Date

Page 2 of 2

A-6005-149 (REV 0)

CHPRC SOFTWARE INSTALLATION AND CHECKOUT FORM

Software Owner Instructions:

Complete Fields 1-13, then run test cases in Field 14. Compare test case results listed in Field 15 to corresponding Test Report outputs. If results are the same, sign and date Field 19. If not, resolve differences and repeat above steps.

Software Subject Matter Expert Instructions:

Assign test personnel. Approve the installation of the code by signing and dating Field 21, then maintain form as part of the software support documentation.

GENERAL INFORMATION:

1. Software Name: The Geochemists Workbench Software Version No.: 12.0.4

EXECUTABLE INFORMATION:

2. Executable Name (include path):

   D:\GWB\Workbench.exe

3. Executable Size (bytes): 17,846,920

COMPILATION INFORMATION:

4. Hardware System (i.e., property number or ID):

   Vendor compiled

5. Operating System (include version number):

   Windows (vendor compiled)

INSTALLATION AND CHECKOUT INFORMATION:

6. Hardware System (i.e., property number or ID):

   INTERA-Blue

7. Operating System (include version number):

   Windows Server 2008 SP2 (32-bit)

8. Open Problem Report? (●) No ( ) Yes PR/CR No.

TEST CASE INFORMATION:

9. Directory/Path:

   \\blue\userfiles\rdockter\

10. Procedure(s):

    CHPRC-01874 Rev. 3, Geochemist's Workbench Integrated Software Management Plan

11. Libraries:

12. Input Files:

    Case1 seawater.rea, Case2 Amazon table 6 7.sp8

13. Output Files:

    ATC-1 React output 4April2019.txt, ATC-2 SpecE8 output 4April2019.txt

14. Test Cases:

    GWB-ITC-1; GWB-ITC-2

15. Test Case Results:

    All tests passed.

16. Test Performed By: Randy Dockter

17. Test Results: (●) Satisfactory, Accepted for Use ( ) Unsatisfactory

18. Disposition (include HISI update):

    Installation added to HISI Entry

Page 1 of 2 A-6005-149 (REV 0)

CHPRC SOFTWARE INSTALLATION AND CHECKOUT FORM (continued)

1. Software Name: The Geochemists Workbench Software Version No.: 12.0.4

Prepared By:

19. WILLIAM NICHOLS (Affiliate) Digitally signed by WILLIAM NICHOLS (Affiliate) Date: 2020.01.16 09:43:36 -08'00' — Software Owner (Signature) | WE Nichols — Print | Date

20. Test Personnel:

Sign	Print	Date
R. Dockter	RE Dockter	1-16-2020

Approved By:

21. Software SME (Signature) | N/A per SMP — Print | Date

A-6005-149 (REV 0)